# The biofouling of reverse osmosis membranes: From characterisation to control.

Powell, Lydia Charlotte

# The biofouling of reverse osmosis membranes – from characterisation to control

*by*

Lydia Charlotte Powell

Submitted to Swansea University in fulfilment of the requirements for the Degree of Doctor of Philosophy

May 2011

Swansea University
Prifysgol Abertawe

*Multidisciplinary Nanotechnology Centre*
*Swansea University*
*Singleton Park,*
*Swansea*
*SA2 8PP*

## Declaration

This work has not been previously been accepted in substance for any degree and is not being concurrently submitted in candidature for any degree.

Signed (candidate): .....

Date: 18/05/11

## Statement 1

This thesis is the result of my own investigations, expect where otherwise stated. Other sources are acknowledged by the use of explicit references. A list of references is included.

Signed (candidate): .....

Date: 18/05/11

## Statement 2

I hereby give consent for my thesis, if accepted, to be available for photocopying and for interlibrary loan, and for the title and summary to be made available to outside organisations.

Signed (candidate): .....

Date: 18/05/11

## Summary

Membrane technology can be utilised for the high purification and desalination of water. However membrane filtration processes are commonly impeded by membrane fouling, which can lead to flux decline and an overall reduction in separation efficiency within the process. Therefore the aim of this research study was a comprehensive investigation of the issue of biofouling on industrial RO membranes through molecular biology techniques, characterisation of surface charge of foulant bacteria and RO membrane surface and AFM imaging and force measurements on clean and fouled membranes for the determination of adhesion force and micromechanical properties. The laboratories within Gwangju Institute of Science and Technology, South Korea and Swansea University, Wales were equipped for the scope of this research work.

Research focused on the extraction of microbial DNA obtained from fouling layers on the surface of Reverse Osmosis Membranes obtained from the Fujairah Water and Power Plant, UAE. The use of the culture independent method of the molecular technique based on the 16S rDNA sequence and constructed gene libraries, was then used to determine the bacterial species that caused significant fouling on the RO membrane. Four bacterial species isolated from the fouling layer from the RO membrane were characterised in terms of electrophoretic mobility and zeta potential to determine the cell surface charge within various industrial relevant environments for the elucidation of cell adhesion mechanisms to the membrane surface. AFM images of virgin and fouled membranes were obtained and analysed to reveal the roughness of the surface which could influence fouling and the surface charge of the membranes were measured through the method of streaming potential at various industrial relevant environments to further elucidate the mechanisms of cell adhesion to the membrane surface. Force measurements were performed to reveal the adhesion force and elasticity values of virgin, process fouled and purposely fouled with the four bacterial isolates, to determine process behaviour in various environmental conditions.

Through this research and future work, it is hoped that a rational strategy for economic and effective cleaning processes will be developed which will maintain efficient membrane operation and prolong membrane life, thus enabling the reduction of operating costs of such processes.

## Dedication

This thesis is dedicated to my Parents

## Acknowledgements

There are many people that I wish to acknowledge and thank for their varying contributions towards the successful completion of this research project:

Dr Chris J. Wright, Multidisciplinary Nanotechnology Centre, Swansea University

Dr Robert Lovitt, Multidisciplinary Nanotechnology Centre, Swansea University

Dr In Seop Chang, Gwangju Institute of Science and Technology (GIST), South Korea

Dr Lewis Francis, Institute of Life Sciences, Swansea University

Dr Dale Rogers, Multidisciplinary Nanotechnology Centre, Swansea University

Dr Paul Williams, Multidisciplinary Nanotechnology Centre, Swansea University

Dr Steven Mandale, Multidisciplinary Nanotechnology Centre, Swansea University

Youngpil Chun, Energy and Biotechnology Laboratory, GIST

British Council for Research Co-operation Funding for research exchange to South Korea

## Contents

## Abbreviations

| | |
|---|---|
| AFM | Atomic Force Microscope |
| BSA | Bovine Serum Albumin |
| DGGE | Denaturing Gel Electrophoresis |
| DMA | Dynamic mechanical analysis |
| ELS | Electrophoretic Light Scattering |
| EPS | Extracellular Polymeric Substance |
| ESWPC | Emirates Sembcorp Water and Power |
| FISH | Fluorescence in Situ Hybridzation |
| IEP | Isoelectric Point |
| JKR | Johnson-Kendall-Roberts |
| MF | MicroFiltration |
| MRSA | Methicillin-resistant *Staphylococcus aureus* |
| NF | NanoFiltration |
| NHS | National Health Service |
| NOM | Natural Organic Matter |
| PBI | Polybenzimidazole |
| PCR | Polymerase Chain Reaction |
| PEM | Polyelectrolyte multilayered thin film |
| PSPD | Position Sensitive Photodiode |
| RFLP | Restriction Fragment Length Polymorphism |
| RO | Reverse Osmosis |
| SEM | Scanning Electron Microscopy |
| SGOMC | Sembcorp Gulf O and M Company |
| SMC | Smooth muscle cells |
| SRB | Sulphate-Reducing Bacteria |
| SWRO | SeaWater Reverse Osmosis |
| UF | UltraFiltration |

# Chapter 1 Introduction

## 1. 1 Introduction

Fresh drinking water is essential for life and as there is current concern about climate change affecting weather patterns and temperature, this has lead to access to pure clean water being an extremely important issue that will grow in magnitude especially for human consumption, agriculture and industry [1]. Areas such as the United Arab Emirates already have had to utilise desalination technology to be able to supply its population with freshwater by converting the surrounding seawater into pure clean drinkable water.

Membrane separation processes is a recent fast emerging technology which has been applied for energy efficient separations within the process industries, since its introduction into the food and biotechnology industries in the 1980's [2]. Membrane technology can be a solution for the production of highly purified water by the purification and desalination of seawater through the application of Reverse Osmosis (RO) and NanoFiltration (NF) membranes for the separation process. However, membrane filtration processes are commonly impeded by membrane fouling, which leads to flux decline within the process and an overall reduction in separation efficiency [3]. Membrane fouling can therefore cause considerable technical problems in processes, such as reduction in water product quality and requirement for higher pressure, and can also cause economic loss as fouling and cleaning agents can shorten the life span of the membranes [2]. Therefore a greater understanding of the membrane fouling process is required for the development of strategies to inhibit and control the biofilm fouling process.

Membrane biofouling is essentially the formation of microbial biofilms attached to the surface of the membrane. Microorganisms within the seawater can attach to the membrane surface and then grow and develop into a biofilm, which is essentially complex layers of microorganisms embedded in a matrix of Extracellular Polymeric Substance (EPS) where EPS is excreted by the microorganisms. Even though the water

treated within the process is relatively low in nutrients, the capture and accumulation of nutrients in the biofilm at the membrane surface promotes substantial microbial growth [2]. Also surface fouling is contributed to by inorganic salts precipitation and organics binding which forms part of the biofilm. The biofilm structure has many advantages over a planktonic mode of existence, such as the ability to resist shear forces which enables the microbes to survive in a submerged environment [4].

Currently operating water desalination plants use a few strategies for the prevention and control of membrane fouling, such as the use of pre-treatment units for the removal of organic and inorganic dissolved substances and the cleaning of the membrane by either back-washing or chemical wash, however these strategies have limited success [5]. Therefore a better understanding of the physical, chemical and biological characteristics regarding the processes regulating biofilm formation and biofouling progression will aid in developing new strategies to prevent or reduce the rate of membrane fouling.

## 1.2 Fouling of Membrane Systems

RO membranes are commercially important membranes that have been used in water treatment, pharmaceutical and food industries for separations processes. These membranes are known to have significant surface roughness, where such membranes prevent the passage of small molecules and simple ions. However due to RO membrane properties, the membranes are susceptible to fouling [6]. In RO systems, there are four types of foulants which are commonly encountered; inorganic fouling (scaling), colloidal fouling, biological fouling and organic fouling. Inorganic fouling or scaling of membrane surfaces is caused by the precipitation of sparingly soluble salts from the concentrated brine. Colloidal fouling of the RO system is due to the presence of suspended solids in the seawater, which tend to clog the system instead of fouling the membrane surface. Bio-fouling occurs when microorganisms attach and grow into a biofilm which subsequently fouls the membrane surface, causing not only a loss of flux within the process but also may physically degrade certain types of membranes. Organic fouling occurs due to what is known as Natural Organic Matter (NOM) which is composed from matter originating from plants and animals being present in raw

waters [7, 8]. Bio-fouling of membrane surfaces is a major component of membrane fouling and therefore the current understanding of its developmental process and the contributing factors involved are further explained.

### 1.2.1 Biofilm Formation

As bio-fouling is a major component in fouling of membrane systems, the mechanism with which bacteria attach and develop into a biofilm needs to be investigated to prevent process disruption. Bacteria normally exist in either a planktonic state, where the bacteria is freely existing in the bulk solution, or in a sessile state where the bacteria is a unit attached to a surface or part of a biofilm. It is thought that about 99% of the world's bacterial population exist within a biofilm at various stages of growth. Biofilms can be described as a microbially derived sessile community characterised by cells that attach to a surface, embedded in a matrix of EPS [9]. The advantages offered to bacteria within a biofilm are numerous, such as protection from antibiotics, disinfectants and dynamic environments. Other advantages include promoted genetic exchange within the biofilm and the ability to survive in nutrient deficient conditions [9, 10]. Biofilms can be found within many industrial, medical and domestic environments. Within such industries as dairy, food, water treatment and maritime, biofilms can be detrimental to the processes as they can be responsible for product contamination, reduced process efficiency, corrosion, pipe blockages and equipment failure [11]. Within medical environments, biofilms within the human body can be the cause of infections which could lead to patient mortality [12]. This problem has been outlined with the recent outbreak of the biofilm forming Methicillin-resistant *Staphylococcus aureus* (MRSA) within the National Health Service (NHS) which is resistance to all but a few antibiotic programs. Also within dentistry, biofilms form on teeth causing the erosion of enamel [13]. However, biofilms have been shown to be useful in the field of bioremediation, where organisms are used to remove contaminants, such as nitrogen compounds and also for the purification of industrial waste water [14, 15]. Therefore, as bacterial biofilms hold important economic and medical consequences, researchers have investigated the mechanisms used by microorganisms to adhere to various surfaces to form biofilms [9].

### 1.2.2 Individual Bacterial Structure

Bacteria are unicellular in nature and a bacterial cell has the following structural components: Nucleoid (DNA), plasmids, ribosomes, cytoplasm, cell membrane and a cell wall. There are two main types of bacterial cell walls, Gram positive and Gram negative. There also are surface structures present on certain bacteria, such as fimbrae or pili which are protein tubes which extend from the outer membrane, S-layers which are two-dimensional arrays of proteins which have a crystalline appearance, capsules which are well organised structures lying outside of the cell wall which may protect bacteria from phagocytosis and desiccation, slime layer composed from EPS excreted from the cells to aid in bacterial adhesion and flagella which are long thin structures which protrude from the cell wall and are responsible for bacterial motility. Bacterial cells lack intracellular membranous compartmentalization which allows the interface between the outer cell envelope and the surrounding environment to dictate a role in the bacteria's overall physiology. It is the outer cell surface that mediates adhesive processes and participates in cell growth and division, therefore it is important to consider the outer surface of a bacterial cell when explaining bacterial adhesion and growth [16].

### 1.2.3 Mechanism of bacterial adhesion and biofilm development

A variety of physical, chemical and biological processes within an environment govern biofilm growth. Characklis and Marshall [17] have described biofilm growth as a eight-step process which considers the formation of a conditioning layer, the reversible and irreversible adhesion of bacteria, population growth and the detachment of bacteria from a mature biofilm for colonisation of other surfaces.

*The conditioning layer*

The first stage involves organic and inorganic particles present in the bulk flow being carried towards the surface by either turbulent flow, diffusion or gravitational force. These particle forms the conditioning layer on top of the substrate which can favourably alter properties of the surface, such as surface charge, potential and tensions, and can

aid in facilitating the attachment of bacteria to the surface and the subsequent biofilm growth [9, 10].

*Reversible adhesion*

After the conditioning layer has formed, microbial cells are transported to a surface from the bulk liquid by either physical forces, such as convective mass transport (where cells are physically transported towards the surface by the movement of the bulk fluid) and by sedimentation, or by active transport mediated by bacterial appendages, such as flagella, fimbriae and pili. Only a fraction of cells reaching the surface reversibly absorbs, where factors such as bacterial orientation, surface functionality, available energy and environment conditions such as temperature and pressure can contribute to bacterial adhesion. The physical forces associated with initial attachment of cells are van der Waals forces, electrostatic (double layer) interaction and steric interactions, which are collectively known as the DLVO forces. The DLVO theory can describe the interaction between a cell and a flat surface as the balance of two additive factors, the attractive van der Waals interactions and the repulsive interactions generated from the overlap of the electrical double layer of the cell and the substrate. Also the extended DLVO theory takes account for the hydrophobic, hydrophilic and osmotic interactions involved [9, 10].

*Irreversible adhesion*

At this stage of bacterial adhesion, the cells remain immobilised and become irreversibly attached to the substrate. A number of factors are thought to be involved in irreversible absorption; these include various short range forces, covalent and hydrogen bonding as well as hydrophobic-hydrophilic interactions of the surface. Also it is suggested that bacterial appendages, such as fimbriae, overcome the repulsive forces of the electrical double layer and make contact with the conditioning layer which stimulates chemical reactions, such as oxidation and hydration, and strengthens the bacteria to surface bond [9, 10].

*Population growth*

The irreversibly attached cells start to divide and daughter cells tend to spread outward and upward to form cell clusters, which typically grow and develop into a mushroom-like structure. It is believed that this mushroom structure allows the passage of

nutrients to bacteria located deep in the biofilm. The rapid increase in population occurs within the exponential growth phase of the cells, after the initial lag phase. The physical and chemical environmental conditions dictate the extent of the growth. At this stage in growth, the formation of a biofilm begins with the cells excreting EPS which helps to form stronger bonds and bind cells together. Also cells within a biofilm show differential gene expression than when they are in a planktonic state to aid to adhesive properties. An example would be the production of bacteria appendages being inhibited in sessile cells as motility is no longer necessary, while the expression of genes for the production of cell surface proteins and excretion products would increase. In one study, as many as 57 biofilm related proteins were found in sessile cells and not in planktonic cells [9].

*Stationary biofilm phase*

At some stage in biofilm development, the cells enter the stationary growth phase where the rate of cell division is equivalent to the rate of cell death. When the cell concentration is high, a series of cell signalling mechanisms are used by the biofilm, which are known as quorum sensing. This is a process where chemical and peptide signals in high concentrations, known as auto inducers, are used to stimulate genetic expression of both mechanical and enzymatic processors of alginates, which forms a crucial part of the extracellular matrix [9].

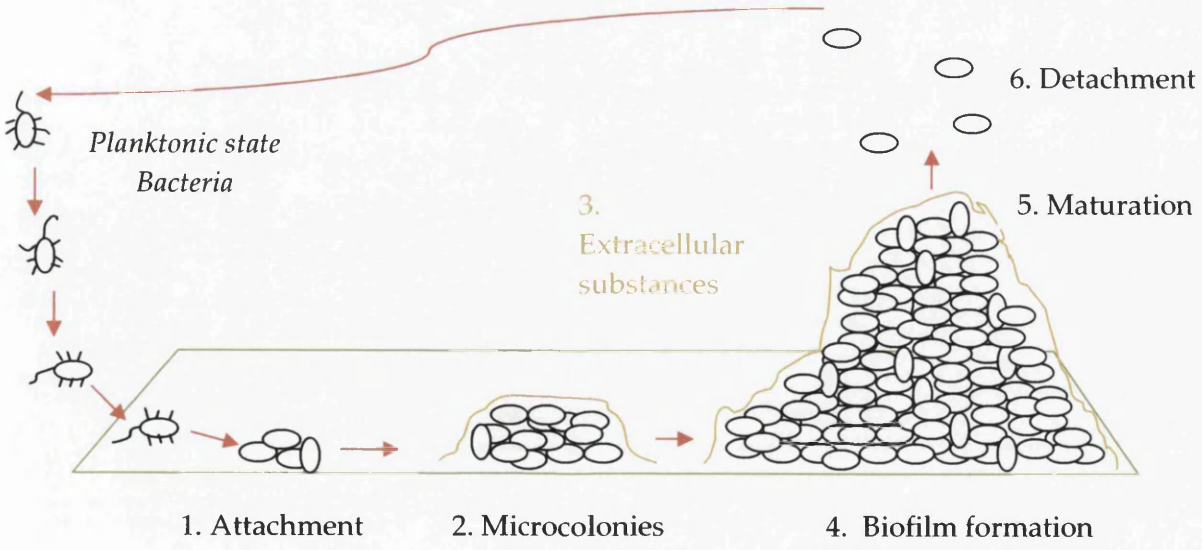


Figure 1.1 Steps involved in bacterial biofilm formation

*Death biofilm phase*

In the death phase, enzymes produced by the biofilm community start to breakdown polysaccharides, which in turn breaks down the structure of the biofilm, allowing the release of surface bacteria. At this stage, the flagella proteins are up regulated for bacterial motility, allowing the bacteria to attach to new surfaces. The bacteria are then available for the colonisation of new surfaces, where the process of biofilm formations will occur again [9].

## 1.3 Forces acting during bacterial adhesion

The mechanism of bacterial adhesion to a surface, such as a membrane, and biofilm development is facilitated and guided by cell-surface force interactions, as was mentioned in section 1.2.3. These interactions are influenced by the ionic strength and pH of the surrounding medium, age of the culture and also by the bacterial cell surface and bacterial surface charge [18]. The bacterial cell surface is involved in such processes as shape maintenance, growth and division and turgor support. Surface charge of microbial cells can influence cell adhesion, aggregation phenomena and cell-ion interactions [16, 19]. Most microorganisms tend to possess a negative surface charge under physiological conditions, which is due to the presence of anionic surface groups, however the charge magnitude can vary between species [10]. Within an aqueous environment of a certain pH, the ultrastructural components of the bacterial surface, such as carboxylate, phosphate and amino groups, are ionized and this creates an electrostatic charge at the cell boundary [16]. A charged bacterial cell in solution is surrounded by various charged ion layers, which results from competition between counter ion neutralization and molecular motion. The various layers are known collectively as the electric double layer and these layers are shown in Figure 1.2. The inner region where a layer of ions are immediately bound to the surface is referred to as the Stern layer, which is an equally but oppositely charged region of counter ions which have built up to balance the surface charge of the bacteria [20]. Outside of the Stern layer is the diffuse layer which consists of a more diffuse distribution of anions and cations determined by the balance of electrostatic forces and random thermal motion. As the distance is increased from the surface asymptotically the ion concentration reaches that of the bulk aqueous environment [21].

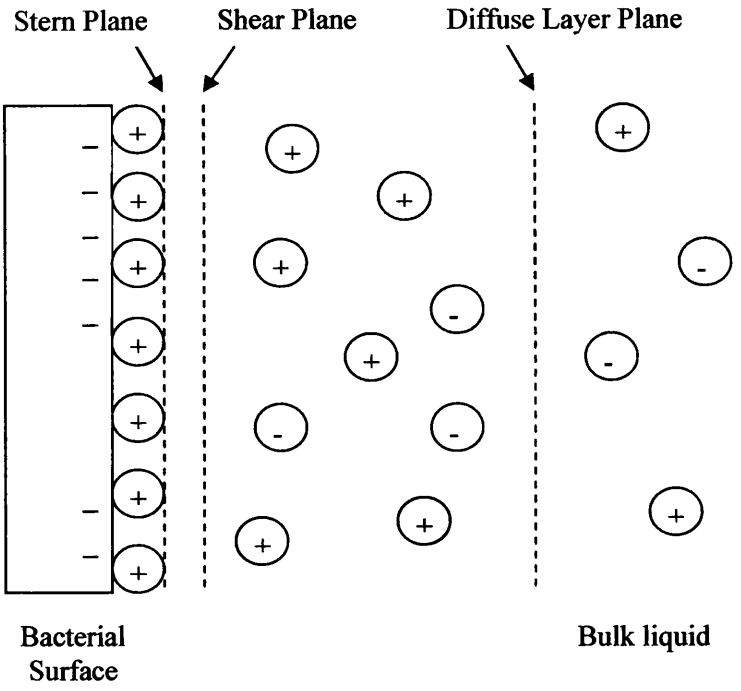


*Figure (a)*

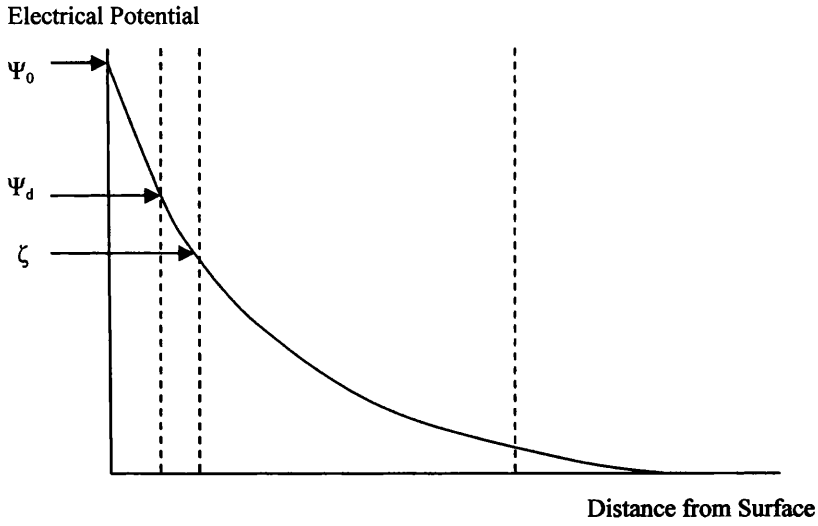


*Figure (b)*

Figure. 1.2 (a) The electric double layer surrounding a bacterial cell. Circles denote ions within the electric double layer and display charge distribution as a function of distance from the bacterial surface. (b) Electrical potential is shown as a function of distance from the bacterial surface, where $\Psi_o$ is the surface potential, $\Psi_d$ is the potential at the stern plane and $\zeta$ is known as the zeta potential.

Bacterial surface charge can be characterized by the zeta potential, which is defined as the electrical potential of the interfacial region between the bacterial surface and the aqueous environment [16]. Zeta potential is measured at the shear plane which is

defined as the distance from the bacterial cell surface, in solution, where the electrolyte ions are not bound to the surface and are not moving as a unit with the bacterial cell [16]. The zeta potential is deduced from the electrophorectic mobility measurements from within an electric field. Through the use of the Smoluchowski model, which is generally used for large particles, the zeta potential is calculated from the electrophoretic mobility.

The Debye length is the characteristic length of the diffuse ion region near the surface and can be given by the inverse Debye length, κ:

$$\kappa = \sqrt{\frac{e^2 \sum_i^N c_{bulk,i} z_i^2}{\varepsilon \varepsilon_0 kT}} \tag{1.1}$$

where e is the electronic charge, z is the valence, c is the concentration of the various ionic species denoted by i, ε is the dielectric constant of the solution, $\varepsilon_0$ is the permittivity of free space, k is the Boltzmann constant and T is the absolute temperature [20].

### 1.3.1 Classical DLVO Theory

Derjaguin, Landau, Verwey and Overbeek (DLVO) in 1941 developed a quantitative theory for the description of the stability of colloid particles within an aqueous solution. The DLVO theory explained that colloid stability is dependent on the balance between the two opposing forces of the attractive van der Waals force, and a repulsive electrostatic force known as the electric double-layer force. In the case of a spherical cell and a flat surface, the net interaction, $V_{TOT}$ between the objects can be described as a balance between two additive factors, $V_A$, resulting from attractive van der Waals interactions and $V_R$, resulting from the repulsive interactions when the electrical double layer of the cell and the surface overlap.

Therefore:

$$V_{TOT} = V_A + V_R \tag{1.2}$$

where $V_A$ is defined as:

$$V_A = -\frac{Ar}{6d} \tag{1.3}$$

A is defined as the Hamaker constant, r is the radius of the cell and d is the separation distance between the cell and the surface.

The repulsive electrical double layer, $V_R$, derives from the Coulomb interaction between charged particles. The range and strength of the double layer is determined by the presence of surrounding ions, as the repelling forces occur due to repulsive osmotic pressure between the ions of the overlapping electrical double layers between two surfaces in close proximity [21]. The repulsive electrical double layer can be related to the surface potential, $\Psi$, and the distance between the cell and the surface, d, incorporating the inverse Debye length, $\kappa$, via the expression:

$$V_R \propto \Psi^2 e^{-\kappa d} \tag{1.4}$$

Plots of Potential Energy as a function of separation distance are useful to account for the forces according to the DLVO theory which particles undergo when they approach each other.

The generalised potential energy curve in Figure 1.3 demonstrates that in the net potential energy curve, there can exist two potential energy minimums and one potential energy maximum, which is known as the energy barrier. For example, consider that two particles or surfaces are brought from infinite separation into approximately close distance, firstly the net potential energy falls to a secondary minimum. The secondary minimum implies that the particles will weakly attract each other. As the particles are brought even more closely together, the potential energy increases from negative to positive and a repulsive force is experienced between the two particles until the potential reaches the energy barrier. If the particles have sufficient energy to overcome the energy barrier, the attractive force begins to dominate the interaction between the particles, such that the potential energy falls to the primary energy minimum and the particles are strongly attracted to each other and in the case of particles coagulated, which is a stable condition for the aggregated particles [22].

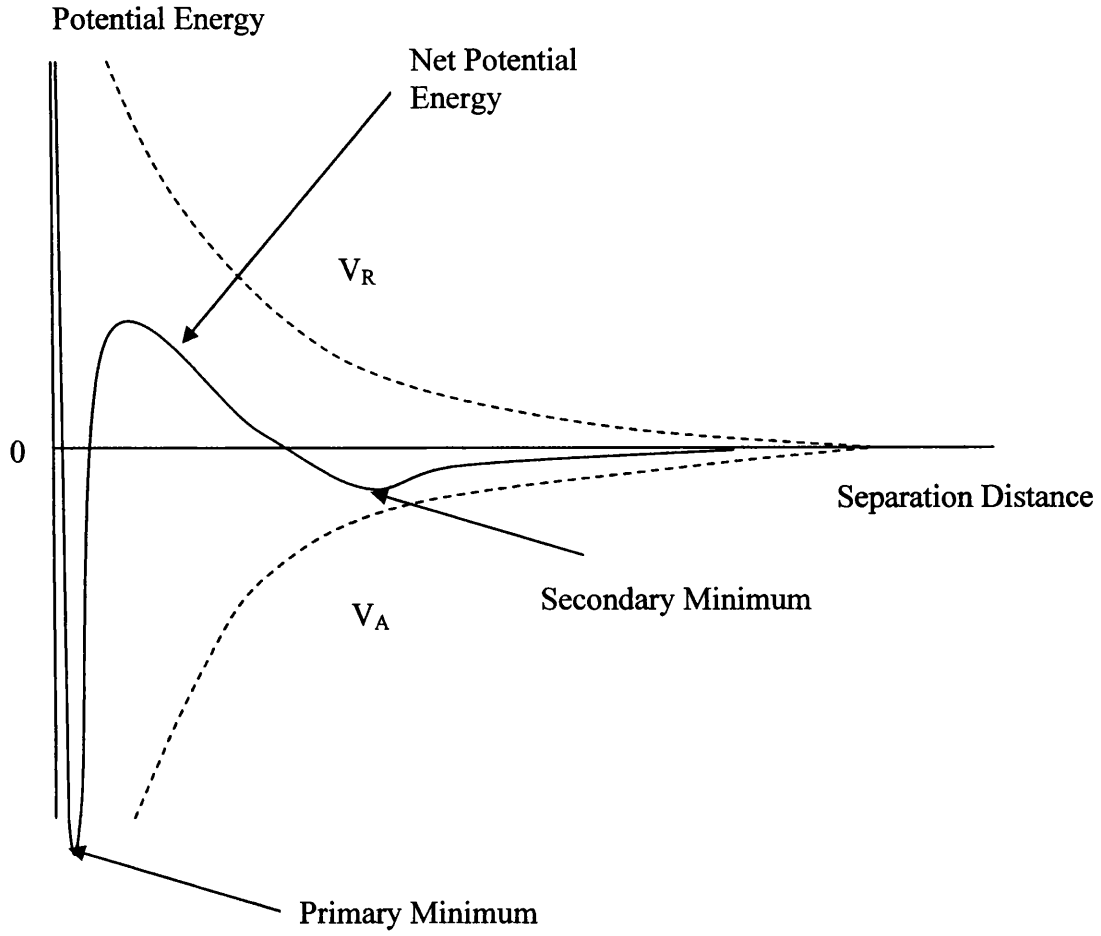


Figure. 1.3 Generalised plot of the Potential Energy as a function of Separation Distance according to the classical DLVO theory.

The forces experienced by particles or surfaces as they approach each other can be greatly affected by the electrolyte concentration and therefore the Potential Energy curve will alter as the electrolyte concentration changes.

The potential energy curves at various electrolyte concentrations is shown in Figure 1.4. In a dilute electrolyte concentration, the net potential energy experiences a primary minimum and a primary maximum and there exists very strong repulsion between charged particles or surfaces. This can lead to a stable colloidal dispersion. In an intermediate electrolyte solution, there may also be a secondary minimum, which could lead to either stable or unstable colloidal dispersions. The secondary minimum leads to a much weaker and potentially reversible adhesion between the particles or surfaces, where weak particle flocs may dissociate under an externally applied force. In a strong

electrolyte concentration, there is only a primary minimum and the interaction experienced by the particles or surfaces is purely attractive van der Waals forces, therefore the colloidal dispersions will coagulate or surfaces will attract each other at all separation distances.

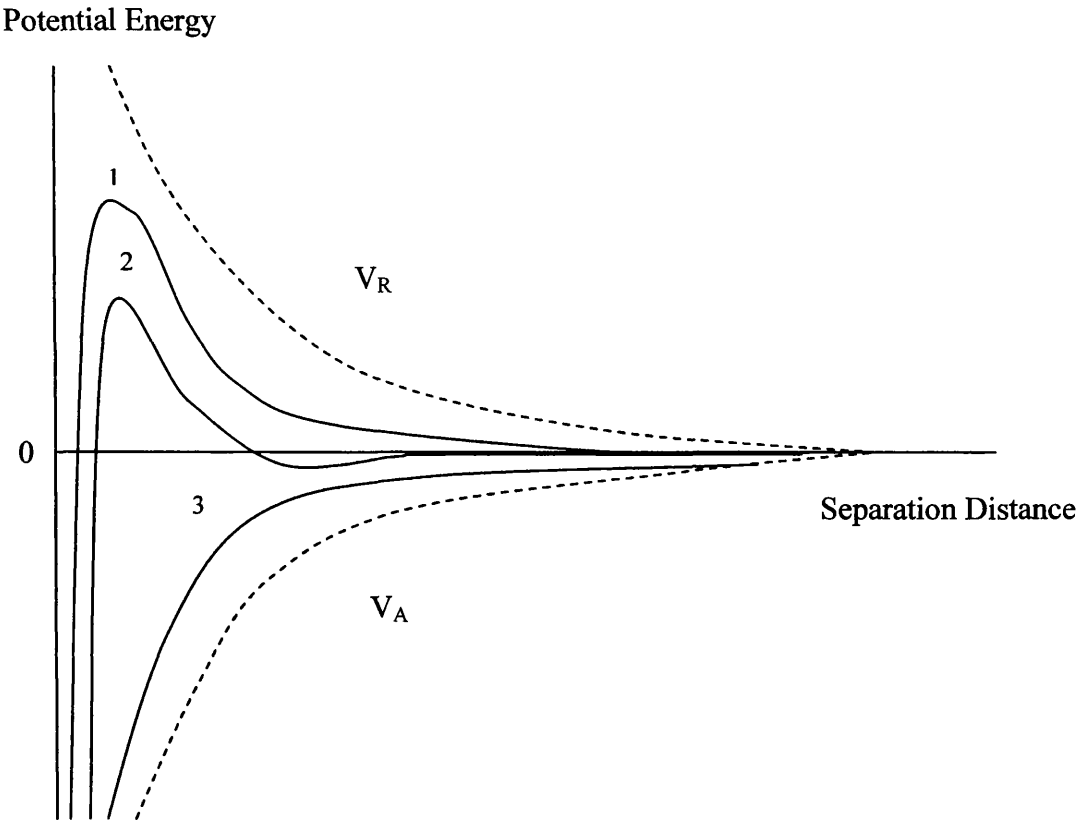


Figure 1.4. Plot of Potential Energy as a function of Separation Distance with various electrolyte concentrations according to the DLVO theory. Plot 1 represents a dilute electrolyte concentration. Plot 2 represents an intermediate electrolyte concentration. Plot 3 represents a strong electrolyte concentration.

Classical DLVO theory has been found to successfully describe long-range interaction forces within a number of systems, such as colloids and surfactant solutions. However once two surfaces or particles come into close contact with each other within a liquid environment , the DLVO theory fails to describe any short-range interaction forces which may be experienced by the surfaces [23]. This may be due to the fact that the van der Waals and electric double layer theories are both continuum theories which are described on the foundation of the solvents bulk properties, such as density and

dielectric constant, whereas the particles or surfaces involved in the interaction have individual characteristics, such as size and their surface chemistry, which are neglected by the classical DLVO theory. Also non-DLVO forces can take part in the interaction between two surfaces, where these forces can be larger in magnitude that van der Waals and electrical double layer forces at small separation distances [23].

### 1.3.2 Non-DLVO Interactions

Many interactions, such as hydrogen bonding, hydration pressure, non-charge transfer Lewis acid base interactions and steric interactions, which exist within environmental systems are not included within in the classical DLVO theory. Recently more cases have been found where the DLVO theory does not sufficiently describe adhesion [24]. A few of these short-range interaction forces which can influence particle and surface adhesion are described in the following paragraphs.

**Hydrophobic Interactions**

Hydrophobic surfaces are non polar and do not have a hydrogen-bonding capacity, therefore are not compatible for bonding with water molecules. Water molecules when in bulk will be significantly structured due to hydrogen bonding, leading to quite large clusters of hydrogen-bonded water molecules forming and breaking down due to unsteady thermal energy, however the water molecules orientation when in contact with a hydrophobic surface is entropically unfavourable. The entropically unfavoured water molecules are expelled into the bulk solution and the total free energy of the system is reduced accordingly. When two hydrophobic surfaces are within close proximity to each other, an attractive force between the hydrophobic surfaces might form due to the trapped water molecules in between the surfaces migrating from the gap to the bulk water where there is unrestricted hydrogen-bonding opportunities. Therefore hydrophobic environmental colloids have a tendency to aggregate in water [23].

**Hydrophilic Interactions**

Hydrophilic interactions occur with particles or surfaces that are mostly polar and have a high hydrogen-bonding capacity with water. Hydrophilic molecules have a strong

affinity with water, therefore tending to dissolve in, mix with or be wetted by water. These forces are associated with aggregation and stabilisation and therefore are important in colloidal systems [25].

***Steric Forces***

Molecules attached to solid surfaces within a liquid environment will have chains with a degree of freedom, which will have a tendency to be suspended in the surrounding liquid where they remain thermally mobile. When two polymer-covered surfaces approach each other, the suspended polymer chains are confined and over-lap and it is the entropy of this confinement that results in a repulsive force. This repulsive force of the overlapping polymer chains is known as the steric repulsion force. Steric repulsion force is not only confined to polymeric molecules but also to layers of small molecules at a much shorter range. Steric interactions also can be attractive in some cases, when the polymer surface interaction is energetically favourable then the polymers will develop a strong attraction and the polymers chains can be built into a bridge between surfaces. There is no simple and comprehensive theory which can describe steric forces due to their complexity. The extent of the steric force between polymer coated surfaces depends on a number of factors, such as the quantity of polymer coating, whether the polymer is simply adsorbed from solution or irreversibly grafted onto the surfaces and also on the quality of the solvent [23, 24].

**Solvation Forces**

The liquid structure when close to a surface interface is ordered into layers different to the bulk solution. As two surfaces approach each other, layers of molecules are forced out of the closed gap. The geometric constraining effect of the approaching wall on the liquid molecules and attractive interactions between the surfaces and the liquid molecules tend to cause a solvation force between the surfaces. Solvation forces rely on both the chemical and physical properties of the surface, such as wettability, surface morphology and rigidity, and on the liquid properties. Hydration force is the solvation force when the system solvent considered is water [23].

### 1.3.3 Extended DLVO Theory

Van Oss proposed an extension of the DLVO theory, generally known as XDLVO theory, for the inclusion of hydrophobic/hydrophilic interactions and Brownian movement forces [26, 27]. This extension was introduced as the current DLVO theory neglected short-range interactions which participated in particle and surface adhesion. Therefore, the extended theory was needed for the description of more complex non-ideal systems which involved various force interactions. Researchers have confirmed the main features of the DLVO theory and extended it with further considerable modifications which include liquid structure, solvation and other forces [28].

### 1.3.4 DLVO theory in microbial adhesion

DLVO theory was first used to explain bacterial adhesion by Marshall *et al* who proposed that bacterial sorption to surfaces involved an initial reversible sorption step and that the effects of electrolyte concentration on this initial reversible phase could be explained by the DLVO theory [21, 29]. Since then the DLVO theory has been used as a qualitative model for the description of bacterial adhesion and also in some ways a quantitative model for the calculation of adhesion free energy changes involved in microbial adhesion. The XDLVO theory has been used as a way to include non-classical DLVO effects, such as hydrophobic/hydrophilic interactions, to better qualitatively predict bacterial adhesion however both DLVO theories still treat bacterial cells as inert particles without the complexities of biological activity and rough heterogeneous cell surfaces and therefore fail to completely describe bacterial adhesion. Also surface structures such as fimbriae, lipopolysacharides and flagella are believed to be involved in bacterial adhesion but are not included in the DLVO theories. Therefore a physico-chemical approach is unlikely to fully describe microbial adhesion but the theories provide a basis to explain bacterial adhesion in which biological components can be added at a later date [21].

## 1.4 Removal of biofilms from membrane surfaces

To prevent bacterial adhesion to membrane surfaces and subsequent biofilm formation water production plants utilising membrane technology normally use a combined cleaning strategy to tackle membrane fouling, by first weakening the biofilm matrix by use of chemical cleaning agents and then the removal of the biofilm by mechanical forces. Cleaning products developed for membranes have five categories of cleaning agents; alkalines, acids, metal chelating agents, surfactants and enzymes. Commercial cleaning solutions are normally mixtures of these components but the actual composition of commercial cleaners are often unknown. However continuous biocide application creates waste-water problems which can be costly for waste treatment and also the wastewater companies must comply with ever tightening environmental regulations [1]. Other cleaning strategies include some pre-treatment systems, such as biological filter systems. The pre-treatment systems are designed to reduce the nutrient and contaminant concentration, hence reduce the biofouling potential of the water, however there is research which suggests that these types of systems could introduce further biofouling capabilities, such as the introduction of new microbes and matter into the water stream [30]. Recent published literature suggests that further research work should be conducted for effective cleaning strategies that minimise the use of cleaning agents or for the development of a biocide-free antifouling process that optimises nutrient-limitation techniques [2]. Research groupings using bench scale equipment stimulating industrial filtration problems have investigated cleaning regimes. Weis [31] results showed that cleaning performance was strongly dependent upon the nature of the foulant whilst Bartlett *et al* [32] evaluated single, multistage and formulated cleaning regimes for ceramic microfiltration membranes, where the results demonstrate the existence of cleaning agents concentration and temperature optima. Therefore selection of an effective chemical cleaning solution depends on the mechanistic understanding of the foulant and the foulant-chemical agent interactions [33], so investigations into the mechanisms of fouling, foulant-membrane, foulant-foulant, foulant-cleaning agent interactions at molecular level need to be performed to obtain high process efficiency.

Membrane interactions and properties of the fouling layer are as a result of foulant characteristics, feedwater solution chemistry (pH, ionic strength, divalent cation

concentration), membrane properties (hydrophobicity, surface charge, roughness) and hydrodynamic conditions (permeate flux, cross-flow or dead-end filtration velocity) and therefore the interactions between the membrane, foulant and cleaning agents are normally specific to a particular membrane process. A few studies have addressed this issue through the use of a combination of experiments to elucidate membrane-foulant behaviour. Li *et al* [33] assessed the adhesion force between a carboxylate modified AFM colloid probe (used as a surrogate for humic acid which is an organic foulant) and a NF membrane. The interfacial force data was assessed alongside the NF membrane water flux measurements to elucidate the mechanisms of organic fouling and chemical cleaning. In this study, force measurements and bench-scale fouling/ chemical cleaning experiments were performed under various solution conditions of total ionic strength, divalent cation concentration and pH to obtain a greater understanding of the role of solution chemistry with membrane fouling. The study discovered that the cleaning efficiency of the membranes was highly dependent on solution pH and the concentration of chemical cleaning agent, which agrees with previous studies where it has been shown that the effectiveness of the chemical cleaning of membranes is dependent upon such factors as temperature, pH, contact time with cleaning solution, concentration of cleaning chemicals and membrane process operating conditions, such as cross-flow velocity and pressure [33]. Therefore more research which assesses the problem of membrane fouling as a combination of many factors and acknowledges that membrane fouling is specific to a particular membrane process is required to develop efficient cleaning agents.

The previous text demonstrates the real industrial problems that membrane bio-fouling poses to desalination plants. Therefore, various studies, techniques and instrumentation have been utilised to unravel the mechanisms involved in membrane bio-fouling. Techniques which are utilised for the current membrane bio-fouling study will now be explained.

## 1.5. Analysis of Microbial Diversity

The ability to quantify the number and species of microorganisms within a community is fundamental to the understanding of the structure and function of an ecosystem. Current research indicates that the 5,000 identified bacterial species is only a minor fraction of all existing bacterial species; therefore only a limited knowledge of the true microbial diversity of the Earth is currently known [34, 35].

Methods for the analysis of microbial diversity within an environment can be divided into two categories: culture dependent studies and culture independent studies [36]. In culture dependent methods, bacteria are isolated from samples and grown in culture medium. Microbial diversity within bacterial communities are usually determined by phenotypic characterization of isolated strains from a sample. Phenotypic methods can be used only on bacteria which can be isolated and cultivated however only less than 1% of bacteria in nature can be cultured with current standard laboratory culturing techniques. Therefore using the culture dependent method for microbial diversity analysis will lead to an incorrect understanding of bacterial communities as most bacteria present within samples will not have the ability to be cultured within a laboratory environment [34, 37].

Recently, the culture-independent molecular technique of analysing the microbial diversity based on the 16S rDNA sequences and the constructed gene libraries has started to be used by researchers, due to the fact that culture independent methods have the strong advantage of direct extraction of nucleic acids from an environmental sample. Culture-independent methods allows for the identification of a large proportion of microbes that are not readily cultured in the laboratory, giving a more accurate population and structural representation of the bacterial community [37].

The 16S rDNA sequence is a gene encoding small subunit ribosomal RNA which is relatively short at 1.5kb. This gene is a section of prokaryotic DNA that is common to all bacteria and archaea and has been highly conserved within bacteria over evolutionary time. The use of universal primers that recognize highly conservative loci as the 16S rDNA encoding gene within a bacterial sequence, allows for species-specific

sequences to be amplified using Polymerase Chain Reaction (PCR) by directly using the bacterial samples genomic DNA as a template. The PCR amplified fragment can then be cloned, resulting in a clone library, containing ribosomal sequences as inserts. The amplified sequences are then compared with a reference-sequence database to determine phylogenetic relationships. By sequencing individual inserts and comparing the obtained sequences with sequences present in databases, it is possible to identify and enumerate the bacterial species of the corresponding bacteria without their cultivation. Therefore the comparison of 16S rDNA sequences from bacteria and archaea is a powerful tool for deducing phylogenetic and evolutionary relationships [38, 39].

Variations of the 16S rDNA sequencing technique have been developed and are currently being used for microbial diversity analysis. Other molecular biological techniques include Denaturing Gel Electrophoresis (DGGE), Restriction Fragment Length Polymorphism (RFLP) have been used in conjunction with molecular techniques to fully analyse the microbial samples, such as the analysis of PCR amplified 16S rDNA sequences and their digestion with restriction endonucleases to obtain RFLP of whole 16S rDNA amplicons [40, 41]. The combination of such molecular biology techniques allows for a more definitive assessment of bacterial diversity and therefore aid in gaining a greater understanding of bacterial populations within their natural environment [40, 41].

Currently there are very limited studies concerning culture independent methods for the analysis of microbial diversity within water treatment membrane processes, especially within the membrane biofilm fouling layers. The few key studies that exist relating to the analysis of the microbial diversity within membrane processes have been performed relatively recently. Bereschenko *et al* [42] used a PCR-DGGE approach combined with analysis of constructed clone libraries, to reveal the differences between the bacterial community within various compartments of a full scale RO water purification plant: RO feed water, wall of UltraFiltration (UF) storage tank, cartridge filter, a biofouled RO membrane, RO product water. In another study, Chen *et al* [43] examined microbial communities of membrane biofilms obtained from UF and RO membranes used in two full-scale water purification processes. Therefore, the identification of the microbial

community within the biofilm fouling layer developed on desalination membranes can lead to conclusions on the dominant bacterial species responsible for membrane bio-fouling and therefore aid in developing strategies to prevent the bacterial adhesion to the membrane surface.

### 1.5.1. Microbial Diversity Analysis using the Culture-Independent technique of 16S rDNA sequencing

The culture-independent technique of 16S rDNA sequencing requires many steps for the identification of bacterial species from genomic DNA [39, 40]. The first step requires that genomic DNA be isolated from a bacterial environmental sample and then purified. PCR technique is then used for amplification of 16S rDNA genes from the genomic DNA sample, where DNA Gel Electrophoresis is then performed to ensure the correct DNA sequence has been amplified. Once the PCR products are purified, the PCR products can be inserted into plasmid vectors, which are then transformed into *Escherichia coli.* The *E.coli* is grown to determine which vectors have been successfully inserted by the PCR product. Colony PCR is then performed on the DNA from the successful colonies of *E.coli* and the results from the PCR are sent away to an outside company to obtain the sequence data of the bacteria present in the Colony PCR product. The sequence data are then analysed to compare the nucleotide sequences to sequence databases through the use of a computer program, which calculates the statistical significance of matches. This process allows the identification of the individual bacteria present within an environmental sample.

The methods used in the process described for microbial diversity analysis are explained in general terms within the following paragraphs.

**Total Genomic Bacterial DNA Extraction**

Genomic DNA can be extracted from a fouled membrane surface by using a sterilised blade to scrap the fouling layer from the surface into a buffer solution. The foulant/buffer solution can then be centrifuged for the achievement of a foulant layer pellet [40].

### Beading Beating Method

Bead beating method is commonly utilised for the release of DNA from cells for genomic studies. Small beads either made from zirconia, silica or glass of a typical size between 0.1mm – 2.5mm are placed with the sample material in a tube and then mechanically shaken to release the DNA by breaking up the structure of the cells. The disruptive effect can be varied according to density of the beads, speed setting and size [40].

### Phenol-Chloroform Method

The Phenol-Chloroform Method is a liquid-liquid extraction technique which is used for isolating DNA. Equal volumes of a phenol:chloroform mixture and an aqueous sample are mixed to form a biphase mixture. The mixture is then vigorously vortexed and then centrifuged to introduce phase separation, where the DNA is concentrated in the upper layer. The upper layer is then carefully removed to a new tube and ethanol is added, where the mixture is vortexed and centrifuged again. This allows phase separation so that the DNA is concentrated by ethanol precipitation [40].

## Purification of DNA Product

The Genomic DNA can be purified by a DNA purification Kit (Gene All PCR DNA Purification Kit by Gene All Biotechnology Co. Ltd) according to the manufacturer's instruction. The Kit provides a simple and rapid method to purify DNA through the use of silica membranes to which the DNA binds to under high salt concentrations and any impurities pass through the membrane into a collection tube. The membranes are washed with an ethanol-containing buffer to remove any traces of proteins, salts and other enzymatic reaction components. The last step involves pure DNA being released from the membrane into a clean collection tube through using water or low ionic strength buffer. The DNA can be used directly for sequencing, cloning and other routine applications without further manipulations.

## PCR for Amplification of Nearly Complete Bacteria 16S rDNA

PCR is a revolutionary technique which was first developed by Kary Mullis in the 1980's and has since been widely used in such research areas as molecular biology, microbiology genetics and environmental science research. Mark R Hughes who is the

deputy director of the National Center for Human Genome Research at the National Institutes of Health stated that 'PCR is the most important new scientific technology to come along in the last hundred years.' PCR capitalizes on the natural function of enzymes, known as polymerases, to copy genetic material. PCR enables DNA polymerase to synthesis new strands of DNA complementary to the given template strand, where the technique can rapidly amplify (replicate many times) a single DNA molecule into many billions of molecules. For the PCR process, a DNA template strand which is the DNA or RNA strand needed for amplification, two primer molecules and DNA polymerase are required. DNA consists of double-stranded nucleotide chains which are formed into a helix shape. Primers are single-stranded short chains of four different nucleotides. The primers nucleotides are in a specific order that will bind to a specific complementary sequence of nucleotides in a piece of single-stranded DNA or RNA, under specific conditions. Through this method almost complete 16S rDNA gene fragments can be amplified from the genomic DNA sample as the universal primers recognize the highly conservative loci as the 16S rDNA encoding gene within the bacterial DNA sequence. The 16S rDNA sequence is a gene encoding small subunit ribosomal RNA which is relatively short at 1.5kb. This gene is a section of prokaryotic DNA that is common to all bacteria and archaea and has been highly conserved within bacteria over evolutionary time. Therefore the amplication of the 16S rDNA sequence allows for species-specific sequences to be amplified using PCR [39].

There are three essential stages within the PCR process. The first stage requires that the DNA template be denatured (helix strands must be unwound and separated forming two single-stranded DNA chains) by heating to 94-96°C. The next stage is the annealing stage, where the temperature is lowered to 50-65°C to allow the primers bind to their complementary nucleotide bases on the single-stranded DNA. The primers are designed to bracket the DNA region to be amplified. The third stage is the synthesis by a polymerase. The temperature is raised to 72°C and the polymerase starts from the primers and then extends to read the template strand and matches the strand with complementary nucleotides, resulting into two double-stranded DNA sections, where each DNA is composed from one of the original strands and its newly assembled complementary strand [39].

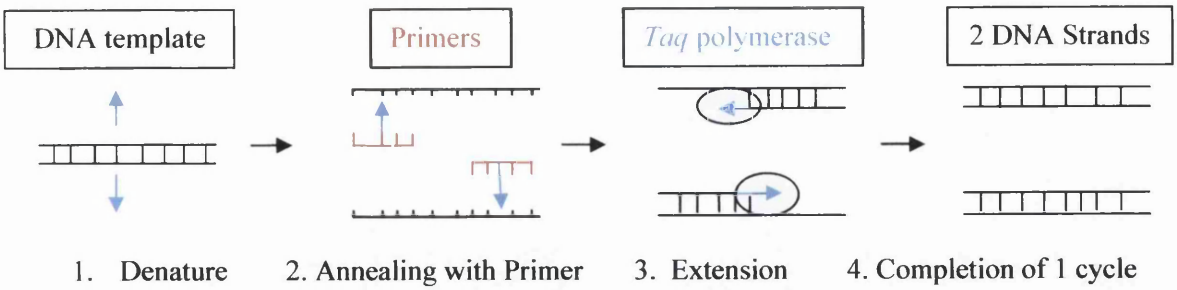


Figure 1.5 Principle of PCR

For the achievement of amplification of the DNA strand, the process needs to be repeated again by denaturing the two newly made double-stranded DNA sections and through the cycles of rapid heating and cooling, the amount of DNA strands present after the process will double in number, therefore after a number of cycles the original DNA template is exponentially amplified, resulting in the production of millions of copies of a specific DNA strand.

However there are some issues which can present themselves within PCR. Contamination of a sample with genetic material could lead to the amplification of unwanted DNA strands, therefore leading to incorrect results.

Automation of the PCR technique through instrumentation has lead to the technique's widely spread usage. The use of *Taq* polymerase is key in the technique's automation. *Taq* polymerase is isolated from *Thermus aquaticus* bacterium which is found in hot springs and was chosen for PCR as the bacterium is stable at high and rapidly fluctuating temperatures [40].

**DNA Gel Electrophoresis**

DNA Gel Electrophoresis is performed using a gel made from agarose placed in an electrophoresis tank filled with a buffer, where a DNA sample is placed into wells located in the top of the gel. An electrical field is applied across the tank via a power supply which causes the DNA to migrate down the gel at a rate determined by their mass. This technique is used as a check once PCR has been performed to ensure the correct DNA sequence has been amplified, through detecting a prominent DNA band in

the gel at 1.4-1.5kb (one kilobase is equal to 1000 bases). The number of Kilobases is determined from a 'DNA ladder' which features fragments of DNA of known size and is used as a reference to indicate the size of the DNA fragment in the PCR product [39].

### Ligation into pGEM-T Easy Vector

Once the PCR products are purified, the PCR product can be inserted into a plasmid vector, which in this case is a commercial vector called pGEM-T Easy vector. Plasmids are generally circular and must be cut or restricted to make space for the PCR product to be inserted. With the pGEM-T Easy Vector system, the plasmids are pre-cut (linearised) and contain overlapping thymines. *Taq* polymerase used during the PCR amplification inserts overlapping adenines on the 3' ends of the DNA, therefore the PCR products will slot into the space in the plasmid. Once treatment with DNA ligase is performed, the DNA insert covalently binds into the vector [39].

### Transformation into the *E.coli*

The term transformation is used to describe the genetic alteration of a cell determination by the uptake and expression of foreign DNA, irrespective of the mechanism involved. Plasmid vectors containing the DNA insert can be used to transform *E.coli* bacteria, by using the bacteria as plasmid 'factories' to produce large amounts of the DNA insert plasmid vector. A method of Heat Shock is used to encourage the bacteria to take up the plasmids. This is where the bacterial cells are chilled and then rapidly heated to around $45^0$C, where the temperature change creates pores in the membrane through which the plasmids can enter. Commercial Competent cells – *E.coli* are used in this step as they have been treated to ensure maximum efficiency in transformation.

The plasmid vector used contains a gene which offers resistance to the antibiotic Ampicillin. Therefore by growing *E.coli* which contains the plasmid vector in the presence of Ampicillin, only the *E.coli* should grow and not any bacterial contamination. Sometimes the plasmid vector closes the gap without the DNA insert, therefore to check that the correct colonies are selected for colony PCR, a differentiation method is employed. The pGEM-T Easy Vector contains a gene for an enzyme called β-galactosidase, which when expresses, acts on the compound X-Gal to produce a blue colour compound. The sequence for the enzyme is based on either side

of the insertion site in the plasmid vector. Therefore if the plasmid vector closes without the DNA insert the sequence for the β-galactosidase is complete and the colonies will produce a blue colour when grown in the presence of X-Gal. When the DNA insert is present in the vector then the β-galactosidase gene remains uncompleted and the colonies produce no colour when they are grown [39].

### Nanodrop 1000 spectrophotometer (Thermo Scientific)

The Nanodrop spectrophotometer enables highly accurate UV/Vis analyses of 1µl sample. The sample retention system eliminates the need for curvettes and capillaries which decreases measurement cycle time. Also the high absorbance capability eliminates the need for most dilutions. The instrument can measure nucleic acid samples up to 2-3700ng/ µl without dilution. The instrument automatically detects high concentration and utilises the 0.2mm pathlength to calculate the absorbance of the sample.

### Sequencing Analysis

Mega 4 is a software tool which aids in the analysis of DNA nucleotide sequence data from a wide range of organisms, as it contains fast computational algorithms and useful statistical methods. Through the input of primer sequences, the program locates the primers in the DNA sequence. Once the primers are found, the target gene is located and the sequence within the data which belong to the *E.coli* vector can be deleted from the overall DNA sequence, leaving only the species-specific sequence isolated from the genomic DNA.

The DNA sequences originally from the bacterial genomic DNA taken from the surface of the membrane can be then be put into National Center for Biotechnology Information (NCBI) website using the Blast tool which stands for Basic Local Alignment Search Tool. The program compares nucleotide sequences to sequence databases and calculates the statistical significance of matches. This allows the identification of the individual bacteria.

## 1.6 Atomic Force Microscopy

The Atomic Force Microscopy (AFM) was invented in 1986 [44] and is recently beginning to be recognised in both the biology, microbiology and surface science world as a powerful analytical tool, due to its enhanced capabilities over other microscopical techniques. The AFM can be used to give high resolution nanometer scale images of the topography of a range of surfaces with little surface preparation and no surface coating and one of the instrument advantages is that it can also study surfaces in different gaseous and aqueous environments. The AFM's main capability is that it can simultaneously provide information on local surface properties and interaction forces. Therefore AFM is a versatile instrument as it not only images the topography of surfaces at high resolution but also allows the measurement of force between an AFM tip and a sample as a function of displacement, so to obtain information on local surface properties and interaction forces. The force data is presented in the form of a force-distance curve, which can provide valuable information on local material properties such as elasticity, hardness, adhesion and surface charge densities. Due to the vast amount of information that can be gained, force measurements have become vital in different fields of research such as microbiology, surface science and materials engineering [38, 45, 46].

### 1.6.1 AFM Operation

A sharp tip is located at the free end of a cantilever, which is systematically scanned across a surface to generate a topographical image. As the tip tracks the surface, the forces between the tip and the surface, such as van der Waals, capillary and electrostatic forces, cause the cantilever to bend. The bending or deflection of the cantilever is measured by an optical lever system, which in most cases is a laser beam reflected off the back of a cantilever onto a position sensitive photodiode (PSPD). The PSPD can measure changes in the position of the incident laser beam as small as 1 nm. The position of the laser on the PSPD activates a feedback loop which moves the AFM scanner to alter the tip-sample distance to achieve a constant deflection of the cantilever. Fine position control of the tip-distance sample is achieved through the

extension and retraction of a piezoelectric ceramic within the scanner. Piezoelectric ceramics are materials that exhibit a change of shape when a voltage is applied across them, therefore allowing high precision sub nanometre positioning of the scanner in the x, y and z directions. It is the scanners movement that is used to generate an accurate topographical image of the sample surface [47]. However in some newer scanner configurations, the tip is mounted on a vertical piezoelectric scanner while the scanned sample in the x and y directions utilise another piezoelectric block.

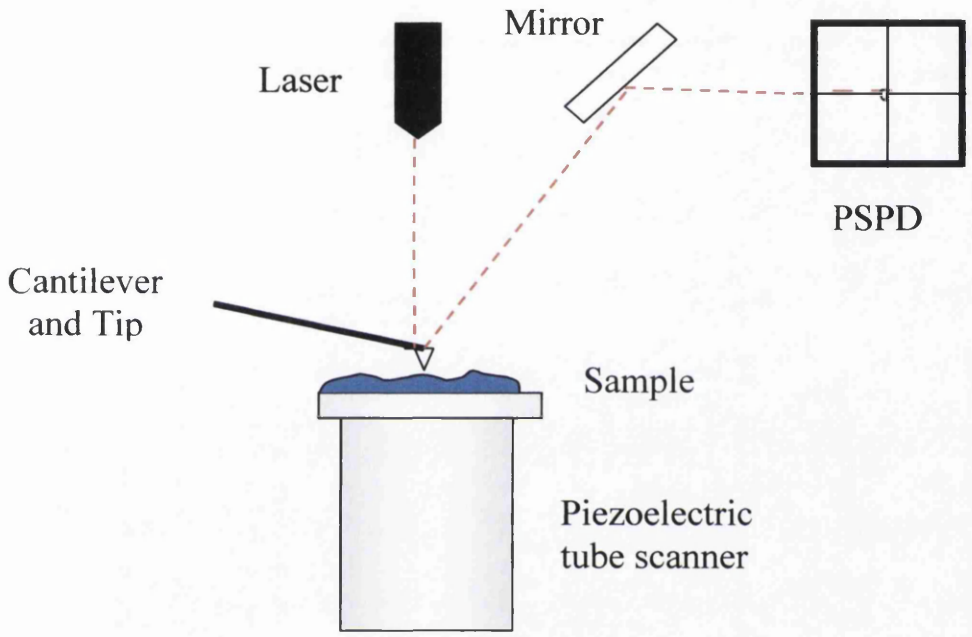


Figure 1.6. Diagram of the basis operation of an AFM.

**AFM modes of operation**

There are three commonly used AFM modes: Contact, Non-contact and Intermittent contact/ Tapping. Each mode is carefully selected according to the material properties of the sample.

*Contact Mode*

The Contact AFM operating mode is where the tip scans the sample in physical contact with the surface. Physical contact is defined as the repulsive force experienced by the atoms at the apex of the tip as the tip approaches the atoms of the sample surface, due to the tip and surfaces electron clouds interacting. One variance of contact mode uses a

constant force so that as the cantilever scans the surface, the feed-back loop operates to maintain a constant deflection of the cantilever so it is the sample height that is adjusted. Another variance of contact mode is constant height mode where the cantilever deflection is directly recorded as the sample is being scanned horizontally, so that constant height of the tip above the surface is maintained. However, a disadvantage of this mode is that it is limited to extremely flat samples as if the sample is rough the tip may crash into peaks on the surface or lose resolution as it passes over valleys [45, 47, 48].

*Non-Contact Mode*

The non-contact AFM operating mode allows the imaging of samples without bringing the tip into contact with the surface. The cantilever is vibrated by an AC driving oscillation and the vibrational parameters, such as amplitude, phase and resonant frequency, are monitored as the tip is brought into proximity with the surface, typically tens of nanometres above the surface. As the tip is scanned over an area, a feed-back loop operates to maintain constant vibrational amplitude as the surface forces change and effect the vibration of the cantilever. This feed-back signal is then used to generate a topographical image of the surface. Non-contact mode can prevent contamination of the tip or damage to the soft or delicate sample surfaces, however this mode will compromise image resolution that can be achieved from images achieved in contact mode [47].

*Intermittent/ Tapping Mode*

The tapping AFM operating mode is a hybrid of non-contact and contact modes. A cantilever is held above the surface and is oscillated at or near the cantilever resonant frequency so that the tip intermittently comes into contact with the surface as it is being scanned. The cantilever's oscillation amplitude changes with sample topography so the topographical image is obtained by monitoring these changes. Currently, tapping mode is commonly used for imaging of soft or biological samples as the intermittent contact reduces the lateral force incident on the soft sample which can reduce surface damage and tip contamination but still provide high quality image resolution [47, 48].

**Imaging**

Topographical imaging is the most widely used form of AFM imaging, where some AFM programs even produce useful presentational 3D images of the sample surface. However there are a few modes of imaging which can extract more information about the sample surface through AFM tip scanning.

*Phase Imaging*

Phase Imaging is a variant of tapping mode AFM imaging which provides nanometer-scale information about surface structure and properties beyond what simple topographical imaging can provide. Applications can include the detection of variations in composition, surface adhesion, friction, viscoelasticity, and numerous other properties of surfaces and also phase imaging can be used for visualisation of soft or adhesive samples [49]. Phase imaging is carried out through the cantilever being excited into resonance oscillation with a piezoelectric driver and this oscillation amplitude is then used as a feedback signal to measure topographic variations of the sample, as in tapping mode. However to produce the phase image, the phase lag of the cantilever oscillation, relative to the signal sent to the cantilevers piezo driver, is simultaneously monitored with topography data. The phase lag is very sensitive to variations in material properties. Both the topographical and phase images are obtained at the same time and can be used as an enhancement technique as the phase imaging can provide clearer observation of fine features which can be obscured by rough topography and is not affected by large-scale height differences [50].

*Amplitude Imaging*

Amplitude imaging is a variant of tapping mode AFM imaging which can provide nanometer scale information about shape of surface features and on softer materials it can often depict subsurface features better than topographical imaging. The amplitude image is arranged from an error signal which is an input into the feedback system. The error signal is composed the difference between the measured cantilever's oscillation amplitude and a setpoint value, however the z-scale is meaningless in terms of samples structure.

**Cantilevers and Tips**

AFM cantilevers are commonly made from silicon or silicon nitride by microfabrication techniques and either has a rectangular or pyramidal structure [45]. However further developments has led to manufacturers producing silicon tips with a variety of properties that can be used for specific applications. Tips have been designed with a chemical or biological coating to encourage specific interaction between the tip and the surface, such as promotion of hydrophobic or hydrophilic interactions between the tip and samples, so that intermolecular force measurement, surface mapping and chemical sensing can be performed [51].

**Cantilever Spring Constants**

Cantilever suppliers normally deliver an approximate spring constant value with their product which has been calculated from the cantilever shape. However these quoted values are not very reliable, therefore to obtain a more accurate value of spring constant, it should be individually measured for each cantilever. A number of methods of measurement of cantilever spring constant exist, such as addition of small removable masses to the apex of the tip. Some AFM software allows the measurement of spring constants through using the thermal tuning method. The thermal tuning method relies on measuring thermal fluctuations in the deflection of the cantilever and using the equipartition theorem to relate these fluctuations to the spring constant. The reason that the measurement can be performed is that thermal energy, calculated from the absolute temperature, should be equal to the energy measured from the oscillation of cantilever spring. A added advantage of measuring the spring constant of the cantilever on the AFM is that the measurement takes account of the cantilever mounted at a 10 degree angle to the sample while AFM manufacturers measure the spring constant perpendicular to the cantilever [52].

**Limitations of AFM Imaging**

Although AFM technology has many advantages over other imaging techniques, there are some limitations and difficulties which have to be considered before a sample is studied. As the AFM is beginning to be more commonly used in various applications, the study of artifacts in AFM imaging is growing more important for high resolution accurate images to be achieved. An artifact tends to distort AFM images and

spectroscopy data through either the design of the microscope or through external factors especially when operating at the nanoscale [53]. A range of imaging artifacts have been detected, such as acoustic noise, electrical interferences, optical interferences and mechanical vibrations. Another common artifact occurs when shadowing or multiplication of small structures is seen on images. This is normally caused by multiple asperities on the tip apex, which can originate from contamination [45]. Velegol *et al* [54] when studying the bacteria *E. coli* observed artifactual lines in tapping mode images which were the result of the cell and pyramidal tip geometries. A study by A. Mendez-Vilas *et al* [53] has investigated optical interference by using a highly reflective surface of polished stainless steel plates and friction maps to uncover a set of regular waves on the images. These types of studies will improve the design, operation and results obtained from the AFM.

Another issue which will limit the resolution of a scanned image is the convolution of the tip and sample where the image will be a combination of the sample topography and the tip geometry. This convolution which is particularly evident in images where structures have a steep topography, where the height variations are in the range of the tips radius of curvature i.e. 10 to 50nm, leading to the sample interacting with the side of the tip. The convolution leads to the broadening of surface features due to the finite size of the AFM tip [45].

**Flattening**

Flattening is a powerful filter that may be used to remove image artifacts due to such issues as vertical (z) scanner drift, image bow or skips that may have resulted in a vertical offset between scan lines. Flattening modifies the image on a line-by-line basis, where it consists of removing the vertical offset between the scan lines by calculating a least-square fit polynomial for a scan line and subtracting the polynomial fit from the original scan line. Flattening can be performed by applying a $0^{th}$, $1^{st}$, $2^{nd}$ or $3^{rd}$ order polynomial fit to each scan line.

**Surface Roughness Measurements**

Surface roughness measurements can be performed over an AFM scanned image using the AFM software. The root mean square RMS ($R_q$) roughness is the standard deviation

of the z values within a given area and is calculated in the software through the use of the equation 1.5,

$$R_{rms} = \sqrt{\frac{\sum_{n=1}^{N}(z_n - \bar{z})^2}{N-1}} \qquad (1.5)$$

where $\bar{z}$ is the average of the z values within a given area, $z_n$ is the current value and N is the number of data points within a given area [48].

## 1.6.2 Force-distance Curves

AFM is a versatile instrument as it not only images the topography of surfaces at high resolution but also allows the measurement of force between an AFM tip and a sample as a function of displacement, so to obtain information on local surface properties and interaction forces. The force data is presented in the form of a force-distance curve, which can provide valuable information on local material properties such as elasticity, hardness, adhesion and surface charge densities. Due to the vast amount of information that can be gained, force measurements have become vital in different fields of research such as microbiology, surface science and materials engineering [38, 45, 46].

The force-distance curve enables the quantification of the variations of interaction forces as the AFM tip, attached to the cantilever, approaches the sample, makes contact and then retracts away from the sample, where the displacement is varied using the extension and retraction of a piezoelectric crystal. The small changes in the deflection of the cantilever are detected by a laser beam being reflected from the back of the cantilever onto a PSPD. For the conversion of deflection into a force value, the spring constant of the cantilever, the cantilever deflection sensitivity and the definition of the zero force need to be known for the calculation [46].

The force-distance curve can provide valuable information on a sample. When the tip-sample separation distance is large, the tip does not experience any force. As the tip approaches the surface, the cantilever may encounter repulsive forces from the surface which may cause the cantilever to bend upwards until it jumps into contact with the

surface, which is due to the attractive forces between the tip-sample exceeding the spring constant of the cantilever. This approach region in a force-distance curve can be used for the measurement of surface force, solvation, hydration and steric/bridging forces. The force is then increased in the contact region on the sample until the force reaches a specified limit, where data from the contact region could provide information on the elasticity of the sample. As the tip is retracted away from the surface, the adhesion of the surface to the tip can influence the movement of the tip to keep the tip in contact with the surface. At a certain distance, the tip overcomes the adhesion force and experiences adhesion 'pull-off' force. This region can be used to estimate the adhesion energy of solids or the binding forces between complementary biomolecules. From this point, the tip does not experience any force and moves to a large separation distance [45].

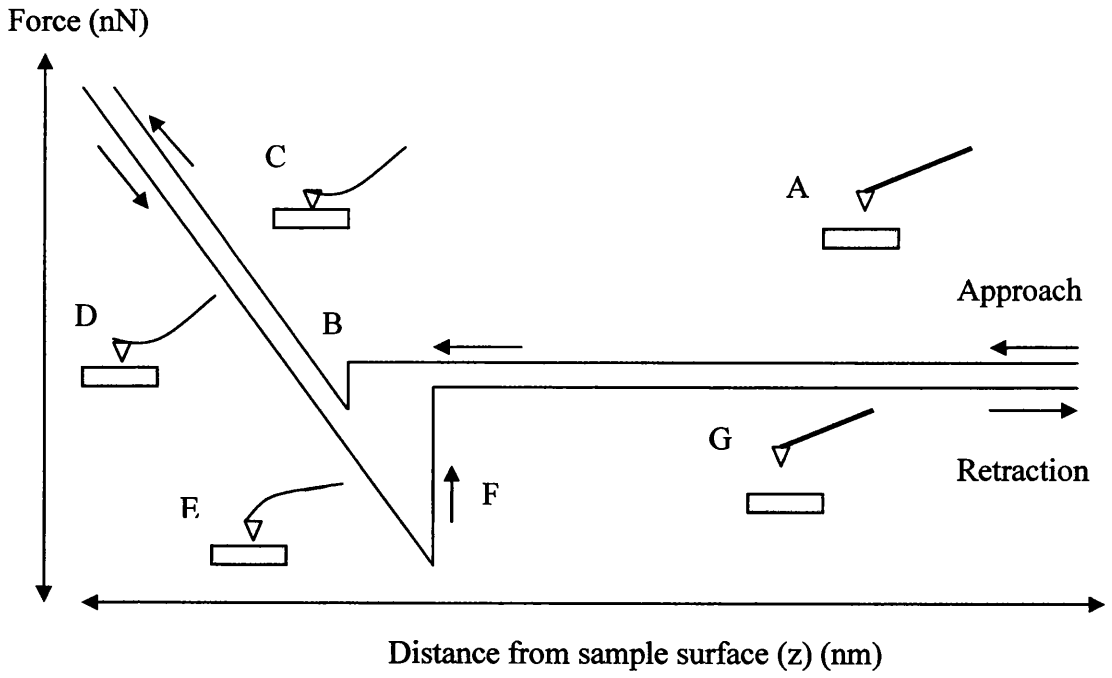


Figure 1.7 Explanation of a basic Force-Distance curve.

A – AFM tip is not in contact with the sample surface. B – Tip experiences a 'jump' into contact with the surface. C– Tip is pushed into the surface, which bends the cantilever, until specified force is reached. D – Tip is withdrawn from the sample surface. E – Tip adheres to the sample surface. F – Tip experiences a 'pull-off' from the surface. G – Tip is retracted away from the surface.

This form of force measurement has been shown to provide insight into the tip-bacteria interaction forces over the various sections of a bacterial cell surface and at various interfacial regions after preliminary formation of biofilms [38, 46, 54 ,55].

**Force measurements performed in different environmental conditions**

Force measurements can be performed in both gaseous and aqueous environments, however the environmental conditions in which the force measurements are made should be carefully chosen. In ambient air, most surfaces are covered by a fluid layer mostly composed of water. This layer is normally several nanometers thick and when an AFM tip approaches the surface, the tip will come into contact with this layer and a meniscus will form. The surface tension of the meniscus will pull the tip onto the surface, where this is known as the capillary force. Capillary forces can be eliminated by submersing the sample and tip into liquid, however some sample surfaces are less robust in liquid and samples such as bacteria and foulant layers present on the surfaces might float off into the liquid environment unless attached to the surface by such adhesives as poly-l-lysine.

### 1.6.3 Colloid Probe Method

Force distance measurements performed with an AFM using a sharp tip tend to suffer from the problem of a poorly defined geometry, which proves difficult for comparison with theory. Also comparison between various researchers work has proved difficult when using irregular shaped commercial tips. However, a technique has been developed which involves replacing the tip at the apex of the cantilever with a colloidal particle of a well defined shape and material composition [28, 56, 57, 58]. Force-distance measurements are then performed upon a surface to obtain measurements such as adhesion, where normalisation of the data based on the colloidal sphere radius allows for comparison between various researchers work. This technique has been coined by Ducker *et al* as the 'colloidal probe technique' [28]. This technique is relatively simple, reproducible and has been applied to a variety of materials and geometries, such as pharmaceutical particles, metal, metal oxides and cells. The colloid probe technique has been used regularly to elucidate the particle-surface interactions that occur within

process environments, where colloid probes are used to quantify adhesion of various materials, such as polymeric latex particles, biological cells and proteins to UF, RO NF membranes. These measurements can provide an assessment of the fouling potential of the membranes by elucidating the mechanical factors that affect membrane fouling without the need of process measurements [59, 60, 61]. The technique has become such a valuable technique for the study of surface interactions that a wide variety of subjects are being investigated. The colloid probe technique has been utilised to study of a wide range of interactions, such as force existing between *Aspergillus niger* to mica surfaces which is of interest to biotechnological industries [62]. Also Gypsum and cellulose colloid probes interactions have been measured for the understanding of the gypsum/cellulose bond within the cellulosic composite wallboard used in residential construction [63], and the direct measurement of interactions between stimulation-responsive nanogel particles as drug delivery vehicles and artificial mucin layers have been performed [64]. Therefore the colloid probe method has become a powerful technique for examination of surface interactions.

### 1.6.4 Indentation

An indentation experiment involves performing a force measurement on a sample, which will produce a force versus distance curve. The slope of the force curve already describes in a qualitative manner the elastic properties of the sample, however to obtain a numerical value for Young's modulus further processing of the force curve data is needed. Hooke's law describes that the applied loading force (F) and the deflection of the cantilever (d) can be related to the spring constant of the cantilever (k). Therefore Hooke's law can be written as:

$$F = kd \tag{1.6}$$

On a infinitely stiff sample compared to the cantilever stiffness, the deflection of the cantilever (d) will be identical to the movement of the piezo in the z direction (z), resulting in the slope of the cantilever deflection versus sample height equaling 1, where the sample height is known after the determination of contact point between the

tip-sample is made. The force curve measured on the hard sample can be used for the calibration of the PSPD sensitivity, allowing the force curve measured in raw units of volts obtained from the AFM to be converted into the cantilever vertical deflection in meters. However when a force measurement is performed on a soft sample, the cantilever tip will indent the sample, which will result in the cantilever deflection being smaller than the sample vertical displacement leading to the slope of cantilever deflection versus sample height curve being lower than 1 . Therefore the difference between the sample height (z) or the cantilever deflection obtained from a force curve performed on a hard surface and the cantilever deflection obtained from a force curve performed on a soft surface (d) will be equal to the indentation depth (δ) of the tip into the sample [65, 66, 67].

$$\delta = z - d \tag{1.7}$$

However using current AFM technology the data needs to be manually processed to obtain the correct values. The deflection of the cantilever when far from the sample surface may not be equal to zero which in part could be due to drift in the detection system and stresses in the cantilever. Therefore the deflection offset can be determined from the average cantilever deflection when the cantilever was far from the surface and then the deflection offset was subtracted from all the deflection values.

Also the contact point where the tip first comes into contact with the sample surface needs to be determined for the calculation of indentation depth into the sample. For the membrane sample there was no sudden jump into contact as seen with other samples quoted in the literature [66] and especially not seen with a colloid probe, therefore the contact point was defined as the height where the cantilever deflection begins to leave the horizontal axis on the deflection versus sample height curve.

Therefore once the deflection offset and contact point is determined, Hooke's law can be utilized for the determination of the loading force from the values of cantilever vertical deflection. This calculation allows for loading force versus indentation curves to be produced for the sample.

### 1.6.5 AFM used in Membrane Studies

AFM imaging technology has been utilised for the quantification of surface morphology, pore size distributions and surface roughness for various types of membranes, such as NF, RO and UF [59, 68, 69, 70]. These measurements are important for process operations as the pore size will determine the particles that will be able to pass through the membrane and also as the literature suggests that surface topography is a factor in fouling potential of filtration membranes. Membrane surfaces which are rough have a tendency to foul easier as the roughness increases the surface area, which in turn increases the number of contact points between foulants and the surface, influencing attachment of colloidal material and attachment of bacterial cells. Large protrusions from the filtration membrane surface can affect local flow fields and shield particles, such as bacterial cells, from detachment [69, 71]. Therefore determination of the surface morphology and surface roughness of membranes is crucial in the study of fouling in these systems.

Force measurements have also been performed on membranes for the direct quantification of membrane/tip and membrane/particle interactions through the measurement of adhesion force, in the hope of the elucidation of process behaviour [59, 60, 61, 68]. The colloid probe technique has been utilised to determine the membrane/particle interactions, as can be demonstrated by Bowen *et al* where force measurements were performed between polystyrene and silica colloids and polymeric UF and RO membranes [6, 68]. Even a protein bovine serum albumin (BSA) colloid probe and a yeast cell probe has been used to directly measure the adhesive force between the probes and two different polymeric membranes [60]. Nano-indentation techniques have also been employed to obtain micromechanical properties, such as elasticity, of membranes and polymeric materials, however there is extremely limited literature on the nano-indentation of commercially available membranes [72].

### 1.6.6 Atomic Force Microscope used in Microbiology

For more than three decades the ultrastructure of microbial surfaces have been studied using electron microscopy however direct information on native surfaces could not be obtained. Other techniques and instrumentation such as X-ray photoelectron spectroscopy, infrared spectroscopy, contact angle, electrophoretic mobility have been used to investigate the chemical composition and physicochemical properties of microbial surfaces, while surface force techniques such as the osmotic stress method, surface force apparatus and the micropipette technique have been used for the measurement of force at biological surfaces. Even though these methods have provided useful information about microbial surfaces, none of these methods can provide direct information with nanometer resolution of these surfaces [73].

Only recently has AFM been developed for a quantitative in-depth study of the molecular mechanisms used in microbial cell attachment [46, 66]. AFM technology has been used increasingly over the last couple of years to investigate microbial surfaces, as the technique offers three-dimensional images of the surface structure with molecular resolution, under physiological conditions whilst in real time and with little sample preparation [45]. AFM technology possesses the advantage of being able to study microorganisms *in situ*, unlike other techniques such as SEM. The AFM can be used to give high resolution images of the morphology of individual microbial cells and bacterial biofilms on solid surfaces, in both dried and hydrated states [12]. AFM imaging of biofilms has proved difficult due to the biofilms deformable nature, which often means that high resolution images are difficult to obtain. However, as the technology has developed to include various imaging modes, such as intermittent contact/tapping mode which greatly reduces the shear forces that could damage soft samples, and the number of studies into microbiological structure increase, more in-depth images are obtained. The AFM has also proven useful in measuring critical dimensions, such as cell size, surface roughness and cell/biofilm height [54]. The AFM has been used to study a wealth of microbial surfaces, such as bacterial cells [74], fungal spores [75], DNA [76] and viruses [77]. Force curves have also been measured from both various microbial cells and biofilms. *E. coli*, *Pseudomonas putida*, *Bacillus subtilis* and *Micrococcus luteus*, *Listeria monocytogenes* are examples of bacterial

biofilms which have been studied through AFM force measurements [74, 78, 79, 80]. Bacterial biofilm formation of *P. aeruginosa* on various materials, such as sheets of aluminum, steel, rubber, and polypropylene, have been investigated by measuring the adhesive properties of biofilm through AFM force measurements [81]. AFM force mapping (force volume) is also used in the study of bacterial biofilms [78, 82]. Force mapping conducts a two-dimensional array of force-distance measurements over a specified area to produce a map image of force variations across the surface. This technique has been used to determine the spatial distribution of adhesive forces between unsaturated fresh and desiccated biofilms of *P. putida* [78] and also the interaction force on a biofilm formed from sulphate-reducing bacteria (SRB) [82].

### 1.6.7 The theoretical framework of AFM mechanical measurements

AFM technology is able to measure micromechanical properties, such as elasticity, of samples through the analysis of the AFM force-distance curves. The determination of elastic deformations has become increasingly important over the last couple of years, especially for the characterization of soft materials, such as biological samples [83]. The force-distance curves are analysed through a chosen mechanical theory which considers the contact and indentation of two surfaces to obtain a value of Young's modulus (Appendix A). Currently there are a number of mechanical theories in use in the literature for the determination of elasticity, however the theory used should be carefully chosen to meet the assumptions of the system. However, it should be noted that when performing indentation experiments, certain characteristics of AFM can effect and introduce error into the determination of the elastic modulus, so researchers should take care when performing indentation experiments. The choice of cantilever spring constant and the tip's accurate calibration can be difficult to determine. As can the location of the contact point in the force curve, as uncertainty in the contact point can lead to significant errors in the estimation of the indentation depth and elastic modulus. Also the wide range of AFM tip shapes available and the small tip-sample contact area make the contact geometry difficult to define [84].

### 1.6.7.1 Hertz and Sneddon Model

Hertz in 1881 introduced a theory to describe the mechanics and stresses of contacting bodies [85]. The Hertzian-based models are commonly used for the determination of elastic modulus and have been demonstrated through experiments to be adequate for use in many applications. In the literature, several relationships for applied force vs. penetration depth for various indenter shapes have been published [84, 86, 87].

The Hertz model describes the simple case of elastic deformation of two perfectly homogeneous smooth bodies touching under load. Two important assumptions of the Hertz model are following: (i) the indenter must have a parabolic shape and (ii) the indented sample is assumed to be extremely thick in comparison to the indentation depth. The first assumption remains a valid one for the case when a spherical tip radius is much bigger than the indentation depth ($h < 0.3R$). As the Hertz model does not take account of tip-surface adhesion, some of the literature deems the use of the model appropriate only if adhesion forces are small or negligible [66].

The equation used to calculate the force on the cantilever F(h) by using the Hertz mechanisms is:

$$F(h) = \frac{4\sqrt{R}}{3} E^* h^{3/2} \tag{1.8}$$

where the tip is approximated by a sphere with the radius R and the depth of indentation is denoted by h. E*is known as the effective modulus of a tip-sample system and is calculated using the following equation:

$$\frac{1}{E^*} = \frac{1-\upsilon^2_{tip}}{E_{tip}} + \frac{1-\upsilon^2_{sample}}{E_{sample}} \tag{1.9}$$

$E_{tip}$, $\upsilon_{tip}$, $E_{sample}$ and $\upsilon_{sample}$ are the denotations for the Young's modulus and the Poisson ratio for the materials of the tip and sample. If the material of the tip is considerably harder than the sample then the following equation can be used:

$$E^* \approx \frac{E_{sample}}{1-\upsilon^2_{sample}} \tag{1.10}$$

Through the substitution of equation 1.10 into the Hertz equation and manipulation of the data from the force-distance curves, the Young's modulus of the sample can be determined.

The Sneddon's variation of the Hertz Model is used for the case of a cone shaped tip cantilever [86, 88],

$$F(h) = \frac{2}{\pi} \tan \alpha \frac{E_{sample}}{1-\upsilon^2_{sample}} h^2 \qquad (1.11)$$

where the half opening angle of the AFM tip is denoted by the symbol α.

### 1.6.7.2 Limitations of Hertzian Models

There are a number of inherent assumptions within Hertzian theories which are not fulfilled by many sample-tip systems.

The assumptions of the Hertz theory are:

- The sample returns to its original shape when the load is withdrawn, therefore demonstrating elastic behaviour.
- The sample is a large system with a flat surface (a half-space).
- The sample is linear and therefore obeys Hooke's Law, where doubling the stress doubles the strain.
- In the bulk sample, there is no preferred direction or point (isotropy and homogeneity).

One of the assumptions of the Hertzian theories is that the tip and sample are assumed to be continuous elastic media. In an ideally elastic material, the tip deforms the sample to a certain depth and the loading and unloading lines overlap in the contact region in a force curve. However, if the sample is plastically deformed, the force of the loading

curve causes the sample to undergo a deformation so that when the tip is withdrawn and the load is decreased, the sample does not regain its shape, whereas the penetration depth remains the same. However most samples have mixed behaviour, so the loading and unloading curves rarely overlap. Also at a large penetration depth, the force of the unloading curve is reduced from the force of the loading curve. The difference between the approach and the retraction contact lines is known as "loading–unloading hysteresis" [86].

When considering living cells, the Hertzian theories basic assumptions become even more invalid [89]. The Hertz theory neglects any adhesion forces acting between the tip and the sample. A considerable fraction of the cell under goes deformation during a force curve which implies that the half-space assumption is incorrect and that finite size is significant. The cells under load may not behave elastically and may show signs of viscoelasticity behavior. Cell structure is composed of regions which are harder than other areas, therefore the cells exhibit inhomogeneity and even anisotropy. Another assumption used in the calculation of the elastic modulus is that the Poisson's ratio is a constant value of 0.5 (the case of incompressible bodies), which is commonly used for cells. However, the Poisson's ratio may vary across the surface of the cell because of intercellular heterogeneities, so the difficulty occurs in that the Poisson's ratio is not measured in the indentation experiment. Therefore from the assumptions of the Hertz model, even though most of the literature focuses on the use of these models, research groups which utilise AFM force measurements on living cells should develop and progress to using more suitable models for their studies which will give more realistic values of elastic moduli.

### 1.6.7.3 JKR Method

In the 1960's, Roberts [90] and Kendall [91] found experimental contradictions to the Hertz model. Kendall and Roberts using both glass and rubber spheres demonstrated that at low loads the contact area between these bodies were larger than predicted by the Hertz model and that the contact area tended towards a constant finite value as the load was reduced to zero [90, 91]. Strong adhesion was observed between the spheres when

the surfaces of the spheres were clean and dry. Therefore these observations suggested that attractive surface forces were operating between the spheres which became of significant importance as the load was reduced towards zero. It is these attractive forces between solid bodies that require a mechanical load to separate the bodies when placed in intimate contact. This led to Johnson, Kendall and Roberts (JKR) [92] to develop an extension of the classical Hertz theory on the deformation of two elastic bodies in contact with one another to include the effect of interfacial energy work of adhesion [92]. The JKR theory can be utilised in the case of large tip radii indenting soft samples with a large adhesion. The adhesion force between the tip and the sample (the short range forces) are taken into account within the contact area and the influence of surfaces forces outside the contact area are neglected in the JKR model [38, 93].

**JKR Calculation**

The work of adhesion W is defined in terms of surface energies $\gamma$ as:

$$W = \gamma_1 + \gamma_2 - \gamma_{12} \tag{1.12}$$

where $\gamma_1$ and $\gamma_2$ are the surface energies of the two solid materials, 1 and 2, and $\gamma_{12}$ is the interfacial energy between the two solid materials.

The maximum adhesion force is given by the equation:

$$F_{ad} = \frac{3}{2}\pi R W \tag{1.13}$$

where $F_{ad}$ is the maximum adhesion force, W is the work of adhesion per unit of contact area and R is the radius of tip.

The calculation of the JKR method from the raw approach data is described below [94]:

$$E = \frac{9}{4}(1-\upsilon^2)RK\Delta_c\left[\frac{P_1}{3Rh}\right]^{3/2} \tag{1.14}$$

where

$$P_1 = (3P_2 - 1)\left[\tfrac{1}{9}(P_2 + 1)\right]^{1/3} \tag{1.15}$$

and

$$P_2 = \left(\frac{Z_{defl}}{\Delta_c} + 1\right)^{1/2} \tag{1.16}$$

E is the reduced Young's modulus of two materials, ν is the poisson ratio, K is the cantilever spring constant, h is the indentation depth, R is the tip radius, $\Delta_c$ is the Cantilever deflection at the point where the tip loses contact with the surface and $Z_{defl}$ is the measured vertical deflection of the cantilever.

### 1.6.7.4 DMT model

DMT theory is used for the case of a small tip indenting stiff samples with a small adhesion. The adhesion of the sample is taken account of outside the contact area but assumes that the surface forces do not modify the deformation from the Hertzian model. The DMT model does not apply to living cells or soft samples [38, 93].

### 1.6.7.5 Oliver-Pharr Model

Modelling indentation contact which includes plasticity involves the use of nonlinear constitutive equations and the use of a number of material parameters which must be included to describe material behaviour. Tabor and Stillwell studies [95, 96] demonstrated that elastic contact solutions exist for each different tip geometry, therefore by taking into account the shape of the perturbed surface after tip unloading, the effect of plasticity on the elastic unloading data can be determined. Oliver, Hutching and Pethica [97, 98] developed a simple method based on the notion that the material conforms to the shape of the indenter to some depth at peak load and if the depth can be determined from the load-displacement data, the projected area of contact can be estimated from shape function.

Doerner and Nix [99] studies assumed that during the initial stages of unloading, the area of contact remains constant and the behaviour is elastic. Therefore the contact area was evaluated by extrapolating the initial linear portion of the unloading curve to zero load, where the extrapolated depth with indenter slope was used to determine contact area. However, the Doerner- Nix assumption of linear unloading was determined to be flawed by load and displacement sensing indentation tests performed by Oliver-Pharr on a large number of materials [100]. It was found that unloading curves are rarely linear even in initial stages of unloading, and therefore could be better described by a power law instead. The Oliver-Pharr method takes account for the curvature in the unloading data and can be used for the determination of the tip indentation depth which can be used in conjunction with the indenter shape function to establish contact area [100, 101]. However, this method again assumes that the indented sample is elastic, isotropic and has negligible adhesion. As soft polymeric materials, cells and tissues often exhibit viscoelastic or time-dependent behavior and may experience adhesive interactions between the tip and the sample, the use of this model should be carefully monitored [102].

**Oliver – Pharr Calculation**

Oliver-Pharr theory states that the unloading data is well described by a simple power law relation [87]. The actual relationship used to describe unloading data for stiffness measurement is:

$$P = \alpha\left(h - h_f\right)^m \tag{1.17}$$

where P is the indenter load, h is the elastic displacement of the indenter, $h_f$ is the residual hardness impression after unloading, m is the material constant, where values for the exponent for some common punch geometries are m = 1 for flat cylinders, m= 1.5 for paraboloids of revolution, and $\alpha$ is the material constant.

The Oliver-Pharr method is a non-linear curve fit method so the constants $\alpha$, m, $h_f$ are all determined by a least squares fitting procedure where the equation can be fitted to the data in the unloading segment, to provide best fits estimates of these constants.

The initial unloading slope can then be found by analytically differentiating this expression with respect to displacement to produce:

$$S = \left.\frac{dP}{dh}\right|_{h=h_{\max}} = \alpha m\left(h_{\max} - h_f\right)^{m-1} \tag{1.18}$$

The derivative can be evaluated at the peak load and displacement to calculate the gradient, where S is the contact stiffness.

**Determination of Contact Area**

When a probe is pushed into the sample, the material deforms in the vicinity of contact. The three displacements which must be accounted are the Total penetration depth, h, Displacement of sample surface, $h_s$ and Contact depth, $h_c$. These displacements are related by:

$$h_c = h - h_s \tag{1.19}$$

From Sneddon's solution, the deflection of the sample surface is determined from:

$$h_s = \lambda\frac{P}{S} \tag{1.20}$$

For pyramidal, conical and spherical indenters, $\lambda = 0.75$, therefore the equation 1.19 becomes:

$$h_c = h - 0.75\frac{P}{S} \tag{1.21}$$

Once contact depth has been determined, it is possible to calculate contact area, where the function for contact area is dependent on the geometry of the probe.

The original Oliver-Pharr model was described for a Berkovich tip where the area of contact, $A_c$, is given by:

$$A_c = 24.56h_c^{\,2} + Ch_c \tag{1.22}$$

where C is a constant.

When indenting soft polymers and tissues, a spherical tip is commonly used to minimize plastic deformation and stress concentrations to avoid damaging the sample. Therefore equation area of a spherical cap to determine the area:

$$A = 2\pi rd \tag{1.23}$$

where A is the contact area, r is the radius of the tip and d is the maximum indentation of probe into cell taken from the force versus indentation curve.

Once the gradient is found then it can be input into the following equation to determine $E_r$:

$$S = \frac{dP}{dh} = \frac{2}{\sqrt{\pi}} E_r \sqrt{A} \tag{1.24}$$

where S is the contact stiffness, A is the contact area, $E_r$ is the relative elastic modulus and dP/dh is the gradient of force displacement data.

### 1.6.7.6 Field and Swain model

The Field and Swain method is another model which can be used for the determination of Young's modulus [103]. This method is similar to Oliver-Pharr method as it considers the unloading curve, however the Field-Swain method fits a single pair of data points (maximum load and some percentage unload data) to the Hertz equation, unlike the Oliver-Pharr where the method uses a series of data points and fits the slope of the initial unloading to the derivative of the Hertz equation. The advantage of this model over the Oliver-Pharr method is that the analysis is quicker and more convenient, however it may produce results which are more susceptible to errors in the data [102, 104].

# 1.7 Surface Charge Measurements

## 1.7.1 Zeta Potential Measurements of bacterial species

Bacterial attachment to such surfaces as membranes, are dictated by the cell-surface interactions. These interactions are influenced by the ionic strength and pH of the surrounding medium, age of the culture and also by the bacterial surface charge [18]. The surface charge of microbial cells can influence cell adhesion, aggregation phenomena and cell-ion interactions, where most microorganisms tend to possess a negative surface charge under physiological conditions [10, 19]. Bacterial surface charge can be characterized by the zeta potential, which is defined as the electrical potential of the interfacial region between the bacterial surface and the aqueous environment [16]. The zeta potential is deduced from the electrophoretic mobility measurements from within an electric field. Through the use of the Smoluchowski model, generally used for large particles, the zeta potential can be calculated from the electrophoretic mobility measurements.

The Smoluchowski equation is derived from Henry's equation, which is:

$$U_E = \frac{2\varepsilon_o \varepsilon_r \zeta}{3\eta} f(\kappa a) \qquad (1.25)$$

where $\varepsilon_0$ is the Relative Dielectric Constant, $\varepsilon_r$ is the Electrical Permittivity of a Vacuum, $\eta$ is the Solution Viscosity, $\zeta$ is the Zeta Potential, f(κa) is the Henry's function which is the ratio of particle radius to double layer thickness, κ is the units of κ are reciprocal length, where 1/κ is equal to the "thickness" of the electrical double layer (the Debye length) and a is the Particle radius

For situations where particles are larger in size and dispersed within an aqueous moderate electrolyte concentration media, then the Smoluchowski approximation can be applied, where f(κa) = 1.5 [16].

Therefore the Smoluchowski equation is:

$$U_E = \frac{\varepsilon_o \varepsilon_r \zeta}{\eta} \tag{1.26}$$

The Smoluchowski approximation is valid for the sizes of most bacteria and viruses.

**Instrumentation**

The basic configuration of instrumentation used for the measurement of zeta potential in the literature is essentially the same even though different manufacturers utilize various geometries, laser powers and scattering angles.

Light scattered from a moving particle experiences a frequency shift. As the frequency of light is high (1014Hz), the shift in frequency can only be measured by an optical mixing or interferometric technique. The incident laser beam is split into two beams, one beam referred to as the scattering beam which passes through the particle dispersion and the other beam called the reference beam which either passes through the sample or is routed around the cell. The main beam is frequency modulated which allows the sign of the electrophoretic mobility to the determined. The two beams must be compared at some point after the scattering beam has passed through the sample (although this could at the crossing point in the sample). Through the comparison in the difference in frequency (i.e. the Doppler shift) between the scattered light and the incident light (the reference beam), the mobility of the particles under the influence of the applied electric field can be determined [16, 105].

## 1.7.2 Streaming Potential Measurements

An important factor which could participate in the fouling of membranes is the surface charge of the membrane. Membrane charge is widely thought to influence the separation performance and fouling tendency of membranes, where fouling substance interaction with the membrane surface in aqueous media can be dependent upon the membrane surface charge [106]. Therefore the study of surface characteristics of

membranes is essential for understanding of membrane fouling. The zeta potential is a value that is typically used to characterise the electrical properties of the membrane surface. The zeta potential of membranes is determined from measuring the electrical potential difference when there is relative motion between a fluid containing charged species and a charged surface caused by hydrostatic pressure gradient. Zeta potential of the membrane surfaces can be calculated from the measured the streaming potential using the Helmholtz-Smoluchowski equation with the Fairbrother-Mastin approach [107, 108].

The Helmholtz-Smoluchowski equation is [108]:

$$\zeta = \frac{dU}{dP}\frac{\mu}{\varepsilon\varepsilon_0}\frac{L}{AR} \tag{1.27}$$

where $\zeta$ is the Zeta Potential, dU/dP is the Slope of streaming potential versus pressure difference across the channel, $\mu$ is the electrolyte viscosity, $\varepsilon$ is the dielectric constant of electrolyte, $\varepsilon_0$ is the permittivity of free space, L is the length of capillary system, A is the cross-sectional area of capillary system and R is the resistance of cell using electrolyte solution.

The Fairbrother-Mastin approach can be used for solutions with low surface conductivity, i.e. when the electrolyte concentration $\geq 10^{-3}$:

$$\frac{L}{A} = \kappa R \tag{1.28}$$

Therefore equation 1.27 becomes:

$$\zeta = \frac{dU}{dP}\frac{\mu}{\varepsilon\varepsilon_0}\kappa \tag{1.29}$$

where $\kappa$ is the specific electrical conductivity of the electrolyte [107].

**Instrumentation**

The zeta potential is measured at the solid/liquid interface of surfaces according to the method of streaming potential. An electrolyte solution flows through a measuring cell

which contains the membrane sample, which depending on the flow resistance of the sample (capillary bundle) a pressure drop is detected across the measuring cell. A pump is used for the electrolyte flow which causes charge transportation in the flow direction along the cell. The resulting potential difference (streaming potential) is detected by measuring electrodes connected at both ends of the measuring cell. As the measurement is taken, the pressure ramp is passed in both flow directions and the pressure drop across the cell and the streaming potential are recorded. The data can be obtained with the flow either through the pores (transmembrane streaming potential) meaning the flow is directed perpendicular to the active layer of membranes or flow horizontally directed along the membrane surface (tangential streaming potential). Transmembrane streaming potential only allows for qualitative results of a multilayer membrane (support layers and skin layer), however tangential streaming potential provides direct data about the membrane skin layer [106]. These values are then used to determine the zeta potential using the Helmholtz-Smoluchowski equation [109].

## 1.8 Combination of Analytical Techniques for membrane fouling investigations

A number of studies have been conducted which combine many techniques for the analysis of membranes and membrane fouling processes to elucidate the mechanisms of fouling. One such study conducted by James *et al* [110] used SEM, AFM and X-ray photoelectron spectroscopy for the characterisation of the surface of virgin and process fouled MicroFiltration (MF) and UF membranes, which were utilised for milk filtration. AFM was determined to be the most appropriate and convenient method for examining surface morphology, whilst SEM was determined to be the best technique for examining the cross-sectional and internal structure of unused or fouled membranes. The membrane structure examined by AFM and SEM was deemed to have a great effect on fouling and filtration performance.

In another study, Pang et al [4] investigated the biofilm formation characteristics of four bacterial isolates which were recovered from RO membranes used for water treatment, with particular attention paid to the investigation of bacterial transport and adhesion

mechanisms. A great number of experiments were conducted to uncover the bacterial isolates ability for biofouling using three different membranes composed of cellulose acetate, polyamide and thin film composite. The experiments conducted were as follows; microtiter plate assay, motility assays, measurement of cell surface hydrophobicity, measurement of cell surface charge, use of AFM and SFM for surface morphology data and surface roughness measurement, contact angle measurement of the membranes, membrane surface zeta potential, Fluorescence in Situ Hybridzation (FISH).

From these two example studies, it can be seen that combination of various analytical techniques for membrane fouling investigations provide useful insights, however there are limited studies on membrane fouling that adopt such a rigorous analytical approach and no such study has yet investigated the mechanical properties of membranes and foulant bacteria alongside comprehensive characterisation of the chosen membrane process.

The Fujairah plant and the problems the plant experiences in terms of membrane fouling is one of the main focuses of the present research for the investigation of fouling mechanisms. This plant was the source of the fouled membranes used in this current study, therefore the operation of the plant processes are described next.

## 1.9 Fujairah Water and Power Plant

The Fujairah Water and Power plant, located in the United Arab Emirates (UAE), was successfully commissioned in September 2003 and is currently the second largest seawater reverse osmosis (SWRO) plant worldwide. The plant uses two technologies for water production, so to obtain lower average water costs as the RO system aids to sustain electricity demand when there is a mismatch between water and electricity demand. The hybrid plant produces 62.5% of water from 5 Multi-Stage Flash Distillation (MSF) units coupled with the power plant and 37.5% of water from SWRO. In 2006, the plant was bought through a joint venture company between Abu Dhabi Water and Electricity Authority and Sembcorp, forming the Emirates Sembcorp Water

and Power Company (ESWPC). The plant is currently being operated under agreement by Sembcorp Gulf O&M Company (SGOMC). The company has committed to supplying 760 megawatts of power and 454,000 $m^3/d$ of water in 2009. The water produced from the plant is mainly used for irrigation purposes in the Al Ayn region (Emirate of Abu Dhabi) [8, 111].

**Description of Fujairah RO Water Plant**

The seawater open intake into the plant is located 380m from the shore and 6m above the sea bed, where the seawater is screened through bar screens and band screens to two pumps which are capable of feeding the RO plant with 20,000 $m^3/h$ of water. The RO pre-treatment of the water begins with a dosing system capable of 25mg/L $H_2SO_4$, 5mg/L $FeCl_3$ and 1.5mg/L of polymer. These chemicals are mixed with the seawater in two static mixers and two coagulation tanks for the destruction of marine growth and algae. The water is then fed to flocculators, where a cationic polyelectrolyte is added, before being gravity fed to 2 lines of 7 open dual-media filters, where each filter is of the Degremont's Mediazur type and capable of handling up to 1,500$m^3/h$ of seawater each. The water is then pumped through 2 lines of 9 cartridge filters, where sodium bisulfate, a de-chlorinating agent, is dosed before and after the cartridge filters.

The required salinity at the outlet of the SWRO plant is expected to be less than 180mg/L, therefore the plant uses a double-pass system, where both passes are also designed into two independent lines. The first pass consists of 18 racks, which in total are 137 process vessels with seven membranes within each vessel. Hydranautics SWC4+ membranes are currently being used in the first pass, however Hydranautics SWC3+ were used until early 2009. The water is pressurized by 18 high-pressure pumps and fed to the first pass racks. 43% of the water is desalinated by SWRO in the first pass. The remaining brine is sent to the energy recovery turbine before being discharged back to the sea. About 80% permeate water produced in the first pass is fed into the second pass to be further desalinated by the process of Brackish water reverse osmosis. The second pass consists of 8 racks with 73 process vessels, each containing 7 Hydranautics ESPA1 low energy membranes. The conversion rate for the water is 90%. The remaining 20% of the first pass permeate flow is blended with the second pass permeate flow before being fed to the product water tanks. The rejected brine

from the second pass is recycled and mixed with incoming seawater before the first pass [8, 111].

### 1.9.1 Membrane History

The membrane sample history was extremely difficult to obtain due to the Doosan Heavy Industries company policy on none disclosure of plant operational data. Doosan Heavy Industries & Construction company constructed the Fujairah RO plant. This policy was strictly enforced due to a recent case where two executives of STX Heavy Industries were arrested on charges of stealing key technology data from their former employer Doosan Heavy Industries & Construction in 2007. The only way to obtain the data was to organise the Dean of GIST and the CEO's of Doosan Heavy Industries to sign a None Disclosure Agreement. Therefore due to the sensitivity surrounding the Fujairah RO process operational data, it was extremely difficult to ascertain the history of the membranes. However, data from previously published papers from plant operators from the Fujairah plant have enabled us to gain an insight into problems with operational procedures at the plant [8].

Even though the overall plant performance has been deemed to be generally good, there have been incidences which have revealed problems in the plant operation, especially in the SWRO first pass racks. In June 2003 there was a sudden increase in normalized differential pressure and again in May – June 2006 there was a decrease in normalized flow which was partly irreversible. In 2006, the membranes were replaced because the autopsy report showed that the membranes in the lead positions were in a poor condition due to fouling. A solution to this problem is the replacement of membranes after extensive use, however this is a timely and expensive solution. Therefore more research is needed for the prevention of membrane fouling in process situations [8].

Also from a presentation given by the Water System Manager from the Fujairah plant in 2008, extra information about the operation of the RO process could be obtained (Appendix B).

## 1.10 Aims and Objectives

The main aim of this research is a comprehensive investigation of the issue of biofouling on industrial RO membranes through molecular biology techniques, characterisation of surface charge of both the isolated bacteria from a fouled membrane and the RO membrane surface and AFM imaging and force measurements on clean and fouled membranes for the determination of adhesion force and micromechanical properties, including elasticity. This rigorous characterisation of membrane fouling in an industrial context will lead the way in developing a rational strategy for economic and effective cleaning processes which will maintain efficient membrane operation and prolong membrane life so enabling the reduction of operating costs of such processes.

There are a number of objectives that need to be achieved for the successful completion of this research, where the research has been facilitated by the School of Engineering located within Swansea University in collaboration with the Energy and Biotechnology Laboratory located within GIST, Korea. The first objective was to identify the different types of microbes that cause significant fouling on membranes, so that methods could be devised to avoid the costly and potentially dangerous problem of membrane biofouling. Using the culture independent method of the molecular technique based on the 16S rDNA sequence and constructed gene libraries, the microbial diversity can be determined within the fouling biofilms and the most significant foulant organisms within the biofilm can be identified. Although these techniques are well established they have not been applied extensively to RO and NF membrane process systems. Four strains of bacteria isolated from the fouled RO membrane using the culture dependent method were chosen and characterised in terms of surface charge at process relevant conditions through the use of Electrophoretic Light Scattering (ELS) technique for measurement of electrophoretic mobility. The results of the first objective are presented in Chapter three.

The second objective was the characterisation of the surface charge of clean and industrial fouled membrane through the use of streaming potential experiments at various pH values and NaCl, $MgCl_2$ and $CaCl_2$ concentrations. Also the AFM was used to characterise clean and industrial fouled membrane surfaces visually and also through

the analysis of the images to obtain data, such as height variation and surface roughness. The analysis of the AFM images could elucidate the fouling potential of the clean membrane surface and determine the foulant coverage of the industrial fouled membrane. The results of the second objective are presented in Chapter Four.

The third objective was the development and application of AFM force measurements to study the mechanical properties of clean and fouled membranes. Clean, industrially fouled and purposefully fouled membranes with the chosen four isolated bacteria from the culture-dependent technique were chosen as model systems. Firstly the loading force and extension time were varied to determine the effect of these AFM parameters on the force curves performed on clean and industrially fouled membranes. Once the optimum settings for the parameters had been chosen force measurements were performed on clean and industrially fouled membranes at various NaCl, $MgCl_2$ and $CaCl_2$ concentrations and three different pH values to achieve measurements of maximum adhesion force and elasticity using both the Hertz and JKR models. The main force measurements used a silica colloid probe, however a comparison study at one NaCl concentration at three different pH values with a sharp silicon nitrate tip was undertaken to see if tip geometry had an effect on the force measurements obtained. Also force measurements were measured on membranes which have been purposely fouled with the four strains of isolated bacteria through the process of high pressure filtration at one NaCl concentration and three different pH values to again achieve measurements of maximum adhesion force and elasticity using both the Hertz and JKR models. The results of the third objective are presented in Chapter five.

The conclusions which summarise the main findings from the result chapters and recommendations for future research work which should be conducted for further elucidation of the issue of membrane biofouling are found in Chapter 6.

# Chapter 2 Materials and Methods

## 2.1 Samples

### 2.1.1 Membrane samples

The Membrane element, SWC3+, used was obtained from Hydranautics, which is a Nitto Denko company. The membrane polymer is composite polyamide and the membrane has a nominal salt rejection of 99.8%. The operational data from the manufacturer is found in the data sheet in Appendix C.

The industrially fouled section of the Membrane element, SWC3+, was obtained from the Fujairah Water and Power plant, located in the UAE. The one section of fouled membrane was sent from the Fujairah RO plant to GIST and another section was sent to Swansea University in October 2008, where the fouled membrane section upon arrival was stored at -20°C until used. The description of the operation of Fujairah Desalination plant is located in section 1.9.

### 2.1.2 Bacterial isolates

The four bacterial species isolated from the industrially fouled membranes and chosen for analysis were *Klebsiella pneumoniae* subsp *Pneumonia, Acinetobacter venetianus, Vibrio* sp. PM6A and an Uncultured Bacterium.

*K.pneumoniae* subsp *Pneumonia, A.venetianus, Vibrio* sp. PM6A are all from the phylum *Proteobacteria* and are also from the same class of *γ-Proteobacteria.* The phylum *Proteobacteria* is a large and extensive complex group that contains over 1,200 species in over 400 genera [112]. The group is diverse in morphology, physiology and life-style. Species contained in the group are important within the medicine, industrial and biological research. It is not known the phylum grouping to which the uncultured bacterium belongs.

***Klebsiella pneumoniae* subsp *Pneumonia***

Bacteria from the genus *Klebsiella* are widely found within soil and water in nature. They also exist in low numbers within the normal flora of the intestinal tract when compared to *E.coli.* The strain *K. Pneumonia* is known for being an opportunistic human pathogen which can cause a variety of diseases, such as pneumonia and urinary tract infections, where *Klebsiella* is known to be the cause of about 10% of urinary tract infections in humans [112].

*Klebsiella* is a gram-negative bacterium, which are straight cylindrical rods of cell dimensions 0.3-1.0μm by 0.6-6.0μm and typical cell dimensions of 0.5 by 2 μm and are non-motile. *Klebsiella* cells have a thick layer of extracellular polysaccharide which is called a capsule. The capsule may confer several advantages when bacteria grow in natural environments, such as the capsule may protect the cells from desiccation and may help the bacteria resist phagocytosis when they are within an animal host [112].

***Acinetobacter venetianus***

The genus *Acinetobacter* contains 17 validly named and 14 unnamed (genomic) species, where the genus *Acinetobacter* is formed from a heterogeneous group of bacterial organisms [113]. Only a relatively small amount is known about the biology of different (genomic) species of *Acientobacter* except for the clinically relevant species *Acientobacter baumannii.* The research conducted within the genus *Acientobacter* has focused on certain human interest, such as in clinical diagnosis, however even though acinetobacters occupy a large variety of ecological niches, little is known about the relevance of acinetobacters in relation to their environment. Di Cello et al discovered fuel-degrading *Acinetobacter* strains which were isolated from Venice Lagoon (Italy) and named the species *A.venetianus* [113]. Further studies by Vaneechoutte *et al* [114] and Yamamoto *et al* [115] found that their isolated strains from Israeli tar deposits and from the Japanese sea had the same pattern as the Di Cello discovered bacterial strain *A.venetianus* [113]. Currently five strains have been discovered of the non validated species '*A.venetianus*'. Three of the strains were isolated independently from sea water and were seen to degrade long chain carbohydrates, one strain was isolated from an aquaculture fish pond in Denmark and another one strain was discovered in vegetables from Hong Kong [113]. The phenotypic characteristics of the bacteria, corresponding

to those of the genus, is that they are gram-negative, strictly aerobic and non-motile coccobacilli. They are capable of growing in mineral media with acetate as sole carbon source and ammonia as sole source of nitrogen and are incapable of dissimilative denitrification [116, 117].

***Vibrio* sp. PM6A**

The *Vibrios* have had an important role in human well being, especially as the strain *Vibrio cholera* causes outbreaks of cholera within the human population [118]. Also *Vibrio* species have been studied by marine microbiologists who observed that bacterial populations in near-shore waters and those associated with sea life were predominantly of the *Vibrio* species. *Vibrios* are important inhabitants of the riverine, estuarine and marine aquatic environments within a wide range of salinities [118]. The phenotypic characteristics of the *Vibrio* genus are straight or curved rods, 0.5-0.8μm in width and 1.4-2.6μm in length, gram negative, and are motile by one or more polar flagella which are enclosed in a sheath continuous with the outer membrane of the cell wall. They facultative anaerobic respiration and are chemoorganotrophic, having both a respiratory and a fermentative type of metabolism [119].

**Uncultured Bacterium**

The uncultured bacterium was obtained from the surface of the fouled RO membrane from Fujairah Desalination Plant. The phylum grouping for this bacterium is unknown.

## 2.2 Growth Media

Three different media were used to grow the bacteria isolated from the membrane: Tryptic Soy Broth (Sigma-aldrich, UK) was used to grow *A.venetianus*, mPlate Count Broth was used to grow uncultured bacterium and Marine Broth 2216 (BD Difco, UK) *K. pneumoniae* subsp *Pneumonia and Vibrio* sp. PM6A.

The mPlate Count Broth was made manually by adding 10g Tryptone, 5g Yeast Extract and 2g Dextrose to a litre of deionised water.

The growth media Tryptic Soy Broth and mPlate Count Broth had 3.5% Sodium Chloride added to the liquid media and all three media had their pH adjusted to 7.5 to simulate seawater salt concentrations and pH conditions prior to sterilization.

To make agar plates for short-term storage of the bacterial species, 2% agar was added to the liquid media. After the media had been sterilized, the liquid agar media was poured into plates in aseptic conditions and left to set before inoculation.

All media had been sterilized in an autoclave at 121°C for 15mins prior to inoculation.

## 2.3 Molecular Analysis using DNA Extraction and 16S rDNA sequencing

### 2.3.1 Total Genomic Bacterial DNA Extraction

Genomic DNA was extracted from a fouled RO membrane obtained from the Fujairah Water and Power Plant, UAE. The samples were sent to GIST, Korea by flight and stored at -80°C until the samples were required for bacterial DNA extraction.

The membrane samples were cut within a sterile environment from the bulk of the sample into 10 x 2cm sections. The membrane was placed in a sterile petri dish and Tris-HCl buffer (50Mm Tris-HCl, 10mM EDTA, 1.5M NaCl) was poured over the membrane surface. A sterilised blade was used to scrap the fouling layer from the surface and into the buffer solution. 10ml of the foulant/buffer solution was then centrifuged at 6,000 rpm for 10 mins to achieve a foulant layer pellet, where the supernatant was discarded. The pellet was then broken up into 1ml of Tris-HCl buffer and the foulant/buffer solution was then transferred into a Power Bead Tube (Mo Bio Laboratories Inc, CA, USA), containing 0.5 g of 0.1mm Zircoria/ Silica beads (Bio Spec Products Inc, OK, USA). 60 µl of 10 % SDS solution was added into the tube. The tube was then vortexed and 300 µl of chloroform solution was added to the tube.

A bead-beating procedure was performed using Mini-Beadbeater (BioSpec Products Inc, CA, USA) to shake the tube at 2500 rpm for 1 min and then vortexing the tube. The bead-beating procedure was performed twice more. The tube was then centrifuged at 12000 rpm, 4°C for 15 mins, the supernatant was removed and put into a new 2ml tube. The same amount of PCI solution (Phenol/Chloroform/ isoamyl alcohol 25:24;1) was added into the tube, as the amount of supernatant present in the tube.

The tube was inverted slowly and the 2ml tube was centrifuged at 12000 rpm, 4°C for 10 mins. The upper phase of the supernatant was removed and placed into another new 2ml tube. The same amount of chloroform was then added into the tube as the amount of supernatant present in the tube. The tube was inverted slowly and the tube was centrifuged at 12000 rpm, 4°C for 10 mins. The upper phase of the supernatant was removed and placed into a two new 2ml tubes and to volume of supernatant retrived, two volumes of ethanol (100% molecular grade) was then added to each of the two tubes, as the amount of supernatant present. The tubes were placed in the refrigerator at -20°C for 2 hours. The tubes were then centrifuged at 12000 rpm, 4°C for 30 mins and the supernatant from the tube was then removed and discarded.

400 µl of 70% ethanol was added into the tubes and the pellet was broken up and suspended in the ethanol. The tube was centrifuged at 12,000 rpm, 4°C for 10 mins and the supernatant was discarded. The tube containing the pellet was left to dry in the fume cupboard for 30 mins.

The DNA sample was dissolved in Tris-HCl Buffer and kept in the freezer at -20°C. The quality and the concentration of the genomic DNA sample was analysed by electrophorthesis on the 1% agarose gel, stained with ethidium bromide to detect the DNA band which is around 20kb. The electrophorthesis was conducted at 100V for 30 min, using 5 µl of the DNA sample and performed within 0.5x TAE Buffer with the Hind III DNA marker which measures up to 23kb.

### 2.3.2 Purification of DNA Product

The genomic DNA was purified using a DNA purification Kit (Gene All PCR DNA Purification Kit by Gene All Biotechnology Co. Ltd) according to the manufacturer's

instruction. The extracted DNA was thoroughly mixed with the company provided solution of acetate and ethanol in the ratio 1:5 and transferred to a filter tube. The filter tube was centrifuged at 12,000 rpm for 1 minute and the flow through was discarded. 700 µl of company provided 70% Ethanol was added into the filter tube and then centrifuge at 12,000 rpm for 1 minute and the flow through was discarded. The filter tube was centrifuged for an additional 2 minutes to remove residual wash buffer and the filter was then transferred to the new 1.5ml tube. 50 µl of elution solution was applied to the centre of the filter to retrieve the DNA by centrifugation for 1 minute at 12,000 rpm. The purified DNA was then stored at -20°C.

3 µl of extracted DNA product were applied on the 1% agarose gel in 0.5X TAE buffer, with the Hind III DNA marker. The electrophothesis was conducted at 100V for 30 min and stained with ethidium bromide to detect the DNA band.

However, it should be noted that purification after genomic DNA extraction does not need to be performed if the DNA band is clear and there are no smears.

### 2.3.3 PCR for Amplification of Nearly Complete Bacteria 16S rDNA

The almost complete 16S rDNA gene fragments were amplified from the total genomic DNA sample using the universal primers 27f and 1492r.
The sequence of conserved primers from 16S rDNA sequence of *E.coli*:

27f: Target site: 27-46: AGAGTTTGATCMTGGCTCAG

1492r: Target site: 1473-1492: GGTTACCTTTGTTACGACTT

For the PCR reaction, a total 50µl volume mixture containing 25 µl of PCR Premix (Bulk AccuPower PCR Premix, Bioneer, Korea), 1 µl of template chromosomal DNA, 0.5 µl of each primer (50 pmol/ µl) and 23 µl of distilled water was prepared and then placed into the MasterCycler gradient PCR machine (Eppendorf, Hamburg, Germany). The reactions were heated to 94°C for 5 mins following by 35 amplification cycles with the parameters: denaturation at 94°C for 45 sec, then annealing at 52°C for 45 sec,

extension step at 72°C for 90s. The reaction ended with the final extension at 72°C for 10 min. The PCR reaction mixture was then stored at 4°C.

### 2.3.4 Purification of PCR Product

The PCR product was purified by the DNA purification Kit (Gene All PCR DNA Purification Kit by Gene All Biotechnology Co. Ltd) according to the manufacturer's instruction, as described in section 2.3.2.

After PCR reaction, 3 µl PCR products and the 1kb marker were applied on the 1% agarose gel, stained with ethidium bromide (0.5 µl/ml) to detect the DNA band at 1.4-1.5kb, in 0.5X TAE buffer. The electrophothesis was conducted at 100V for 30 min.

### 2.3.5 Ligation into pGEM-T Easy Vector

The pGEM-T Easy vector system (Promega, WI, USA) was used for the cloning of PCR products. A mixture of 0.5 µl of pGEM-T vector (50 ng/ µl), 1 µl of purified PCR product, 1 µl of $T_4$ Ligase, 5 µl of rapid buffer for $T_4$ ligase (2X), and 2.5 µl sterilised distilled water was used for a 10 µl mixture. The mixture was incubated at 4°C for 9 hours.

However, the amount of PCR product used depends on the concentration of the purified PCR product. 150ng of the purified PCR product was used for a 10ml reaction. The concentration of DNA within the purified PCR product was measured using the Nanodrop machine.

### 2.3.6 Transformation into the *E.coli*

The ligated vector was transformed into *E.coli* competent cell (HIT competent cell, RBC BioScience, Taiwan) which was stored at -70°C. The competent cell was kept on ice until it just thawed. The entire ligation product was added into 100 µl competent cell and the mixture was kept in ice for 30 minutes. Heat shock of the mixture at 42°C for 90 seconds was performed, where immediately afterwards it was cooled on ice for 2 minutes. 600 µl of LB medium was added to the mixture before being incubated in a

shaking incubator at 37°C for 1 hour. The concentrations of 50, 100 and 200 µl of transformed cell suspension were spread onto three individual 1.5% LB agar plates containing 75 µg/ml of ampicillin, 0.5mM of IPTG and 80 µg/ml of X-gal and incubated for 10-12 hours at 37°C. The white colonies which grew and contained the target gene inserted into the vector, were picked up randomly, being careful not to select the blue colonies which do not possess the target gene. The white colonies were then streaked onto individual 1.5% LB agar plate containing 75 µg/ml of ampicillin, 0.5mM of IPTG and 80 µg/ml of X-gal and incubated for 10-12 at 37°C.

### 2.3.7 Colony PCR

To prepare the samples for colony PCR, the streaked colonies were again checked for a white colour and individually removed from the plate and placed into 10-20µl of Tris-HCl buffer. The mixture was then heated to 95°C for 15 mins to lyse the cells. The sample was then centrifuged at 12,000 rpm for 10 mins and the supernatant was used as the DNA template for the PCR reaction.

For the PCR reaction, a total 25µl volume mixture containing 12.5 µl of PCR Premix (Bulk AccuPower PCR Premix, Bioneer, Deajon, Korea), 2 µl of DNA template, 0.25 µl of both primers (50 pmol/ µl) and 10 µl of distilled water was prepared and then placed into the MasterCycler gradient PCR machine (Eppendorf, Hamburg, Germany). The mixture was heated to 94°C for 5 mins followed by 30 amplification cycles with the parameters: denaturation at 94°C for 45 sec, then annealing at 52°C for 45 sec, extension step at 72°C for 90s. The reaction ended with the final extension at 72°C for 10 min. The PCR reaction was stored at 4°C.

After PCR reaction, 3 µl PCR products and the 1kb marker were applied on the 1% agarose gel, stained with ethidium bromide (0.5 µl/ml) to detect the DNA band at 1.4-1.5kb, in 0.5X TAE buffer. The electrophothesis was conducted at 100V for 30 min.

### 2.3.8 Purification of DNA Product

The PCR Product was purified using the DNA purification Kit (Gene All PCR DNA Purification Kit by Gene All Biotechnology Co. Ltd) according to the manufacturer's instruction, as described in section 2.3.2.

### 2.3.9 Sequencing Analysis

About 100 purified Colony PCR samples were sent for sequencing (SolGent Co., Ltd, Korea). The sequences were analysed using MEGA version 4.0 program and compared with those in the BLAST GenBank (http://www.ncbi.nlm.nih.gov/blast/).

## 2.4 Electrophoretic Mobility and Zeta Potential Measurements of bacterial species

### 2.4.1 Sample Preparation

The four bacterial species were prepared for electrophoretic mobility measurements using the following protocol. Bacterial cells previously grown on agar plates were removed from the refrigeration unit at 4°C, where single colonies of each bacterium were picked up from the agar by a sterilized inoculating loop and transferred to the corresponding media. Three different types of media were used; Tryptic Soy Broth, mPlate Count Broth and Marine Broth. After the bacterial inoculation of the media, the bacteria inoculated media contained in conical flasks were moved into an incubator shaker at 30°C for 22 hours to allow for bacterial growth. After this time, two amounts of 1ml of the bacterial suspension were taken from the conical flasks and placed into 1.5ml sized eppendorfs. The eppendorfs were then placed into a centrifuge, whilst ensuring that the centrifuge was evenly balanced and spun at 12,000 rpm for 6mins. The eppendorfs were then removed from the centrifuge, where the supernatant was carefully discarded, leaving a solid bacterial mass at the bottom of the eppendorfs. The bacterial mass was then resuspended into 1ml deionised water, placed back into the centrifuge and spun 12,000 rpm for 6 mins for the removal of any impurities left in the bacterial

mass from the media. The supernatant was again discarded leaving a bacterial mass at the bottom of the eppendorf. The bacterial mass was then resuspened in 20ml electrolyte of various pH values and salt concentrations.

For static growth conditions, the samples were prepared in the same manner apart from the bacteria inoculated media contained in conical flasks were moved into an incubator at 30°C for 22 hours to allow for bacterial growth, instead of being shaken.

### 2.4.2 Electrolyte solution preparation

A number of electrolyte solutions spanning industrial important environments, especially for desalination plants were prepared to investigate the effect of pH values and NaCl, $MgCl_2$, $CaCl_2$ concentrations on the cell surface charge. 0.1M, 0.3M, 0.6M and 0.8M NaCl electrolyte solutions were prepared. The pH of the NaCl solutions were adjusted to values of 3, 4, 5, 6, 7, 8, 9 by adding small amounts of HCl and NaOH. Also the concentrations of the combined solutions of NaCl - $MgCl_2$ and NaCl - $CaCl_2$ were varied, whilst ensuring the ionic strength of the solutions were kept constant, to determine the effect of $Mg^{2+}$ and $Ca^{2+}$ ions on the cell surface charge. The ionic strength of NaCl is lower than the ionic strength of the $MgCl_2$ and $CaCl_2$, due to the charge on the $Mg^{2+}$ and $Ca^{2+}$ ions, therefore to maintain the same ionic strength in the combined solutions of NaCl, $MgCl_2$ and $CaCl_2$, the ionic strength of each of these solutions had to be calculated using the equation:

$$I = \frac{1}{2}\sum_{i=1}^{n} c_i z_i^2 \qquad (2.1)$$

where $c_i$ is the molar concentration of the ion, $z_i$ is the charge on the ion and the sum is taken over all the ions in the solution.

The variations of the amount of NaCl, $MgCl_2$ and $CaCl_2$ used in the experiments are shown below in Tables 2.1 and 2.2. The electrophorectic mobility measurements were performed at two ionic strengths of 0.1M and 0.6M for NaCl - $MgCl_2$ and NaCl - $CaCl_2$ combined solutions at pH 7. One extra measurement was performed at the ionic

strength of 0.6M to simulate the typical seawater concentration of $NaCl_2$ - 0.5595mol, $MgCl_2$ – 0.0135mol, $CaCl_2$ – 0.0037mol. The solution measurements performed at the ionic strength of 0.6M are contained in Table 2.1, whilst the solution measurements performed at the ionic strength of 0.1M are contained in Table 2.2

| NaCl (mols) | $MgCl_2$ (mols) |
|---|---|
| 0.6 | 0 |
| 0.5595 | 0.0135 |
| 0.5 | 0.033 |
| 0.4 | 0.066 |
| 0.3 | 0.1 |
| 0.2 | 0.133 |
| 0.1 | 0.166 |
| 0 | 0.2 |

| NaCl (mols) | $CaCl_2$ (mols) |
|---|---|
| 0.6 | 0 |
| 0.5595 | 0.0037 |
| 0.5 | 0.033 |
| 0.4 | 0.066 |
| 0.3 | 0.1 |
| 0.2 | 0.133 |
| 0.1 | 0.166 |
| 0 | 0.2 |

Table 2.1 Electrophoretic mobility measurements performed at ionic strength of 0.6M to investigate the effect of increasing $Mg^{2+}$ and $Ca^{2+}$ ions on bacterial surface charge.

| NaCl (mols) | $MgCl_2$ (mols) |
|---|---|
| 0.1 | 0 |
| 0.0833 | 0.0055 |
| 0.0667 | 0.0111 |
| 0.0500 | 0.0167 |
| 0.0333 | 0.0222 |
| 0.0167 | 0.0278 |
| 0 | 0.0333 |

| NaCl (mols) | $CaCl_2$ (mols) |
|---|---|
| 0.1 | 0 |
| 0.0833 | 0.0055 |
| 0.0667 | 0.0111 |
| 0.0500 | 0.0167 |
| 0.0333 | 0.0222 |
| 0.0167 | 0.0278 |
| 0 | 0.0333 |

Table 2.2 Electrophoretic mobility measurements performed at ionic strength of 0.1M to investigate the effect of increasing $Mg^{2+}$ and $Ca^{2+}$ ions on bacterial surface charge.

### 2.4.3 Data Acquisition

The Zetasizer 2000 from the manufacturer 'Malvern Instruments' was used to determine the electrophoretic mobility of the four species of bacteria. 10ml of deionised water was injected into the Zetasizer, to ensure that the measurement cell was clean and not contaminated, whilst carefully ensuring that no air bubbles were introduced into the instrument. 10ml of the bacterial electrolyte solution was then injected into the Zetasizer where 20 measurements of electrophoretic mobility at 25°C for each particular sample were measured to obtain an average value of mobility of the bacteria.

### 2.4.4 Data Analysis

The Smoluchowski model can be applied in the case of these bacterial species, which is described by the equation:

$$U_E = \frac{\varepsilon_o \varepsilon_r \zeta}{\eta} \tag{2.2}$$

where, $U_E$ is the electrophoretic mobility, $\varepsilon_o$ is the Electrical Permittivity of a Vacuum, $\varepsilon_r$ is the Relative Dielectric Constant, $\eta$ is the Solution Viscosity and $\zeta$ is the Zeta Potential.

Therefore from the electrophoretic mobility measurements from the Zetasizer and the use of the Smoluchowski model, the zeta potential of the bacterial species can be determined in various aqueous environments.

## 2.5 Streaming Potential

### 2.5.1 Samples Preparation

The virgin membrane element, SWC3+ and the industrially fouled section of the membrane, SWC3+ were used within this experiment. The clean and industrially fouled membrane samples were cut from provided templates into two rectangular shaped

pieces with specific holes for liquid flow, which were suitable for the rectangular fluid cell used for streaming potential measurements.

The clean membrane samples were soaked in deionised water at 4°C for 24 hours for the removal of any contamination. The industrially fouled membranes were removed from -20°C storage and the underside of the membrane placed in a small amount of deionised water and left to soak at 4°C for 24 hours. This enabled the membrane to be hydrated with only minimal disruption of the foulant layer, as if placed in a large amount of deionised water the foulant layer could float off into the surrounding liquid.

After 24 hours, the cut membrane sample pieces were clamped between two measuring cell parts separated by a defined streaming channel within the rectangular fluid cell.

### 2.5.2 Electrolyte solution preparation

A number of electrolyte solutions spanning industrial important environments, especially for desalination plants were prepared to investigate the effect of pH and NaCl, $MgCl_2$, $CaCl_2$ concentrations on the membrane surface charge. 0.01M and 0.1M NaCl electrolyte solutions were prepared. The pH values of the NaCl solutions were adjusted to 3, 4, 5, 6, 7, 8, 9 by adding small amounts of HCl and NaOH.

Also the concentrations of the combined solutions of NaCl - $MgCl_2$ and NaCl - $CaCl_2$ were varied, whilst ensuring the ionic strength of the solutions were kept constant, to determine the effect of $Mg^{2+}$ and $Ca^{2+}$ ions on the membrane surface charge. The ionic strength of each of these solutions had to be calculated as described in section 2.4.2. Zeta potential measurements were performed at two ionic strengths of 0.01M and 0.1M for NaCl - $MgCl_2$ and NaCl - $CaCl_2$ electrolyte solutions at pH values of 3, 4, 5, 6, 7, 8, 9. The solution measurements performed at the ionic strength of 0.01M are contained in Table 2.3, whilst the solution measurement performed at the ionic strength of 0.1M are contained in Table 2.4.

| NaCl (mols) | $CaCl_2$ (mols) |
|---|---|
| 0.0100 | 0 |
| 0.0080 | 0.00067 |
| 0.0060 | 0.00133 |
| 0.0040 | 0.00200 |
| 0.0020 | 0.00267 |
| 0 | 0.00333 |

| NaCl (mols) | $MgCl_2$ (mols) |
|---|---|
| 0.0100 | 0 |
| 0.0080 | 0.00067 |
| 0.0060 | 0.00133 |
| 0.0040 | 0.00200 |
| 0.0020 | 0.00267 |
| 0 | 0.00333 |

Table 2.3 Streaming potential measurements performed at ionic strength of 0.01M to investigate the effect of increasing $Mg^{2+}$ and $Ca^{2+}$ ions on membrane surface charge.

| NaCl (mols) | $CaCl_2$ (mols) |
|---|---|
| 0.100 | 0 |
| 0.080 | 0.00667 |
| 0.060 | 0.01333 |
| 0.040 | 0.02000 |
| 0.020 | 0.02667 |
| 0 | 0.03333 |

| NaCl (mols) | $MgCl_2$ (mols) |
|---|---|
| 0.100 | 0 |
| 0.080 | 0.00667 |
| 0.060 | 0.01333 |
| 0.040 | 0.02000 |
| 0.020 | 0.02667 |
| 0 | 0.03333 |

Table 2.4 Streaming potential measurements performed at ionic strength of 0.1M to investigate the effect of increasing $Mg^{2+}$ and $Ca^{2+}$ ions on membrane surface charge.

### 2.5.3 Data Acquisition

The Electro Kinetic Analyzer from the manufacturer 'Anton Paar' was used to determine the streaming potential of clean and industrial fouled membranes at different pH values and NaCl, $MgCl_2$ and $CaCl_2$ concentrations. Firstly, calibrations of the pH and conductivity probes were performed, followed by a rinse cycle of both the bypass and the fluid cell in both directions within the analyser with deionised water. Then a rinse cycle was performed with the specified salt solution, taking care to ensure that any air bubbles were removed from the rectangular fluid cell, and with the outside pH and conductivity probes placed in the salt solution. Once the preliminary rinse cycles were

performed, the pH of the salt solution was adjusted and another rinse cycle performed for mixing of the solution within the analyser. The pH was adjusted during this rinse cycle until the pH value stabilised at the correct value. The zeta potential measurements were repeated three times for each pH value in each direction of fluid flow.

### 2.5.4 Data Analysis

Zeta potential of the membrane surfaces was calculated from the measured streaming potential using the Helmholtz-Smoluchowski equation with the Fairbrother-Mastin approach.

$$\zeta = \frac{dU}{dP}\frac{\mu}{\varepsilon\varepsilon_0}\kappa \qquad (2.3)$$

where $\zeta$ is the Zeta Potential, dU/dP is the Slope of streaming potential versus pressure difference across the channel, $\mu$ is the electrolyte viscosity, $\varepsilon$ is the dielectric constant of electrolyte, $\varepsilon_0$ is the permittivity of free space and $\kappa$ is the specific electrical conductivity of the electrolyte.

## 2.6 AFM Imaging

### 2.6.1 Samples Preparation

The virgin membrane element, SWC3+ and the industrially fouled section of the membrane, SWC3+ were used within this experiment. To prepare the clean and industrially fouled membranes for AFM imaging, the clean membrane samples were soaked in deionised water at 4°C for 24 hours for the removal of any contamination. The industrially fouled membranes were removed from -20°C storage and the underside of the membrane placed in a small amount of deionised water and left to soak at 4°C for 24 hours. This enabled the membrane to be hydrated with only minimal disruption of the foulant layer, as if placed in a large amount of deionised water the foulant layer could float off into the surrounding liquid.

After 24 hours, the clean and industrially fouled membrane samples were cut into small sections of 15 mm x 15 mm within a sterile environment and left to air dry. Each cut membrane sample was then attached one side of a 20mm glass cover slip using double sided adhesive tape, in preparation for imaging.

### 2.6.2 Data Acquisition

The Dimension 3100 AFM (Digital Instruments – Veeco Metrology group, Santa Barbara, California) was used for the majority of membrane imaging. Non Contact Cantilevers were used from the manufacturer Veeco, model number OTESPAW. These cantilevers are composed from non-conductive silicon nitride and the manufacturer specifies that the spring constant value was 0.08N/m. The membrane images were achieved using tapping mode within an air environment of 21°C and a relative humidity of 40%. The topographical, phase and amplitude data was obtained simultaneously. The scan rate of 0.4Hz and an image resolution of 1024 x 1024 were chosen for most images, however for the largest scan size of 100μm, a scan rate of 0.2Hz was used to achieve a higher quality image.

### 2.6.3 Data Analysis

The captured images were analysed using Nanoscope offline software. Measurements of the software computed Peak-to-Valley and RMS roughness were obtained from the captured images. RMS roughness and Peak-to-Valley measurements were performed over 1x1, 10x10, 100x100$\mu m^2$ scan images for the clean and industrially fouled membranes. Also, RMS roughness and Peak-to-Valley measurements of 1x1 $\mu m^2$ areas were taken from 10x10$\mu m^2$ images to determine the roughness of the foulant layer and then used to compare to similar measurements taken on the clean membrane. The measurements of the 1x1 $\mu m^2$ areas were obtained by using the cursor to draw a box on the scanned image and utilising the software to calculate the values.

## 2.7 Force Measurements performed on Clean and Industrially fouled membranes

### 2.7.1 Samples Preparation

The virgin membrane element, SWC3+ and the industrially fouled section of the membrane, SWC3+ were used within this experiment. For AFM preparation, the clean membrane samples were soaked in deionised water at 4°C for 24 hours for the removal of any contamination. The industrially fouled membranes were removed from -20°C storage and the underside of the membrane placed in a small amount of deionised water and left to soak at 4°C for 24 hours. This enabled the membrane to be hydrated with only minimal disruption of the foulant layer, as if placed in a large amount of deionised water the foulant layer could float off into the surrounding liquid.

In preparation for AFM force measurements, the clean and industrially fouled membrane samples were cut into small sections of 8 mm x 12 mm within a sterile environment. Each cut membrane sample was attached one side of a 25mm circular glass cover slip using double sided adhesive tape. The glass cover slips were cleaned before use. A circular 25mm plastic fluid cell was then placed over the cover slip and secured in place with silica gel to form a water tight seal. The chosen liquid of specified pH value and salt concentration was placed into the fluid cell carefully using a pipette, so not to disrupt the foulant layer, to the amount of 3ml. The liquid and the membrane sample within the fluid cell was then left for 40 mins to reach equilibrium before use.

### 2.7.2 Procedure for AFM Colloid Probe construction

AFM colloid probes were made through the use of a Micromanipulator (Singer Instruments). The process involves the use of a tipless cantilever (Veeco) which was placed into a tipholder and positioned at the end of a micromanipulator rod. This rod was then placed directly underneath a optical microscope. A clean glass slide had a layer of Loctite Glass bond glue applied evenly to one end of the slide, and one the other end of the slide, cleaned silica spheres of a size ranging from 3-10μm were

dropped onto the surface using a clean pipette. The glass slide was inverted and inserted into the slide holder in the micromanipulator, which was positioned just above the cantilever. The stage was then moved using a fine position joystick to place the cantilever underneath the glue, where the cantilever was then dipped into the glue layer. The cantilever was then moved and brought up onto a clean section of the glass slide to remove excess glue. The stage was then moved to locate a suitable silica sphere on the surface, of which a photo was taken using the software which was later used for sphere sizing. Silica colloids of 3μm radius were chosen for use within the force curve experiments. The cantilever was then placed underneath the suitable sphere and the cantilever was then lightly pressed into the sphere for a few seconds and then the cantilever was moved away from the surface with the silica sphere firmly attached to its apex.

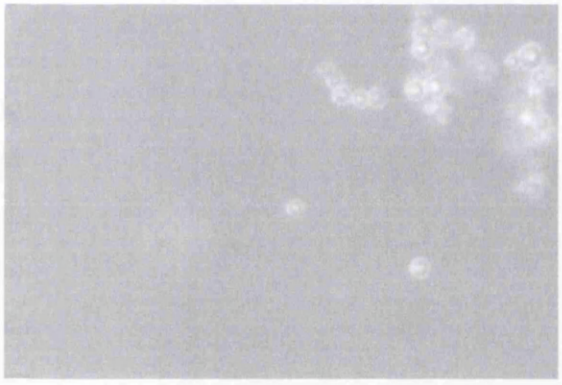

Figure 2.1. Image taken of Silica Sphere

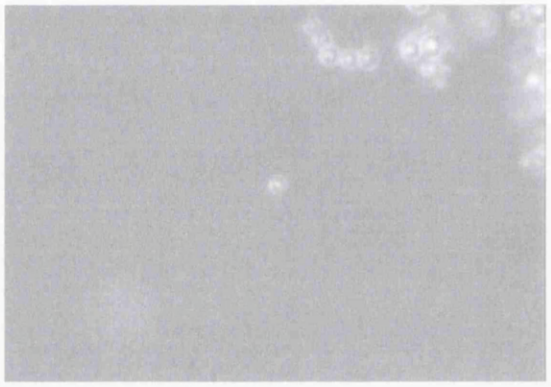

Figure 2.2. Image taken after tip made contact with Silica Sphere

To ensure that the colloid probe had been constructed properly, with the silica sphere placed at the apex of the cantilever and without being swamped with glue, the cantilever was rotated underneath the optical microscope to obtain a side view of the colloid probe for visual inspection. Through using the photo of the silica sphere and a photo of a calibration slide taken at the same objective, imaging software was then used to determine the size of the sphere. The Loctite Glass glue was UV curing so to firmly attach the colloid to the cantilever the cantilever was placed underneath a UV lamp for 5 mins. The probes were thoroughly rinsed with distilled water before use.

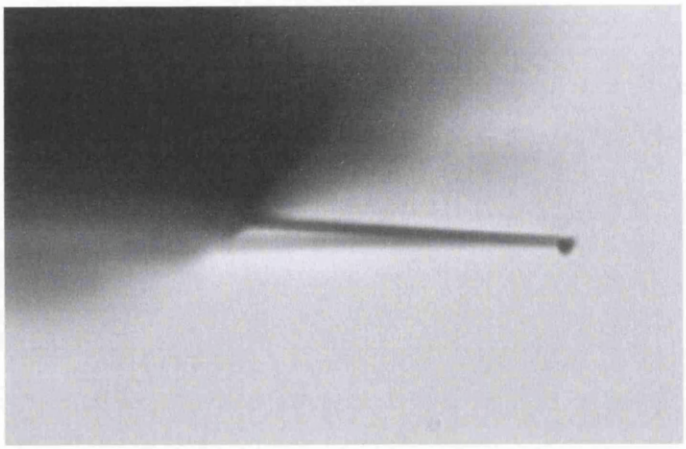

Figure 2.3. Optical Image of Silica Colloid Probe

**Colloid Probe Preparation before experimental use**

Before each force measurement experiment, an optical microscope was used to determine if the silica colloid probe was suitable for use, such that it was clean, free from debris from previous experiments and the sphere was still located at the apex of the cantilever. After the colloid suitability determination, the colloid probe was rinsed with deionised water to ensure it was clean before use. The colloid probe was then mounted onto the AFM head and a calibration force measurement was taken on a clean glass surface. Then the colloid probe's cantilever spring constant was measured via the thermal tune method using the Nanowizard AFM (JPK) software.

### 2.7.3 Instrumentation and Data Acquisition

The NanoWizard II BioAFM with TopView Optics (JPK Instruments) was used for the majority of the force measurements on all membrane surfaces. Contact Cantilevers were used from the manufacturer Vecco, model number DNP. These cantilevers were composed from silicon nitride and the manufacturer specifies that the nominal spring constant value was 0.32N/m. The spring constant of the tips were also determined through the use of thermal tuning software on the AFM, and when the tip's spring constant determined by thermal tuning was close to the manufacturers nomail spring constant value, the tip was used. The silica colloid probes were constructed as described

in section 2.7.2, and the spring constant of the probes were determined by using the thermal tuning present in the AFM software.

The chosen cantilever was secured into place on the glass AFM head and a drop of the chosen liquid was placed in between the glass head and the cantilever to prevent air bubbles forming when the cantilever entered the fluid cell. The fluid cell was placed directly underneath the AFM head and the cantilever was brought slowly down into the liquid. The cantilever was positioned above the glass cover slip surface and brought into contact for the achievement of force curves on the glass surface for the determination of the cantilever's deflection sensitivity. The cantilever was then positioned over the centre of the membrane surface and the tip was brought into contact with the membrane surface for the achievement of force curves.

Loading force, extension speed and tip geometry experiments were performed on the clean and industrially fouled membrane surfaces to investigate the effect of these parameters on the values of adhesion and elasticity using the silica colloid probe. The loading force and extension speed experiments were performed in 0.01M NaCl solution at pH 7. The loading force measurements were taken at 10nN, 20nN, 40nN, 60nN, 80nN, 100nN at a speed of 0.3μm/s and the extend speed measurements were taken at 0.1, 0.3, 0.5, 0.7 and 0.9μm/s at a loading force of 40nN. The AFM optics were used to choose a representative location on the surface of the membrane. The tip was brought into contact with the membrane surface over a scan range of 10μm, where 5 force measurements were performed over the area. In total 4 representative locations were chosen on the membrane surface therefore 20 force measurements were achieved for each loading force and extension speed measurement.

After the force curve parameters experiments, settings of 20nN loading force, extend speed of 0.3μm/s and the use of a colloid probe were chosen. Force measurements on the membranes at various salt concentrations and pH values were performed by the tip being brought into contact with the membrane surface over a scan range of 10μm, where 5 force measurements were performed over the area. In total 5 representative locations were chosen on the membrane surface, therefore 25 force measurements were achieved for each liquid environment.

The clean and industrially fouled membranes were characterized using force measurements at NaCl concentrations of 0.1M and 0.6M at each pH value of 3, 7 and 9. The membrane - colloid probe interactions were also measured at a $MgCl_2$ and $CaCl_2$ concentration of 0.1M ionic strength at each pH value of 3, 7 and 9.

## 2.8 Force Measurements performed on bacteria fouled membranes

### 2.8.1 Samples Preparation

**Membrane Preparation**

The virgin membrane element, SWC3+ was used for this experiment. For AFM preparation, the clean membrane samples were soaked in deionised water at 4°C for 24 hours for the removal of any contamination. The membranes were then cut using a sterilized scalpel blade into a circular 49mm diameter template for use in the high pressure filtration unit.

**Bacteria Preparation**

The four bacterial species were prepared using the following protocol. Bacterial cells previously grown on agar plates were removed from the refrigeration unit, where single colonies of each bacterium were picked up from the agar by a sterilized inoculating loop and transferred to the corresponding media. Three different types of media were used, as described in section 2.2. The media had been sterilized in an autoclave at 121°C for 15mins prior to inoculation. After the bacterial inoculation of the media, the bacteria inoculated media contained in conical flasks were moved into an incubator shaker at 30°C for 22 hours to allow for bacterial growth. After this time, 40ml of the bacterial suspension was taken from the conical flasks and placed into 50ml conical tubes. The conical tubes were then placed into a centrifuge, whilst ensuring that the centrifuge was evenly balanced and spun at 4,000 rpm for 5 mins. The tubes were then removed from the centrifuge, where the supernatant was carefully discarded, leaving a solid bacterial mass at the bottom of the tube. The bacterial mass was then resuspended into 40ml deionised water, placed back into the centrifuge and spun 4,000 rpm for 5 mins for the removal any impurities left in the bacterial mass from the media. The

supernatant was again discarded leaving a bacterial mass at the bottom of the tube. The bacterial mass was resuspended in a 10ml of deionised water, were 2ml of the bacterial solution was removed and added to 70ml of deionised water.

### 2.8.2 Filtration to produce bacteria fouling films

The high pressure filtration unit was utilised for the achievement of a thin layer of bacterial mass on the surface of the SWC 3+ membrane, which was later characterisated with force measurements. The filtration was conducted using Sterlitech HP4750 stainless steel cell which has a maximum pressure rating of 69 bar and is ideally suited to RO filtration. The filtration experiment was performed at 20 bar at room temperature and the filtration was left to run over night due to the long filtration time. The filtration experiment in terms of time and amount of filtrate was logged by a computer program.

Once the filtration experiment had finished, the bacteria fouled membrane surfaces were used immediately for force measurements. The samples were cut into small sections of 8 mm x 12 mm within a sterile environment. Each cut membrane sample was attached one side of a 25mm circular glass cover slip using double sided adhesive tape, where the glass cover slips were cleaned before use. A circular 25mm plastic fluid cell was then placed over the cover slip and secured in place with silica gel to form a water tight seal. The chosen liquid of specified pH value and salt concentration was placed into the fluid cell carefully using a pipette, so not to disrupt the foulant layer, to the amount of 3ml. The liquid and the membrane sample within the fluid cell were then left for 40 mins to reach equilibrium before use.

### 2.8.2 Data Acquisition

The NanoWizard II BioAFM with TopView Optics (JPK Instruments) was used for the majority of the force measurements on all membrane surfaces. The Silica Colloid probes were constructed and prepared as described in section 2.7.2. The spring constants of the probes were determined from the AFM thermal tuning software. The cantilever was positioned above the glass cover slip surface and brought into contact for the achievement of force curves on the glass surface for the determination of the

cantilever's deflection sensitivity. The cantilever was then positioned over the centre of the membrane surface for the achievement of force curves from the membrane surface. The AFM optics were used to select a representative location on the fouled membrane surface. The tip was brought into contact with the membrane surface over a scan range of 10μm, where 5 force measurements were performed over the area. In total 5 representative locations were chosen on the membrane surface, therefore 25 force measurements were achieved for each environmental condition. Settings of 20nN loading force and extend speed of 0.3μm/s were chosen for the force measurements due to previous loading force and extend time experiments, see section 2.7.3. The force curves were performed in 0.6M NaCl solution at pH values of 3, 7, 9.

## 2.9 Force Curve Analysis

The data was analysed manually through excel spreadsheets using the raw data exported from the JPK instrument in parameters of Force in Volts and Z-detector height in Meters. The data was manipulated as explained in section 1.6.4 to achieve values of Maximum Adhesion Force (lowest force data point in the force-distance curve) and the models Hertz and JKR were used to obtain Young's modulus values as explained in sections 1.6.7.1 and 1.6.7.3. The Hertz model was used as this is the most commonly used model in the literature for elasticity measurements and the JKR model was chosen as the model which considered the adhesion within the contact area of the tip and the surface, which is more suited to the present study. The contact point was defined as the height where the cantilever deflection begins to leave the horizontal axis on the deflection vs sample height curve [66].

# Chapter 3 Identification and Characterisation of Bacterial Membrane foulants

## 3.1 Introduction

Membrane technology can be utilised for the production of highly purified water through the purification and desalination of seawater, however membrane filtration processes are commonly impeded by membrane bio-fouling [3]. Bio-fouling occurs when microorganisms attach to a membrane surface and develop into a biofilm, which consists of cells embedded in a matrix of extracellular substances, that subsequently foul the membrane surface [8]. Membrane fouling can cause considerable technical problems, such as reduction in water product quality, loss of flux, and can also cause economic loss as fouling and cleaning agents can shorten the life span of the membranes [2]. Some bacterial biofilms may even physically degrade certain types of membranes. RO membranes are commercially important membranes that have been regularly used in water treatment, however due to the RO membrane properties of significant surface roughness and extremely high salt rejection, the membranes are susceptible to fouling [6]. Therefore a better understanding of the physical, chemical and biological characteristics regarding the processes regulating biofilm formation and biofouling development on RO membrane surfaces will aid in developing new strategies to prevent or reduce the rate of membrane fouling.

As the issue of membrane bio-fouling is economically important, a number of studies have been conducted by various research groups to elucidate the bacterial processes within desalination plants. A number of researchers have inserted glass coupons into a RO plant and also into intake water bays in Saudi Arabia to study bacterial attachment and biofilm formation as a way of determining membrane fouling [120, 121]. The glass coupons were examined by SEM or microscopically to examine the formed biofilm and the pour plate technique was utilised to determine the number of bacteria (CFU) per $cm^2$, however this technique is indirect and will give an inaccurate representation of the bacterial community [120, 121]. For the investigation into membrane bio-fouling, accurate identification of the microbial diversity within the biofilm fouling layer developed on desalination RO membranes is important for the determination of the

different types of microbes that cause significant fouling on membranes. The Culture Independent Method of the molecular technique based on the 16S rDNA sequence and constructed gene libraries can be utilised for the direct identification of the most significant foulant organisms within the biofilm [29]. The Culture Independent Method has the advantage over other techniques, such as the culture dependent method, of direct extraction of nucleic acids from an environmental sample. Only less than 1% of bacteria in nature can be cultured with current standard laboratory culturing techniques, therefore the direct extraction of genomic DNA from the foulant biofilm on the membrane surface allows for the identification of a large proportion of microbes that are not readily cultured within a laboratory setting. This gives a more accurate population and structural representation of the bacterial community present within the foulant biofilm [34, 37]. Although the culture independent method is well established they have not been applied extensively to RO membrane process systems.

Currently there are very limited studies concerning culture independent methods for the analysis of microbial diversity within water treatment membrane processes, especially within the membrane biofilm fouling layers. The few key studies that exist relating to the analysis of the microbial diversity within membrane processes have been performed relatively recently. Bereschenko *et al* [42] used a PCR-DGGE approach combined with analysis of constructed clone libraries, where larger PCR fragments of 16S rRNA gene and DGGE screening of the isolated clones were used to reveal the differences between the bacterial community within various compartments of a full scale RO water purification plant: RO feed water, wall of UF storage tank, cartridge filter, a biofouled RO membrane and RO product water. In another study, Chen *et al* [43] examined microbial communities of membrane biofilms obtained from UF and RO membranes used in two full-scale water purification processes. The membrane biofilms were characterised using a polyphasic approach that utilised bacterial cultivation, 16S rDNA clone library and fluorescence in situ hybridization (FISH) techniques, in the hope to provide better insights into microbial community structure and function in an engineered environment to unravel the processes of biofouling on membranes. Lee *et al* [122] also utilised the 16S rDNA sequence and constructed gene libraries to examine the microbial communities of RO membrane samples and the seawater intake.

There are also few studies that have attempted to fully analyse membrane fouling in terms of the biological, chemical and physical aspects all together. A study by Pang *et al* [4] progressed into investigating biofilm formation characteristics of four bacterial isolates recovered from RO membranes utilised in potable water treatment, with particular attention paid to the investigation of bacterial transport and adhesion mechanisms. A number of experiments were conducted to uncover the bacterial isolates ability for biofouling using three different membranes composed of cellulose acetate, polyamide and thin film composite. The experiments conducted were as follows; microtiter plate assay, motility assays, measurement of cell surface hydrophobicity, measurement of cell surface charge, use of AFM and SFM for surface morphology data and surface roughness measurement, contact angle measurement of the membranes, membrane surface zeta potential and Fluorescence in Situ Hybridzation (FISH). The study isolated the *Sphingomonas* species as an important organism which could aid in biofouling on RO membranes as observations revealed the organisms ability for twitching and swarming motility could facilitate membrane surface colonization. Also the organisms ability to produce large amounts of viscous extracellular polymeric substances could allow for the adhesion and colonisation of membrane surfaces, even with membranes of varying surface roughness values. Bacterial adhesion to the membrane surface for both *Dermacoccus* and *Microbacterium* species seemed to be facilitated by cell surface hydrophobicity as it was suggested that hydrophobic interactions could mediate bacterial adhesion. *Rhodopseuomonas* species possessed a hydrophilic cell and did not demonstrate any signs of motility, therefore the mechanism for adhesion must be facilitated low surface charge, as the membrane surface in the experiment possessed a negative charge. Even though the research conducted by Pang *et al* [4] is important for the elucidation of the mechanisms of bio-fouling, the experiments conducted were not extended to consider whether changes in pH or salt concentrations had an effect on the fouling potential of these bacteria, which could have provided a more encompassing view of bacterial adhesion and biofilm formation.

In the present study, the Culture Independent Method based on the 16S rDNA sequence and constructed gene libraries for the identification of the microbial diversity within the fouling layer developed on RO membranes obtained from Fujairah desalination plant was conducted in the Gwangju Institute of Science and Technology (GIST), South Korea. This research enabled the identification of the different types of microbes that

cause significant fouling on membranes. This research work was part of a larger volume of work performed by YoungPil Chun, a Masters student who studied at GIST. Youngpil used the same fouled RO membranes to determine microbial diversity through the culture dependent method. Even though the culture dependent method has disadvantages as discussed earlier, the technique has the advantage of isolation of the bacterial species from the membrane. The isolation of the bacteria allows for the continuation of the research as the bacterial species obtained from the RO fouling layer can then be examined by experimental methods. The four strains of bacteria isolated from the fouled RO membrane using the culture dependent method were given by YoungPil and the bacteria was then characterised in terms of surface charge at process relevant conditions at Swansea University.

The determination of surface charge properties is of great importance for the understanding of cell function and behaviour within various environments, as the surface charge of microbial cells can influence cell adhesion, aggregation phenomena and cell-ion interactions. Therefore, determination of cell surface charge can aid in the elucidation of cell adhesion to membrane surfaces within process conditions [16, 18, 19]. Bacterial surface charge can be characterized by the zeta potential through the technique of ELS, which has been proven to be a rapid and relatively easy technique of zeta potential determination [16]. The zeta potential can be deduced from the electrophoretic mobility measurements obtained from within an electric field, through the use of the Smoluchowski model. The first ELS experiment was performed in 1972 by Ware and Flygare, since then ELS has been used for investigations in bacterial cell charge. Bayer *et al* [123] measured the electrophoretic mobility of a variety of gram-negative and gram-positive bacteria, such as various *E.coli* strains and *Cytophaga* U67, under standard growth conditions and neutral pH. Bayer discovered that all the cells under standard growth conditions and neutral pH displayed a negative electrophoretic mobility. Blake *et al* [124] measured the electrophoretic mobility of *Thiobacillus ferroxidans*, which was grown on iron, pyrite and sulphur, under physiological conditions and then further calculated the zeta potential. While Van der Mei *et al* [125] measured the zeta potential of fully hydrated oral *Streptococci* cells as a function of pH in dilute potassium phosphate, yielding isoelectric points (IEP) for the different strains. Therefore in the literature, ELS has become an established tool for the determination of electrophoretic mobility and zeta potential measurements for many types of cells, such

as *Calothrix* sp., *Anoxybacillus flavithermus*, and even bacteria isolated from different wastewater treatment plants [126, 127, 128]. Some ELS investigations into bacterial physiology have focused on the contribution of cell surface charge within the process of bacterial adhesion to solid surfaces. Van Loosdrecht *et al* [129] discovered that the bacterial cell surface charge influenced their binding to negatively-charged polystyrene, while Vanhaecke *et al* [16] published research demonstrating there was negligible effect of cell surface charge on the binding of *Pseudomonas aeruginosa* strains to stainless steel.

However, only a limited amount of research has been performed to determine the surface charge of bacterial cells isolated directly from RO membranes. Pang *et al* [4] only measured the cell surface charge, expressed as zeta potential, of four bacterial isolates from RO membranes in the limited conditions of 10mM potassium phosphate buffer at pH 7.3. Therefore, there is scope for more research to be performed to determine the cell surface charge of the chosen four species of bacteria at process relevant conditions and at different pH values and NaCl, $MgCl_2$, $CaCl_2$ concentrations.

## 3.2 Methods

The experimental methods for the 16S rDNA sequencing for the determination of microbial diversity from the foulant layer are given in section 2.3, while information regarding the fouled membrane is given in section 2.1.

The experimental methods for determination of the electrophoretic mobility and zeta potential are given in section 2.4. The description of the bacterial isolates used in this experiment is given in section 2.1, while the growth media description is given in section 2.2.

## 3.3 Results and Discussion

This following section represents the results of the DNA extraction and 16S rDNA sequencing performed on the process fouled RO membranes for the identification of bacterial membrane foulants. After this work, the electrophoretic mobility of the

bacterial isolates were characterized at various process relevant pH values and salt concentrations.

### 3.3.1 DNA Analysis of RO membrane

16S rDNA sequencing performed on DNA extracted from process fouled RO membranes allowed for the determination of microbial community structure present in the membrane fouling layer. A total number of 100 clones were obtained from the experimental procedure and sequenced. The sequences were then identified through comparison of the sequences with the internet database GenBank using Blast search. Table 3.1 shows the 100 clone results of the DNA analysis performed on the RO membrane. The sequenced clones had similarity which ranged from 84% to 99% and 7 phylum-based different microbial groups were identified. Figure 3.1 shows the most abundant bacterial groups present within the foulant layer. *Proteobacteria* (17%) was determined to be the most abundant identified group, with *γ-Proteobacteria* making up a large fraction of the *Proteobacteria* phylum. The next most abundant grouping was the *Bacterioidetes* (10%) and *Plantomycetes* (10%), where the most predominant bacteria within these groupings were the uncultured bacterium of each phylum. *Chloroflexi* and *Nitrospira* were also discovered but were not included within Figure 3.1 due to each phylum only composing of 1% of the total clones sequenced from the membrane.

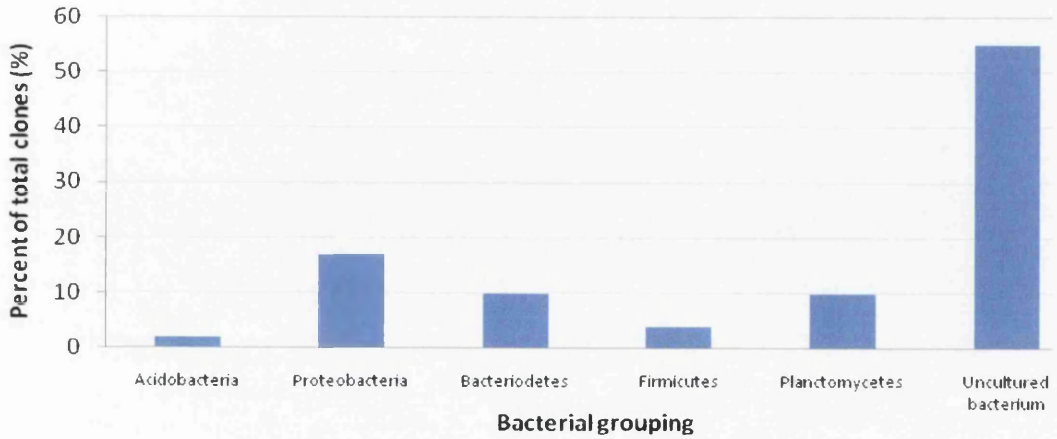


Figure 3.1 – Microbial community structure on fouled RO membrane as identified by GenBank

**Table 3.1 Results from DNA Analysis of fouled RO Membrane by GenBank**

| Phylogenetic lineages | Closest Relative in Gen Bank | No of Clones | Similarity % |
|---|---|---|---|
| Acidobacteria | Uncultured Acidobacteria bacterium clone A6C | 2 | 84 - 87 |
| α-Proteobacteria | Uncultured Alpha-proteobacterium clone HCM3MC91_7A_FL | 1 | 95 |
| β-Proteobacteria | Limnobacter sp. DG1290 | 2 | 98 - 99 |
| | Uncultured beta proteobacterium clone HB123 | 1 | 92 |
| γ-Proteobacteria | Balneatrix alpaca | 2 | 93 |
| | Simiduia agarivorans strain SA1 | 1 | 98 |
| | Cellvibrio mixtus subsp. Mixtus | 1 | 97 |
| | Gamma proteobacterium N2yML2 | 2 | 95 |
| | Endosymbiont of unidentified scaly snail | 1 | 89 |
| | Escherichia coli | 1 | 99 |
| | Natronocella acetinitrilica strain ANL 6-2 | 1 | 85 |
| δ-Proteobacteria | Uncultured delta proteobacterium | 2 | 89 - 91 |
| | Uncultured delta proteobacterium clone ss1_B_04_30 | 1 | 90 |
| | Uncultured delta proteobacterium clone ss1_B_08_37 | 1 | 96 |
| Bacteriodetes | Uncultured Bacteroidetes bacterium | 2 | 91 - 95 |
| | Uncultured Bacteroidetes bacterium clone 9NBGBact_75 | 3 | 92 - 95 |
| | Uncultured Bacteroidetes bacterium clone TDNP_Bbc97_188_1_50 | 1 | 91 |
| Chloroflexi | Uncultured Chloroflexi bacterium clone LC1-24 | 1 | 86 |
| Nitrospirales | Uncultured Nitrospira sp. clone l11F | 1 | 84 |
| Firmicutes | Clostridium sp. Enrichment culture clone MB3_7 | 1 | 99 |
| | Clostridium sp. JB-1 | 1 | 99 |

Table 3.1 continued.

| | | | |
|---|---|---|---|
| | Sporacetigenium mesophilum strain ZLJ115 | 2 | 98 |
| Planctomycetes | Uncultured planctomycete clone GASP-77KB-802-B05 | 3 | 89 |
| | Uncultured planctomycete clone 170 | 3 | 90 |
| | Uncultured planctomycete clone Sylt 10 | 1 | 93 |
| | Uncultured planctomycetales bacterium clone TDNP_Wbc97_76_1_225 | 1 | 90 |
| | Uncultured planctomycete | 1 | 92 |
| | Uncultured Planctomycetales bacterium | 1 | 90 |
| Sphingobacteria | *Flexibacteraceae* bacterium MOLA 398 | 1 | 94 |
| | Uncultured *Sphingobacteriales* bacterium clone B255_A11 | 3 | 91 – 92 |
| Unknown Group | Uncultured bacterium (clones include Elev_16S_1117, S25_868, LC1537B-77, SD04D09, FFCH12445, Y36, C51, Y118, KspoB2, E77, MABRDTU36, SHFH544, KGB200711-093, P9X2b3F05, SC89, BH58, S25_1406, 165B42, D8S-106, Illimani_c9, Hg92C9, 5C231539, SHFG578, C13S-30, A59, 061F22, LC1537B-77, tios39a, MC1_16S_85, KZNMV-10-B77 , Aeroplankton_a7) | 47 | 84 – 99 |
| | uncultured crenarchaeote | 1 | 90 |
| | Unidentified bacterium wb1_H02 | 1 | 90 |
| | Unidentified bacterium wb1_D15 | 1 | 86 |
| | Uncultured soil bacterium clone 1_A5 | 1 | 88 |
| | uncultured soil bacterium | 1 | 88 |
| | Uncultured organism clone ctg_NISA320 | 1 | 99 |
| | Bacterium DG981 | 1 | 97 |
| | Candidate division OP11 clone LGd2 | 1 | 89 |

The highest number of clones obtained were 3 clones for uncultured *plantomycete* bacterium and 3 clones for uncultured *bacteriodetes* bacterium, therefore no dominant species could be identified from these results. The obvious observation is the amount of unculturable bacterial clones which could not be identified through comparison to the database GenBank. 55 clones of bacterial species have been identified which could not be placed within a phylogenetic grouping, which then makes it extremely difficult to draw conclusions on the dominant grouping or species present in the fouling layer. However, a more recent taxomony database, EzTaxon, published in 2007, was utilised to try to identify the unculturable bacterial clones. EzTaxon is a free web-based tool for the analysis of all prokaryotic type strains 16S rRNA gene sequences to achieve identification of isolates based on pairwise nucleotide similarity values and phylogenetic inference methods. EzTaxon taxomony database has the advantage over other databases in that other public databases have been flooded with sequences of non-type strains including environmental clones and may contain erroneous and mislabeled sequences [130]. Therefore through the use of EzTaxon, the unculturable bacterial clones could be identified and conclusions on the dominant groupings present within the foulant biofilm can be made.

Table 3.2 shows the results of the DNA analysis, including the identified unculturable bacterial clones using the EzTaxon database. The sequenced clones had similarity which ranged from 73% to 99% and 7 phylum-based different microbial groups were identified. Figure 3.2 shows the most abundant bacterial groups present within the foulant layer. *Proteobacteria* (47%) was determined to be the most abundant identified group, with *γ-Proteobacteria* being the most predominant class within the phylum. The next most abundant grouping was the *Bacterioidetes* (23%) and *Plantomycetes* (12%). The *Bacterioidetes* phylum consisted of two classes of bacterium, *Sphinghobacteria* and *Flavobacteria*. Previous bacterial identification with the GenBank database did not show a representation of *Flavobacteria* class of bacteria but only showed *Sphingobacteria*. There were a few bacterial species which demonstrated high clone numbers. 5 clones of *Gemmata obscuriglobus* UQM 2246 from the phylum *Planctomycetes* were obtained with a similarity of 83-85% and 6 clones were obtained for *Haliangium tepidum* from the phylum *δ-Proteobacteria* with a similarity of 90-93%. However, due to the relatively low similarity values it cannot be said that these are the actual bacterial species present in high clone numbers. The results obtained using

EzTaxon cannot be taken as very accurate, due to the low similarity values obtained and the fact that the database is relatively recent and has yet to be extensively used within the literature. However, this approach has allowed for the dominant phylum and class to be identified within the foulant layer present on the RO membrane.

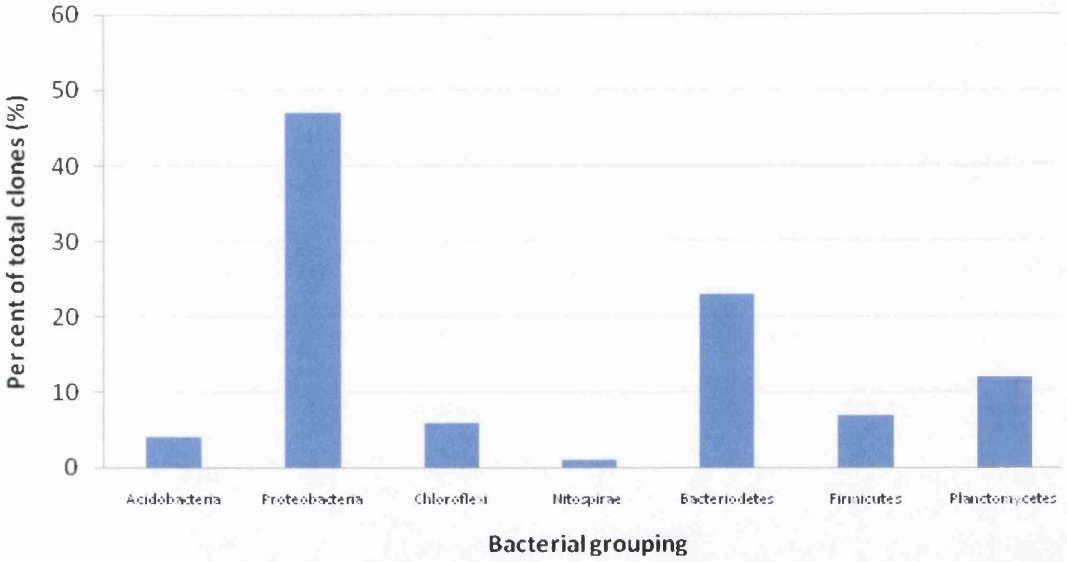


Figure 3.2 – Microbial community structure on fouled RO membranes as identified by EzTaxon

The microbial diversity analysis has shown a complex and varied community of many bacterial species present within the membrane fouling layer. A possible explanation for the appearance of such a complex community of bacterial species with varying physiological traits is most likely due to selective promotion of growth of the different species under changing process conditions, as RO plant conditions are highly dynamic and are operated under a high pressure environment.

**Table 3.2 Results from DNA Analysis of fouled RO Membrane using EXtaxon database**

| Phylogenetic lineages | Closest Relative in Gen Bank | No of Clones | Similarity % |
|---|---|---|---|
| Acidobacteria | Candidatus Solibacter usitatus Ellin6076 | 4 | 81 – 85 |
| α-Proteobacteria | Prosthecomicrobium consociatum | 1 | 91 |
| | Parvularcula bermudensis HTCC2503 | 3 | 87 – 94 |
| | Wenxinia marina | 1 | 85 |
| | Loktanella koreensis | 1 | 87 |
| | Tropicimonas isoalkanivorans | 1 | 95 |
| | Erythrobacter flavus | 1 | 99 |
| β-Proteobacteria | Limnobacter sp. DG1290 | 2 | 98 - 99 |
| | Limnobacter thiooxidans | 3 | 90 - 96 |
| | Curvibacter delicates | 2 | 98 |
| | Thauera terpenica | 1 | 88 |
| | Azoarcus communis | 1 | 83 |
| | Azoarcus indigens | 1 | 85 |
| | Malikia spinosa | 2 | 85 |
| γ-Proteobacteria | Balneatrix alpaca | 2 | 93 |
| | Simiduia agarivorans strain SA1 | 1 | 98 |
| | Cellvibrio mixtus subsp. Mixtus | 1 | 97 |
| | Gamma proteobacterium N2yML2 | 2 | 95 |
| | Endosymbiont of unidentified scaly snail | 1 | 89 |
| | Escherichia coli | 1 | 99 |
| | Natronocella acetinitrilica strain ANL 6-2 | 1 | 85 |
| | Shigella flexneri | 2 | 99 |
| | Thermomonas haemolytica | 2 | 86 – 87 |
| | Thiohalocapsa marina | 2 | 87 |
| | Legionella gresilensis | 1 | 83 |

Table 3.2 continued.

| | | | |
|---|---|---|---|
| δ-Proteobacteria | Sorangium cellulosum | 1 | 85 |
| | Desulfonatronum cooperativum | 1 | 77 |
| | Desulfonatronum lacustre | 1 | 78 |
| | Haliangium tepidum | 6 | 90 - 93 |
| | Geobacter metallireducens GS-15 | 1 | 85 |
| | Hippea maritime | 1 | 73 |
| Chloroflexi | Caldilinea aerophila | 4 | 83 - 86 |
| | Leptolinea tardivitalis | 1 | 83 |
| | Bellilinea caldifistulae | 1 | 82 |
| Nitrospirales | Nitrospira marina Nb-295 | 1 | 84 |
| Firmicutes | Clostridium sp. Enrichment culture clone MB3_7 | 1 | 99 |
| | Clostridium sp. JB-1 | 1 | 99 |
| | Sporacetigenium mesophilum strain ZLJ115 | 2 | 98 |
| | Bacillus massiliensis | 1 | 80 |
| | Fusibacter paucivorans | 1 | 95 |
| | Geosporobacter subterraneus | 1 | 95 |
| Planctomycetes | Uncultured planctomycete clone GASP-77KB-802-B05 | 1 | 89 |
| | Zavarzinella Formosa | 4 | 83 – 85 |
| | Blastopirellula marina DSM 3645 | 1 | 84 |
| | Gemmata obscuriglobus UQM 2246 | 5 | 83 – 85 |
| | Blastopirellula marine DSM 3645 | 1 | 87 |
| Sphingobacteria | *Flexibacteraceae* bacterium MOLA 398 | 1 | 94 |
| | Marinoscillum pacificum | 1 | 87 |
| | Flexibacter sp. R2A36-4 | 1 | 85 |
| | Thermonema lapsum | 3 | 83 - 84 |
| | Candidatus Aquirestis calciphila | 4 | 85 |

Table 3.2 continued.

| | | | |
|---|---|---|---|
| | Adhaeribacter aquaticus | 3 | 85 - 86 |
| Environmental Sample | Caldithrix abyssi LF 13 | 1 | 86 |
| Flavobacteria | Owenweeksia hongkongensis | 4 | 86 – 89 |
| | Fluviicola taffensis | 1 | 92 |
| | Winogradskyella poriferorum | 1 | 90 |
| | Yeosuana aromativorans | 2 | 87 – 86 |
| | Flavobacterium indicum | 2 | 84 |

In a similar investigation Bereschenko *et al* [42] utilised 16S rRNA gene sequencing to determine the microbial community present on a biofouled RO membrane. The majority of the microorganisms in the biofilm (59%) were related to the phylum *Proteobacteria*, where α-*Proteobacteria* subdivision was the most numerically encountered in the biofilm at 35%, *β-Proteobacteria* subdivision was the second largest fraction at 14% and γ- *Proteobacteria* bacterial clones made up 9% of the membrane community. A dominance of *Sphingomonas* species was observed within the membrane and throughout the RO plant as 27% of all clones were of the *Sphingomonas* species. Therefore the authors suggested that this is an important organism contributing to the biofouling of the RO membrane.

Chen *et al* [43] found that the results through 16S rDNA sequencing revealed a diverse range of bacteria divisions in the microbial communities present on UF and RO membranes obtained from full-scale water purification processes. Overall *Proteobacteria* was found to be the predominant group in UF and RO membrane biofilm samples, where α-*Proteobacteria* was the largest microbial fraction followed by the second largest microbial fraction, γ-*Proteobacteria,* for both membranes. Also *Planctomycetes* and *Fibroacter/Acidobacteria* were the second most predominant bacterial clones on both RO and UF membranes. The authors suggested that members of the α-*Proteobacteria* and γ- *Proteobacteria,* could be responsible for part of the biofouling problem on the membranes. Lee *et al* [122] also utilised the 16S rDNA

sequence and constructed gene libraries to examine the microbial communities of RO membrane samples and the seawater intake. *α-Proteobacteria* was found to be the most abundant bacterial group on the membrane surface, while the next most abundant clones were *Bacteriodetes* and *Flavobacteria.* The phylum *Firmicute* and *Planctomycetes* were also found in the foulant layer on the RO membranes.

Therefore from previous investigations into the microbial community present on fouled RO membranes, the *Proteobacteria* is identified as the most predominant phylum existing in the fouling layer. This confirms the findings of this current study as *Proteobacteria* was determined to be the most abundant identified group, using GenBank (17%) and EzTaxon (47%). All three previous investigations identified α-*Proteobacteria* subdivision as the largest microbial fraction, however the current findings identify γ-*Proteobacteria* (16%) as the largest microbial fraction, with β-*Proteobacteria* (12%) as the second largest microbial fraction within the *Proteobacteria* phylum. However, Chen *et al* [43] identified that second largest microbial fraction was γ-*Proteobacteria* in the fouled RO membrane. Therefore, from previous and current investigations it can be seen that fouling layers found on RO membranes from differing water purification processes are composed predominantly from the *Proteobacteria* phylum and therefore the bacteria from this phylum can pose major biofouling hazard to RO membranes. Other bacterial groupings identified from previous investigations, such as *Planctomycetes*, *Acidobacteria*, *Bacteriodetes* and *Firmicute*, have also been found within the RO fouling layer currently under study, therefore suggesting common foulant bacteria groupings. This present research successfully allowed the identification of the different types of microbes that cause significant fouling on RO membranes retrieved from the Fujairah desalination plant.

This research work was conducted in collaboration with YoungPil Chun, a Masters student who studied at GIST, South Korea as part of a British Council funded project investigating membrane fouling. Youngpil used the same fouled RO membranes to determine microbial diversity through Culture Dependent Method, see Appendix D. The culture-dependant method results showed that the most abundant grouping was *γ-Proteobacteria,* which confirms the results of the current culture-independent method performed on the same sample. The culture-dependent method only identified 3 phylum-based different microbial groups; α -, *β-Proteobacteria*, *Firmicutes* and

*Sphingobacteria*, unlike the culture-independent method which discovered 7 phylum-based groups. This demonstrates the limitation of the culture-dependent technique for determination of microbial diversity. Only less than 1% of bacteria in nature can be cultured with current standard laboratory culturing techniques which accounts for the limitation in culture-dependent methods [34, 37]. Therefore the culture-independent method of direct extraction of genomic DNA from the foulant biofilm on the membrane surface is again confirmed to allow for the identification of a large proportion of microbes that are not readily cultured within a laboratory setting, giving a more accurate population and structural representation of the bacterial community within RO membrane fouling layers.

For the continuation of the research, the four bacterial species isolated from the RO fouling layer using the culture-dependant method performed by Youngpil Chun were then examined by experimental methods to unravel the mechanisms of bacterial adhesion to the RO membrane. Three bacterial species, *Vibrio* sp. PM6A *A.venetianus, K.pnuemoniae* subsp. *pneumonia*, all from the subdivision *γ- Proteobacteria* were chosen as *γ- Proteobacteria* was the most abundant microbial grouping with the phylum *Proteobacteria* present within the RO membrane foulant layer. One uncultured bacterium that could not be identified was chosen due to high unculturable bacterium obtained from the RO membrane when using the established database GenBank. Another reason the bacterial species were chosen was due to their ability to display high colony units when grown and therefore were determined to be easily culturable in laboratory conditions. The bacteria species were then characterised in terms of surface charge at process relevant conditions at Swansea University for the understanding of the role surface charge plays within the mechanism of bacterial adhesion.

## 3.2.2 Bacterial Surface Charge

The determination of surface charge properties is of great importance for the understanding of cell function and behaviour within various environments, as determination of cell surface charge can aid in the elucidation of cell adhesion to membrane surfaces within process conditions [16, 18, 19]. For the determination of bacterial surface charge the technique of ELS has been utilised for determination of electrophoretic mobility at various process relevant NaCl concentrations and $MgCl_2$ and

$CaCl_2$ concentrations. The electrophoretic mobility of each bacterial species was measured at NaCl concentrations of 0.1, 0.3, 0.6 and 0.8M, at pH values 3 to 9 to determine the effect on bacterial surface charge. Also the effect of increasing $Mg^{2+}$ and $Ca^{2+}$ ion concentration, whilst maintaining a constant ionic strength at pH 7, was also investigated to determine if the $Mg^{2+}$ and $Ca^{2+}$ ion concentration had an effect on bacterial cell surface charge. The electrophoretic mobility values have been plotted to visualize the trends in the data instead of values of zeta potential as there may be slight discrepancies in the values of viscosity and dielectric constant for the high salt concentration solutions. However, the zeta potential values have been calculated, as shown in Tables 3.3 and 3.4 for comparison to previous literature.

Figures 3.3, 3.4 and 3.5 show that for *Vibrio* sp. PM6A, *A.venetianus* and *K.pnuemoniae* subsp. *Pneumonia,* the electrophoretic mobility becomes more negative with increasing pH where the mobility values level off at higher pH values. However, for *Vibrio* sp. PM6A (Figure 3.3) the electrophoretic mobility performed at 0.8M shows only a gentle slope of the mobility becoming less positive with increasing pH values. For the uncultured bacterium (Figure 3.6), the mobility values fluctuate slightly with increasing pH but do not show significant changes in mobility as seen with the other bacteria. Table 3.3 shows the values and ranges for electrophoretic mobility and zeta potential experienced by the bacterial species over conditions of varying NaCl concentrations and pH values.

| **Bacterial species** | **Electrophoretic Mobility ($\mu m\ cm\ V^{-1}\ s^{-1}$)** | | | **Zeta Potential (mV)** | | |
|---|---|---|---|---|---|---|
| | *minimum* | *maximum* | *Mean St Dev (+/-)* | *minimum* | *maximum* | *Mean St Dev (+/-)* |
| *Vibrio sp. PM6A* | -1.104 | 0.372 | 0.12 | -14 | 4.7 | 1.58 |
| *K.pnuemoniae* subsp. *Pneumonia* | -1.759 | 0.267 | 0.15 | -22.4 | 3.4 | 1.91 |
| *A.venetianus* | -1.886 | 0.219 | 0.15 | -24 | 2.8 | 1.87 |
| Uncultured bacterium | 0.1 | 0.616 | 0.13 | 1.3 | 7.8 | 1.67 |

Table 3.3 The range of Electrophoretic Mobility and Zeta Potential measurements obtained at pH 3 to 9 for the four bacterial isolates grown in stirred conditions.

Figures 3.3, 3.4 and 3.5 also show the trend that as the NaCl concentration increases, the electrophoretic mobility becomes less negative for the pH values 3 to 9. This trend exists for all three *γ- Proteobacteria* bacterial species, *Vibrio* sp. PM6A *A.venetianus, K.pnuemoniae* subsp. *pneumonia.* This could be due to the compression of the electric double layer surrounding the bacterial species with increasing salt concentration as explained by the DLVO theory (see section 1.3) in which the electrophoretic mobility measurements of the bacterial species become less negative for all pH values. However, the uncultured bacterium exhibited only marginal changes in electrophoretic mobility becoming more positive with increasing NaCl concentrations (Figure 3.6). From Table 3.3 it can be seen that *A.venetianus* experiences the most negative mobility values, followed by *K.pnuemoniae* subsp. *Pneumonia* which experiences slightly less negative mobility values, followed by *Vibrio* sp. PM6A, which experiences much less negative mobility values when compared to the other two bacterial species. However, again the uncultured bacterium displays dissimilar behavior to the other bacterial species as all the mobility values for the uncultured bacterium at all NaCl concentrations and pH values are positive unlike the other bacterial species which have both positive and negative electrophoretic mobility values.

The isoelectric point is normally defined as zero zeta potential, i.e. the pH value when the plot of zeta potential versus pH crosses the zero axis. It is an important parameter as it is normally the point where colloidal systems are the least stable. *Vibrio* sp. PM6A displays two IEP's, one at pH 3.2 for 0.3M and at pH 3.9 for 0.6M NaCl. *A. venetianus* displays one IEP at pH 3.3 for 0.8M NaCl and also *K. pnuemoniae* subsp. *pneumonia* displays one IEP at pH 3.4 for 0.8M. However uncultured bacterium does not display a IEP, due to the bacterium having all positive electrophoretic mobility values. The context of the zeta potential and the IEP values with previous research is discussed below.

*Vibrio* sp. PM6A, *A.venetianus* and *K.pnuemoniae* subsp. *Pneumonia* all belong to the bacterial grouping *γ-Proteobacteria* and show similar behaviour in electrophoretic mobility in variations of pH values and NaCl concentrations. It is not known to what phylum the uncultured bacterium belongs, however the results obtained for this bacterium are dissimilar to the other bacterium which seems to indicate that this bacterium may not be part of the *γ-Proteobacteria* grouping. The three bacterial species

from most predominant grouping, *γ-Proteobacteria,* display a negative surface charge in similar conditions to seawater, 0.6M and pH 7 - 8. The negative charge on the bacteria could influence bacterial attachment to the membrane surface as if the membrane surface is also negative (see Chapter four) in seawater conditions then it is an unfavourable condition for bacterial cell attachment, as the bacterial surface will experience repulsive forces from the membrane surface. Therefore the mechanism of cell attachment and subsequent biofilm formation within the Fujairah desalination plant for these bacterial species could be due to other bacterial cell characteristics, such as surface hydrophobocity. However the uncultured bacterium displays a positive surface charge in conditions similar to seawater so the bacterium would experience attractive forces towards a possible negative membrane surface and therefore this situation would be favourable for cell attachment to the membrane surface. Also the measurement of the membrane surface charge in different salt solutions is required for explanation of the results obtained from this present study (Chapter 4).

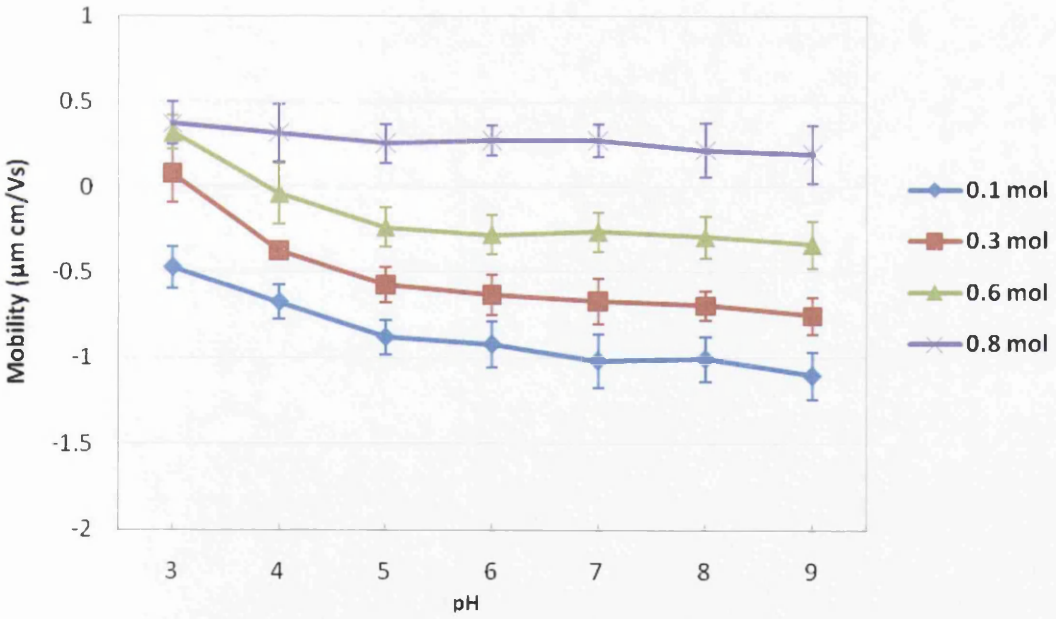


Figure 3.3 Electrophoretic mobility of *Vibrio* sp. PM6A at varying NaCl conc. as a function of pH in stirred conditions at a constant temperature.

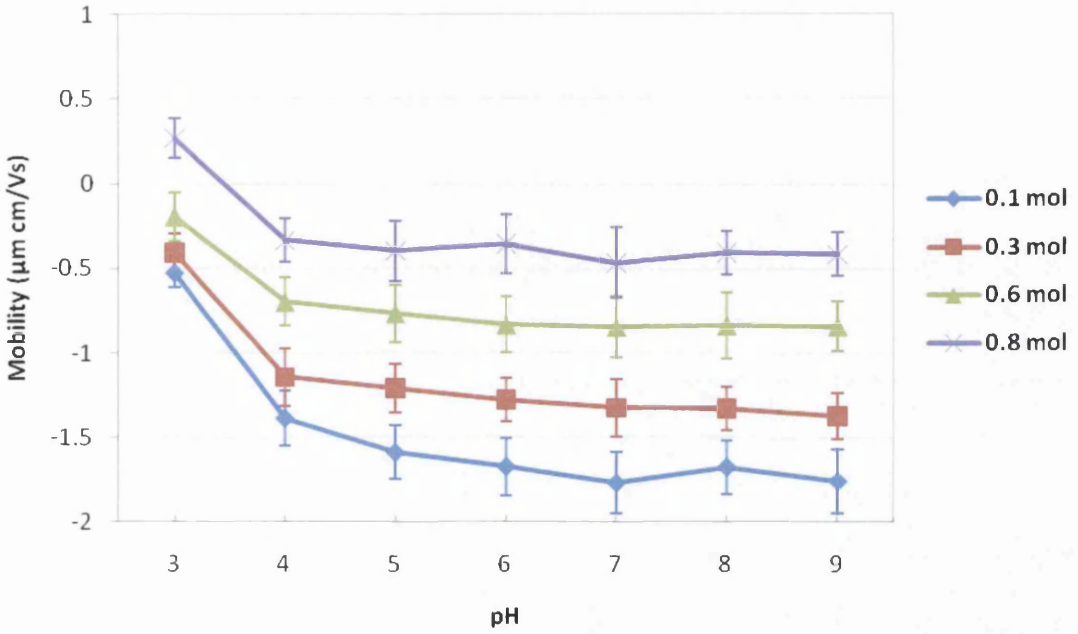


Figure 3.4 Electrophoretic mobility of *K.pneumoniae* subsp. *Pneumonia* at varying NaCl conc. as a function of pH in stirred conditions at a constant temperature.

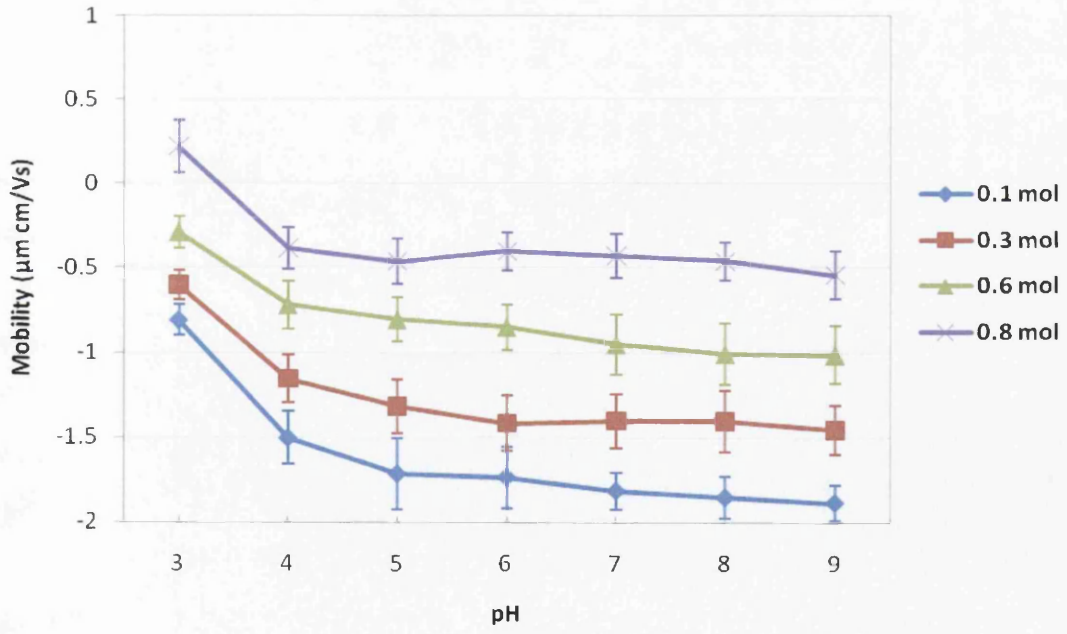


Figure 3.5 Electrophoretic mobility of *A.venetianus* at varying NaCl conc. as a function of pH in stirred conditions at a constant temperature.

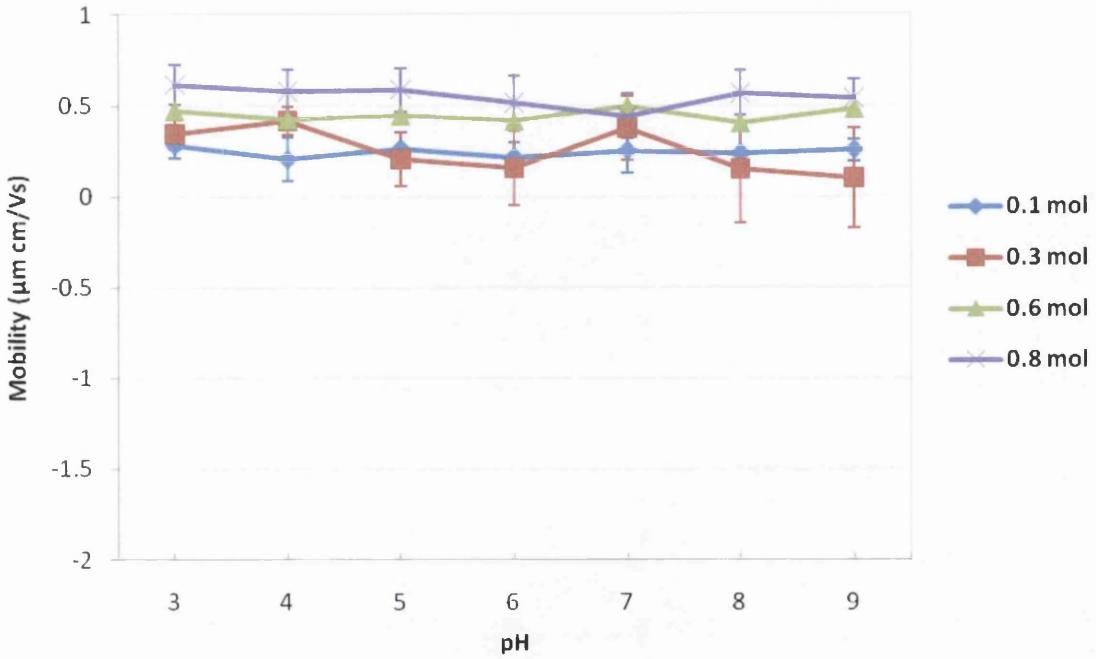


Figure 3.6 Electrophoretic mobility of Uncultured bacterium at varying NaCl conc. as a function of pH in stirred conditions at a constant temperature.

Another experiment was performed by altering the growth conditions of the bacterial species. During plant operation, there will be changing conditions within the highly dynamic and high pressure environment of the RO plant, where the different conditions during plant operation could favour selective promotion of different bacterial species due to their varying physiological traits. Therefore, the growth conditions were altered so that the bacteria were grown in stationary conditions, such that the bacteria inoculated media was not shaken during growth but just kept at a constant temperature. This experiment was performed on all four bacterial species isolates, again measuring the electrophoretic mobility at different NaCl concentrations of 0.1, 0.3, 0.6 and 0.8M, at pH values 3 to 9.

Figures 3.7, 3.8 and 3.9 show for *Vibrio* sp. PM6A, *A.venetianus* and *K.pnuemoniae* subsp. *Pneumonia,* that the electrophoretic mobility becomes more negative with increasing pH, where the mobility values level off at higher pH values. The changes in growth conditions have not altered the shape of curve for the bacterial species, only

slight changes have been observed between the growth condition curves. For *Vibrio* sp. PM6A (Figure 3.7) the electrophoretic mobility performed at 0.8M shows only a gentle slope in the mobility becoming more negative with increasing pH values. For the uncultured bacterium (Figure 3.10), the mobility values show a gentle change in becoming more negative with increasing pH for the NaCl concentrations of 0.1M and 0.3M however, no significant change in mobility is seen for the concentrations of 0.6M and 0.8M. Table 3.4 shows the values and ranges of electrophoretic mobility and zeta potential experienced by the bacterial species over all the salt concentrations and pH values conditions.

Figures 3.7, 3.8 and 3.9 also show the trend that as the NaCl concentration increases, the electrophoretic mobility becomes less negative for the pH values 3 to 9. This trend still exists for all three *γ- Proteobacteria* bacterial species, *Vibrio* sp. PM6A *A.venetianus, K.pnuemoniae* subsp. *pneumonia* with changing growth conditions. The uncultured bacterium (Figure 3.10) exhibited only a small change in the electrophoretic mobility becoming more positive with increasing NaCl concentrations, however this was a greater change in mobility values than that seen with stirred growth conditions. From Table 3.4 it can be seen that *A.venetianus* experiences the most negative mobility values, followed by *K.pnuemoniae* subsp. *Pneumonia* which experiences slightly less negative mobility values, followed by *Vibrio* sp. PM6A, which experiences much less negative and more positive mobility values when compared to the other two bacterial species. However, the uncultured bacterium displays dissimilar behavior to the other bacterial species as all the mobility values it displays are positive unlike the other bacterial species which display either negative or both positive and negative electrophoretic mobility values. Similar behavior was exhibited in stirred conditions.

*Vibrio* sp. PM6A displays three IEP's, one at pH 3.15 for 0.1M, pH 3.3 for 0.3M NaCl and at pH 5.6 for 0.6M. Also *K. pnuemoniae* subsp. *pneumonia* displays three IEP's at pH 3 for 0.3 mol, pH 3.5 for 0.6M and at pH 4 for 0.8M. However, the uncultured bacterium and *A. venetianus* do not display a IEP, due to the uncultured bacterium having all positive electrophoretic mobility values and the *A. venetianus* having all negative mobilities.

| Bacterial species | Electrophoretic Mobility ($\mu m\ cm\ V^{-1}\ s^{-1}$) | | | Zeta Potential (mV) | | |
|---|---|---|---|---|---|---|
| | *minimum* | *maximum* | *Mean St Dev (+/-)* | *minimum* | *maximum* | *Mean St Dev (+/-)* |
| *Vibrio sp. PM6A* | -0.953 | 0.501 | 0.12 | -12.1 | 6.4 | 1.52 |
| *K.pnuemoniae* subsp. *Pneumonia* | -1.747 | 0.318 | 0.18 | -22.2 | 4 | 2.3 |
| *A.venetianus* | -2.071 | -0.183 | 0.17 | -26.4 | -2.3 | 2.2 |
| Uncultured bacterium | 0.048 | 0.561 | 0.14 | 0.6 | 7.1 | 1.77 |

Table 3.4 The range of Electrophoretic Mobility and Zeta Potential measurements obtained at pH 3 to 9 for the four bacterial isolates grown in stationary conditions.

Through comparison to the stirred growth conditions it can be seen that the uncultured bacterium and *A. venetianus* have slightly more negative electrophoretic values when grown in stationary conditions unlike *Vibrio* sp. PM6A and *K. pnuemoniae* subsp. *Pneumonia* which have slightly more positive values, which leads to an increase in the number of IEP obtained in the different NaCl concentrations for these bacterial species. However the standard deviation of the electrophoretic mobility measurements are relatively large due to the sample being biological and therefore heterogeneous in nature. This may account for the slight change in the electrophoretic charge for the stationary conditions when compared to the stirred conditions. Growth conditions are thought to influence the cell surface characteristics [112], therefore as zeta potential is dependent on the cell surface, it was thought that growth conditions may have an effect on cell surface charge, however from the results it can be determined that a change from stationary to stirred growth conditions have not had a dramatic impact on the values of electrophoretic mobility.

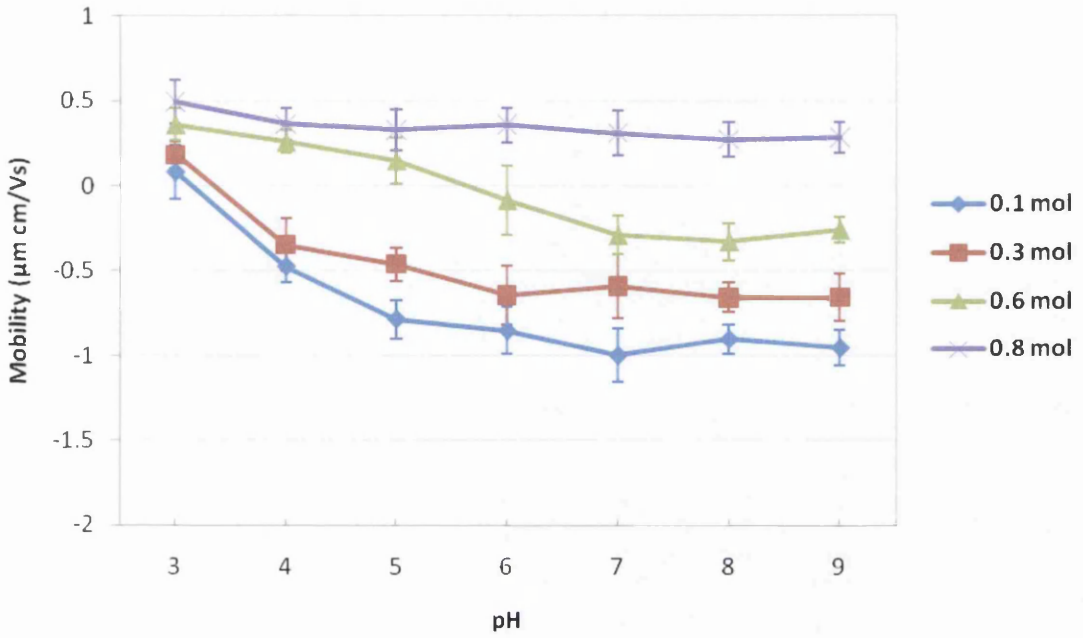


Figure 3.7 Electrophoretic mobility of *Vibrio* sp. PM6A, grown in stationary conditions at a constant temperature, at varying NaCl conc. as a function of pH.

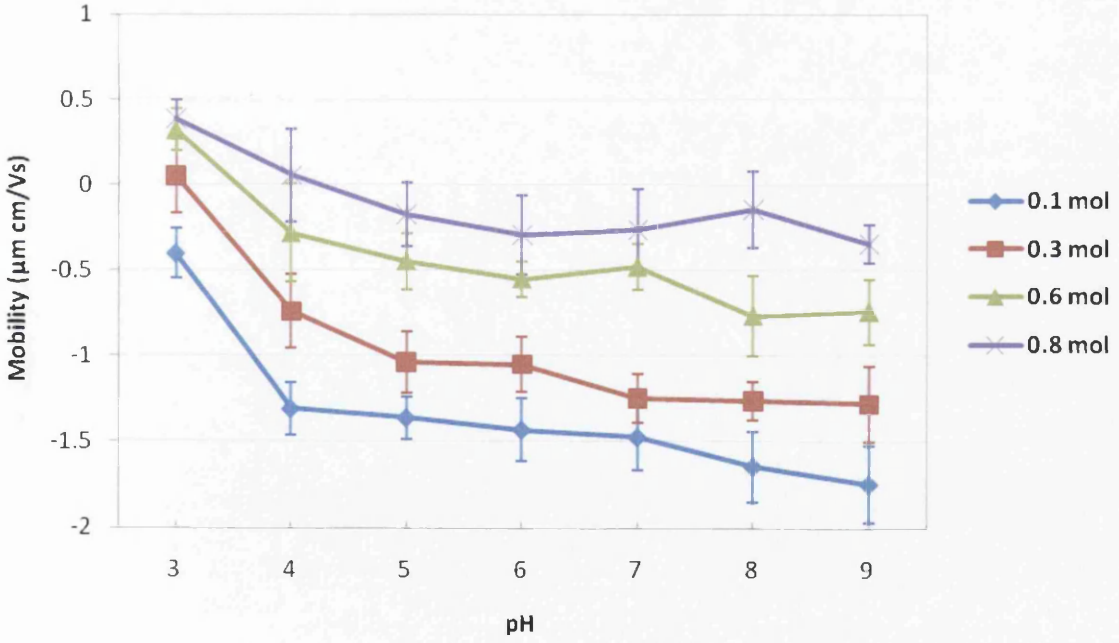


Figure 3.8 Electrophoretic mobility of *K.pneumoniae* subsp. *Pneumonia*, grown in stationary conditions at a constant temperature, at varying NaCl conc. as a function of pH.

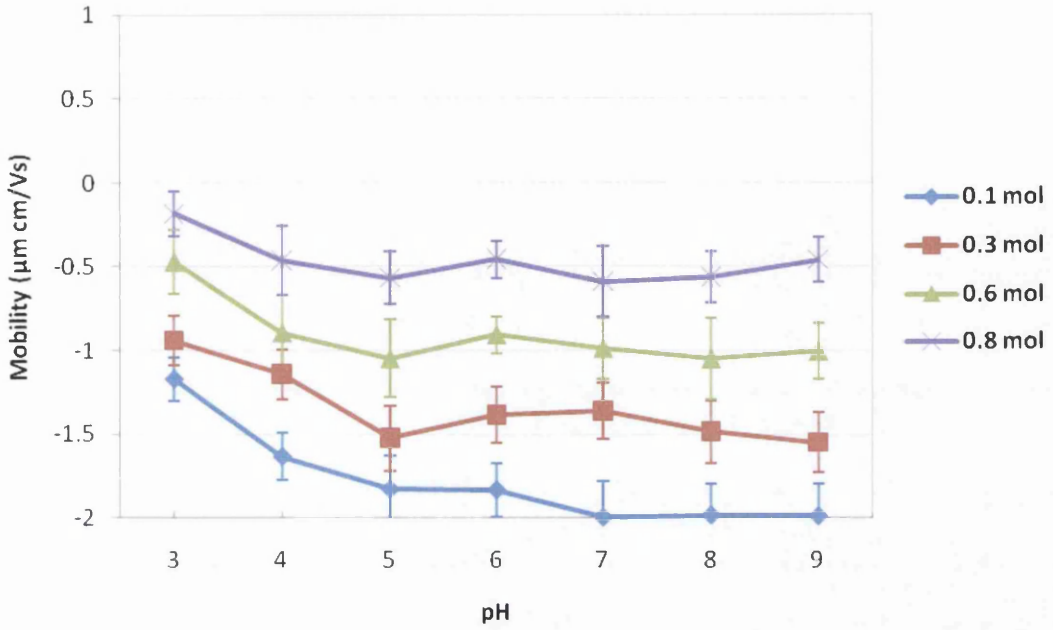


Figure 3.9 Electrophoretic mobility of *A.venetianus*, grown in stationary conditions at a constant temperature, at varying NaCl conc. as a function of pH.

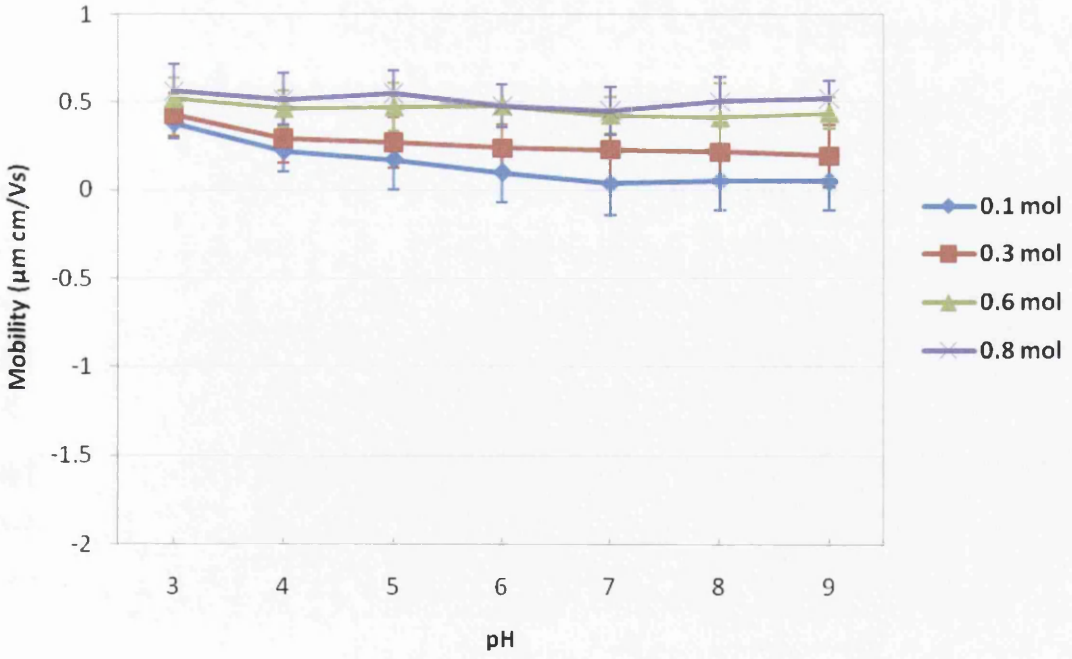


Figure 3.10 Electrophoretic mobility of Uncultured bacterium, grown in stationary conditions at a constant temperature, at varying NaCl conc. as a function of pH.

Previous research from other research groups have measured zeta potentials for a wide range of gram-positive and gram-negative bacteria, where the zeta potentials values become more negative systemically with increasing pH revealing an isoelectric point of 1 to 4 [16, 131]. Also Bayer *et al* [123] performed electrophoretic mobility on a variety of gram-negative and gram-positive bacteria, where under standard growth conditions and neutral pH all cells displayed a negative electrophoretic mobility. This confirms the results of this current study for the bacterial species *Vibrio* sp. PM6A, *A.venetianus* and *K.pnuemoniae* subsp. *pneumonia.* However the results for the uncultured bacterium are not confirmed by previous research findings, due to the bacterium possessing all positive values of zeta potential.

There are only extremely limited studies which have examined the cell surface charge of these four bacterial strains. Baldi *et al* [132] measured the zeta potential of a recently described *A. venetianus* VE-C3 in only the conditions of 0.1M NaCl at the pH of 6.5 where the electrophoretic mobility -1.04 $x10^{-8}$ $m^2V^{-1}s^{-1}$ and a zeta potential of -13.3 mV was measured. Baldi also measured this bacterial species in seawater at pH 8.0 where the electrophoretic mobility was $-0.81x10^{-8}$ $m^2V^{-1}s^{-1}$ and the zeta potential was -10.5 mV. Dorobantu *et al* [133] briefly measured the zeta potential of the newly named *A. venetianus* RAG-1 in 0.1M phosphate buffer at pH 7.0 to be -13.7 +/-0.4 mV. The current study has found for the stirred conditions that at 0.1M NaCl and pH 7, the electrophoretic mobility was -1.855 $x10^{-8}m^2V^{-1}s^{-1}$ and the zeta potential was -23.6 +/-2.5mV. At 0.6M NaCl at pH 8.0 the electrophoretic motility was -1.006 $x10^{-8}$ $m^2V^{-1}s^{-1}$ and the zeta potential was -12.8 +/- 2.3 mV. Therefore when compared to the previous research by Baldi and Dorobantu conducted at 0.1M salt concentration at pH 6.5 – 7, the results obtained by this current study are more negative. Also compared to the experiment conducted in sea water at pH 8, the closest current conditions are at 0.6M NaCl at pH 8, where the results obtained by this current study are only slightly more negative. This difference could be accounted for as *A.venetianus* is only a newly found bacterial species and only 5 strains have been identified for the species. Therefore the bacteria under study may be of a different strain to the bacteria studied in the literature. Baldi [132] also demonstrated for *A.venetianus* that an increase in salt concentration from 0.1M NaCl to seawater exhibited in less negative electrophoretic mobility values. This correlates well with the findings of the present study.

Camprubf *et al* [134] measured the zeta potential of *K. pnuemoniae* in 0.5mM $NaH_2PO_4$ and Szabo *et al* [135] measured the zeta potential of *K. pnuemoniae* grown in one high and one low nutrient concentration in just the one buffer condition of 0.05M $KH_2PO_4$ at pH 7.2. The electrophoretic mobility of the full strength culture was -1.96 +/-0.26 μm cm $V^{-1}$ $s^{-1}$ (zeta potential: -24.7+/-3.3mV), while the dilute culture was -2.85+/- 0.17 μm cm $V^{-1}$ $s^{-1}$ (zeta potential: -35.9 +/-2.2 mV). However no literature has been found for *K. pnuemoniae* subsp. *pneumonia.* The current study has found for the stirred conditions at 0.1M NaCl at pH 7, the electrophoretic mobility is -1.768 $x10^{-8}m^2V^{-1}s^{-1}$ and the zeta potential was -22.5 +/- 2.3mV of *K.pnuemoniae* subsp. *pneumonia.* These results correlate well with the electrophoretic mobility values obtained by Camprubf *et al* [134] for the *K. pnuemoniae* grown in a high nutrient concentration.

Zeta measurements of *V.alginolyticus* cells have also been performed but no literature has been found of the zeta measurements for the bacterial species *Vibrio* sp. PM6A [136]. Morisaki *et al* [136] calculated the electrophoretic mobility of *V. alginolyticus* to ranges between $-1.6x10^{-8}$ to $-1.9 \times 10^{-8}$ $m^2V^{-1}s^{-1}$ for ionic strengths 0.01 to 0.15M at pH 7.4. The zeta potential calculations ranged from -20.2 to -24.4 mV for ionic strength 0.01 to 0.15M. Current results performed at 0.1M at pH 7 show the electrophoretic mobility to be $-1.018 \times 10^{-8}$ $m^2V^{-1}s^{-1}$ and the zeta potential to be -13 +/- 2mV. The current values obtained in this study are therefore less negative than those obtained for other *Vibrio* species, however this difference could be accounted for as the *Vibrio* species under study is a different species to the one reported in the literature. Morisaki [136] also found that at low ionic strengths (0.02M), mobility became slightly less negative with the increment increase in ionic strength, but the mobility leveled off at high ionic strengths (0.15M). The results obtained from current study show that as the ionic strength increases, the electrophoretic mobility of *Vibrio* sp. PM6A becomes less negative incrementally for both low and high ionic strength values.

Figures 3.11 and 3.12 show the plots of electrophoretic mobility versus magnesium ion concentrations at the constant ionic strength of 0.1M and 0.6M at pH 7 to determine if $Mg^{2+}$ ion concentration had an effect on bacterial cell surface charge. At the constant ionic strengths of 0.1M (Figure 3.12) and 0.6M (Figure 3.11), the electrophoretic mobility becomes less negative and more positive gradually as the $Mg^{2+}$ ion concentration increases for the bacterial species *Vibrio* sp. PM6A, *A.venetianus* and

*K.pnuemoniae* subsp. *Pneumonia*. However the electrophoretic mobility fluctuates only slightly with increasing $Mg^{2+}$ ion concentration for the uncultured bacterium.

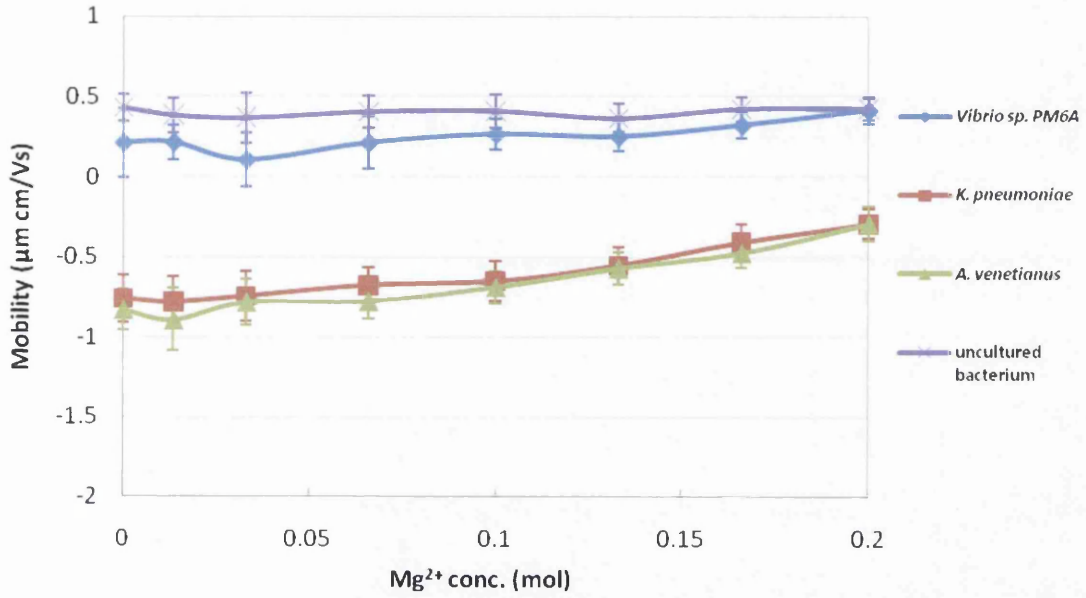


Figure 3.11 Electrophoretic mobility of four bacterial isolates at varying $Mg^{2+}$ conc. at 0.6M ionic strength.

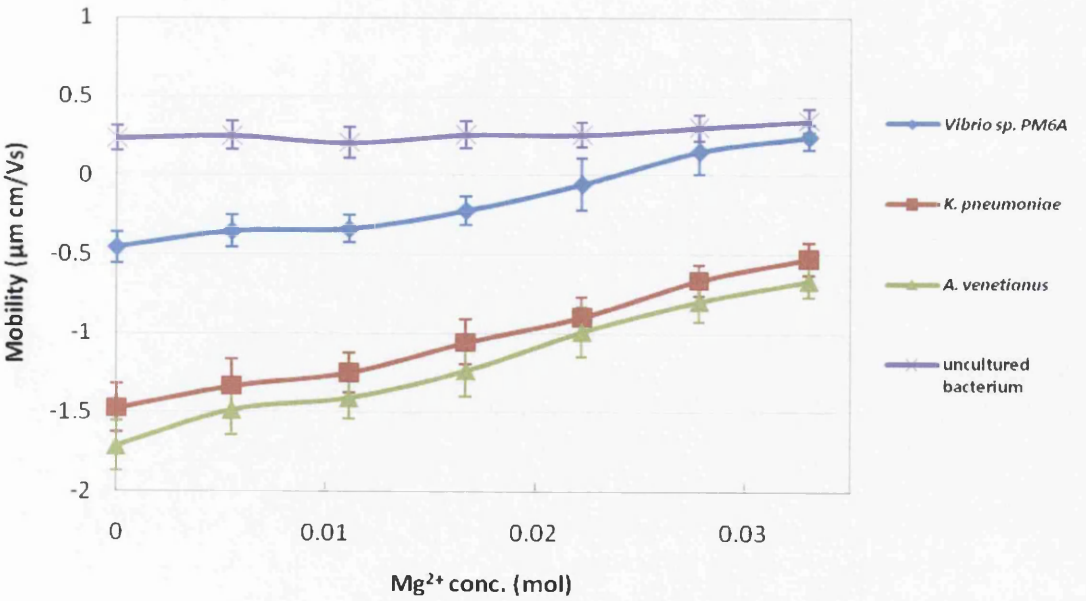


Figure 3.12 Electrophoretic mobility of four bacterial isolates at varying $Mg^{2+}$ conc. at 0.1M ionic strength.

For the 0.1M ionic strength, there is a steeper change in the electrophoretic mobility becoming less negative with increasing $Mg^{2+}$ ion concentration than that observed for the 0.6M ionic strength for all three bacterial species *Vibrio* sp. PM6A, *A.venetianus* and *K.pnuemoniae* subsp. *Pneumonia.* However for the uncultured bacterium, the change in $Mg^{2+}$ ion concentration does not seem to have an effect on the electrophoretic mobility values.

Figures 3.13 and 3.14 show the plots of electrophoretic mobility versus calcium ion concentration at the constant ionic strengths of 0.1M and 0.6M at pH 7 to determine if $Ca^{2+}$ ion concentration had an effect on bacterial cell surface charge. At the constant ionic strengths of 0.1M (Figure 3.14) and 0.6M (Figure 3.13), the electrophoretic mobility becomes less negative and more positive gradually as the $Ca^{2+}$ ion concentration increases for the bacterial species *Vibrio* sp. PM6A, *A.venetianus* and *K.pnuemoniae* subsp. *Pneumonia.* However the electrophoretic mobility fluctuates only slightly with increasing $Ca^{2+}$ ion concentration for the uncultured bacterium. For the 0.1M ionic strength, there is a steeper change in the electrophoretic mobility becoming less negative with increasing $Ca^{2+}$ ion concentration than that observed for the 0.6M ionic strength for all three bacterial species *Vibrio* sp. PM6A, *A.venetianus* and *K.pnuemoniae* subsp. *Pneumonia.* However for the uncultured bacterium, the change in $Ca^{2+}$ ion concentration does not seem to have much influence on the electrophoretic mobility values.

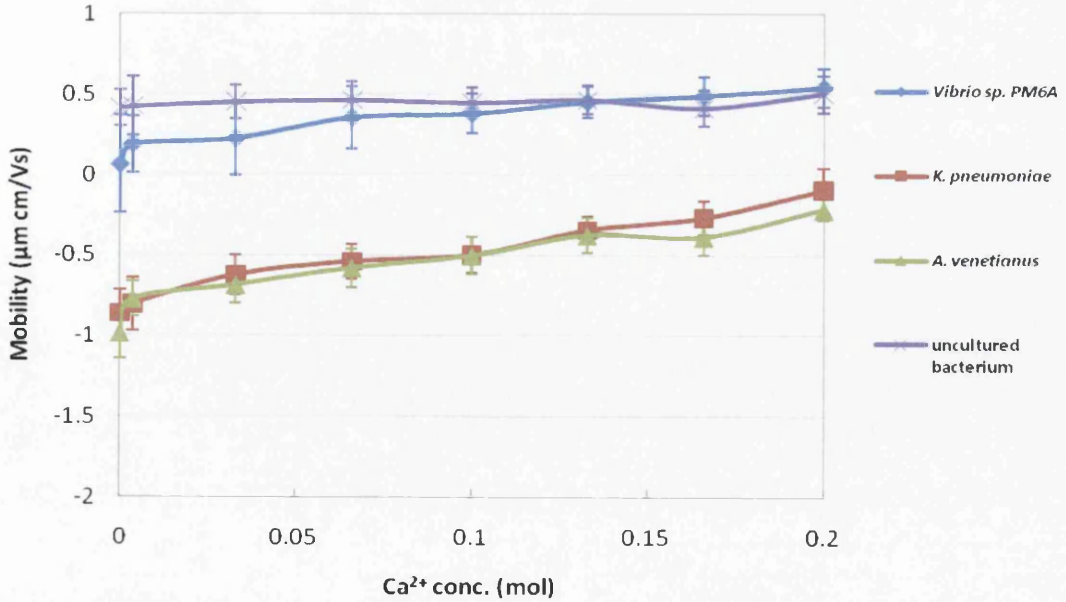


Figure 3.13 Electrophoretic mobility of four bacterial isolates at varying $Ca^{2+}$ conc. at 0.6M ionic strength.

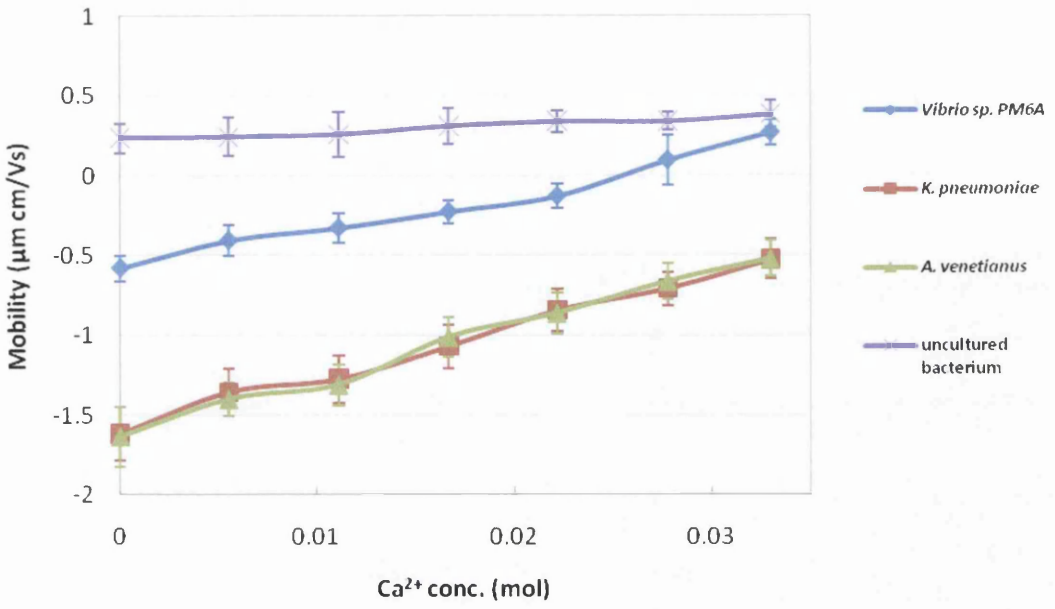


Figure 3.14 Electrophoretic mobility of four bacterial isolates at varying $Ca^{2+}$ conc. at 0.1M ionic strength.

Therefore for the three bacterial species from the class *γ-Proteobacteria,* as the divalent ions, $Mg^{2+}$and $Ca^{2+}$, increased in concentration, the electrophoretic mobility values, which infers cell surface charge, became less negative. The reason for this change could be due to the divalent ions forming part of the ion layers surrounding the bacterial cell, therefore masking the negative charge of the cell surface. The importance of such measurements are related to the composition of seawater. Seawater consists of a number of different cations, of which $Mg^{2+}$ and $Ca^{2+}$ are present in significant concentrations. RO membrane used in Fujairah desalination plant has a very high salt rejection of 99.8% (Appendix B) which means that not only will there be a concentration gradient of $Na^{+}$ at the membrane surface, but also a concentration gradient of the divalent ions $Mg^{2+}$ and $Ca^{2+}$. Also due to the divalent charge on the ions, the ions will be in a more favourable position to move towards a negatively charged membrane surface (Chapter 4) in seawater conditions and therefore the concentration gradient of divalent ions present at the membrane surface could influence the bacterial attachment to the membrane surface. The change in cell surface charge with increased concentrations of $Mg^{2+}$and $Ca^{2+}$ means that bacterial cell attachment to the RO membrane is more favourable with a concentration gradient of divalent ions

present at the membrane surface, which might explain the reason why high salt rejection RO membranes are susceptible to membrane fouling. No literature has been found relating the divalent ion concentration to the cell surface charge regarding these bacterial species.

## 3.4 Conclusions

The microbial diversity analysis has shown a complex and varied community of many bacterial species present within the membrane fouling layer. *Proteobacteria* was determined to be the most abundant identified group, with *γ-Proteobacteria* being the most predominant class within the phylum. The next most abundant grouping was the *Bacterioidetes* and *Plantomycetes*. Previous and current investigations indicate that fouling layers found on RO membranes from differing water purification processes are composed predominantly from the *Proteobacteria* phylum and therefore the bacteria from this phylum can pose a major biofouling hazard to RO membranes. Also, other bacterial groups identified from previous investigations, such as *Planctomycetes*, *Acidobacteria*, *Bacteriodetes* and *Firmicute*, have also been found within the RO fouling layer currently under study, therefore suggesting common foulant bacterial groupings. This research successfully allowed the identification of the different types of microbes that cause significant fouling on membranes. The identified bacteria were then used in the subsequent research of the thesis to bring industrial relevance to the study.

For the continuation of the research, the four bacterial species isolated from the RO fouling layer using the culture-dependant method were obtained; *Vibrio* sp. PM6A, *A.venetianus* and *K.pnuemoniae* subsp. *Pneumonia,* and an uncultured bacterium, where the three named bacterial species were chosen as they belong to the subdivision *γ-Proteobacteria,* which was determined to be the most abundant microbial grouping within the RO membrane foulant layer.

Cell surface charge was successfully measured over the bacterial species. The electrophoretic mobility results showed a strong dependence on pH and NaCl concentration for the bacterial species *Vibrio* sp. PM6A, *A.venetianus* and

*K.pnuemoniae* subsp. *Pneumonia.* These bacteria also possessed a negative surface charge under standard growth conditions and neutral pH, apart from 0.8M NaCl for the *Vibrio* sp. PM6A, which displayed a positive charge. However no strong dependence on pH and NaCl concentration was found for the uncultured bacterium and the bacterium showed a positive charge under standard growth conditions and neutral pH. Physical growth conditions were also determined not to have a significant effect on the electrophoretic mobility values. It was discovered that increasing the divalent ion concentration $Mg^{2+}$ and $Ca^{2+}$, altered the cell surface charge values for the three bacterial species *Vibrio* sp. PM6A, *A.venetianus* and *K.pnuemoniae* subsp. *Pneumonia.* However, the uncultured bacterium did not display a dependence on increasing $Mg^{2+}$ and $Ca^{2+}$ ion concentration. The importance of such measurements are related to the composition of seawater. Seawater consists of a number of different cations of which $Mg^{2+}$ and $Ca^{2+}$ are present in significant concentrations. RO membranes used in the Fujairah desalination plant have a very high salt rejection which means there will be a concentration gradient of the divalent ions $Mg^{2+}$ and $Ca^{2+}$ at the membrane surface, and therefore this concentration gradient of divalent ions at the surface could influence the bacterial attachment to the membrane surface. The changes in cell surface charge with increasing concentrations of $Mg^{2+}$and $Ca^{2+}$ means that bacterial cell attachment to the RO membrane is more favourable due to a concentration gradient of divalent ions present on the membrane surface, which might explain the reason why high salt rejection RO membranes are susceptible to membrane bio-fouling.

*Vibrio* sp. PM6A, *A.venetianus* and *K.pnuemoniae* subsp. *Pneumonia* all belong to the bacterial grouping *γ- Proteobacteria* and show similar behaviour in electrophoretic mobility in changes of pH and salt concentrations. However, it is not known the phylum the uncultured bacterium belongs to, however the results obtained for this bacterium are dissimilar to the other bacterial species which seems to indicate that this bacterium may not be part of the *γ- Proteobacteria* grouping.

These results will aid in the elucidation of mechanisms involved in bacterial cell adhesion to membrane surfaces within the RO desalination process conditions that result in biofouling. In addition, the bacterial zeta potential measurements will aid in the analysis of interaction data presented in Chapter 5.

# Chapter 4 Membrane Characterisation

## 4.1 Introduction

RO membranes are commercially important membranes that have been commonly used in water treatment, where these membranes prevent the passage of small molecules and simple ions. Due to RO membrane properties, such as significant surface roughness, RO membranes are susceptible to fouling [6]. The Fujairah Water and Power plant, located in the UAE, utilizes RO membranes for the desalination of seawater. The plant has experienced problems of increase of normalized differential pressure and decrease in normalized flow within plant operation, especially in the year 2006. When an autopsy was performed on old membranes after they were replaced in 2006, it was discovered that the membranes in the lead positions were in a poor condition due to fouling. Membrane replacement is a timely and expensive procedure which could be limited if membrane fouling could be reduced [8].

Membrane interactions and properties of the fouling layer are as a result of foulant characteristics, feedwater solution chemistry (pH, ionic strength, divalent cation concentration), membrane properties (hydrophobicity, surface charge, roughness) and hydrodynamic conditions within the plant (permeate flux, cross-flow or dead-end filtration velocity). Therefore the interactions between the membrane and foulant are normally specific to a particular membrane process and thus membrane fouling research should assess the fouling as a combination of many factors. Therefore to investigate the fouling mechanisms within the specific membrane process from Fujairah Water SWRO plant, the AFM was used to characterise clean and industrial fouled membrane surfaces through imaging and also through the analysis of the images to obtain data, such as height variation, foulant surface thickness and surface roughness. The analysis of the AFM images could help elucidate the fouling potential of the clean membrane surface and determine the foulant coverage of the industrially fouled membrane.

The morphology of RO membranes have been examined using a number of techniques such as SEM and even visually, however AFM has many advantages over these

techniques, such as little sample preparation which means that AFM is more appropriate for surface roughness measurements [137, 138].

AFM imaging technology has been established in the literature for the quantification of surface morphology, pore size distributions and surface roughness for various types of membranes, such as NF, RO and UF [59, 68, 69, 70]. Kwak *et al* [139, 140] used AFM to determine the surface morphology of RO membranes and used the surface roughness data to relate surface roughness to permeability. Bowen's research group within Swansea University focused on the investigation into membranes using AFM imaging for visualizing the surface [60, 61, 68]. In one such study, Bowen *et al* [59] used the AFM for quantification of surface morphology, pore size distributions and particle adhesion for three NF membranes. Analyses of AFM images are vitally important as current literature suggest that the fouling potential of filtration membranes can be determined by its surface topography. It is thought that membrane surfaces which are rough, have a tendency to foul easier as the roughness increases the surface area, which in turn increases the number of contact points between foulants and the surface. Large protrusions from the filtration membrane surface can affect local flow fields and shield particles, such as bacterial cells, from detachment and lateral peak-to-peak and peak-to-valley distances on the surface can influence attachment of colloidal material and attachment of bacterial cells [71]. Therefore determination of surface roughness of membranes is crucial in the study of particle fouling in these systems. However it is difficult to compare different roughness values from the literature as there is a lack of uniformity in the AFM methods due to several modes of AFM and different scan areas being used for the determination of surface roughness [48]. Scan area is especially important as roughness is not independent of scale.

AFM technology has also been utilized for the imaging and analyses of bacterial biofilms. One of the earliest AFM examinations of biofilms was performed by Bremer *et al* [141]. AFM was used to image hydrated freshwater bacterial biofilms formed on polished and unpolished copper surfaces. The biofilms were observed to be heterogeneous in nature in both depth and cell distribution and also bacterial cells were associated with pits seen on the surface of the unpolished copper. Following this study, further research was conducted in which pure and mixed bacterial biofilms were grown

on different types of steel surfaces and analysed with AFM [142, 143]. The biofilm surface and the steel surface after the removal of the biofilms were imaged for the purpose of gaining qualitative and quantitative information on biofilm structure *in situ* at high resolution and also to determine the biodeterioration of steel in the presence of biofilms, where a degree of pitting corrosion on the steel was observed. Beech *et al* [143] also used AFM image analysis software for the estimation of the width and height of the individual bacterial cells and exopolymeric capsule. These studies paved the way for other research groups to investigate biofilms through AFM technology. Following these papers, more in-depth investigations into bacterial biofilms using AFM has been conducted by various research groups. *Haemophilus influenza, P. putida, E.coli* O157:H7 and *Staphylococcus epidermidis* are just a few of the types of biofilms investigated by AFM imaging and force-distance measurements [78, 79, 144, 145].

Early AFM studies on biofilm usually focused on gaining topographical and morphological information of the features present on the surface. However, limitations of AFM for the study of biofilms include the inability to obtain a large area survey scan and the AFM tip's incapacity for imaging the side walls of bacterial cells. Also the soft and gelatinous nature of the biofilm might be damaged by the imaging of the surface, especially within a liquid environment. Auerbach *et al* [78] imaged unsaturated fresh and desiccated biofilms of *P. putida* to determine if surface morphology and roughness of the biofilms were affected by the drying of the unsaturated biofilms. It was observed that drying biofilms grown in humid air (unsaturated conditions) caused little change in morphology, roughness, or adhesion forces when compared to the moist biofilms, unlike the structural changes that occur when biofilms grown in fluid are dried for AFM analysis. Recently more AFM studies into various bacterial biofilms have been performed in aqueous conditions in the attempt to understand the more realistic properties, such as interaction and attachment to surfaces, of whole biofilms in aqueous conditions. Arce *et al* [144] studied the pathogen *Nontypeable H.influenza* through the use of AFM in an aqueous environment to image and characterise structural details, such as Hif-type pili, of the live bacteria at early stage of biofilm formation.

AFM technology has also been utilized for the imaging of biofilm layers and foulant layers on membranes, which have either been purposely fouled within laboratory conditions [69] or fouled within a process [146, 147]. However, there seems to be a

limited amount of studies which have used AFM imaging for the analysis of process fouled membranes in comparison to the imaging of purposely fouled membranes. This could be due to the ability to obtain the membranes from plants as the membranes are only replaced periodically. Therefore the literature has shown that AFM is an established technique for the imaging and analysis of membranes and biofilm layers and therefore can be utilized for the imaging of clean and fouled RO membranes from the Fujairah Water and Power plant.

Another important factor which could participate in the fouling of membranes is the surface charge of the membrane. Membrane charge is widely thought to influence the separation performance and fouling tendency of membranes, where fouling substance interaction with the membrane surface in aqueous media can be dependent upon the membrane surface charge. Therefore the study of surface characteristics of membranes is essential for understanding of membrane fouling. The zeta potential is a value that is typically used to characterise the electrical properties of the membrane surface. The zeta potential of membranes is determined from measuring the electrical potential difference when there is relative motion between a fluid containing charged species and a charged surface caused by hydrostatic pressure gradient. The data can be obtained with the flow either through the pores (transmembrane streaming potential) meaning the flow is directed perpendicular to the active layer of membranes or flow horizontally directed along the membrane surface (tangential streaming potential). Transmembrane streaming potential only allows for qualitative results of a multilayer membrane (support layers and skin layer), however tangential streaming potential provides direct data about the membrane skin layer [106]. The zeta potential value can be then calculated from the Helmholtz-Smoluchowski equation [148].

Streaming potential analysers have been used extensively over the last 20 years to determine the zeta potential of various types of membranes. Nystrom *et al* [149] published research on the use of the measurements of streaming potential versus pressure relationships as a method of characterisation of UF membranes, where three different membranes with various pore sizes at different pH and ionic strengths were studied. Elimelech *et al* [150] used a streaming potential analyser to measure the zeta potential of cellulose acetate and composite polyamide RO membranes at various NaCl concentrations, pH and dissolved humic substances. The results indicated that the

solution chemistry had a marked effect on the electrokinetic properties of RO membranes. Deshmukh *et al* [151] performed streaming potential measurements on RO membranes using actual membrane feedwater, where the results showed a more positive zeta potential in the presence of the feedwater, probably due to the presence of divalent cations. Some research teams have used membrane surface charge as a correlating parameter for the investigation into the fouling characteristics of various UF membranes, where such studies revealed that the greatest fouling occurs under conditions of the solute and the membrane having a large opposite net charge [152]. Burns *et al* [152] assessed the buffer effects on the zeta potential of polyethersulfone UF membranes, commonly used in food and bioprocessing industries, by investigating effective surface charge of the membrane in the presence of a variety of monovalent and multivalent ions, in biologically significant buffers. Measurements were made using both negatively and positively charged membranes with the zeta potential evaluated from streaming potential measurements in the presence of the buffer ions. The study found that very different behaviour was seen with standard and positively-charged polyethersulfone membranes due to the difference in potential-determining ions for these membrane systems. The zeta potential of the positively-charged membrane was strongly dependent on the buffer with the absorption of di- and tri-valent anions causing a large reduction in zeta potential. From this study it can be determined that membrane charge can have a large effect on performance of many UF processes. Al-Amoudi *et al* [106] investigated the zeta potential of virgin and fouled NF membranes before and after chemical cleaning. Various agents were used in the study, including HCl, NaOH and commercial grade agents used in commercial plants, and also the pH and temperature were investigated. The study concluded that the fouled DK (GE Osmonics) membrane were found to be almost negatively charged with no isoelectric point when compared to a virgin DK membrane, however after cleaning by NaOH followed by HCl, at a low pH the zeta potential measurements from the fouled DK were in close agreement with those from the untreated virgin membrane. Also the cleaning agent SDS had the highest effect on surface charge for both virgin and fouled NF membranes. This study demonstrates the use of streaming potential measurements for the measurement of cleaning performance and membrane integrity. Childress and Elimelech [153] investigated the effect of solution chemistry on the surface charge of four commercial RO and NF membranes. The zeta potentials of the membranes were analysed in various salt solutions such as NaCl and solutions containing divalent ions

$CaCl_2$, $Na_2SO_4$, and $MgSO_4$ over a pH range of 2 to 9. The isoelectric points of the various membranes at 0.01M NaCl ranged from 3.0 to 5.2, while the divalent salt solutions suggested that divalent cations more readily adsorbed to the membrane surface than divalent anions, especially at higher pH range.

Therefore streaming potential measurements used to determine the zeta potential of membrane surfaces have been well established within the literature to produce relevant results to determine the fouling potential of clean and fouled membranes. The surface charge of clean and industrial fouled membranes were characterised through the use of streaming potential experiments at various pH values and NaCl, $MgCl_2$ and $CaCl_2$ concentrations to help build a wealth of data to unravel the mechanisms of bio-fouling.

## 4.2 Methods

The experimental methods for the membrane AFM imaging are given in section 2.6, while information regarding the fouled membrane is given in section 2.1.

The experimental methods for determination of the zeta potential through streaming potential measurements are given in section 2.5.

## 4.3 Results and Discussion

AFM images selected from the characterization work performed on virgin and process fouled SWC 3+ RO membranes are displayed within this section, where the observations and analyses of the images are discussed. Following this work, further characterization of the membrane surface is presented in the determination of membrane surface charge through streaming potential measurements.

### 4.3.1 AFM Imaging of membranes

AFM topographical images have been performed on virgin and process fouled SWC 3+ RO membranes. 1x1, 10x10 and 100x100 $\mu m^2$ size images have been taken over each membrane surface, where the corresponding phase images have been included for the virgin membranes and the corresponding amplitude images included for the fouled membranes. The phase and amplitude images have been included for further elucidation of surface structures which might not have been clearly shown in the topographical images. It was found for the virgin membrane images that phase imaging displayed the surface images more clearly, unlike the fouled membrane images where amplitude images was deemed to be more appropriate for the display of surface features. Also AFM images of interesting surface features on the fouled membrane have been included which show the complex structure of the foulant layer.

1x1, 10x10 and 100x100 $\mu m^2$ topographical images of the virgin membrane clearly show the structure of the RO membrane surface in Figures 4.1, 4.2 and 4.3. The quality of the images is good due to a high resolution of 1024x1024 pixels, slow scan speed and the use of a sharp tip. It can be seen that the surface of the membrane is composed from peaks and valleys, where the shading intensity shows the vertical profile of the surface. The lightest regions are the highest regions and the darkest regions are the depressions present on the surface. The structural surface of the RO membrane imaged in this current work is similar to that observed in a study by Kwak *et al* [140] where four different types of RO membranes were imaged using AFM and SEM.

1x1, 10x10 and 100x100 $\mu m^2$ topographical images of the fouled membrane clearly show the fouled state of the RO membrane surface in Figures 4.4, 4.5 and 4.6. Again the quality of the images is good due to a high resolution of 1024x1024 pixels, slow scan speed and the use of a sharp tip. The fouling layer on the RO membrane can be seen clearly especially in 10x10 and 100x100 $\mu m^2$ scans where the structure of the RO membrane can be seen in gaps within the fouling layer. From the 100x100 $\mu m^2$ scans it can be seen that the fouling layer does not cover the entire RO membrane surface, nor is there an even distribution of the layer on the surface but rather there is a relatively non uniform distribution of foulant structures present on the surface. From the 10x10 $\mu m^2$

scans, the appearance of the foulant layer suggests that EPS i.e. slime layer, is present. Microorganisms that attach to the membrane excrete EPS to aid in adhesion to the surface and for the formation of a biofilm. The presence of EPS suggests that bio-fouling is occurring on the membrane and is facilitating in the formation of a cohesive foulant layer. Images of varying scan sizes have also been included to further demonstrate the non uniform distribution of the foulant layer in Figures 4.7. AFM technology has also been previously utilized for the imaging of foulant layers on membranes which have been fouled within a process [146, 147], however they are generally of poor quality and shown alongside much clearer SEM images to elucidate the foulant structure on the membrane. Previous AFM and SEM images show a non-uniform distribution of foulant structures which confirms the findings of this current work. In this study, clear high resolution images have been achieved on the fouled membrane surface without surface modification techniques.

The images were analysed through AFM Nanoscope software to obtain peak to valley and surface roughness measurements for both the virgin and fouled membranes at each scan size. The surface roughness and peak to valley measurements are shown in Table 4.1. From Table 4.1 it can be seen that as the scan size increases, the surface roughness and peak to valley measurements increase. Boussu *et al* [48] studied six NF membranes to investigate the influence of using both noncontact AFM mode and tapping AFM and also the size of the scan area on the roughness values for the different membranes. The results showed that there was little difference found between the two modes of AFM in ranking the membranes with respect to their surface roughness, even though larger differences between the roughness of the membrane were obtained with tapping AFM mode. Also it was discovered that an increase in roughness values were obtained with increasing scan area from $0.5x0.5\mu m^2$ to $10x10\ \mu m^2$ for both AFM modes. The author suggested that increasing surface roughness could be related to the dependency of the roughness of spatial wavelength on the scanned area or the frequency, i.e. in a small scan area only the roughness of the 'higher' frequencies is measured. However, when a larger scan area is chosen, the increase in roughness could be caused by additional lower frequencies which are then taken into account. Also another explanation given is that when the scan size is changed, it is possible to get a different surface topography, therefore resulting in a different roughness value [48]. Therefore the current results confirm Boussu *et al* [48] findings that surface roughness increases with scan area.

From Table 4.1, it can also be seen that fouled membrane surface has the larger peak to valley measurements for all scan sizes when compared to the virgin membrane. However, the fouled membrane surface has larger surface roughness values for scan sizes 1x1 and 100x100 $\mu m^2$ but for the 10x10 $\mu m^2$ scan size shows the fouled membrane surface to be smoother than the virgin membrane. The measurements obtained from the fouled membrane images only assess the fouled membrane image as a whole, with the underlying structure of the RO membrane being taken into account when gaps in the foulant layer are present. Therefore to determine the roughness of the foulant layer 1x1$\mu m^2$ areas were selected on 10x10 $\mu m^2$ scan images, where the difference between the foulant layer and the RO membrane surface can be clearly identified, and the surface roughness and Peak-Valley measurements taken. 30 measurements in total were taken over three 10x10 $\mu m^2$ scan images, which reveal that the fouling layer is much smoother than the unfouled RO membrane surface. This could be due to the presence of the EPS within the foulant layer. The topography, surface roughness and peak to valley measurements show that the virgin RO membranes used within Fujairah desalination plant are susceptible to biofouling.

Previous research by Bowen *et al* [6] measured the surface roughness as 66nm and peak to valley as 560nm of virgin AFC99RO membrane from a 4x4$\mu m^2$ scan image. Kwak *et al* [140] measured the surface roughness and peak to valley of 4 different types of virgin RO membranes using 10x10$\mu m^2$ scan images. The maximum peak to valley ranged from 400 to 780 nm and the RMS surface roughness ranged from 50 to 104nm. These results confirm with current findings which show a RMS surface roughness of 107.9+/- 9.68 nm and peak to valley measurement of 786.0 +/- 116.58 nm.

Other images included in Figure 4.7 show long thin structures present on the surface of the fouled membrane, forming part of the foulant structure. It is not known what these structures are, whether they are from the seawater or the RO plant pre-treatment schemes.

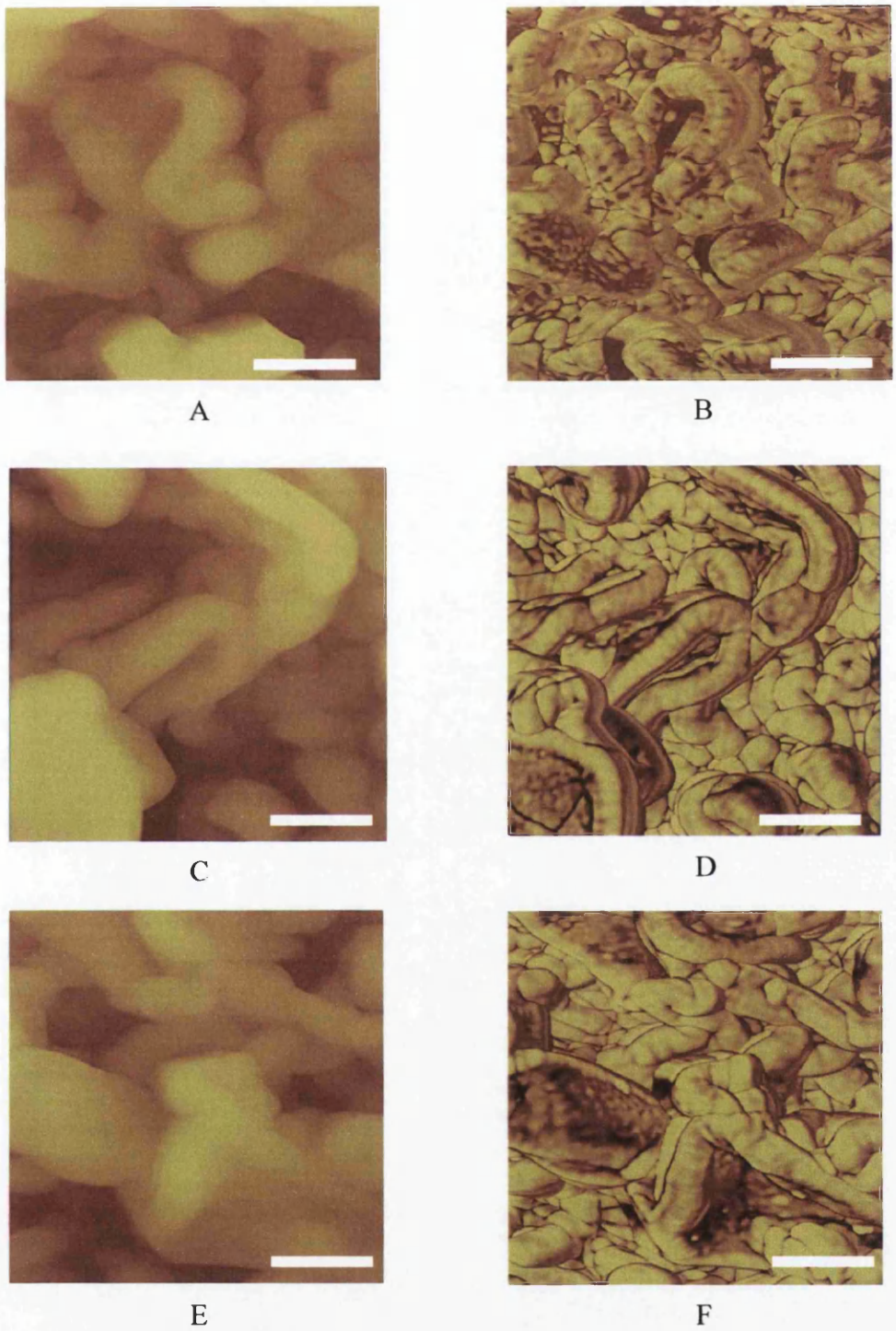


Figure 4.1 Tapping mode AFM topographic and corresponding phase 1μm images of virgin SWC 3+ RO Membrane. The scale bars in images A to F represent 0.3μm. A, C, E images show the topography of virgin SWC 3+ membrane, while B, D, F shows the corresponding phase images of the membrane. Z range is 1 μm.

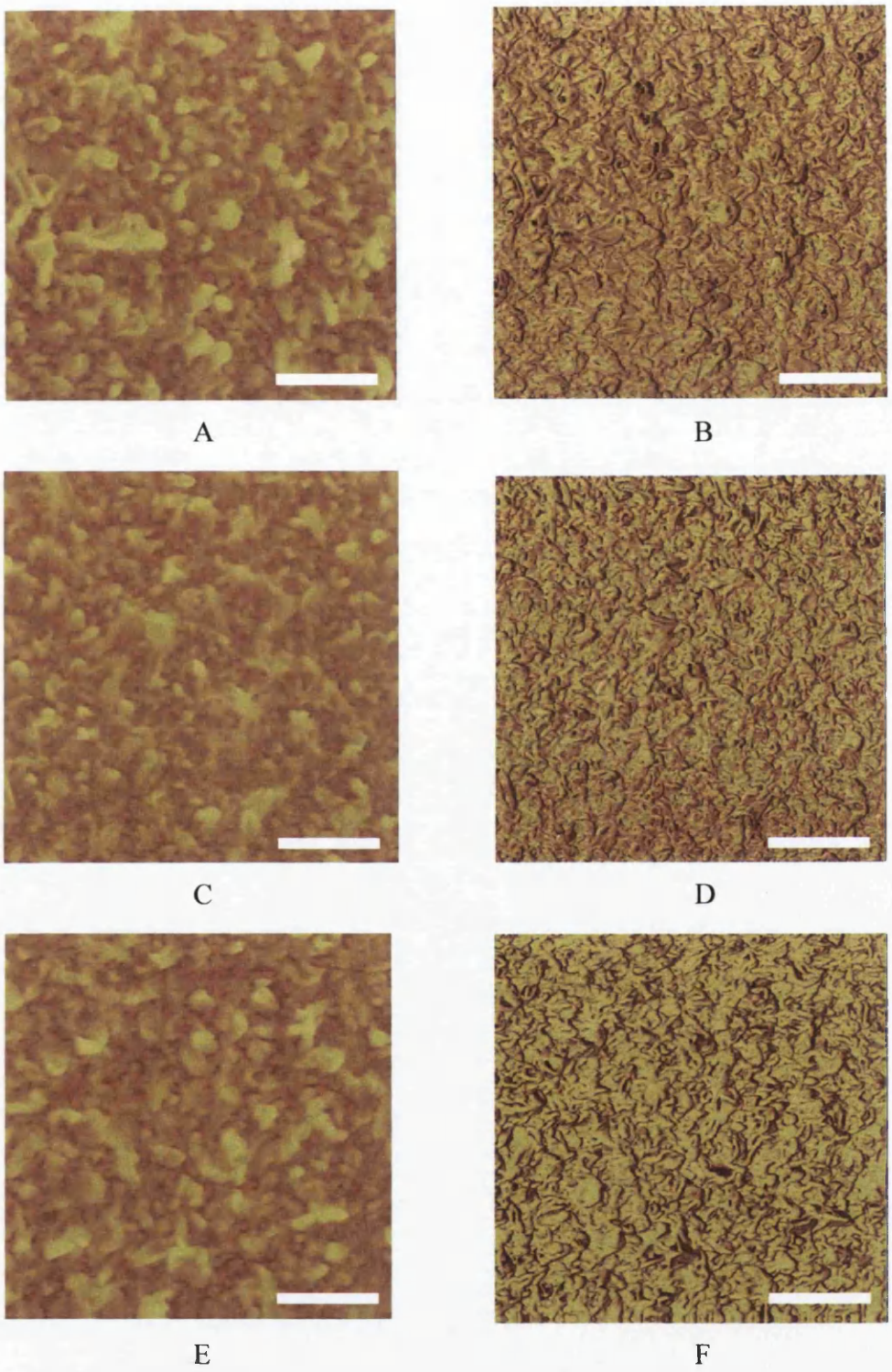


Figure 4.2 Tapping mode AFM topographic and corresponding phase 10μm images of virgin SWC 3+ RO Membrane. The scale bars in images A to F represent 3μm. A, C, E images show the topography of virgin SWC 3+ membrane, while B, D, F shows the corresponding phase images of the membrane. Z range is 2.0μm.

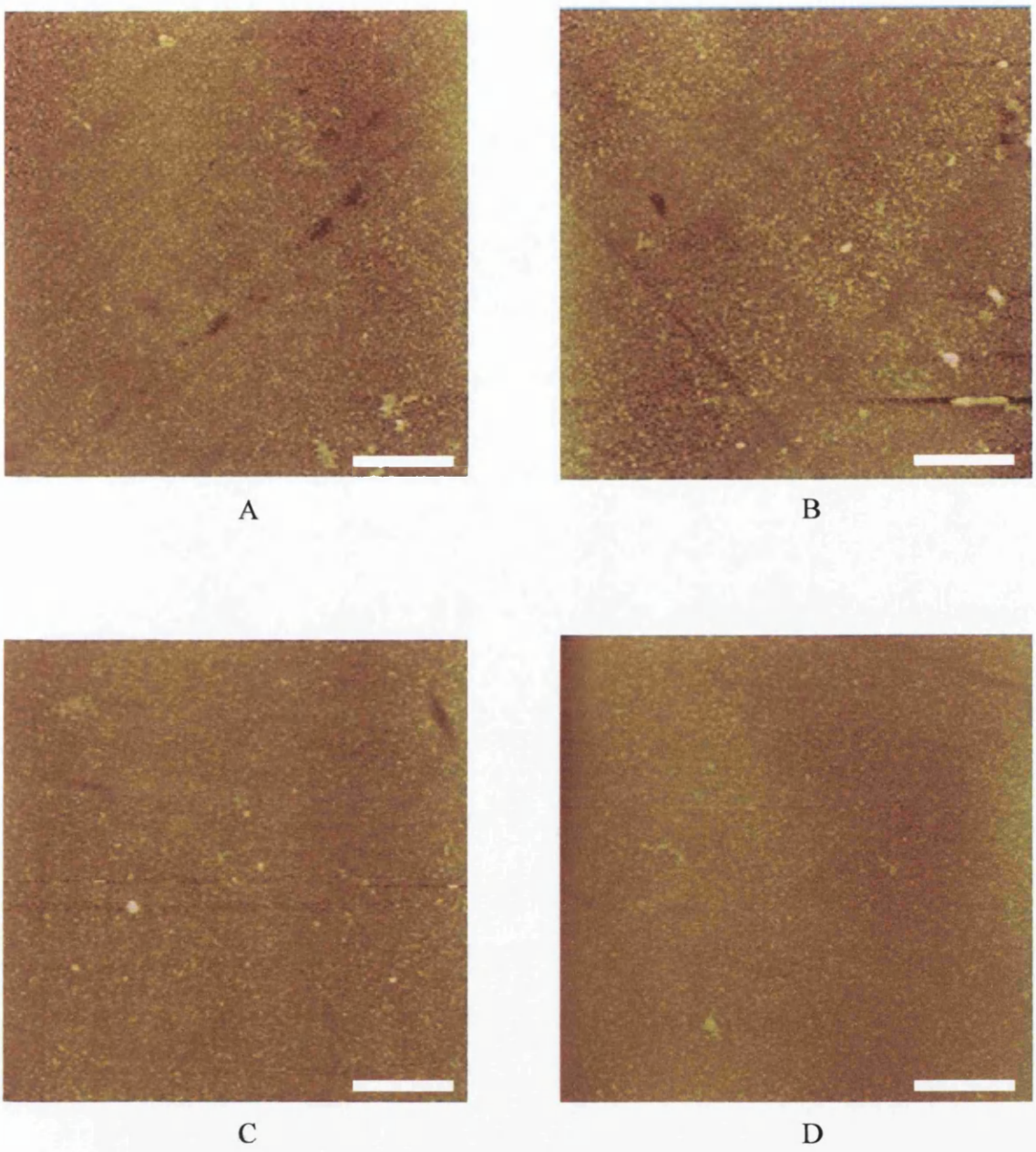


Figure 4.3 Tapping mode AFM topographic 100μm images of virgin SWC 3+ RO Membrane. The scale bars in images A to D represent 30μm. A, B, C, D images show the topography of virgin SWC 3+ membrane. Z range is 2 μm.

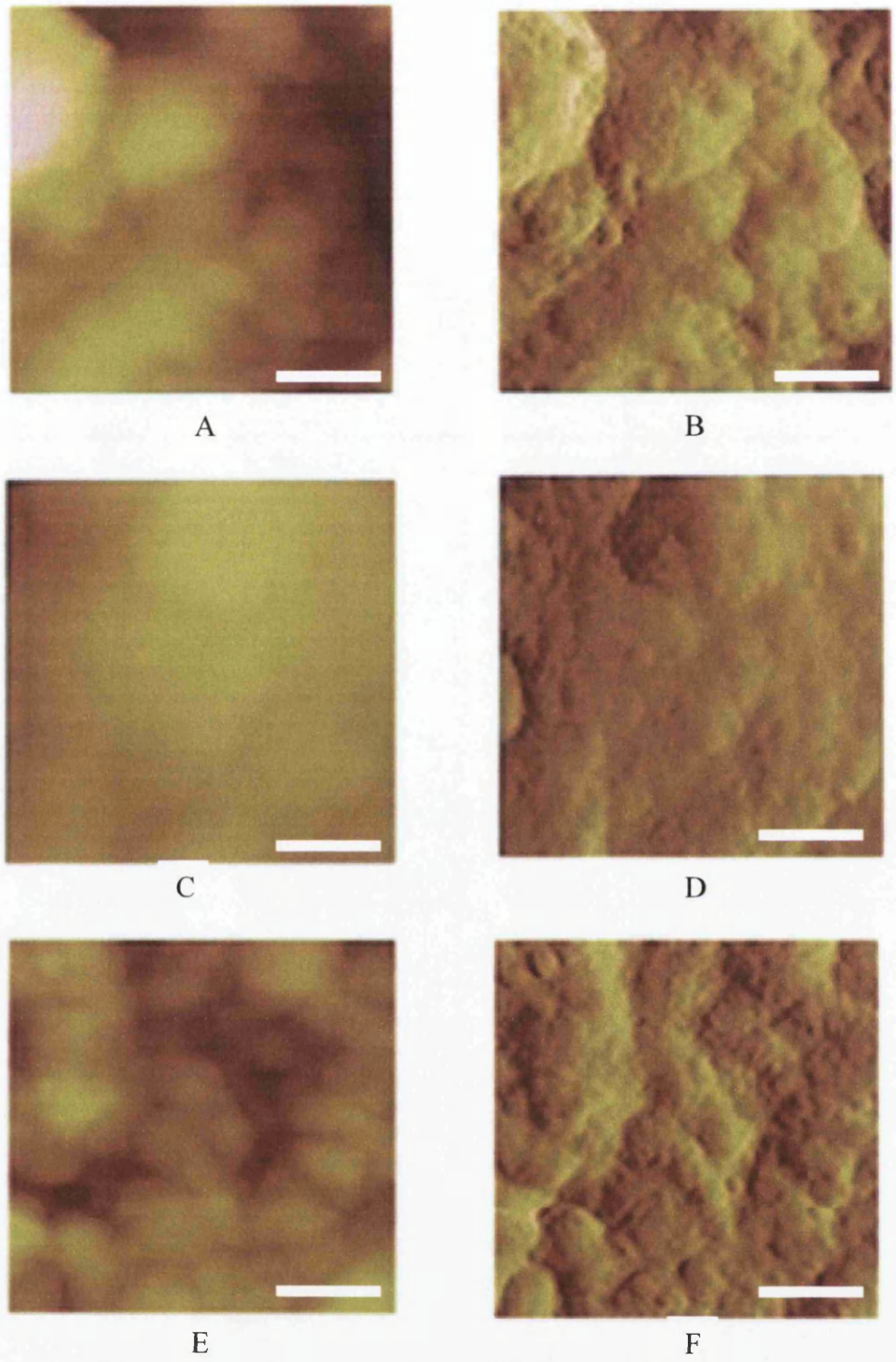


Figure 4.4 Tapping mode AFM topographic and corresponding amplitude 1μm images of process fouled SWC 3+ RO Membrane. The scale bars in images A to F represent 0.3μm. A, C, E images show the topography of virgin SWC 3+ membrane, while B, D, F shows the corresponding amplitude images of the membrane. Z range is 1μm.

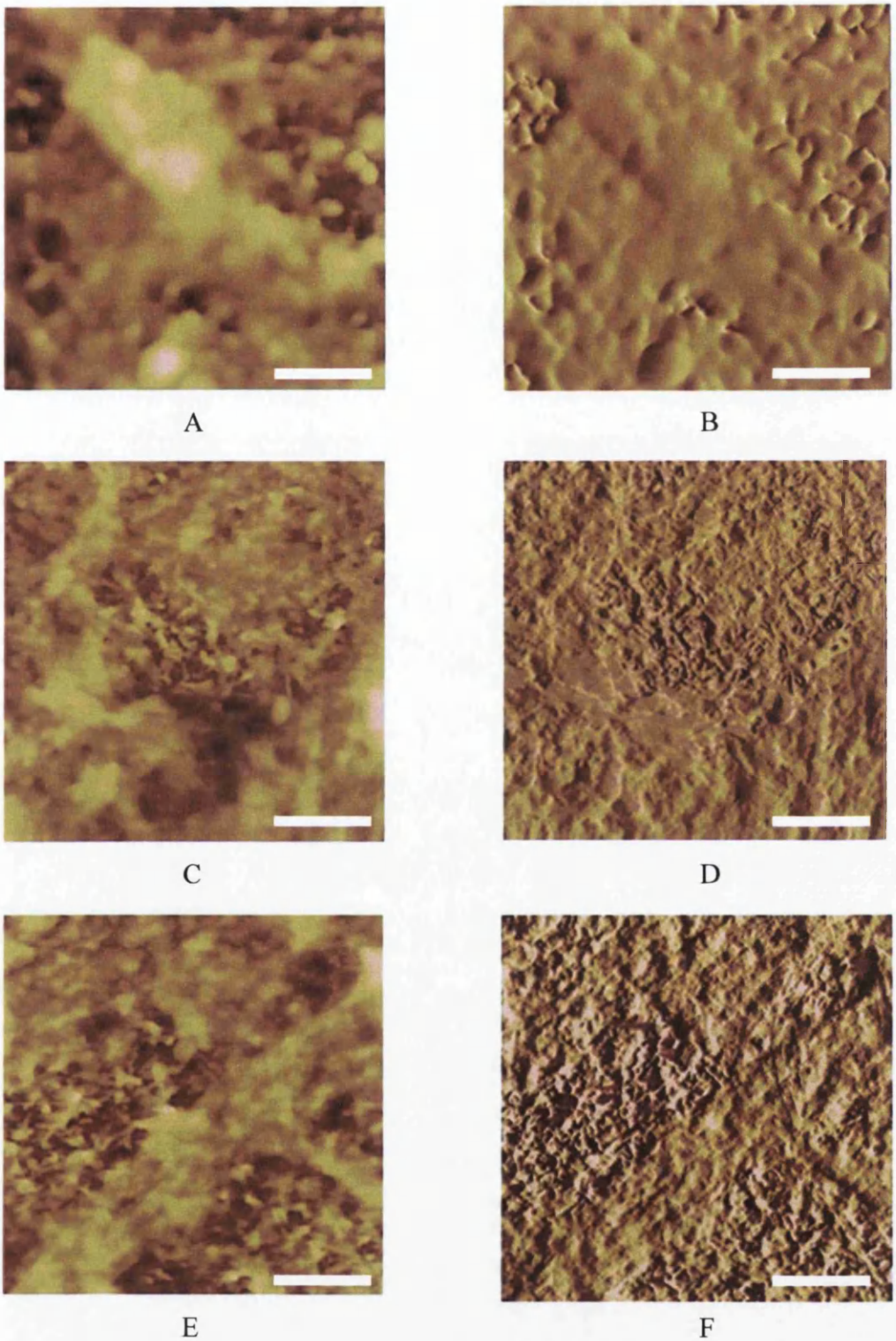


Figure 4.5 Tapping mode AFM topographic and corresponding amplitude 10μm images of process fouled SWC 3+ RO Membrane. The scale bars in images A to F represent 3μm. A, C, E images show the topography of fouled SWC 3+ membrane, while B, D, F shows the corresponding amplitude images of the membrane. The Z range is 2μm

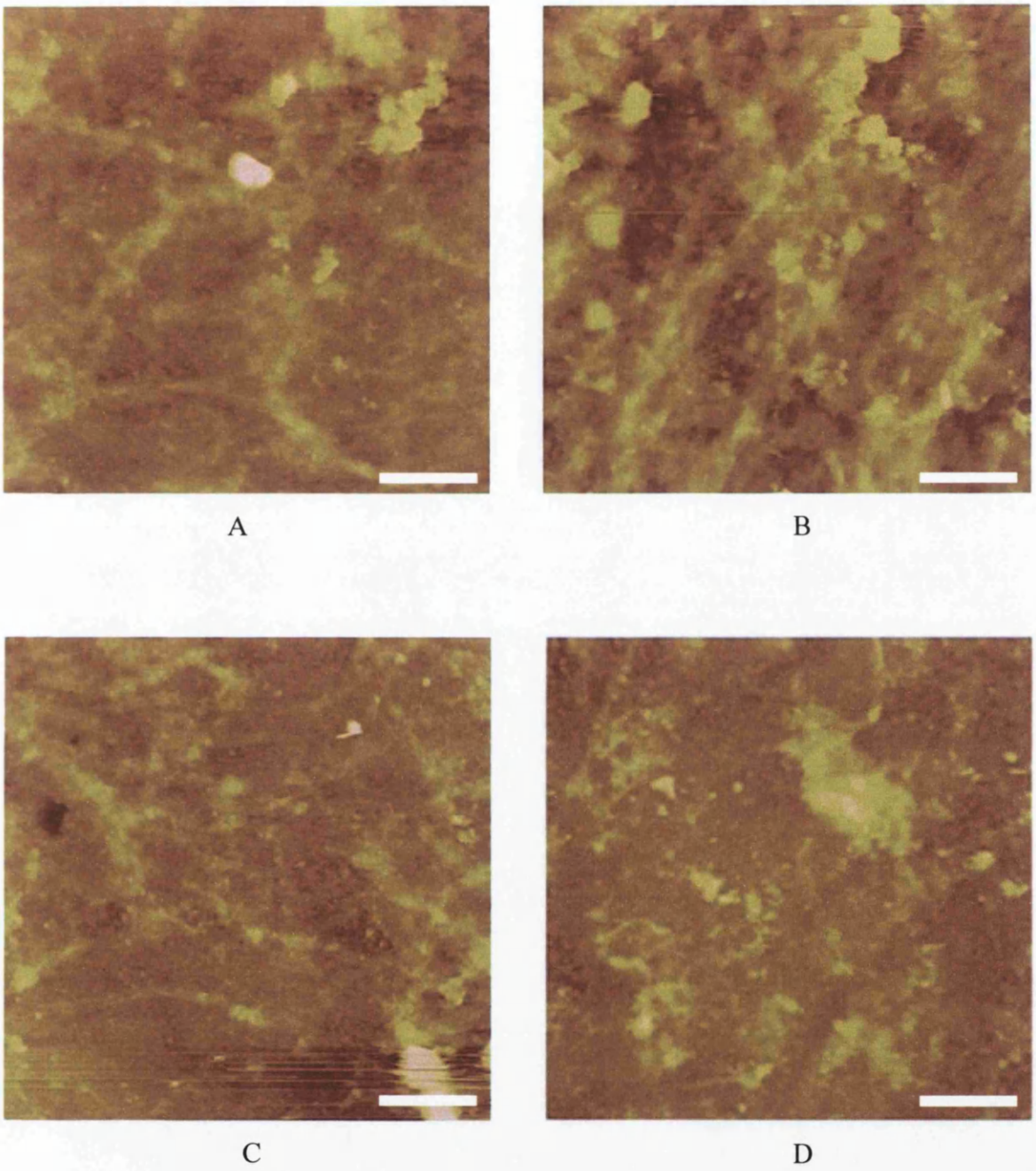


Figure 4.6 Tapping mode AFM topographic 100μm images of process fouled SWC 3+ RO Membrane. The scale bars in images A to D represent 30μm. A, B, C, D images show the topography of fouled SWC 3+ membrane images of the membrane. Z range is 2 μm.

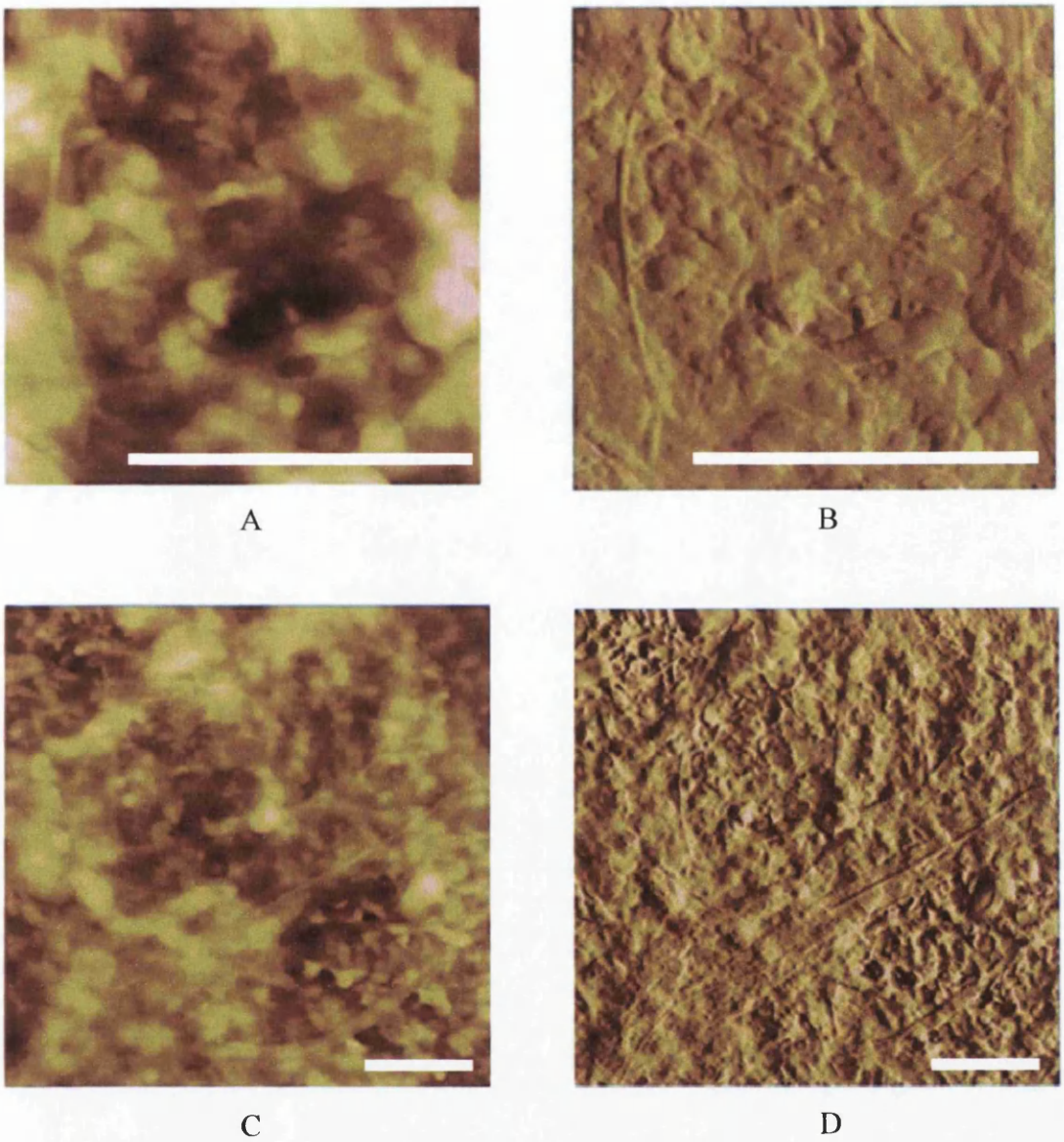


Figure 4.7 (a) Tapping mode AFM topographic images of process fouled SWC 3+ RO Membrane displaying interesting surface features. The scale bars in images A to D represent 3μm. A and C images show the topography of fouled SWC 3+ membrane, while B and D shows the corresponding amplitude images of the membrane.

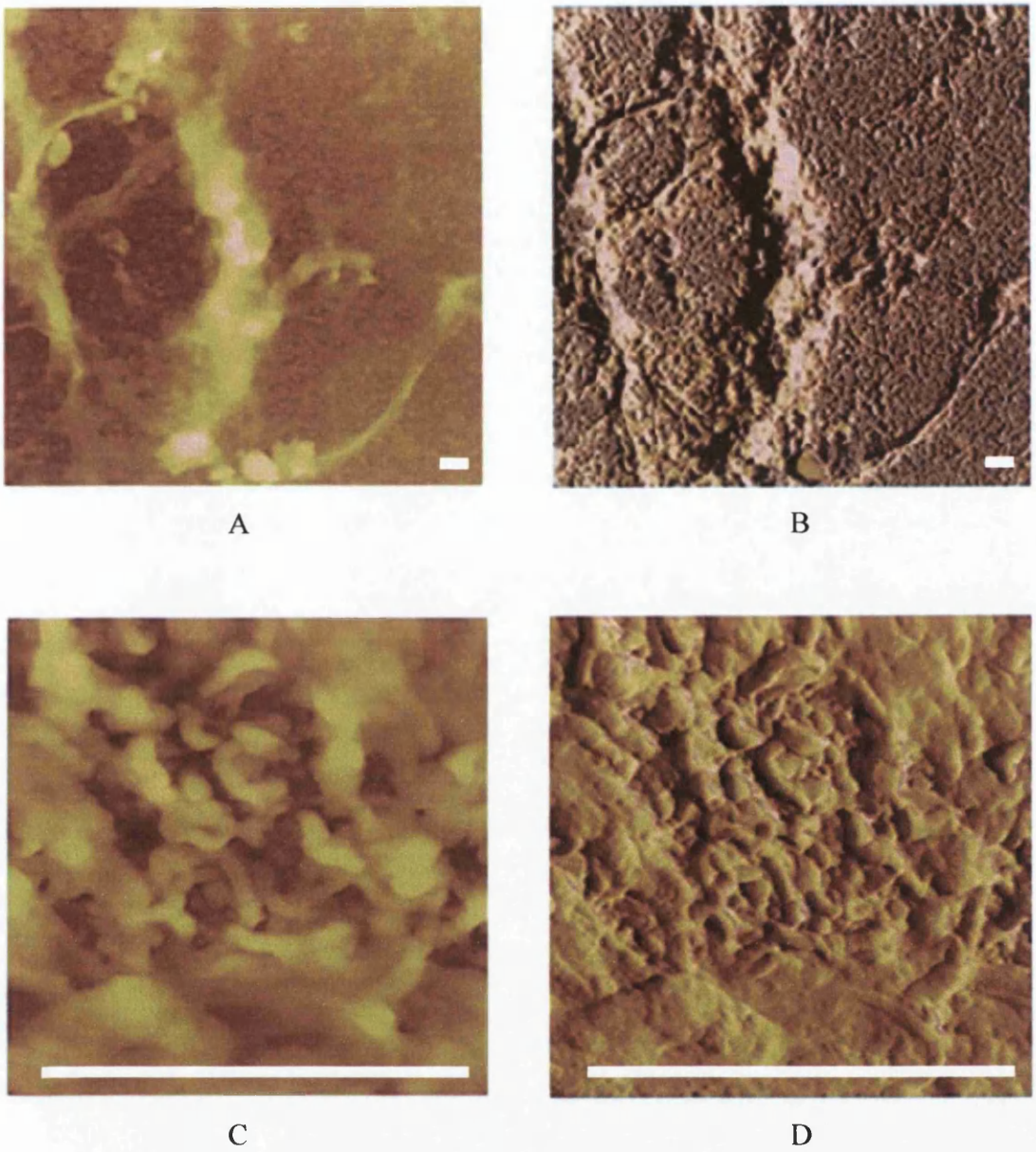


Figure 4.7 (b) Tapping mode AFM topographic images of process fouled SWC 3+ RO Membrane displaying interesting surface features. The scale bars in images A to D represent 3μm. A and C images show the topography of virgin SWC 3+ membrane, while B and D shows the corresponding amplitude images of the membrane.

**Virgin Membrane**

| Membrane Size (μm) | RMS (nm) | | Peak to Valley (nm) | |
|---|---|---|---|---|
| | *average* | *st. dev* | *average* | *st. dev* |
| 1 | 69.70 | 13.70 | 444.33 | 112.10 |
| 10 | 107.90 | 9.68 | 786.00 | 116.58 |
| 100 | 173.67 | 25.89 | 1974.67 | 756.77 |

**Process Fouled Membrane**

| Membrane Size (μm) | RMS (nm) | | Peak to Valley (nm) | |
|---|---|---|---|---|
| | *average* | *st. dev* | *average* | *st. dev* |
| 1 | 87.45 | 11.21 | 490.24 | 109.57 |
| 10 | 99.60 | 14.25 | 824.33 | 112.54 |
| 100 | 297.67 | 44.23 | 3837.00 | 1013.26 |

**1μm x 1μm area surface roughness measurements**

| Membrane Type | RMS (nm) | | Peak to Valley (nm) | |
|---|---|---|---|---|
| | *average* | *st. dev* | *average* | *st. dev* |
| Virgin | 221.01 | 66.40 | 484.23 | 100.85 |
| Process Fouled | 41.48 | 12.53 | 93.01 | 25.32 |

Table 4.1 Surface roughness measurements

### 4.3.2 Membrane Zeta Potential Measurements

Membrane charge is widely thought to influence the separation performance and fouling tendency of membranes, where fouling substance interaction with the membrane surface in aqueous media can be dependent upon the membrane surface charge. Therefore, the membrane charge has been determined for the clean and fouled membrane surfaces. The salt concentrations of 0.001, 0.01 and 0.1M NaCl were used as increasing the salt concentration to process relevant conditions caused very large standard deviation values and no trend could be established for the zeta potential. Also the streaming potential equipment was only designed to be operated at certain salt concentrations which were far below process relevant salt concentrations.

The results of zeta potential versus pH for the virgin RO membrane at various NaCl concentrations are shown in Figure 4.8. The virgin membrane was positively charged at low pH and negatively charged at high pH for all NaCl concentrations. However as the

concentration of NaCl increases, the membrane becomes less positively and negatively charged, resulting in less steep curves. This could be due to compression of the electric double layer with increasing salt concentration as explained by the DLVO theory (see section 1.3) in which the zeta potential values of the membrane come closer to the isoelectric point (zero zeta potential) for all pH values.

The isoelectric points were determined to be pH 3.75 for 0.001M, pH 3.9 for 0.01M and pH 4.0 for 0.1M, therefore the IEP increases slightly as the NaCl concentration increases. The zeta potential versus pH curves for the virgin membrane display the characteristic shape of surfaces with acidic and basic functional groups. The results of zeta potential versus pH for the fouled RO membrane at various NaCl concentrations are shown in Figure 4.9. The fouled membrane was entirely negatively charged over the pH range and therefore had no isoelectric points, which indicates that the foulant material was mainly negatively charged. The negative charge on the foulant material present on the membrane could be partially explained by the zeta measurements of the bacterial species obtained in Chapter 3. The zeta potential of three bacterial species, *Vibrio* sp. PM6A, *A.venetianus* and *K.pnuemoniae* subsp. *Pneumonia,* all belonging to the class *γ-Proteobacteria* show negative electrophoretic mobility values over pH values 3 to 9 for 0.1M NaCl, which become more negatively charged with increasing pH values. *γ-Proteobacteria* was determined to be the most predominant bacterial grouping found within the foulant layer present on processed fouled membranes (Chapter 3) therefore this grouping was responsible for part of the fouling on the RO membrane. This present study on fouled membrane surface charge experiments seems to add evidence to the finding that *γ-Proteobacteria* is partially responsible for biofouling, due to the negative charge present on the fouled membrane at all pH values.

As the concentration of NaCl increased from 0.01M to 0.1M the zeta potential measurements of the fouled membrane for all pH values becomes less negative, which could be due to the compression of the electric double layer with increasing salt concentration, as explained by the DLVO theory (see section 1.3). However at 0.001M NaCl concentration, the zeta potential measurements only show a gentle slope in becoming more negative with increasing pH which is dissimilar to the other NaCl concentrations. Also the zeta potential measurements at 0.001M NaCl are less negative at higher pH values when compared to zeta potential measurements obtained at 0.01M

and 0.1M NaCl concentrations. The foulant substances present on the membrane surface seem to be displaying less negative zeta potential values at very low NaCl concentrations.

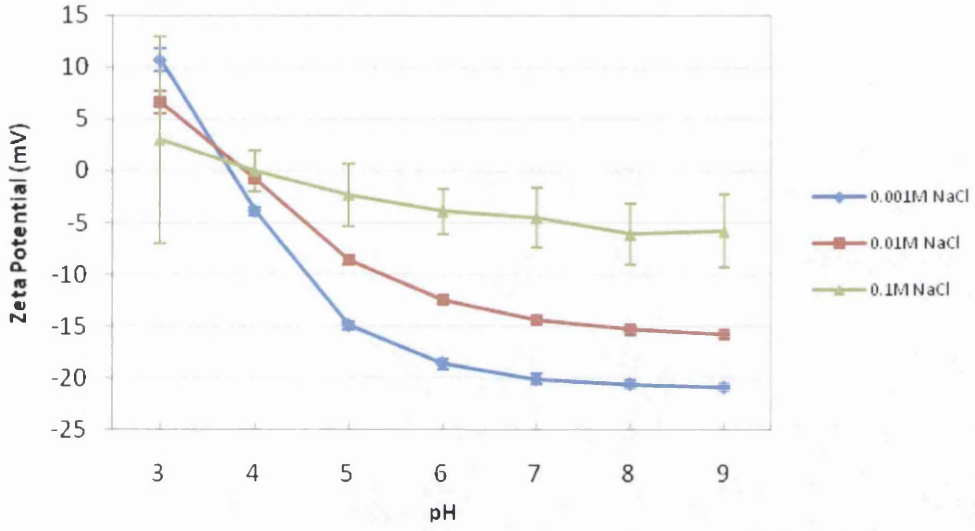


Figure 4.8 Zeta potential measurements of virgin RO membrane at various NaCl concentrations.

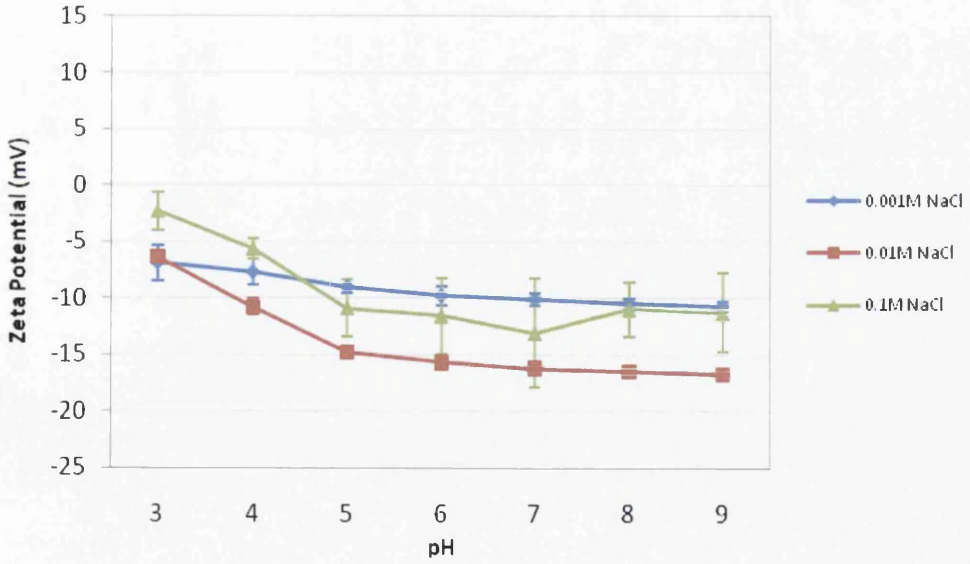


Figure 4.9 Zeta potential measurements of process fouled RO membrane at various NaCl concentrations.

Previous research by Al-Amoudi *et al* investigated the zeta potential of three virgin and one fouled NF membrane at different pH values [106]. The study concluded that the fouled NF membranes were found to be negatively charged between the zeta potential ranges of -13 to -21mV with no isoelectric point, however virgin NF membranes were positively charged at low pH, between the zeta potential ranges of 8 to -8mV for pH 3, with an isoelectric point between pH 3-4 and negatively charged at high pH between the zeta potential ranges of -18 to -24mV for pH 10.35. This confirms the current research conducted over clean and fouled membranes, even though the membrane under test in this study are RO membranes and not NF as was used in Al-Amoudi research.

The divalent ions, $Mg^{2+}$ and $Ca^{2+}$, were used to see if these cations had an effect on the zeta potential measurements at the conditions of 0.01M and 0.1M ionic strength. Figures 4.10 and 4.11 show that at the ionic strength of 0.01M as the divalent ion concentration increases, the zeta potential of the virgin membrane becomes less negative, where this effect is more pronounced at pH values of 7 to 9. Even though the zeta potential values become less negative, the membrane surface still remains negatively charged at high pH values. A possible explanation for the change in zeta potential, especially at pH values of 7 to 9 when the experiment is performed with divalent ions is due to the adsorption of the divalent cation, either $Ca^{2+}$ or $Mg^{2+}$, to the membrane surface. The membrane is negatively charged at higher pH values, which is a favourable position for the absorption of the divalent ions. This absorption masked the strongly negatively surface charge, which in turn leads to changes in zeta potential.

Figures 4.12 and 4.13 show that at the ionic strength of 0.1M, as the divalent ion concentration increases, the zeta potential of the virgin membrane becomes slightly less negative, where this effect is more pronounced at pH values of 7 to 9. Even though the zeta potential values become less negative, the membrane surface still remains negatively charged at high pH values. However it must be noted that the standard deviation of the data is relatively high so only 2 other measurements were taken for $Mg^{2+}$ and $Ca^{2+}$ ion concentrations to more clearly see any trend which might be present. The values of zeta potential at 0.1M ionic strength are much less negative and positive than those obtained for the ionic strength of 0.01M and some data points especially at pH 3 to 5 are closer to the isoelectric point.

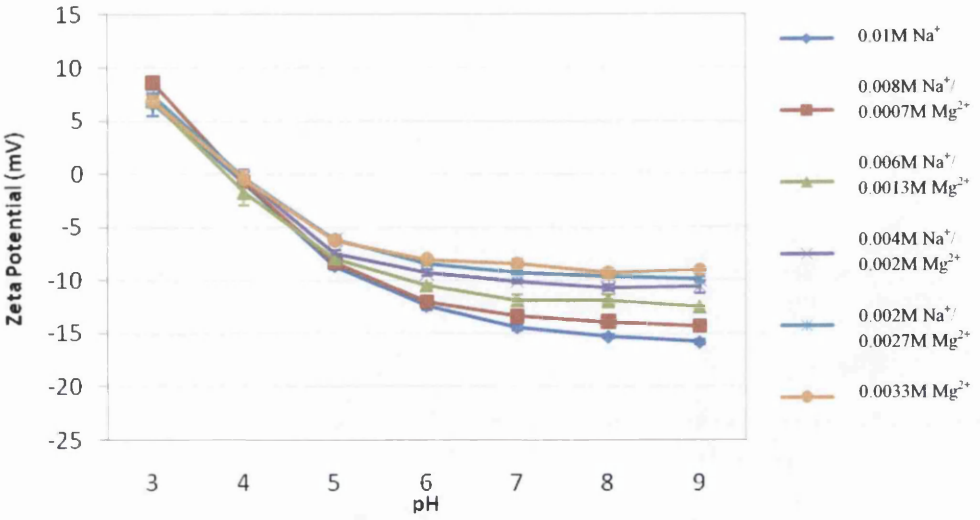


Figure 4.10 Zeta potential measurements of virgin RO membrane at various $MgCl_2$ and NaCl concentrations at the ionic strength of 0.01M.

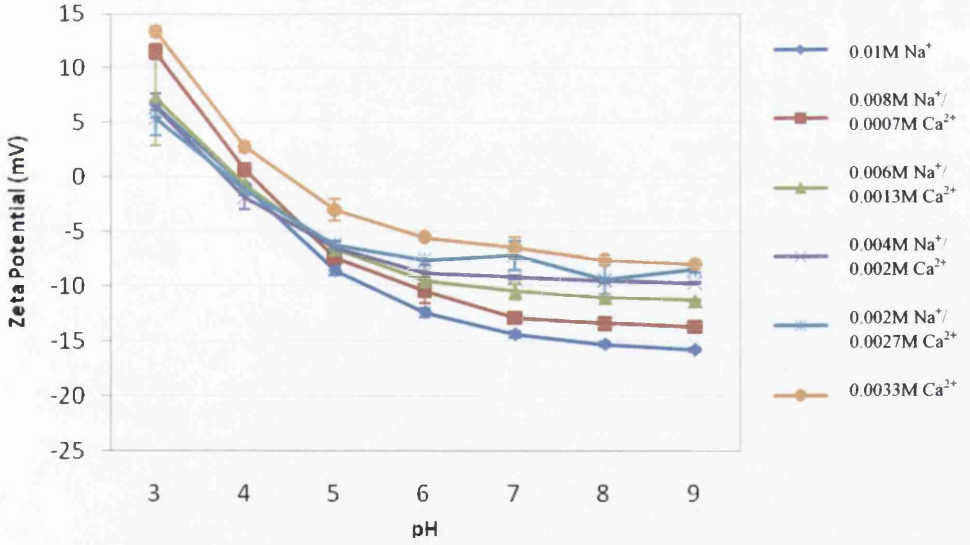


Figure 4.11 Zeta potential measurements of virgin RO membrane at various $CaCl_2$ and NaCl concentrations at the ionic strength of 0.01M.

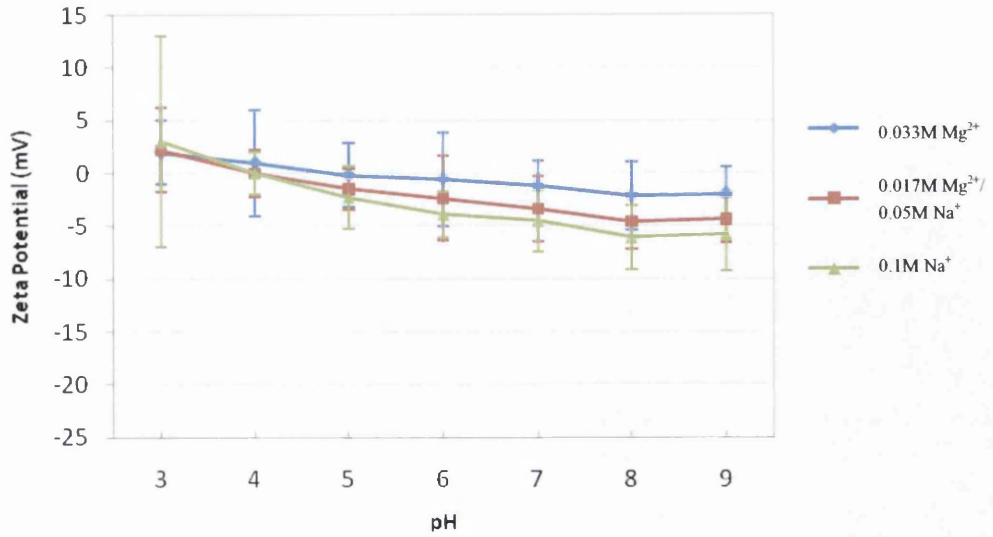


Figure 4.12 Zeta potential measurements of virgin RO membrane at various $MgCl_2$ and NaCl concentrations at the ionic strength of 0.1M.

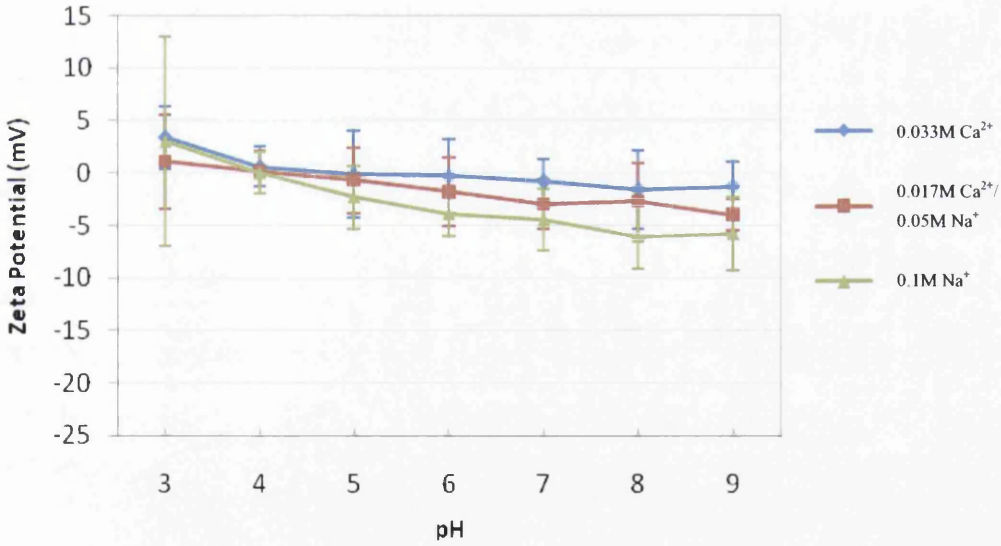


Figure 4.13 Zeta potential measurements of virgin RO membrane at various $CaCl_2$ and NaCl concentrations at the ionic strength of 0.1M.

Figures 4.14 and 4.15 show that at the ionic strength of 0.01M as the divalent ion concentration increases, the zeta potential of the fouled membrane becomes less negative, where again this effect is more pronounced at pH values of 7 to 9. Even

though the zeta potential values become less negative, the fouled membrane surface still remains negatively charged at all pH values.

Figures 4.16 and 4.17 show that at the ionic strength of 0.1M as the divalent ion concentration increases, the zeta potential of the fouled membrane becomes slightly less negative, where even though the zeta potential values change, the membrane surface still remains negatively charged at all pH values. However it must be noted that the standard deviation of the data is relatively high so only 2 other measurements were taken for $Mg^{2+}$ and $Ca^{2+}$ ion concentrations to more clearly see any trend which might be present. The values of zeta potential at 0.1M ionic strength are within the range of those obtained for the ionic strength of 0.01M.

Previous research by Burns *et al* [152] assessed the buffer effects on the zeta potential of polyethersulfone UF membranes, commonly used in food and bioprocessing industries, by investigating effective surface charge of the membrane in the presence of a variety of monovalent and multivalent ions, in biologically significant buffers. Measurements were made using both negatively and positively charged membranes with the zeta potential evaluated from streaming potential measurements in the presence of the buffer ions. The study found that very different behaviour was seen with standard and positively-charged polyethersulfone membranes due to the difference in potential-determining ions for these membrane systems. The zeta potential of the positively-charged membrane was strongly dependent on the buffer with the absorption of di- and tri- valent anions causing a large reduction in zeta potential. From this study it can be determined that membrane charge can have a large effect on performance of many UF processes.

In similar research to the current study, Childress [153] investigated the effect of solution chemistry on the surface charge of four commercial RO and NF membranes. The zeta potentials of the membranes were analysed in various salts containing divalent ions $CaCl_2$, $Na_2SO_4$, and $MgSO_4$ over a pH range of 2 to 9. The isoelectric points for the two RO membranes at 0.01M NaCl ranged from 3.0 to 5.2 and were positively charged at low pH between the ranges 7.5 to 3.5 mV and negatively charged at high pH between the ranges -9 to -16mV. For the TFCL RO membrane, the divalent ions had no effect on the zeta potential of the membrane, however for the other TFCS RO

membrane $CaCl_2$ had a noticeable effect on surface charge. The current study confirms some of the research results by Childress [153]. The isoelectric points for RO membrane currently under study falls within the pH range 3.0 - 5.2 and the membrane was positively charged at low pH values and negatively charged at high pH values. The current study confirms with the TFCS RO membrane surface where $CaCl_2$ had a noticeable effect on surface charge.

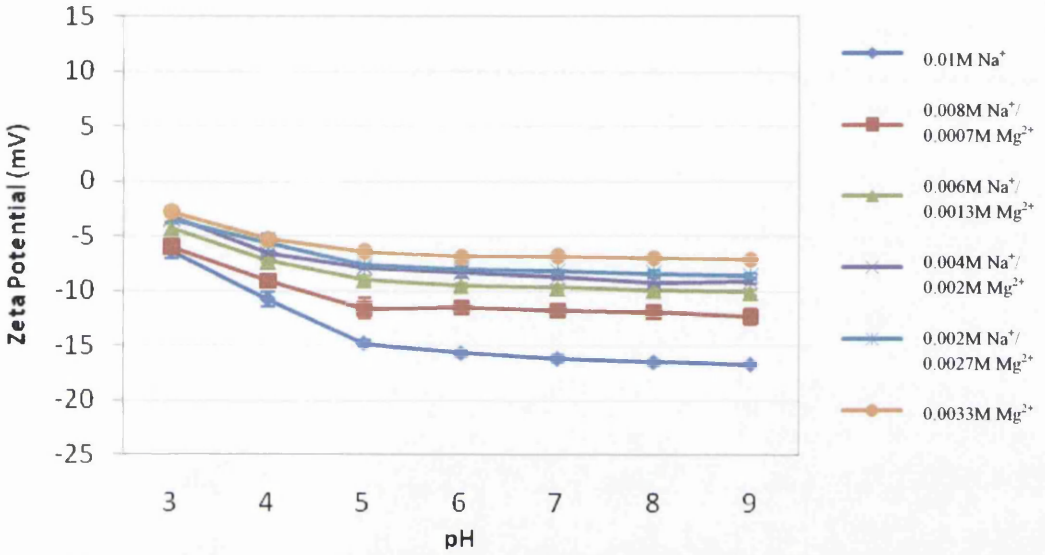


Figure 4.14 Zeta potential measurements of process fouled RO membrane at various $MgCl_2$ and NaCl concentrations at the ionic strength of 0.01M.

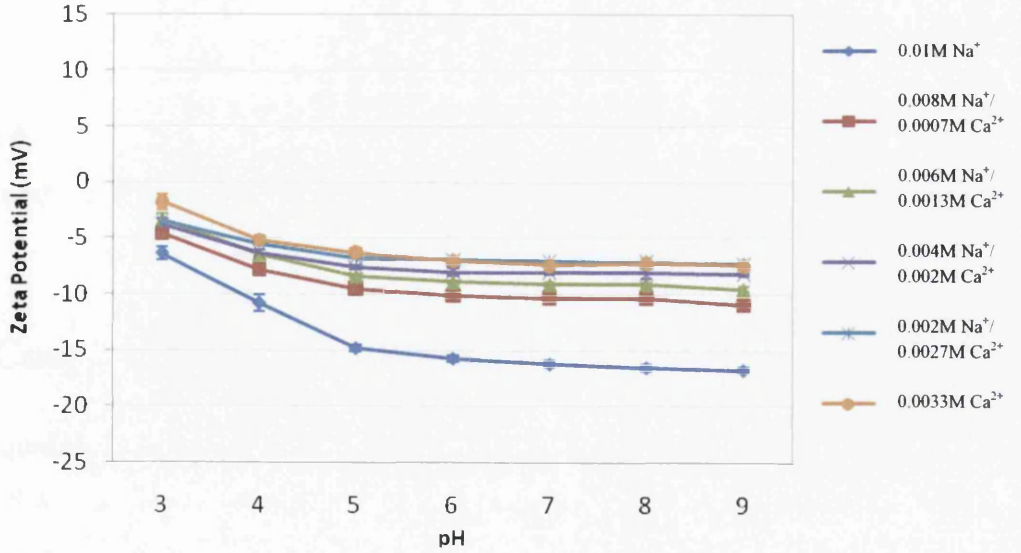


Figure 4.15 Zeta potential measurements of process fouled RO membrane at various $CaCl_2$ and NaCl concentrations at the ionic strength of 0.01M

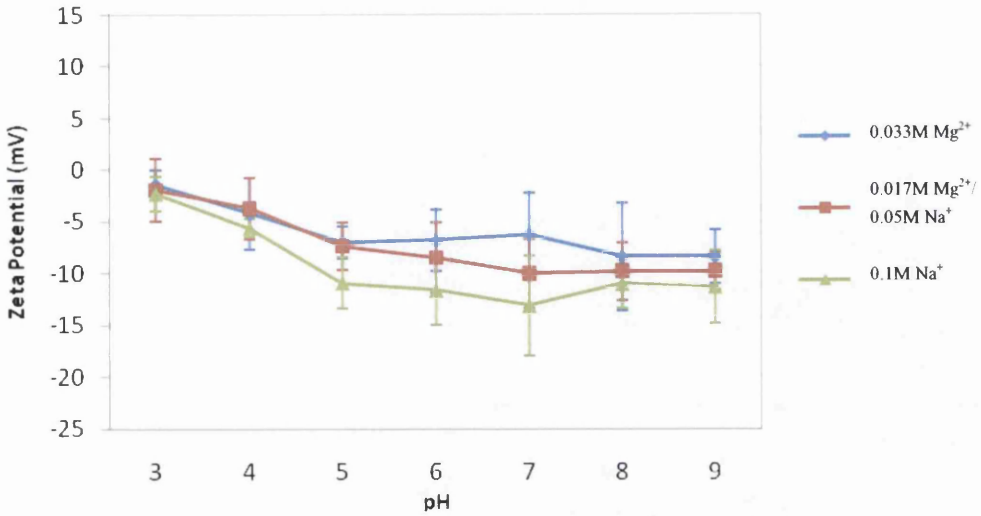


Figure 4.16 Zeta potential measurements of process fouled RO membrane at various $MgCl_2$ and NaCl concentrations at the ionic strength of 0.1M.

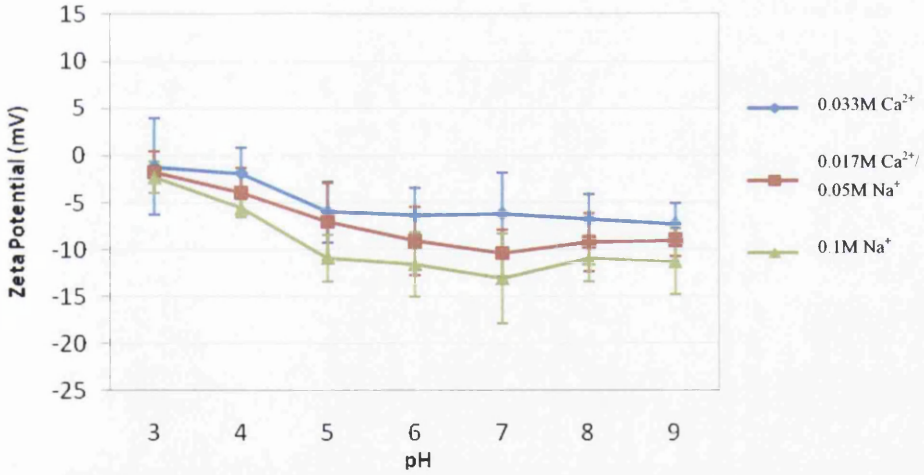


Figure 4.17 Zeta potential measurements of process fouled RO membrane at various $CaCl_2$ and NaCl concentrations at the ionic strength of 0.1M.

## 4.4 Conclusions

Good quality AFM topographical images have been obtained for virgin and process fouled SWC 3+ RO membranes. 1x1, 10x10 and 100x100 $\mu m^2$ size images have been taken over each membrane surface. From the virgin membrane images, it can be seen that the surface of the membrane is composed from peaks and valleys and displays a

structure typical of RO membranes. From the fouled membrane scans it can be seen that the fouling layer does not cover the entire RO membrane surface, nor is there an even distribution of the layer on the surface but rather there is a relatively non uniform distribution of foulant structures. On the images there is evidence of EPS, which indicates that microorganisms are present and are responsible for the development of the fouling layer. Roughness measurements of the virgin membrane surface reveal a typically rough RO surface. Roughness and peak to valley measurements reveal that the fouling layer is much smoother than the unfouled RO membrane surface, which could be due to the presence of the EPS within the foulant layer.

The surface charge of clean and industrial fouled membrane were characterised through the use of streaming potential experiments at various pH values and NaCl and $MgCl_2$ and $CaCl_2$ concentrations to help build a wealth of data to unravel the mechanisms of bio-fouling. Results reveal that the zeta potential is strongly dependent on pH and NaCl concentration for both the virgin and fouled membrane, where the foulant material present is determined to be negatively charged at all NaCl concentrations and pH values measured. It was shown that divalent ion concentration had a marked effect on the zeta potential of the membranes, especially at the ionic strength of 0.01M. However the zeta potential of the virgin and fouled membranes at high pH still remains negative at these conditions, therefore the membrane surface remains negatively charged.

The chapter has characterized the virgin and fouled membranes in terms of topography and streaming potential, this information along with bacterial studies (presented in Chapter 3) can be extended to enable greater process and biofouling control through the characterization of the mechanical properties of the fouling material now discussed in Chapter 5.

# Chapter 5 Determination of micromechanical properties of clean and fouled membranes.

## 5.1 Introduction

Biofilms mechanical properties will affect the shape and stability of the biofilm structure and therefore can determine the failure and detachment of a biofilm in reaction to a physical force such as fluid-induced shear and also the accumulation of such biofilms in industrial environments [154]. Through the understanding of these properties, a foundation of information for effective biofilm control within industrial environments can be established. AFM can be used in the elucidation of biofilm and membrane mechanical properties.

The AFM is a versatile instrument as it not only produces high resolution topographical images of surfaces but also allows the measurement of force between an AFM tip and a sample as a function of displacement. The force data is presented in the form of a force-distance curve which can provide valuable information on interaction forces and local material properties such as elasticity, hardness, adhesion and surface charge densities. Due to the vast amount of information that can be gained, force measurements have become vital in different fields of research such as microbiology, surface science and materials engineering [38, 45, 46].

Force measurements have been performed on membranes for the direct quantification of membrane/tip and membrane/particle interactions through the measurement of adhesion force, in the hope of the elucidation of process behaviour [59, 60, 61, 68]. The colloid probe technique has been utilised to determine the membrane/particle interactions, due to the technique possessing the advantage of a well defined shape colloidal particle and known material composition [28, 56, 57, 58]. Also, force-distance measurements performed using a colloid probe can be analysed with a normalisation method based on the colloidal sphere radius which allows for the advantage of comparison between various researchers work [28]. The colloid probe technique has been used regularly to elucidate the particle-surface interactions that occur within process environments. Bowen *et al* has extensively used colloid probes to

quantify adhesion of various materials, such as polymeric latex particles, polystyrene and silica colloids probes to UF, RO and NF membranes which are used in such industries as pulp and paper and desalination industries [6, 68]. Bowen continued his membrane research by using silica colloid probes to perform force measurements on RO membranes to determine that adhesion of the probes were greater in the valleys than at the peaks of the membrane. It was also discovered that the difference in adhesion between the peak and the valleys increased with decreasing salt concentration [6]. These measurements can provide an assessment of the fouling potential of the membranes by the elucidation of mechanical factors that affect membrane fouling without the need of process measurements [59, 61]. Bowen *et al* [62] also demonstrated that the colloid probe technique can be used as a method for evaluating the specific interactions of biological material, such as *A.niger* to mica surfaces, which might be of interest to biotechnological industries. Also Bowen *et al* [68] used an AFM in conjunction both with a protein bovine serum albumin (BSA) coated silica colloid probe to directly measure the adhesive force between protein BSA and two different membranes. The functionalising of the colloid particle allows for more specific interactions between the particle and the surface to be studied, where the BSA colloid probe and a yeast cell probe has been used to directly measure the adhesive force between the probes and two different polymeric membranes [60]. Lee *et al* [155] utilised the colloid probe technique to determine the adhesion force between bulk organic foulants and foulants deposited on the surface of the membranes under various solution chemistries through initial flux and cross-flow velocity. The NOM fouling was more severe at solution chemistries that resulted in larger adhesion forces, such as lower pH, higher ionic strength and the presence of calcium ions (but not magnesium ions).

Force-distance curves have been utilised for the achievement of adhesion force measurements with various tip geometries on membrane surfaces as such measurements provide an important assessment of the fouling potential of the membranes by the elucidation of mechanical factors that affect membrane fouling without the need of process measurements. Force measurements have also been employed to obtain micromechanical properties, such as elasticity, of such samples as membranes, polymeric materials, bacterial cells and biofilms through the use of the nano-indentation technique [72]. Recently substrate elasticity is an emerging as an important physical factor in the response of many cell types. Some research groups consider that the

elasticity of a substrate will have an effect on the cell rigidity, therefore the stiffness of a substrate is intrinsic to the cells in vitro response of attachment and differentiation. Pelham *et al* [156] investigated culturing rat kidney epithelial and 3T3 fibroblastic cells on a collagen-coated polyacrylamide substrate of varying elasticity, while maintaining a constant chemical environment. When compared to firm substrates, the cells on more elastic substrates showed reduced spreading, increased rates of motility and irregularly shaped adhesion structures. Engler *et al* [157] also used varying elasticity collagen-coated polyacrylamide for culturing smooth muscle cells (SMC), where SMC spreading shows a hyperbolic dependence in projected cell area versus Young's modulus of the gel. Solon *et al* [158] measured the elastic moduli of fibroblasts grown on fibronectin-coated polyacrylamide gels of rigidity varying between 500 to 40,000 Pa. The indentation measurements showed that the cells elastic moduli was equal to, or slightly lower, than those of the substrates for a range of soft gels, reaching a saturating value at substrate rigidity of 20kPa. Through these types of studies, it has been implied that some cells can respond to differences in substrates elasticity by altering their adhesion structures, morphology or cellular behaviour. Although, there seems to be only a few studies performed on the mechanical properties of bacterial cells grown on soft elastic surfaces. Bakker *et al* [159] investigated the deposition of three marine strains, *Halomonas pacifica*, *Marinobacter hydrocarbonoclasticus* and *Psychrobacter* sp. onto polyurethane coated glass with varying elastic modulus in stagnation point flow chamber. It was shown that the bacteria adhered in higher numbers to hard surfaces than to coatings of lower elastic moduli. Lichter *et al* [160] engineered weak polyelectrolyte multilayered (PEM) thin films over the elasticity range 1MPa < E< 100MPa to investigate if surface elasticity affects bacterial adhesion. The adhesion of viable *S. epidermidis* and *E. coli* was found to correlate positively with increasing elastic modulus of PEM, independently of surface roughness, surface interaction energy and surface charge density of the surface. This study demonstrates that the stiffness of nanoscale polymeric substrata can strongly affect the adhesion of bacteria in aqueous suspensions. These studies demonstrate that local mechanical properties measurements of a substrate and bacterial cells are required for the understanding of cell responses on surfaces which display an elastic response [155, 161]. Therefore, bacterial cells should be examined on the substrate, as would be the case in the process environment, as the substrate could have an effect on the biofilm formation and bacterial cells elasticity values. Membrane elasticity could be a key factor in bacterial cell adhesion and hence

biofilm formation and therefore force measurements could provide an assessment of membrane bio-fouling potential within process environments.

Currently there is limited literature on the nano-indentation of commercially available membranes [72]. The bulk mechanical properties of membranes, such as polybenzimidazole (PBI), have been investigated for the determination of tensile strength, storage modulus and Young's modulus, using such techniques as dynamic mechanical analysis (DMA) [162, 163]. Most of these techniques have considered the mechanical behaviour of the bulk of the polymer, however the local mechanical properties of the polymer vary from the bulk, which could lead to incorrect conclusions on the mechanisms of membrane fouling. Therefore the nano-indentation technique allows for a simple, convenient measurement of local Young's modulus of membranes, although there is limited literature on the nano-indentation of membranes. Franceschini *et al* [72] determined the elastic moduli of nafion, PBI and poly [2, 5-benzimidazole] membranes, both undoped and phosphoric acid doped, using AFM force spectroscopy. The fore mentioned membranes were being tested as possible candidates to replace nafion as proton exchange membranes in methanol fuel cells. An average value of Young's modulus from 30 force curves taken on each membrane was obtained for each membrane, where differences were observed for doped and undoped membranes. However, AFM nano-indentation has been used to measure the Young's modulus and hardness of various polymers, such as polyethylene, polyvinyl alcohol, ultrahigh molecular weight polyethylene, polyvinyl chloride, polycarbonate, Nylon6, poly(methyl methacrylate), polystyrene and polyacrylic acid [164, 165]. The extremely limited literature on membrane material elasticity using nano-indentation demonstrates that the research community does not currently consider such measurements to be of importance, however as can be demonstrated from the recent research which suggests that substrate elasticity is emerging as an important physical factor in the response of many cell types, the nano-indentation technique on membrane surfaces can elucidate a possible key factor in membrane bio-fouling.

AFM force spectroscopy has been widely utilised within many research groupings for the measurement of mechanical properties of microbial cells on a local scale. Microbial cells are surrounded by thick and mechanically strong cell walls, which dictates the shape of the cell and also allow the cells to resist turgor pressure. The mechanical

properties of a microbe's cell wall are also involved in cell growth and division processes and also in controlling interfacial interactions such as cell adhesion and aggregation [19, 66]. Therefore force measurements are performed by pressing the AFM probe onto cells or isolated cell wall components to assess the cells mechanical properties. One of the first studies into cell surface elasticity was performed by Xu *et al* [166] where the elastic modulus of the archcon *Methanospirillum hungatei* GP1, which revealed large modulus values of $2x10^{10}$ to $4x10^{10}$ N/m that indicated that the sheath could withstand an internal pressure of 400atm. The method used in this paper was the 'depression technique' which entails allowing a solution containing a microbial cells and cell wall components to dry on a hard substrate [45].

Force measurements have also been widely utilised to investigate bacterial biofilms, as microbial cells develop into a biofilm, so the mechanical properties of these cells within a biofilm become vitally important. Oh *et al* [79] investigated the influence of culture conditions of both low and high nutrient media on *E.coli* O157:H7 biofilm formation by AFM. The morphology of the biofilms were examined through AFM imaging while force-distance curves on individual bacterial cells at varying early biofilm stages demonstrated that as the biofilm matured, the adhesion force between a tip and surface of the biofilm increased which indicated that EPS appear to accumulate over the cell surface upon initial attachment of bacterial cells to surfaces. Volle *et al* [167] also performed force measurements on cells within a biofilm. Five bacterial strains, *E. coli ML35*, *E. coli ZK1056*, *P. putida*, *B. subtilis* and *M.luteus*, were chosen for AFM analysis, as all formed simple biofilms on glass. The cells' spring constants and adhesion to the AFM tip were determined from a series of force curves in liquid. The spring constants and adhesion profiles of the five bacteria were distinctive, depending on the biology of the bacteria. The cellular spring constants varied between 0.16 +/- 0.01 and 0.41 +/- 0.01 N/m but it was noted that the gram-positive cells had larger spring constants than the gram-negative cells. Force measurements were also performed on both bacterial species of *E. coli* ZK1056 and *B. subtilis* in two different states; chemically fixed free-swimming planktonic cells and native biofilm cells without chemical fixation. Chemically fixed planktonic cells had different elasticity and adhesive profiles from the corresponding biofilm cells. This demonstrates that the physical properties of chemically fixed planktonic cells are significantly different from those of native biofilm cells.

Volle *et al* in 2008b [167] studied the elasticity and adhesive properties of normal *E. coli* prey cells and invaded prey cells by *B. bacteriovorus* (bdelloplasts). *B. bacteriovorus* is a small, predatory bacterium that invades and consumes other gram-negative bacteria, such as *E.coli* biofilms. On average, the spring constant of normal *E. coli* cells was 3 times stiffer than that of the bdelloplast and the bdelloplasts adhered to the AFM tip with much larger pull-off forces when compared to normal *E. coli* cells. The strength of these adhesion forces decreased with increasing ionic strength, which indicated that there was an electrostatic component to the adhesion events. This important work demonstrates that dynamic events in living unfixed cells can be imaged and investigated using AFM.

Only a few studies have investigated the forces associated with cells within an established biofilm. Fang *et al* [82] demonstrated that the AFM can be used for the quantification of the tip-cell interaction force and the measurement of surface elasticity on a biofilm formed from sulphate-reducing bacteria (SRB). A force map was created over the forming biofilm, where individual force measurements were performed on bacteria within a biofilm. The forces between the AFM tip and the bacterial cell surface were relatively constant while the cell-cell interface and periphery of the cell-substratum contact surface experienced greater adhesion forces, which were argued to be due to the accumulation of EPS. Their results also showed that elasticity varied over the cell surface. Auerbach *et al* [78] also used force mapping of a biofilm surface to determine the adhesion between unsaturated fresh and desiccated biofilms of *P. putida*. The force maps were analysed graphically for the determination of the median adhesion force for each force map for the comparison of different biofilm treatment effects, fresh and dried biofilms which had been washed or left unwashed at varying stages of biofilm growth. No consistent trend for the differences in median adhesion force was found between the biofilms subjected to different treatments.

The formation of biofilms is strongly dependent on the characteristics of the solid substrate. Oh *et al* [81] used sheets of aluminum, steel, rubber, and polypropylene to examine the effects on formation of *P. aeruginosa* biofilms with AFM. The surface morphology of the biofilm, bare substrate and the biofilm after hot water treatment were examined using AFM imaging. Force measurements revealed that the adhesion forces are higher when the biofilms matured on the substrate but when the biofilms are treated

with hot water the biofilm adhesion forces are reduced which indicates a loss of extra-cellular matrix from the biofilm. Rodriguez *et al* [80] investigated the effects of contact time, pressure, relative humidity (%RH), and material type on the adhesive strength of the food poisoning bacteria *L. monocytogenes* at a cellular level using AFM. Listerial biofilms were grown on stainless steel and through the AFM force measurements it was determined that neither contact time, loading force or relative humidity had a significant effect on biofilm adhesiveness. This work also used two different colloid probes ($SiO_2$ and polyethylene) to identify that *Listeria* biofilms adhered more strongly to hydrophobic surfaces then hydrophilic surfaces at a cellular level.

Currently, there have only been a few studies which focused on the investigation of bacteria isolated from a marine source using AFM. Nishino *et al* [168] used AFM to study a natural seawater sample and four bacterial strains; *Vibrio alginolyticus* 138-2, *Vibrio harveyi* ATCC 14126T and *Halomonas marina* IAM 12928 and *B.subtilis* IAM 12118T. The bacteria was either retained on a filter or placed on glass and dried for AFM imaging. The size, shape, effect of fixation and filtration and the choice of suitable filter were investigated. The natural seawater sample showed that the attached cells commonly possessed filamentous structures and/or many submicron particles surrounding them, however bacteria concentrated by a filter showed in a cross sectional image that both rod and coccoid cells were flattened, the former usually having a two-humped shape. Zhao *et al* [169] isolated the *γ-Proteobacteria* strains of *Shewanella* sp. strain T1 and *Pseudoalteromonas* sp. strain T8 from a water sample taken from the German Wadden Sea. Part of the investigation used AFM to achieve images of the adhered bacteria to differently terminated alkanethiolate self-assembled monolayers on gold. On one of the surfaces to which the bacteria was adhered, changes in bacteria shape and excretion of EPS were observed.

Therefore from the above experimental studies it can be concluded that it is important to study bacterial cells as part of a biofilm, as the cells would be found in an industrially setting. The physical properties of chemically fixed planktonic cells are significantly different from those of native biofilm cells [167]. In addition it is important to not only determine the elasticity of the membrane but also the bacterial cell biofilm as part of a whole system, as substrate elasticity is emerging as an important physical factor in the

response of many cell types. Thus, the substrate could alter the bacteria elasticity and effect bacterial cell adhesion [157, 161].

From literature review there are only a few AFM imaging studies and no AFM force studies of bacterial cells deposited on a commercial membrane surface. Studies investigating the physicochemical factors governing initial rates of microbial deposition through direct microscopic observation of bacterial cells onto RO and NF membranes have been performed, however AFM technology was only used for imaging surface topography [170].

**Experimental Considerations**

There are a number of considerations which need to be taken into account before performing any force measurements on surfaces, to ensure accurate and representative data. The surface of soft or bacterial surfaces can deteriorate and become unrepresentative if too many repeat force or indentation measurements are taken. This can indicate that the microbial surface was being damaged by the force applied upon it, however the number of force measurements that can be performed without damage does depend on the microbial sample used [62].

In addition when performing AFM nanoindentation measurements on thin films the experimental method needs to be carefully selected. Indentation depth into the sample, especially when indenting thin layers, should be deep enough to minimize any surface effects, which could emerge especially if the surface is relatively rough. However, the indentation depth should be less than 5-10% of the total film thickness due to the effect of the hard substrate that the film is mounted on. As the indentation depth into the film increases and the sample becomes more compressed, stiffening due to the rigid hard substrate and tip geometry become increasingly important which leads to a nonrepresentative elastic moduli of the thin film. Also the AFM probe parameters of cantilever spring constant, tip shape and the piezoelectric scanner movement should be calibrated to produce accurate values of Young's modulus [164]. Another factor to be considered is the use of sharp tips and colloid probes for indenting thin films which will help in accurately determining elastic moduli [157].

AFM force measurements on clean, industrially fouled and purposefully fouled membranes with the chosen four isolated bacteria from the culture-dependent technique have been performed. Firstly the loading force and extension time were varied to determine the effect of these AFM parameters on the force curves performed on clean and industrially fouled membranes. Once the optimum settings for the parameters had been chosen force measurements were performed on clean and industrially fouled membranes at various NaCl, $MgCl_2$ and $CaCl_2$ concentrations and three different pH values to match previous studies, Chapters 3 and 4, to achieve measurements of maximum adhesion force and elasticity using both the Hertz and JKR models. The main force measurements were performed using a silica colloid probe, however a comparison study at one NaCl concentration at three different pH values were performed with a sharp silicon nitrate tip to see if tip geometry had an effect on the force measurements obtained. Force measurements were also performed on membranes which had been purposely fouled with the four strains of isolated bacterial species through the process of high pressure filtration at one NaCl concentration and three different pH values to again achieve measurements of maximum adhesion force and elasticity using both the Hertz and JKR models.

## 5.2 Methods

The experimental methods for the force measurements performed on the clean and industrially fouled membranes are given in section 2.7, while information regarding the fouled membrane is given in section 2.1. The silica colloid probes were made as described in the section 2.7.2.

The experimental methods for the force measurements performed on the purposely fouled membrane through filtration are given in section 2.8. The description of the bacterial isolates used in this experiment is given in section 2.1, while the growth media description is given in section 2.4.

## 5.3 Results and Discussion

This section contains a thorough analysis of the effect of such AFM parameters as loading force, extension speed and tip geometry on the measurement of adhesion force

and elasticity values, for both Hertz and JKR models, performed on virgin and industrially fouled membranes. Adhesion force and elasticity values, again for both Hertz and JKR models, measured through AFM force measurement are then shown for clean and industrially fouled membranes at various salt concentrations and pH values. Also adhesion force and elasticity values for both models achieved from purposefully fouled membranes with the chosen four isolated bacterial species from the culture-dependent technique at industrially relevant conditions are then shown.

## 5.3.1. Contact Tip Experiment

For the achievement of force measurements that give both accurate and relevant data from RO membranes, a number of experiments need to be performed to investigate the effect of AFM parameters on the values of adhesion force and elasticity achieved on both clean and fouled membranes. The AFM study of both clean and fouled membrane is important as not only do the mechanisms involved in cell to membrane adhesion need to be investigated for the prevention of biofilm formation but also mechanisms involved in cell to biofilm, (or silica to biofilm) need to be investigated for the control and limitation of biofouling on membranes. Therefore both clean and fouled membranes were investigated in the parameter study to determine the optimum parameters suitable for force measurements on each membrane. Firstly tip geometry was investigated through the use of a sharp contact tip and a silica colloid probe. The experiment was performed in conditions of 0.1M NaCl at three different pH values of 3, 7 and 9. The pH values were chosen as pH 3 is close to the isoelectric points of the virgin membrane and the bacterial isolates, pH 7 as it is neutral and industrially relevant as it is close to the pH of seawater and pH 9 to test alkaline conditions. Table 5.1 displays the variation of adhesion force with changing pH for both virgin and fouled membranes using a contact tip. The range of values of adhesion force experienced by the contact tip for the virgin membrane ranged from 1.95 +/- 1.64 to 2.56 +/- 1.46 nN. The range of values of adhesion force experienced by the contact tip for the fouled membrane ranged from 1.54+/- 1.64 to 2.46 +/- 1.39 nN. There appears to be a weak trend that as the pH value is increased the adhesion force decreases, however the values of standard deviation are relatively high and therefore this trend cannot be confirmed. Table 5.2 shows the variation of adhesion force with changing pH for both virgin and fouled membranes using a silica colloid tip. The range of values of adhesion force

experienced by the colloid probe for the virgin membrane ranged from 0.84 +/- 0.69 to 9.21 +/- 6.13 nN, while for the fouled membrane ranged from 0.81 +/- 0.20 to 1.45 +/- 0.93 nN. The adhesion values at pH 3 are much higher than those obtained for pH 7 and 9 and there are differences between the virgin membrane and the fouled membrane at pH 3, which is due to the difference in surface material. There are large standard deviations for adhesion force values which shows that the adhesion values fluctuate widely over the virgin and fouled membranes, however at pH 7 and 9 the values for adhesion are relatively constant over the virgin and fouled membranes surfaces.

Therefore the comparison between the contact tip and the silica colloid probe for achieved adhesion values demonstrate that the silica colloid probe is more sensitive to pH values than the contact tip, especially at pH 3, however the ranges of adhesion ranges, especially for pH 7 and pH 9 are similar.

| pH | Adhesion Force (nN) | | | |
|---|---|---|---|---|
| | Virgin membrane | | Fouled membrane | |
| | Average | stdev | Average | stdev |
| 3 | 2.56 | 1.40 | 2.46 | 1.40 |
| 7 | 2.01 | 1.50 | 1.93 | 1.50 |
| 9 | 1.95 | 1.64 | 1.54 | 1.64 |

Table 5.1 Adhesion Force for virgin and industrially fouled RO membranes using a contact tip.

| pH | Adhesion Force (nN) | | | |
|---|---|---|---|---|
| | Clean membrane | | Fouled membrane | |
| | Average | stdev | Average | stdev |
| 3 | 9.21 | 6.13 | 1.45 | 0.93 |
| 7 | 1.66 | 1.00 | 0.70 | 0.66 |
| 9 | 0.84 | 0.69 | 0.81 | 0.20 |

Table 5.2 Adhesion Force for virgin and industrially fouled RO membranes using a silica colloid probe.

Table 5.3 displays the variation of Young's modulus achieved with the Hertz model with pH and Table 5.4 displays the variation of Young's modulus achieved with the JKR with pH for both the virgin and fouled membranes using a contact tip. The range of values of Young's modulus for the virgin membrane achieved using the Hertz model

of values of Young's modulus for the virgin membrane achieved using the Hertz model are 546 +/- 165 to 603 +/- 160 kPa and the Young's modulus achieved using the JKR model for the virgin membrane are 562 +/- 186 to 646 +/- 235 kPa. The range of values of Young's modulus for the fouled membrane achieved using the Hertz model are 419 +/- 192 to 567 +/- 180 kPa and the Young's modulus achieved using the JKR model for the fouled membrane are 410 +/- 196 to 633 +/- 205 kPa. There appears to be a slight decrease in Young's modulus from pH 3 to pH 7 and a large decrease in Young's modulus between pH 7 to pH 9 for both Hertz and JKR models, however again in should be noted that large values of standard deviation were achieved for each measurement and therefore this trend cannot be confirmed. There seems to be a slight increase in the values achieved using the JKR model compared to those achieved for the Hertz model. Table 5.5 displays the variation of Young's modulus achieved with the Hertz model with pH and Table 5.6 displays the variation of Young's modulus achieved with the JKR model with pH for both the virgin and fouled membranes using a silica colloid tip. The range of values of Young's modulus for the virgin membrane achieved using the Hertz model are 52.33 +/- 13.51 to 59.56 +/- 12.29 kPa and Young's modulus achieved using the JKR model for the virgin membrane are 58.26 +/- 12.57 to 69.92 +/- 20.21 kPa. The range of values of Young's modulus for the fouled membrane achieved using the Hertz model are 28.90 +/- 5.32 to 32.20 +/- 7.96 kPa and Young's modulus achieved using the JKR model for the fouled membrane are 30.43 +/- 6.60 to 33.01 +/- 8.10 kPa. The silica colloid probe values of Young's modulus seem to remain relatively stable over the pH value range for those achieved with the Hertz model, however for the JKR model there seems to be a decrease in Young's modulus from pH 3 to pH 7 for the virgin membrane, however the standard deviation is very large which might account for this decrease in Young's modulus. There does not seem to be any significant difference between the Hertz model and the JKR model for this experiment using the colloid probe.

Therefore it can be seen that tip geometry does have an effect on values achieved using force measurements, especially in the values of Young's modulus obtained. The contact tip demonstrated a much higher value of Young's Modulus than those achieved using a colloid probe. Dimitriadis *et al* [171] performed a comparison study of sharp tips and microsphere probes indenting a thin layer poly (vinyl alcohol) gel, where the results demonstrate the inappropriateness of sharp tips for thin, soft samples while

showing the accuracy of Young's modulus values when using microspheres of either 2 or 5 μm radius where the results were deemed excellent.

| pH | Hertz Young's modulus (kPa) | | | |
|---|---|---|---|---|
| | Virgin membrane | | Fouled membrane | |
| | Average | stdev | Average | stdev |
| 3 | 602.65 | 160.34 | 567.02 | 180.34 |
| 7 | 598.43 | 174.04 | 536.51 | 204.04 |
| 9 | 546.26 | 164.74 | 419.12 | 191.74 |

Table 5.3 Hertz Young's modulus for virgin and industrially fouled RO membranes using a contact tip.

| pH | JKR Young's modulus (kPa) | | | |
|---|---|---|---|---|
| | Clean membrane | | Fouled membrane | |
| | Average | stdev | Average | stdev |
| 3 | 646.34 | 235.46 | 633.17 | 205.46 |
| 7 | 603.58 | 192.20 | 571.95 | 212.20 |
| 9 | 562.15 | 186.20 | 440.95 | 196.20 |

Table 5.4 JKR Young's modulus for virgin and industrially fouled RO membranes using a contact tip.

| pH | Hertz Young's modulus (kPa) | | | |
|---|---|---|---|---|
| | Clean membrane | | Fouled membrane | |
| | Average | stdev | Average | stdev |
| 3 | 52.33 | 13.51 | 28.90 | 6.63 |
| 7 | 55.07 | 12.06 | 32.20 | 7.96 |
| 9 | 59.56 | 12.29 | 31.57 | 5.32 |

Table 5.5 Hertz Young's modulus for virgin and industrially fouled RO membranes using a silica colloid probe.

| pH | JKR Young's modulus (kPa) | | | |
|---|---|---|---|---|
| | Clean membrane | | Fouled membrane | |
| | Average | stdev | Average | stdev |
| 3 | 69.92 | 20.21 | 30.43 | 6.60 |
| 7 | 58.26 | 12.57 | 33.01 | 8.10 |
| 9 | 60.99 | 12.47 | 31.69 | 4.68 |

Table 5.6 JKR Young's modulus for virgin and industrially fouled RO membranes using a silica colloid probe.

Therefore the silica colloid probe was chosen for the adhesion and indentation studies of the membranes. This is due to two reasons. RO membranes are susceptible to fouling by colloidal particles due to their properties, such as high surface roughness. Silica particles have manifested to be a type of foulant on membrane surfaces [6]. Boubakri *et al* [172] discovered from a RO membrane autopsy from Djerba island desalination station, that the fouling layer was mostly composed from organic matter, silica, iron and $CaCO_3$. The high amount of silica is thought to be due to loose sand particles from the pre-treatment sand filters due to the filtration on the particle/water suspension being conducted under high pressure. Fujairah RO Water Plant utilises dual-media filters for the pre-treatment of the seawater which contains sand and pumice and therefore the membranes may be susceptible to silica fouling [111]. Therefore through adhesion measurements of silica to the clean and fouled membrane surfaces, conclusions about colloidal fouling can be obtained, especially for process fouled membrane surfaces, as it seems that this research has not yet been performed in the literature. The second reason for the use of a silica colloid probe is for its shape. The colloid probe technique allows for a well-defined shape colloid probe [28]. The silica colloids are spherical in size and have a much larger 1.5-5 μm radius than the typically manufactured silicon nitride sharp tips, roughly 2 - 20 nm radius, whose radius of curvature is given by the manufacturer and is given between limits. This means that on a soft surface, the silica colloid probe will more likely compress the surface, unlike sharp tips which could puncture and disrupt the surface as sharp tips induce local strains that can far exceed the linear material regime. Therefore silica colloid measurements of elasticity will be more representative of the surface as it is taken over a larger area, due to the radius of the sphere and also the measurement will be of the elasticity of the surface, rather than the layers underneath.

However, it must be noted that the use of the colloid probe for indentation with use of the Herztian models for calculation of elasticity will lead to a reduced value of Young's modulus as when compared to that for a sharp tip [171]. Due to incorrect assumptions in the elasticity models, researchers currently suggest that force measurements should be used in comparison with other results obtained in a similar method instead of taking the value of Young's modulus as absolute. Therefore the silica colloid probe is argued to be suitable for use within this experiment.

### 5.3.2 Loading Force Experiments

The second AFM parameter to be investigated is the loading force applied to the membrane surface. This is a crucial parameter as the loading force influences the indentation depth into the sample surface and therefore where the measurements of elasticity will be taken from. The loading force was varied from 10 to 100nN using the silica colloid probe on the virgin and fouled membrane surfaces and the values of adhesion force and Young's modulus using both Hertz and JKR models measured. Figure 5.1 shows the variation of adhesion force with varying loading force for both virgin and fouled membranes using a colloid probe. The range of values of adhesion force experienced by the probe for the virgin membrane ranged from 3.83+/- 1.94 to 5.51 +/- 3.19 nN and for the fouled membrane the range is 0.69+/- 0.76 to 3.22 +/- 2.87 nN. From Figure 5.1, it is observed that loading force has a negligible effect on the values of adhesion force for the virgin membrane, however as for the fouled membrane, as the loading force increases so does the adhesion force. This can be explained as the increased loading force means that the indentation depth into the fouled membrane is increased, therefore the contact area between the colloid probe and the surface is increased, resulting in a larger adhesion value.

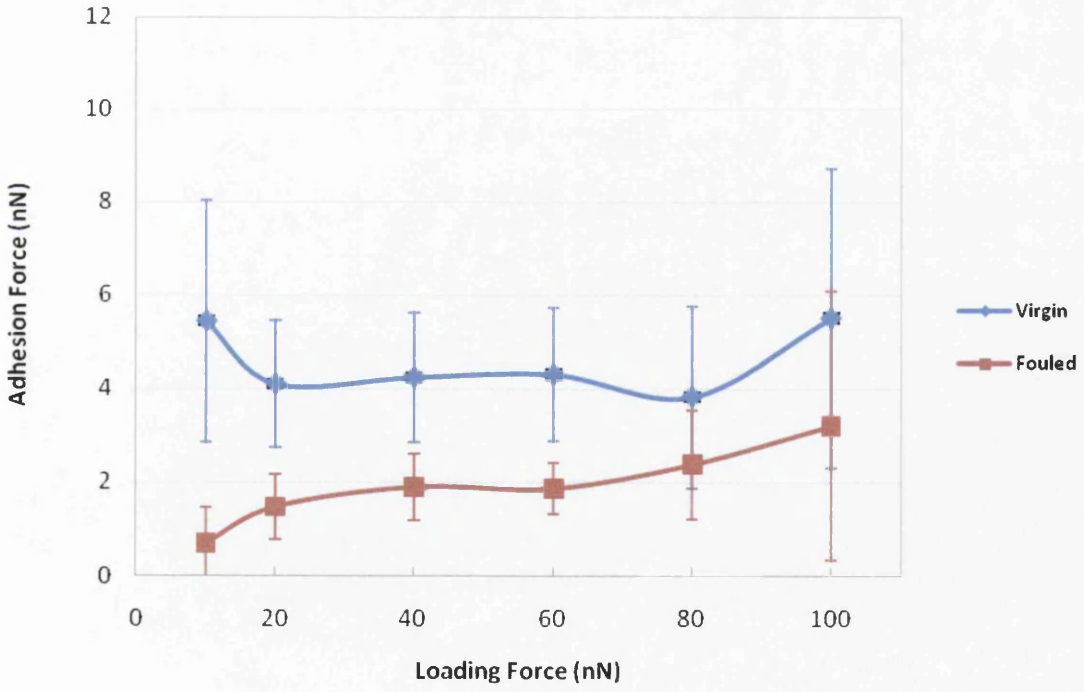


Figure 5.1 Adhesion Force for virgin and industrially fouled RO membranes at various loading forces.

Figure 5.2 shows the variation of Young's modulus achieved with the Hertz model with loading force and Figure 5.3 shows the variation of Young's modulus achieved with the JKR with loading force for both the virgin and fouled membranes using a silica colloid probe. The range of values of Young's modulus for the virgin membrane achieved using the Hertz model are 36.75 +/- 4.75 to 57.83 +/- 23.94 kPa and Young's modulus achieved using the JKR model are 38.35 +/- 4.86 to 77.47 +/- 28.55 kPa. From Figures 5.2 and 5.3, there appears to be a decrease in Young's modulus with increasing loading force for the virgin membrane for both models, Hertz and JKR models, however the decrease in Young's modulus is more pronounced with the JKR model. Also the standard deviation for the data is high at low loading forces but decreases in magnitude with increasing loading force, therefore the values obtained for Young's modulus fluctuate across the membrane surface at low loading forces. This could be due to the inherently rough surface of the RO membrane having an effect on Young's modulus values at low indentation depths. The range of values of Young's modulus for the fouled membrane achieved using the Hertz model are 25.54 +/- 3.97 to 32.13 +/- 7.34 kPa and Young's modulus achieved using the JKR model for the fouled membrane are 26.29 +/- 9.76 to 33.52 +/- 8.18 kPa. Loading force does not seem to have a significant effect on Young's modulus obtained from the fouled membrane for both the Hertz and JKR models.

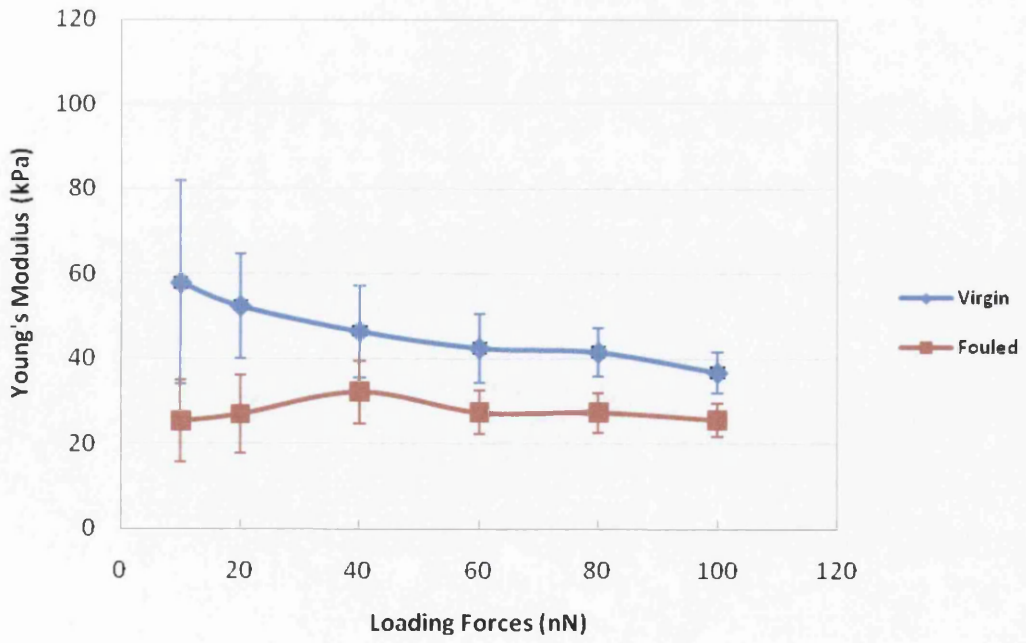


Figure 5.2 Hertz Young's modulus for virgin and industrially fouled RO membranes at various loading forces.

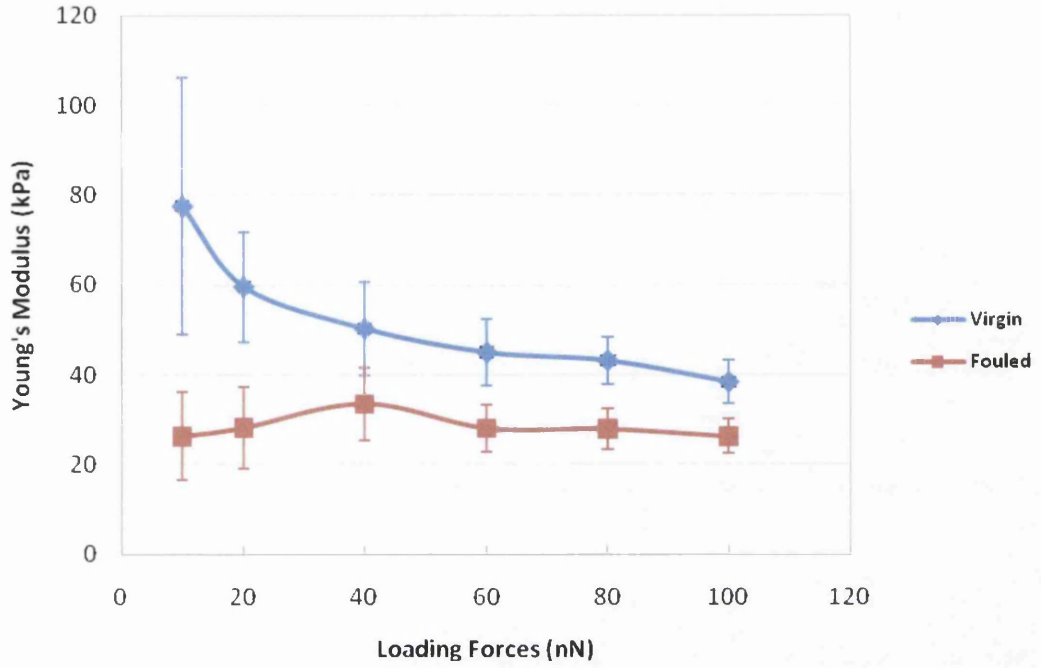


Figure 5.3 JKR Young's modulus for virgin and industrially fouled RO membranes at various loading forces.

## 5.3.3 Extension Speed Experiments

The third AFM parameter to be investigated is the extension speed applied to the colloid probe. The extension speed is the speed at which the tip approaches the surface. The extension speed was varied from 0.1 to 0.9 μm/s, using the silica colloid probe on the virgin and fouled membrane surfaces and the values of adhesion force and Young's modulus using both Hertz and JKR models measured. Figure 5.4 shows the variation of adhesion force with varying extension speed for both virgin and fouled membranes using a colloid probe. The range of values of adhesion force experienced by the probe for the virgin membrane ranged from 4.24 +/- 1.38 to 9.60 +/- 2.62 nN and for the fouled membrane the range is 1.47 +/- 1.22 to 2.83 +/- 2.15 nN. From Figure 5.4, it can be seen that the values of adhesion force fluctuates as the extension speed is increased, especially for the virgin membrane. No trend can be established as the standard deviation of the data is relatively high for both the virgin and fouled membranes.

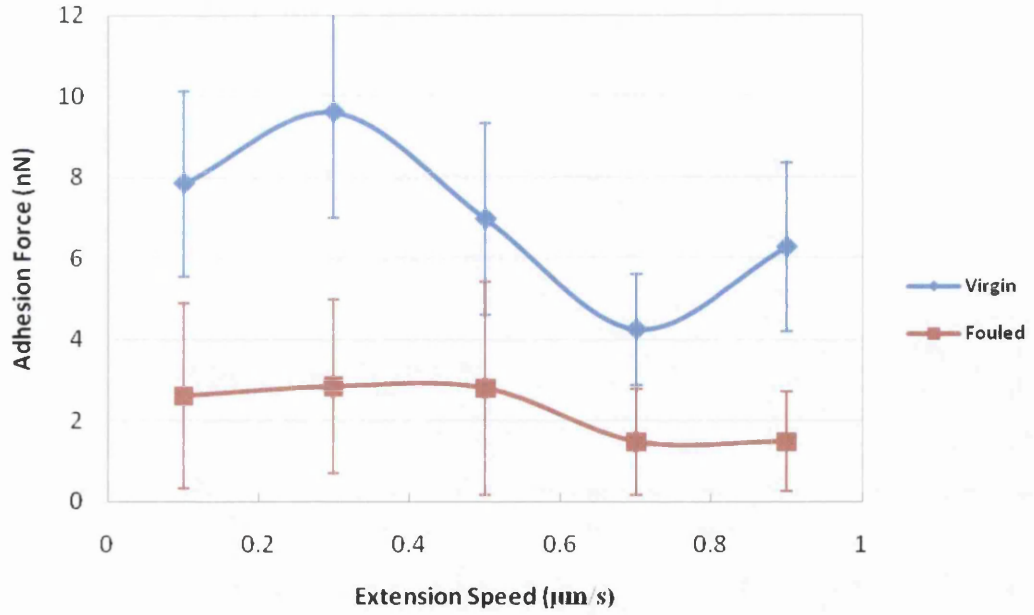


Figure 5.4 Adhesion Force for virgin and industrially fouled RO membranes at various extension speeds.

Figure 5.5 shows the variation of Young's modulus achieved with the Hertz model with extension speed and Figure 5.6 shows the variation of Young's modulus achieved with the JKR model with extension speed for both the virgin and fouled membranes using a silica colloid probe. The range of values of Young's modulus for the virgin membrane achieved using the Hertz model are 38.34 +/- 10.56 to 46.42 +/- 10.82 kPa and Young's modulus achieved using the JKR model for the virgin membrane are 44.55 +/- 11.23 to 51.61 +/- 10.44 kPa. The range of values of Young's modulus for the fouled membrane achieved using the Hertz model are 24.74 +/- 9.41 to 33.50 +/- 9.74 kPa and Young's modulus achieved using the JKR model for the fouled membrane are 25.97 +/- 9.79 to 34.40 +/- 9.75 kPa. From Figures 5.5 and 5.6 it can be seen Young's modulus fluctuates slightly, with large standard deviations values, so no trend could be established. Therefore extension speed does not seem to have a significant effect on Young's modulus obtained from the fouled membrane for both the Hertz and JKR models.

A similar study has been performed by Xu *et al* [173]. Xu *et al* determined the effect of residence time, loading force, pH and ionic strength on the adhesion forces between colloids and dextran, lysozyme and BSA coated surfaces, where increasing residence time and the increasing loading force both increased the adhesion force measured during the retraction of the tip. Adhesion force decreased with increasing pH.

However, no literature has been found for the effect of such parameters using commercial membrane surfaces, where the results have more significant industrial relevance.

It was decided to use a low loading force regime so that any plastic deformations which might occur are minor, as plastic deformations are expected to depend on the value of loading force. However from the results a 20nN loading force was chosen as 10nN had a large standard deviation of data. In addition, for the foulant layer on the industrial membranes and bacterial layer achieved by filtration, force measurements should only have a small indentation depth into the sample or the underlying membrane will have an effect on the values of elasticity obtained from foulant layers, so a low loading force was used. The approach speed was chosen at 0.3μm/s so that the contact between the sample and the tip would be long enough to measure relatively high values of adhesions for both the virgin and fouled membranes.

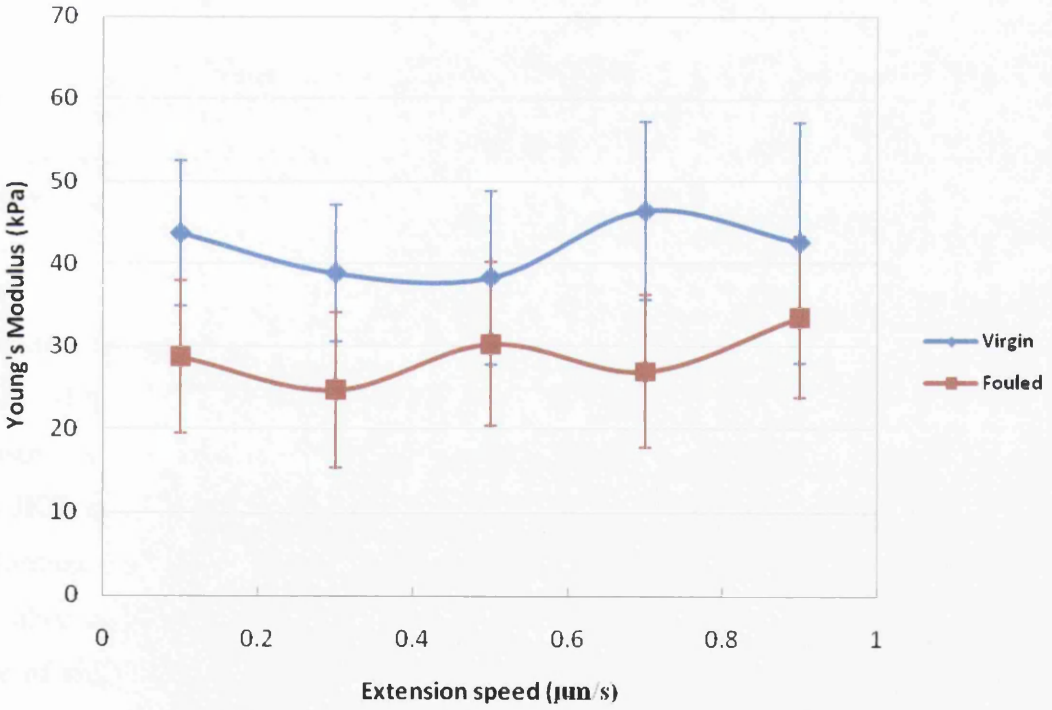


Figure 5.5 Hertz Young's modulus for virgin and industrially fouled RO membranes at various extension speeds.

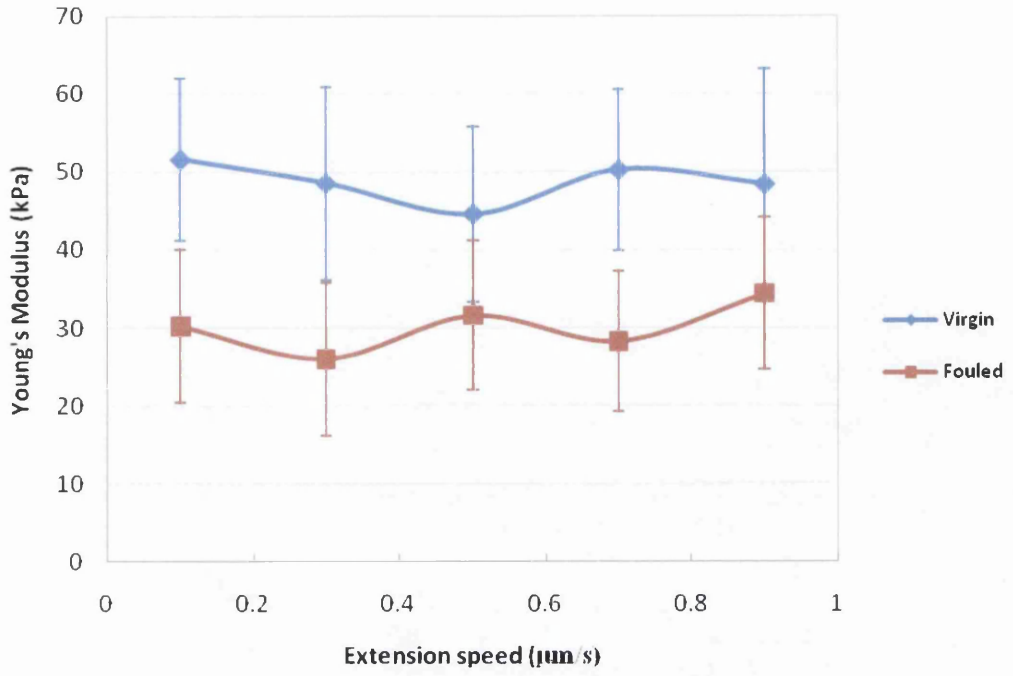


Figure 5.6 JKR Young's modulus for virgin and industrially fouled RO membranes at various extension speeds.

## 5.3.4. Effect of pH and Salt Concentration on the Adhesion Force and Elasticity of both virgin and industrially fouled membranes

Once the optimum settings for the AFM parameters had been chosen, force measurements were performed on clean and industrially fouled membranes at various NaCl, $MgCl_2$ and $CaCl_2$ concentrations and three different pH values to achieve measurements of maximum adhesion force and elasticity using both the Hertz-Sneddon and JKR models. Force measurements at 0.6M NaCl concentration and pH 7 were performed due to its industrial relevance as its close to conditions of seawater, however the other measurements were performed to see the effect of certain conditions in the hope of aiding cleaning regimes associated with RO desalination processes. Table 5.7 displays the variation of adhesion force with pH for different salt concentrations for the virgin membrane using a colloid probe. The range of values of adhesion force experienced by the probe for the virgin membrane at 0.1M NaCl ranged from 0.84 +/- 0.69 to 9.21 +/- 6.13 nN and for the 0.6M NaCl the range is 0.97+/- 0.72 to 6.09 +/- 4.22 nN. The values of adhesion force obtained for the divalent ions at ionic strength of

0.1M are very similar for both Magnesium and Calcium ions. The values of adhesion force for the divalent ions range from 1.61 +/- 0.87 to 2.70 +/- 2.05 nN. As seen in Table 5.7, the adhesion force from the virgin membrane in the presence of the divalent ions at the ionic strength of 0.1M does not vary much over the range of pH, however in the presence of monovalent ions at the ionic strength of 0.1M, the adhesion force decreases with increasing pH. Also there seems to be a slight decrease in the adhesion force values obtained for 0.6M NaCl when compared to 0.1M NaCl, even though the trend of adhesion force decreases with increasing pH values still exist. However the values of large standard deviation obtained at pH 3 shows that the adhesion force varies much across the surface of the membrane at this pH 3 for the monovalent ion.

Table 5.8 shows the variation of adhesion force with pH at various salt concentrations for fouled membranes using a colloid probe. The range of values of adhesion force experienced by the probe for the fouled membrane at 0.1M NaCl ranged from 0.70 +/- 0.66 to 1.45 +/- 0.93 nN and for the 0.6M NaCl the range is 0.63 +/- 0.78 to 0.90 +/- 0.10 nN. The values of adhesion force obtained for the divalent ions at ionic strength of 0.1M are very similar for both Magnesium and Calcium ions. The values of adhesion force for the divalent ions range from 1.03 +/- 1.00 to 2.53 +/- 3.49 nN. As seen in Table 5.8, the adhesion force obtained from the fouled membrane for all salt conditions does not vary much over the range of pH when considering the standard deviations, apart from a slightly rise in adhesion force at pH 9 for the divalent ions. This is a marked difference from the virgin membrane where the membrane showed a dependence on pH 3 and monovalent salt concentration.

For the virgin membrane, the maximum adhesion occurred at pH 3, where surface charge of the membrane is positively charged, and is close to the isoelectric point of the membrane (see Chapter 4) therefore the electric double layer is relatively thin [174]. The changes in adhesion forces measured as a function of pH could be due to the change in the ionization state of the membrane surface. As the pH is increased, the membrane becomes negatively charged and the silica colloid is strongly negatively charged at high pH values [174], so as the particle approaches the membrane surface in these conditions, the colloid experiences increasing electrostatic double-layer repulsive force which opposes the motion of the colloid. Due to the repulsive force, the particle may be prevented from coming into intimate contact with the membrane surface, which

leads to a lower adhesion force. This is a favorable condition for the prevention of membrane fouling [6]. For the fouled membrane, the surface charge of the membrane is negative over all pH values (Chapter 4) which means that the colloid experiences a repulsive force over all pH values and therefore the adhesion force values show only a slight variation with pH values [175].

Previous adhesion force measurement studies by Bowen *et al* [83] on an virgin RO membrane using silica colloid probes have chosen a constant probe movement of 0.1μm/s and a maximum loading force of 120nN – 140nN. The force measurements were performed in varying NaCl solutions of concentrations $10^{-3}$M, $10^{-2}$M and $10^{-1}$M and at pH 9. The study revealed that as NaCl concentration increased the value of adhesion force measured increased. For the force measurements performed on peaks of the membrane, the adhesion increased from 0.3 +/- 0.17mN/m to 2.3 +/- 0.48 mN/m and for the force measurements performed within the membrane valleys, the adhesion increased from 6.5 +/- 6.5 to 8.7 +/- 4.0mN/m [83]. The results obtained during this study have investigated 0.1M and 0.6M NaCl concentrations, however the results obtained at 0.1M NaCl at pH 9 reveal adhesion force values of 0.83 nN, which when normalized for colloid radius of 3μm the adhesion value is 2.77mN/m, which falls between the adhesion values achieved for the membrane peak and valleys.

| pH | Adhesion Force (nN) | | | | | | | |
|---|---|---|---|---|---|---|---|---|
| | 0.1M $Na^+$ | | 0.6M $Na^+$ | | $Ca^{2+}$ | | $Mg^{2+}$ | |
| | Average | stdev | Average | stdev | Average | stdev | Average | stdev |
| 3 | 9.21 | 6.13 | 6.09 | 4.22 | 1.73 | 1.34 | 2.70 | 2.05 |
| 7 | 1.66 | 1.00 | 1.67 | 1.13 | 1.61 | 0.87 | 1.80 | 1.07 |
| 9 | 0.84 | 0.69 | 0.97 | 0.72 | 2.18 | 1.51 | 1.82 | 1.57 |

Table 5.7 Adhesion Force for virgin RO membranes at various salt concentrations.

| pH | Adhesion Force (nN) | | | | | | | |
|---|---|---|---|---|---|---|---|---|
| | 0.1M $Na^+$ | | 0.6M $Na^+$ | | $Ca^{2+}$ | | $Mg^{2+}$ | |
| | Average | stdev | Average | stdev | Average | stdev | Average | stdev |
| 3 | 1.45 | 0.93 | 0.63 | 0.78 | 1.84 | 1.75 | 1.82 | 1.86 |
| 7 | 0.70 | 0.66 | 0.90 | 0.10 | 1.12 | 1.12 | 1.03 | 1.00 |
| 9 | 0.81 | 0.20 | 0.79 | 0.93 | 1.63 | 2.47 | 2.53 | 3.49 |

Table 5.8 Adhesion Force for industrially fouled RO membranes at various salt concentrations.

Table 5.9 shows the variation of Young's modulus with pH at various salt concentrations achieved with the Hertz model and Table 5.10 with the JKR model for the virgin membrane using a silica colloid probe. Table 5.11 shows the variation of Young's modulus with pH at various salt concentrations achieved with the Hertz model and Figure 5.12 with the JKR model for the fouled membrane using a silica colloid probe. The range of values of Young's modulus for the virgin membrane at 0.1M NaCl achieved using the Hertz model are 52.33 +/- 13.51 to 59.56 +/- 12.29 kPa and Young's modulus achieved using the JKR model for the virgin membrane are 58.26 +/- 12.57 to 69.92 +/- 20.21 kPa. The range of values of Young's modulus for the virgin membrane at 0.6M NaCl achieved using the Hertz model are 52.01 +/- 7.56 to 58.77 +/- 7.64 kPa and Young's modulus achieved using the JKR model for the virgin membrane are 53.72 +/- 8.07 to 71.95 +/- 13.76 kPa. The range of values of Young's modulus for the virgin membrane at 0.1M ionic strength of the divalent ions achieved using the Hertz model are 55.96 +/- 10.19 to 61.71 +/- 10.35 kPa and Young's modulus achieved using the JKR model for the virgin membrane are 59.56 +/- 11.15 to 67.05 +/- 10.99 kPa. From Table 5.9, achieved using the Hertz model, it can be seen that the Young's modulus all for conditions of salt concentration does not significantly vary with pH, when considering the large values of standard deviation, however Table 5.10, achieved using the JKR model, shows a slight decrease from pH 3 to pH 7 for 0.1M and 0.6M NaCl and also for 0.1M ionic strength $MgCl_2$. Therefore the Hertz model suggest no dependence on salt concentration or pH values on the values of Young's modulus, however JKR suggests a slight dependence on pH values, especially at pH 3.

| **pH** | **Hertz Young's modulus (kPa)** | | | | | | | |
|---|---|---|---|---|---|---|---|---|
| | 0.1M $Na^+$ | | 0.6M $Na^+$ | | $Ca^{2+}$ | | $Mg^{2+}$ | |
| | Average | stdev | Average | stdev | Average | stdev | Average | stdev |
| 3 | 52.33 | 13.51 | 58.77 | 7.64 | 55.96 | 10.19 | 61.71 | 10.35 |
| 7 | 55.07 | 12.06 | 55.57 | 6.83 | 58.36 | 11.83 | 56.40 | 10.67 |
| 9 | 59.56 | 12.29 | 52.01 | 7.56 | 56.88 | 7.68 | 59.29 | 8.77 |

Table 5.9 Hertz Young's modulus for virgin RO membranes at various salt concentrations.

| pH | JKR Young's modulus (kPa) | | | | | | | |
|---|---|---|---|---|---|---|---|---|
| | 0.1M $Na^+$ | | 0.6M $Na^+$ | | $Ca^{2+}$ | | $Mg^{2+}$ | |
| | Average | stdev | Average | stdev | Average | stdev | Average | stdev |
| 3 | 69.92 | 20.21 | 71.95 | 13.76 | 59.56 | 11.15 | 67.05 | 10.99 |
| 7 | 58.26 | 12.57 | 58.84 | 7.86 | 61.64 | 12.78 | 59.71 | 11.55 |
| 9 | 60.99 | 12.47 | 53.72 | 8.07 | 60.95 | 8.30 | 63.01 | 10.30 |

Table 5.10 JKR Young's modulus for virgin RO membranes at various salt concentrations.

Table 5.11 shows the variation of Young's modulus with pH at various salt concentrations achieved with the Hertz model and Table 5.12 with the JKR model for the fouled membranes using a silica colloid probe. The range of values of Young's modulus for the fouled membrane at 0.1M NaCl achieved using the Hertz model are 28.90 +/- 6.63 to 32.20 +/- 7.96 kPa and Young's modulus achieved using the JKR model for the fouled membrane are 30.43 +/- 6.60 to 33.01 +/- 8.10 kPa. The range of values of Young's modulus for the fouled membrane at 0.6M NaCl achieved using the Hertz model are 19.47 +/- 6.81 to 26.89 +/- 9.15 kPa and Young's modulus achieved using the JKR model for the fouled membrane are 20.02 +/- 6.96 to 27.78 +/- 9.48 kPa. The range of values of Young's modulus for the fouled membrane at 0.1M ionic strength of the divalent ions achieved using the Hertz model are 19.35 +/- 7.21 to 38.61 +/- 10.33 kPa and Young's modulus achieved using the JKR model for the fouled membrane are 20.04 +/- 7.58 to 40.29 +/- 10.71 kPa. From Table 5.11, achieved using the Hertz model, it can be seen Young's modulus may have a slight dependence on salt concentrations and pH. The values of Young's modulus for 0.6M NaCl are slightly reduced from the 0.1M NaCl and the Young's modulus of 0.1M $MgCl_2$ are slightly reduced from 0.1M $CaCl_2$. Also the Young's modulus for the divalent ions seem to decrease from pH 3 to pH 7 but rise slightly from pH 7 to pH 9. Table 5.12 achieved using the JKR model shows the same trend. Thus, Young's modulus values for the fouled membrane may have a weak dependence on pH and salt concentrations. This could be due to the nature of the foulants within the fouling layer present on the membrane responding weakly to the environmental conditions and thereby slightly altering the value of Young's modulus achieved.

There is extremely limited literature on the nanoindentation of membranes, and no literature was found for RO membranes, indenting membranes with a silica colloid

probe, and the effect of industrially relevant conditions on the elasticity of the membrane. In one of the few studies into nanoindentation on commercial membranes, Franceschini *et al* [72] determined the elastic moduli of nafion, PBI and poly [2, 5-benzimidazole] membranes, both undoped and phosphoric acid doped, using AFM force spectroscopy. A sharp contact tip was used and the force measurements were performed in dry conditions in a $N_2$ environment. The elasticity values measured for the different membranes ranged from 0.104 +/- 0.036 to 6.17 +/- 0.93 GPa. The measurements for the RO membranes using a contact tip ranged from 419 +/- 191 to 567 +/- 180 kPa using the Hertz model, while using the silica colloid probe was approximately 50kPa. The difference between these values is due to the environment in which the measurements are taken in. The indentation experiments in this study are performed in a liquid environment, as would be in the industrial process, which means that the membrane is hydrated and therefore its elasticity value would decrease. Also a different type of membrane is used which could also account for this difference. The studies performed here are industrially relevant at salt concentrations which would be present within the desalination process, unlike other studies [72].

| pH | Hertz Young's modulus (kPa) | | | | | | | |
|---|---|---|---|---|---|---|---|---|
| | 0.1M $Na^+$ | | 0.6M $Na^+$ | | $Ca^{2+}$ | | $Mg^{2+}$ | |
| | Average | stdev | Average | stdev | Average | stdev | Average | stdev |
| 3 | 28.90 | 6.63 | 23.56 | 7.20 | 38.61 | 10.33 | 24.46 | 10.70 |
| 7 | 32.20 | 7.96 | 26.89 | 9.15 | 24.29 | 13.80 | 19.35 | 7.21 |
| 9 | 31.57 | 5.32 | 19.47 | 6.81 | 25.70 | 10.21 | 21.29 | 5.56 |

Table 5.11 Hertz Young's modulus for industrially fouled RO membranes at various salt concentrations.

| pH | JKR Young's modulus (kPa) | | | | | | | |
|---|---|---|---|---|---|---|---|---|
| | 0.1M $Na^+$ | | 0.6M $Na^+$ | | $Ca^{2+}$ | | $Mg^{2+}$ | |
| | Average | stdev | Average | stdev | Average | stdev | Average | stdev |
| 3 | 30.43 | 6.60 | 24.04 | 7.21 | 40.29 | 10.71 | 25.50 | 10.53 |
| 7 | 33.01 | 8.10 | 27.76 | 9.48 | 25.35 | 15.13 | 20.04 | 7.58 |
| 9 | 31.69 | 4.68 | 20.02 | 6.96 | 27.59 | 12.12 | 23.04 | 8.10 |

Table 5.12 JKR Young's modulus for industrially fouled RO membranes at various salt concentrations.

## 5.3.7. Effect of pH and Salt Concentration on the Adhesion Force and Elasticity of bacterial isolates fouled membranes

Force measurements were undertaken on membranes which had been purposely fouled with the four strains of isolated bacteria through the process of high pressure filtration at one NaCl concentration and three different pH values to again achieve measurements of maximum adhesion force and elasticity using both the Hertz-Sneddon and JKR models.

Table 5.13 shows the variation of adhesion force with pH for 0.6M NaCl for the four bacterial isolates using a colloid probe. The range of values of adhesion force experienced by the probe for the *Vibrio* sp. PM6A ranged from 0.80 +/- 0.69 to 1.49 +/- 1.27 nN, adhesion force values for *A.venetianus* ranged from 0.62 +/- 0.45 to 1.56 +/- 0.74 nN, adhesion force values for *K.pnuemoniae* subsp. *Pneumonia* ranged is 0.74 +/- 0.57 to 0.92 +/- 0.76 nN and adhesion force values for the uncultured bacterium ranged from 0.21 +/- 0.21 to 0.70 +/- 0.60 nN. As seen in Table 5.13, there is no common trend of the adhesion force values for all the bacterial species, with the uncultured bacterium and *K. pneumoniae* showing a slight increase in adhesion force over the pH values 3 to 9, while *Vibrio sp. PM6A* shows a decrease in adhesion force with increasing pH and *A.venetianus* shows a dramatic increase in adhesion force from pH 3 to pH 7. The standard deviation values obtained for all the adhesion force measurements were relatively high therefore it cannot be said conclusively that these trends exist.

| pH | Adhesion Force (nN) | | | | | | | |
|---|---|---|---|---|---|---|---|---|
| | *Vibrio* sp. PM6A | | *K.pnemoniae* | | *A.venetianus* | | Uncultured bacterium | |
| | Average | stdev | Average | stdev | Average | stdev | Average | stdev |
| 3 | 1.49 | 1.27 | 0.74 | 0.57 | 0.62 | 0.45 | 0.21 | 0.21 |
| 7 | 1.00 | 0.69 | 0.76 | 0.65 | 1.56 | 0.74 | 0.43 | 0.57 |
| 9 | 0.80 | 0.69 | 0.92 | 0.76 | 1.54 | 0.56 | 0.70 | 0.60 |

Table 5.13 Adhesion Force for the four bacterial isolates at various pH values.

Table 5.14 shows the variation of Young's modulus with pH for the four bacterial isolates using a colloid probe achieved with the Hertz model and Table 5.15 with the

JKR model. The Young's modulus values for the bacterial species were obtained at 0.6M NaCl and pH 7. The range of values of Young's modulus achieved with the Hertz model for the *Vibrio* sp. PM6A ranged from 2.47 +/- 0.82 to 4.11 +/- 4.09 kPa, Young's modulus values for *A.venetianus* ranged from 13.14 +/- 12.69 to 18.51 +/- 14.17 kPa, Young's modulus values for *K.pnuemoniae* subsp. *Pneumonia* ranged from 14.63 +/- 6.96 to 31.46 +/- 14.22 kPa and Young's modulus values for the uncultured bacterium ranged from 5.71 +/- 2.69 to 16.54 +/- 10.54 kPa. The range of values of Young's modulus achieved with the JKR model for the *Vibrio* sp. PM6A ranged from 2.59 +/- 0.84 to 4.24 +/- 4.21 kPa, Young's modulus values for *A.venetianus* ranged from 14.14 +/- 13.67 to 18.16 +/- 14.33 kPa, Young's modulus values for *K.pnuemoniae* subsp. *Pneumonia* ranged from 14.90 +/- 7.01 to 32.08 +/- 14.46 kPa and Young's modulus values for the uncultured bacterium ranged from 5.78 +/- 2.73 to 16.76 +/- 10.65 kPa. As seen in Table 5.14 and 5.15, there is no common trend of the Young's modulus values for the bacterial species, with *Vibrio* sp. PM6A showing the lowest values of Young's modulus with a possible weak dependence on pH 3 to 7, for uncultured bacterium, the Young's modulus increase rapidly from pH 3 to pH 7 then decrease from pH 7 to pH 9 and *K. pneumoniae* showing a decrease in Young's modulus from pH 3 to pH 7 and then a slight increase over the pH values 7 to 9, while *A.venetianus* shows a decrease in Young's modulus from pH 3 to pH 9. The standard deviation values obtained for all the elasticity measurements were relatively high therefore it cannot be said conclusively that these trends exist.

| **pH** | **Hertz Young's modulus (kPa)** | | | | | | | |
|---|---|---|---|---|---|---|---|---|
| | *Vibrio* sp. PM6A | | *K.pnemoniae* | | *A.venetianus* | | Uncultured bacterium | |
| | Average | stdev | Average | stdev | Average | stdev | Average | stdev |
| 3 | 2.47 | 0.82 | 31.46 | 14.22 | 18.51 | 14.17 | 5.71 | 2.69 |
| 7 | 4.11 | 4.09 | 14.63 | 6.96 | 14.31 | 2.83 | 16.54 | 10.54 |
| 9 | 4.03 | 4.09 | 17.22 | 11.01 | 13.14 | 12.69 | 9.32 | 4.23 |

Table 5.14 Hertz Young's modulus for the four bacterial isolates at various pH values.

| pH | JKR Young's modulus (kPa) | | | | | | | |
|---|---|---|---|---|---|---|---|---|
| | *Vibrio* sp. PM6A | | *K.pnemoniae* | | *A.venetianus* | | Uncultured bacterium | |
| | Average | stdev | Average | stdev | Average | stdev | Average | stdev |
| 3 | 2.59 | 0.84 | 32.08 | 14.46 | 18.16 | 14.33 | 5.78 | 2.73 |
| 7 | 4.24 | 4.21 | 14.90 | 7.01 | 14.84 | 2.95 | 16.76 | 10.65 |
| 9 | 4.12 | 4.21 | 17.81 | 11.46 | 14.14 | 13.67 | 9.43 | 4.34 |

Table 5.15 JKR Young's modulus for the four bacterial isolates at various pH values.

The zeta potential measurements obtained from the four bacterial species (Chapter 3) would indicate that there would be differences observed between the pH values, especially for the adhesion force measurements and that differences could be observed between the uncultured bacterium and the other *γ-Proteobacteria* bacteria. However no significant differences or trends could be established from the data obtained for the adhesion and elasticity values for the four bacterial species, due to variation in the data and the large standard deviations for each measurement. A possible explanation for the wide variation of data obtained from the four bacterial species over the pH values could be due to the high membrane surface roughness. Result of the analyses of AFM virgin membrane images show a relatively high membrane surface roughness, composed of peaks and valleys (Chapter 4). Filtration of the bacterial species onto the membrane surface is thought to have resulted in a non uniform bacterial film depth, as the film would have a greater thickness over the membrane valleys and a lesser thickness over the membrane peaks. Therefore it is thought that when force measurements were performed on the thin bacterial film which was over the membrane peaks, the high elasticity values of the membrane (section 5.3.4) had more of an influence on the elasticity value measured for the bacterial film due to the thin bacterial film depth, however when the force measurements were performed on the bacterial film over the membrane valleys, there is a greater bacterial film depth and the elasticity values measured are more indicative of the actual elasticity of the bacterial film. Also the variation of the adhesion values over the four bacterial species could also be due to the non uniform bacterial thin film depth. Over the membrane peaks, the indentation into the thin film is less due to the higher values of elasticity measured, however over the membrane valleys, the indentation into the thin layer is greater due to the lower values of elasticity. The greater the indentation into a soft sample means that the contact area of the tip and the sample is increased which could increase the values of adhesion force

achieved. Therefore this could be a possible explanation for the wide variation between the adhesion and elasticity measurements obtained for the four bacterial species. A way to reduce the effect of the membrane surface is to increase the depth of the thin film by increasing the amount of bacteria filtered onto the surface, however previous experimental work performed during this study, showed that thicker bacterial films had a tendency to detach from the membrane when surrounded in a liquid environment, due to weak cell to cell forces within the thin film. Therefore there is a need for extremely carefully controlled experiments to determine the optimum bacterial thin film thickness for these force curve experiments and also demonstrates the requirement for the AFM imaging of the virgin membrane. However, this is not a solution of the problem when studying biofilms from real systems.

The variation of elasticity measured over the biofilm film is that biofilms on a membrane surface is a heterogenous system so a normal distribution of parameters measured over an area should be expected. If more force curves had been measured the force data could be plotted as a frequency distribution, and so enable statistical analysis between different aqueous environments to determine if any significant differences were obtained for the different pH values.

### 5.3.6. Example Approach Curves analysed to obtain Elasticity values

Force curve analysis normally utilizes a model, such as Hertzian, for the determination of a numerical value of Young's modulus from the force versus indentation curves, where the gradient of the approach data is taken for use within the model. This allows for a single value of Young's modulus for the system. However this approach is limited for more complex systems which may show multiple gradients on the approach data. A more suitable method is to calculate the Young's modulus at each data point independently on the approach curve, where a graph of Young's modulus versus Indentation can then be drawn. The elasticity value strongly fluctuates at low indentations around the contact point but will reach a plateau with increasing indentation. If the force value is relatively high on a soft sample, the substrate stiffness can have an effect on the elasticity values, causing the Young's modulus value to increase again with increasing indentation. By producing a graph of Young's modulus

versus Indentation for each force curve, the indentation value where the Young's modulus approaches a constant value should be used to determine a single value of Young's modulus [67, 94, 171].

This method of plotting graphs of Young's modulus vs. indentation modulus has been utilized throughout this study to determine a single value of Young's modulus where the value reaches a plateau. However, when examining the force curves performed on the RO membranes fouled with bacterial isolates, due to the complex nature of the thin film, multiple gradients on the approach curves were discovered on a few force curves. The multiple gradients were found on a few force curves from all four bacterial isolates. A few examples of the approach curves exhibiting multiple gradients and the corresponding Young's modulus versus indentation graphs have been included and are shown in Figures 5.7, 5.8 and 5.9. Figure 5.7 (a) shows the approach curve taken on *Vibrio* sp. PM6A, where two gradients can be clearly seen. Figure 5.7 (b) of Young's modulus plotted over indentation shows a break in Young's modulus at approximately 1.80μm, where the Young's modulus rises again. This break corresponds to the first gradient exhibited on the approach curve. Figure 5.8 again shows a break in Young's modulus which occurs at approximately 0.6μm which corresponds to the first gradient on the approach curve. Figure 5.9 shows that even though the approach curve is relatively straight, when the Young's modulus is plotted against indentation, the Young's modulus seems to fluctuate downwards. This method allows for a new way to examine multilayered biofilms, as Young's modulus at various layers within the biofilm can be measured as well as the biofilm layer depth from the surface can be known from the indentation depth. No literature has been found where the elasticity of a biofilm has been investigated at various layers within the biofilm; however such information could aid in determining the ability to break up the developed biofilm on the surface of the membrane and reduce the foulant substances present on the membrane surface.

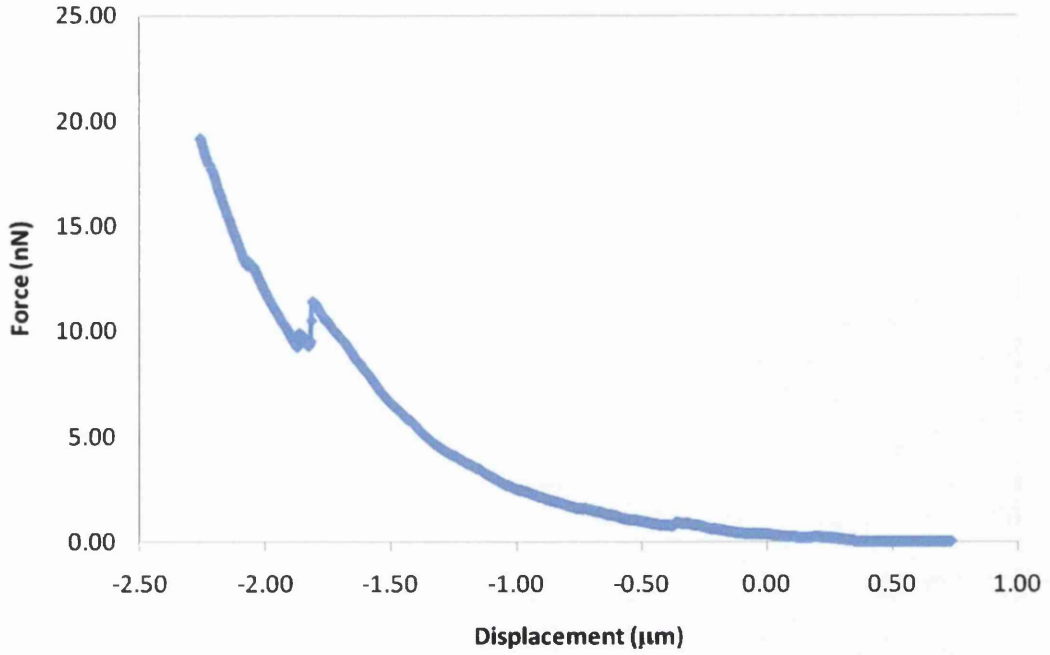


Figure 5.7 (a) Approach Force curve on *Vibrio* sp. PM6A at pH 3 and 0.6M NaCl.

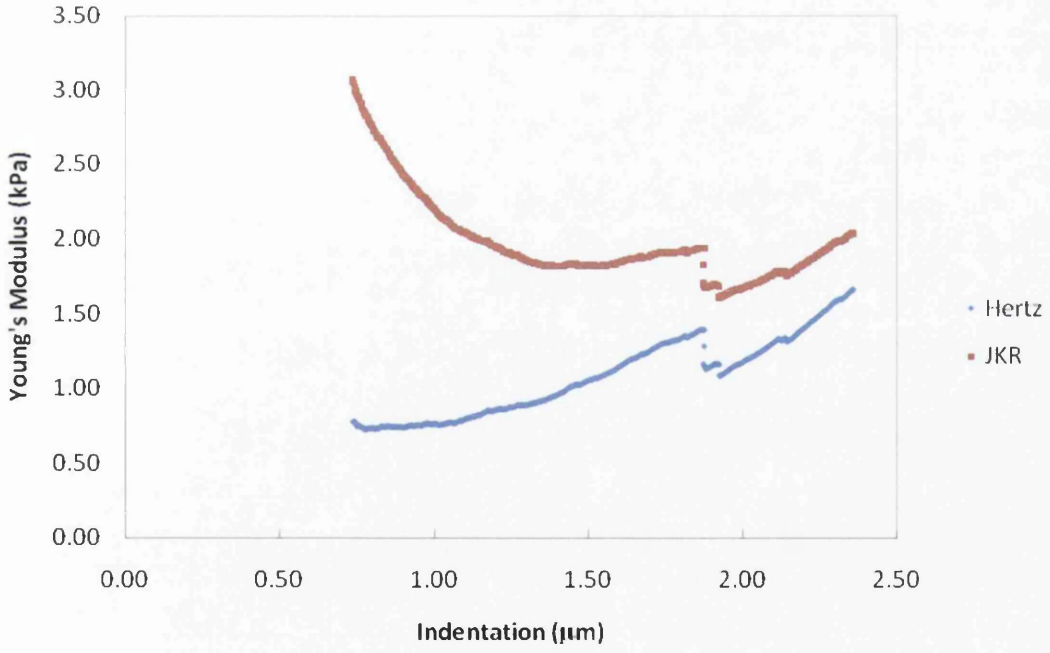


Figure 5.7 (b) Young's modulus variation over approach curve for *Vibrio* sp. PM6A at pH 3 and 0.6M NaCl

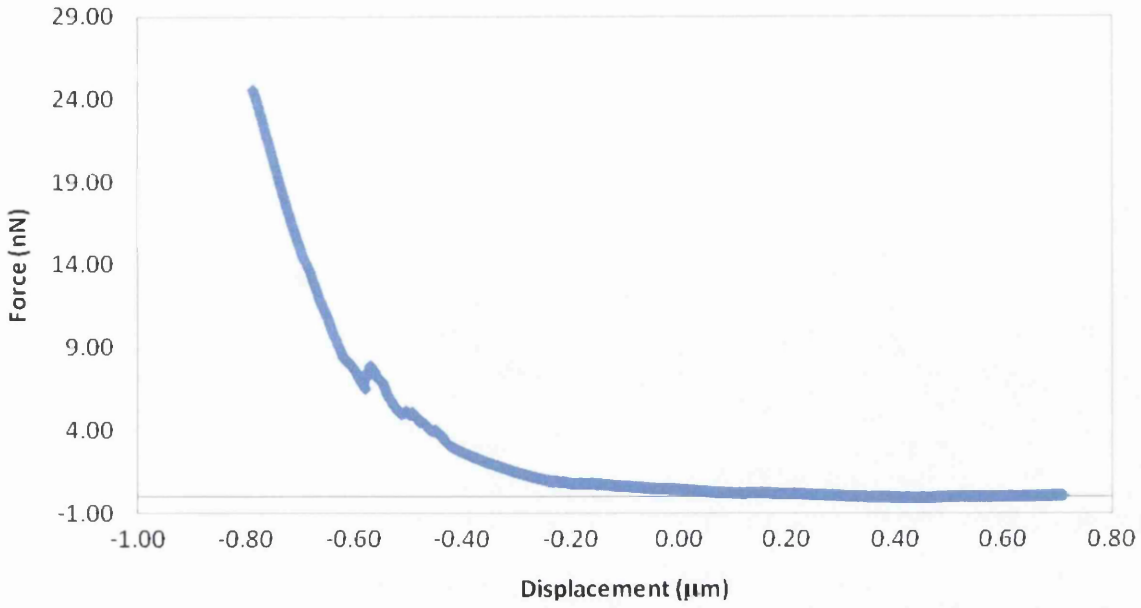


Figure 5.8 (a) Approach Force curve on *K.pnemoniae* at pH 3 and 0.6M NaCl.

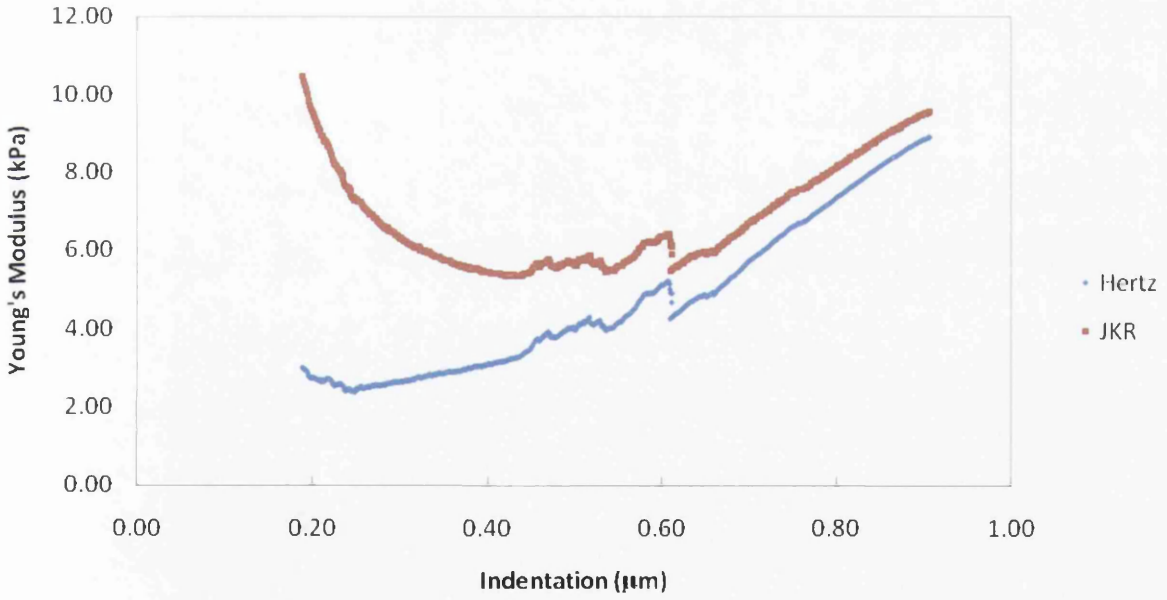


Figure 5.8 (b) Young's modulus variation over approach curve for *K.pnemoniae* at pH 3 and 0.6M NaCl

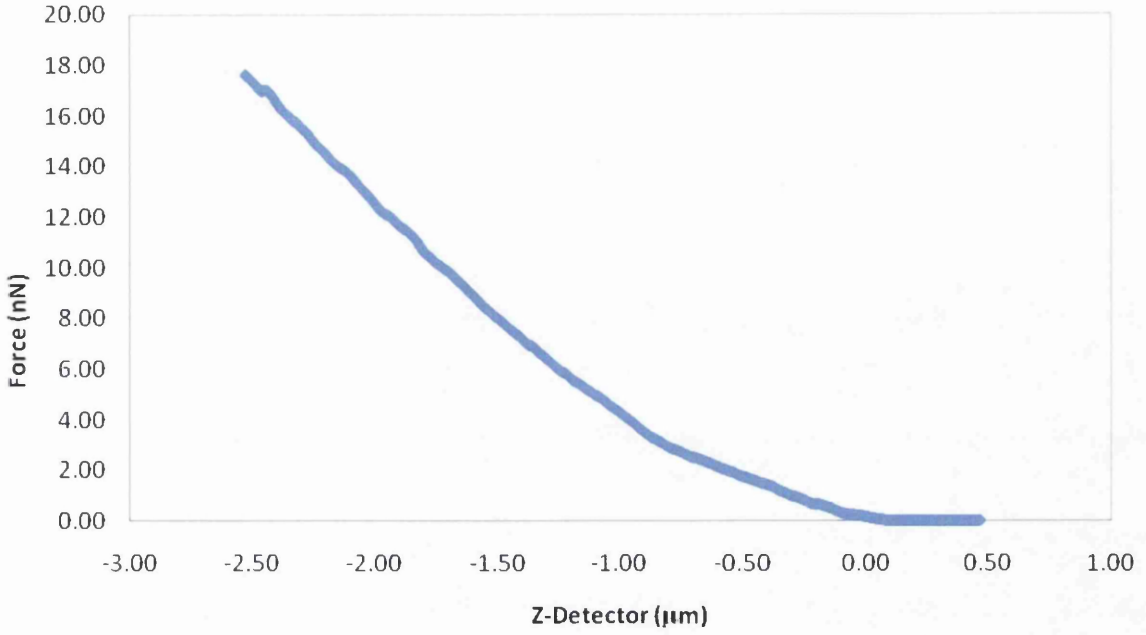


Figure 5.9 (a) Approach Force curve on *A.venetianus* at pH 3 and 0.6M NaCl.

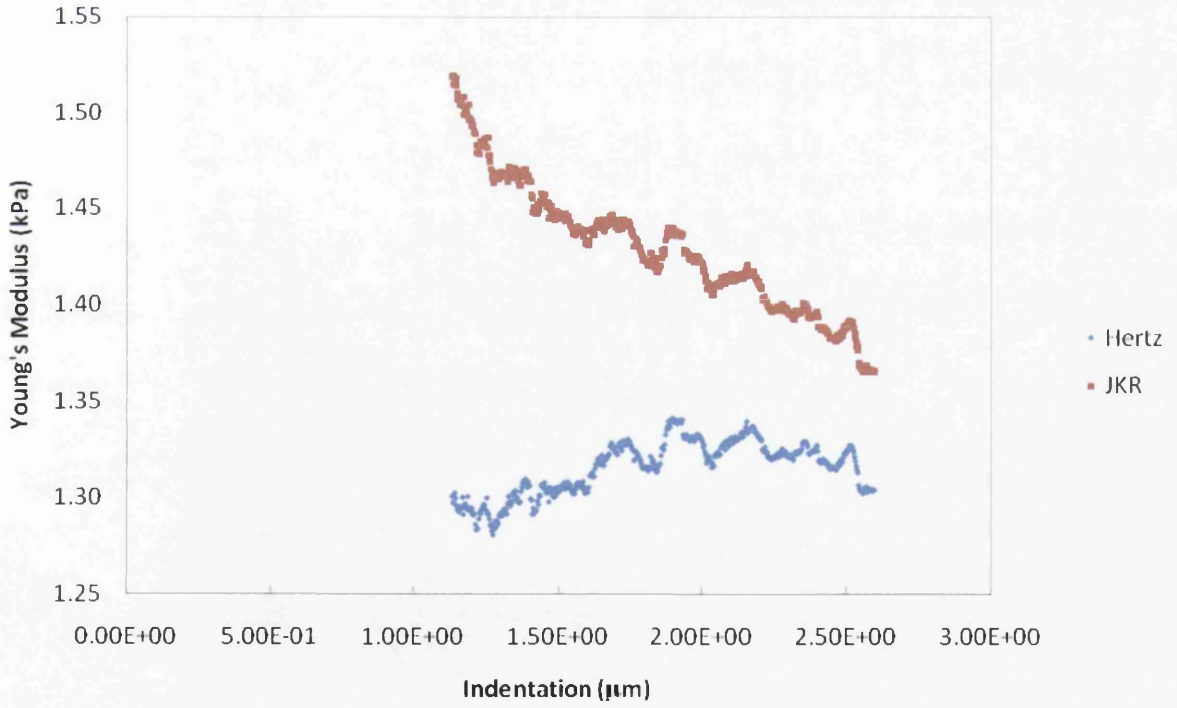


Figure 5.9 (b) Young's modulus variation over approach curve for *A.venetianus* at pH 3 and 0.6M NaCl

## 5.4 Conclusions

Force measurements have been performed on membranes for the direct quantification of membrane/tip and membrane/particle interactions through the measurement of adhesion force and determination of elasticity in the hope of the elucidation of biofouling process behaviour. A thorough analysis of the effect of such AFM parameters as loading force, extension speed and tip geometry on the achievement of adhesion force and elasticity values, for both Hertz and JKR models, on virgin and industrially fouled membranes have been performed. These experiments were necessary to achieve both accurate and relevant data from RO membranes and to define the membrane characterization parameters in this proof of concept study.

A comparison study between the contact tip and the silica colloid probe was undertaken where the contact tip provided a much higher value of Young' modulus than those achieved using a colloid probe. Therefore it can be seen that tip geometry does have an effect on values achieved using force measurements, especially in the values of Young's modulus obtained. The silica colloid probe was chosen for the adhesion and indentation studies of the membranes due to its well defined tip geometry and silica being a possible contaminate within the Fujairah desalination plant.

The second AFM parameter to be investigated was the loading force applied to the membrane surface. This is a crucial parameter as the loading force influences the indentation depth into the sample surface and therefore where the measurements of elasticity will be taken from. Loading force was determined to have a negligible effect on the values of adhesion force for the virgin membrane, however for the fouled membrane, as the loading force increases so did the adhesion force experienced by the colloidal tip, which could be due to increased contact between the colloid and the foulant material on the membrane. Also for elasticity measurements on the virgin membrane, as the loading force increased there appeared to be a decrease in Young's modulus, with a decrease in standard deviation of the data, however on the fouled membrane as the loading force increased, the Young's modulus did not appear to be dramatically affected, apart from slight fluctuations.

The third AFM parameter to be investigated was the extension speed applied to the colloid probe during a force measurement. No trend for adhesion force could be established as the standard deviation of the data was relatively high for both the virgin and fouled membranes. In addition, the extension speed did not seem to have a significant effect on Young's modulus obtained for both the virgin and fouled membrane. A low loading force was chosen so that any plastic deformations which might occur are minor and the indentation into the thin film sample was small so that the underlying membrane did not have an effect on the values of elasticity.

The adhesion forces measured from the virgin membrane in the presence of monovalent ion at the ionic strength of 0.1M and 0.6M decreases with increasing pH. Also there was a slight decrease in the adhesion force values obtained for 0.6M NaCl when compared to 0.1M NaCl. However the adhesion force from the virgin membrane and fouled membrane in the presence of the divalent ions at the ionic strength of 0.1M does not vary much over the range of pH when considering the standard deviations, apart from a slight rise in adhesion force at pH 9 for the divalent ions. This rise could be because of the absorption of $Ca^{2+}$ and $Mg^{2+}$ onto the membrane surface, decreasing the negative charge of the membrane surface. Therefore within seawater conditions of 0.6M, the virgin membrane adhesion force is not favourable for bacterial attachment however as the pH of seawater can vary around 7.5 to 8.0 then the presence of $Ca^{2+}$ and $Mg^{2+}$ on the membrane surface could lead to a slightly greater value of adhesion force and therefore more favourable conditions for bacterial attachment to the RO membrane surface.

Elasticity values achieved using the Hertz model for the virgin membrane showed that the values of Young's modulus for all conditions of salt concentration did not significantly vary with pH, especially when considering the large values of standard deviation, however values achieved using the JKR model shows a slight decrease from pH 3 to pH 7 for 0.1M and 0.6M NaCl and also for 0.1M ionic strength $MgCl_2$. Therefore the Hertz model suggests no dependence on salt concentration or pH values on the values of Young's modulus, however JKR model suggests a slight dependence on pH values, especially at pH 3. However for the fouled membrane, there is evidence that there might be a weak dependence on pH and salt concentrations for the Young's modulus values. This could be due to the nature of the foulants within the fouling layer

present on the membrane responding weakly to the environmental conditions and thereby slightly altering the value of Young's modulus achieved. Therefore the elasticity of the foulant surface present on the membrane surface could vary with industrial conditions. If the optimum conditions could be determined where the elasticity of the foulant layer is at its lowest, then cleaning regimes within the Fujairah desalination plant such as cross-flow could be more effective in removing and breaking up the foulant biofilm.

Adhesion force and elasticity values for both models performed at industrially relevant conditions were determined from force measurements achieved on purposefully fouled membranes with the chosen four isolated bacteria from the culture-dependent technique. There was no common trend for the adhesion force and elasticity measurements obtained from the bacteria and the standard deviation values obtained for all the adhesion force measurements were relatively high, therefore it cannot be said conclusively that these individual bacterial species trends exist. However it is suggested that this could be due of the non-uniform bacterial film present on the membrane surface due to the high surface roughness of the RO membrane, for the bacterial film on the membrane peaks, the elasticity of the membrane had more of an effect on the elasticity value of the bacterial film unlike at the valleys where the biofilm film has a greater depth and therefore the elasticity values are more indicative of the actual biofilm elasticity. The elasticity of the bacterial film was much lower than that obtained for the industrially fouled membrane, which could be due to a greater coverage of the RO membrane with foulant material and also due to the bacterial cells being freshly harvested and biologically functional. The results demonstrate that although the elasticity of the biofilm film is a lot lower than the industrially fouled membranes and therefore more susceptible to being broken up and detached from the membrane surface, the valleys located on the membrane surface could shield the biofilm from the mechanical cleaning forces which would enable the biofilm to grow and develop.

The use of the Hertz and the JKR model to determine Young's modulus has been applied throughout this present study into membrane and biofilm elasticity. The results showed that the JKR model revealed slightly higher values of Young's modulus than those achieved for the Hertz model and in some cases revealed a slight trend in the data which was not seen when using the Hertz model. The JKR model was determined more

suitable for use as the model takes into account adhesion force between the tip and the sample within the contact area, unlike the Hertz model which assumes completely elastic behaviour [92]. Most research groups use the Hertz model due to its simplicity for analysis of biological samples, however it is flawed for biological analysis due to its inherent assumptions [86] and therefore should not be used for biological samples.

Therefore AFM indentation experiments for determination of elasticity when applied to RO membranes as a method to elucidate the mechanisms of biofouling is extremely novel. There is limited literature about the indentation into commercially available membranes and biofilm, and no literature has been found for indentation experiments using a silica colloid probe for the indentation into the process membranes, and indentation of bacterial biofilms on membrane surfaces. This proof of concept study has been extended further by performing AFM indentation experiments in different salt concentrations and pH values. Therefore elasticity measurements are a novel technique as applied to RO membranes, and hold promise for further elucidation of the mechanisms involved in membrane bio-fouling. This proof of concept study demonstrates that the methods utilised in this research could be standardised to allow for comparison between different fouled membranes and biofilms on different surfaces, such as food processing, heat exchangers and medical implants.

# Chapter 6 Conclusions and Recommendations for Future Research

## 6.1 Conclusions

The objective of this thesis was to comprehensively investigate the issue of biofouling on industrial RO membranes through molecular biology techniques, characterisation of surface charge of isolated bacteria from a fouled membrane and RO membrane surface, and AFM imaging and force measurements on clean and fouled membranes for the determination of adhesion force and micromechanical properties of elasticity. This objective was successfully achieved through the research performed and documented in this thesis, where some of the techniques used are novel when used in conjunction with RO membrane samples. It is hoped that this rigorous characterisation of membrane fouling in an industrial context will aid in developing a rational strategy for biofilm formation prevention or economic and effective cleaning processes which will maintain efficient membrane operation and prolong membrane life.

Microbial community diversity present within foulant layers found on industrial RO membranes, obtained from the Fujairah Water and Power plant, were analysed through 16S rDNA sequencing performed on DNA extracted from process fouled membranes. The microbial diversity analysis showed a complex and varied community of many bacterial species present within the membrane fouling layer, where *Proteobacteria* was determined to be the most abundant group of identified bacterial species. *γ-Proteobacteria* was the most predomnaint class within the phylum *Proteobacteria.* The next most abundant groupings of bacterial species were the *Bacterioidetes* and *Plantomycetes.* Previous and current investigations indicate that fouling layers found on RO membranes from differing water purification processes are composed predominantly from the *Proteobacteria* phylum and therefore the bacteria from this phylum can pose a major biofouling hazard to RO membranes. However, the few studies within the literature that utilise this technique for the identification of foulant layers, retrieved from desalination plants, identify *α-Proteobacteria* as the most predomnaint class of identified bacterial species within the *Proteobacteria* phylum, which differs from the findings of this study, which suggest specialised fouling

conditions within the Fujairah desalination plant. This study has successfully allowed the identification of the different types of microbes that cause significant fouling on membranes. Therefore it is concluded that bacteria from the phylum *Proteobacteria* should be investigated thoroughly to determine common characteristics and behaviour which causes the bacteria to attach and thrive in growth to develop into biofilms on the RO membranes with desalination plants.

For the continuation of the research, the four bacterial species isolated from the RO fouling layer using the culture-dependant method were obtained; *Vibrio* sp. PM6A, *A.venetianus* and *K.pnuemoniae* subsp. *Pneumonia,* and uncultured bacterium. The three identified bacteria, were chosen as they belong to the subdivision *γ-Proteobacteria,* which was determined be the most predominant class within the phylum *Proteobacteria* and therefore these bacteria were determined to cause significant fouling on the RO membrane surfaces. For the elucidation of common characteristics and behaviour of the bacteria species from *γ-Proteobacteria* and the uncultured bacterium, cell surface charge was successfully measured over the bacterial species. The determination of surface charge properties is of great importance for the understanding of cell function and behaviour within various environments, as cell surface charge can aid in the elucidation of cell adhesion to membrane surfaces within process conditions. A number of industrially relevant environmental conditions were studied to see if environmental changes would alter the cell surface characteristics. The electrophoretic mobility results showed a strong dependence on pH and NaCl concentration for the bacterial species *Vibrio* sp. PM6A, *A.venetianus* and *K.pnuemoniae* subsp. *Pneumonia.* The electrophoretic mobility measurements infer that the surface charge of the bacterial species becomes less negative and more positive with increasing NaCl concentration. This is due to compression of the electric double layer with increasing salt concentration. Also as the pH values increase, the electrophoretic mobility values which infers cell surface charge becomes more negative. These bacteria also possess a negative surface charge under standard growth conditions and neutral pH, apart from 0.8M NaCl for the *Vibrio* sp. PM6A, which displayed a positive charge. However, no strong dependence on pH and NaCl concentration was found for the uncultured bacterium and the bacterium showed a positive charge under all conditions of salt and pH. Physical growth conditions were also determined not to have a significant effect on the electrophoretic mobility values.

The three bacteria species, *Vibrio* sp. PM6A, *A.venetianus* and *K.pnuemoniae* subsp. *Pneumonia*, from the most predominant bacteria fouling class, *γ-Proteobacteria,* displayed similar behaviour and had a negative charge in seawater conditions. The negative charge on the bacteria could influence bacterial attachment to membrane surface, as the RO membrane surface charge is also negative in seawater conditions (Chapter 4). In this case, this is an unfavourable condition for bacterial cell attachment, as the bacterial surface will experience repulsive forces from the membrane surface. Therefore the mechanism of cell attachment and subsequent biofilm formation within the Fujairah desalination plant for these bacterial species could be due to other bacterial cell characteristics, such as surface hydrophobocity. However the uncultured bacterium displays a positive charge in seawater conditions which would experience attractive forces towards the negatively charged membrane surface and would be favourable for cell attachment to the membrane surface.

Also it was observed that increasing the divalent ion concentration $Mg^{2+}$and $Ca^{2+}$, caused the electrophoretic mobility to become less negative and more positive, therefore changing the cell surface charge values for the three bacterial species *Vibrio* sp. PM6A, *A.venetianus* and *K.pnuemoniae* subsp. *Pneumonia*. However the uncultured bacterium did not display a dependence on increasing $Mg^{2+}$ and $Ca^{2+}$ ion concentration. Seawater consists of a number of different cations of which $Mg^{2+}$ and $Ca^{2+}$ are present in significant concentrations. RO membrane used in the Fujairah desalination plant has a very high salt rejection of 99.8% (Appendix B) which means that not only will there be a concentration gradient of $Na^{+}$ at the membrane surface, but also $Mg^{2+}$ and $Ca^{2+}$ will have a concentration gradient at the surface. Also due to the divalent charge, the ions will be in a more favourable position to move towards the negatively charged membrane surface in seawater conditions. Therefore from the electrophoretic mobility results obtained for the bacterial species belonging to the class *γ-Proteobacteria,* the gradient of divalent ions present at the membrane surface could influence the bacterial attachment of bacterial cells to the membrane surface. The less negative electrophoretic mobility values with increasing concentrations of $Mg^{2+}$and $Ca^{2+}$ means that these bacterial cell attachment to the RO membrane is more favourable with a concentration gradient of divalent ions present on the membrane surface, which might be another factor why high salt rejection RO membranes are susceptible to membrane fouling.

*Vibrio* sp. PM6A, *A.venetianus* and *K.pnuemoniae* subsp. *Pneumonia* all belong to the bacterial grouping *γ-Proteobacteria* and show similar behaviour in electrophoretic mobility in changes of pH and divalent ion concentrations. It is not known what phylum the uncultured bacterium belongs, however the results obtained for this bacterium are dissimilar to the other bacteria, which seems to indicate that this bacterium may not be part of the *γ-Proteobacteria* grouping.

Good quality AFM topographical images have been performed on virgin and process fouled SWC 3+ RO membranes where the virgin membrane images reveals that the surface of the membrane is composed from peaks and valleys and displays a structure typical of RO membranes. From the fouled membrane scans it can be seen that the fouling layer does not cover the entire RO membrane surface and there is a relatively non uniform distribution of foulant structures. On the images there is also evidence of EPS, which indicates that microorganisms are present and are responsible for the development of the fouling biofilm layer. Roughness measurements performed on the virgin membrane surface revealed a typically rough RO surface. Current literature suggests that membrane surfaces which are rough have a tendency to foul easier as the roughness increases the surface area, which in turn increases the number of contact points between foulants and the surface and large protrusions from the filtration membrane surface can affect local flow fields and shield particles, such as bacterial cells from detachment. The rough surface of the RO membrane is therefore determined to be at susceptible to fouling and therefore again demonstrates the importance of this biofouling study, regarding the use of these membranes within desalination operations. Also roughness and peak to valley measurements reveal that the fouling layer is much smoother than the unfoaled RO membrane surface, which could be due to the presence of the EPS within the foulant layer. The topography, surface roughness and peak to valley measurements show that the RO membranes used in the Fujairah desalination plant are susceptible to biofouling.

Membrane charge is widely thought to influence the separation performance and fouling tendency of membranes, where fouling substance interaction with the membrane surface in aqueous media can be dependent upon the membrane surface charge. Therefore the study of surface characteristics of membranes is essential for

understanding of membrane fouling. The surface charge of clean and industrial fouled membrane were characterised through the use of streaming potential experiments at various pH values and NaCl and $MgCl_2$ and $CaCl_2$. Results revealed that the zeta potential is strongly dependent on pH and NaCl concentration for both the virgin and fouled membranes, where the foulant material present on the membrane surface was determined to be negatively charged at all NaCl concentrations and pH values measured. It was shown that divalent ion concentration had a marked effect on the zeta potential of the membranes, especially at the ionic strength of 0.01M. This could occur as negative charge of the membrane surface at high pH values is a favorable position for $Ca^{2+}$ and $Mg^{2+}$ to be adsorbed onto the surface of the membrane, which would alter the zeta potential of the membranes to be less negative. However the zeta potential of the virgin and fouled membranes at high pH still remain negative at all salt conditions. A concentration gradient of $Ca^{2+}$ and $Mg^{2+}$ could be present at the membrane surface due to the high salt rejection of the RO membrane as explained earlier in the conclusions, therefore as the membrane surface charge becomes less negative with increasing divalent ion concentration, the negatively charged bacterial cells in seawater conditions (Chapter 3) would encounter less repulsive force from the membrane surface and therefore the situation for bacterial cell attachment becomes more favourable. This is another factor within the Fujairah desalination plant which could facilitate bacterial attachment and subsequent biofilm formation.

Force measurements have been performed on membranes for the direct quantification of membrane/tip and membrane/particle interactions through the measurement of adhesion force and determination of elasticity in the hope of the elucidation of biofouling process behaviour. A thorough analysis of the effect of such AFM parameters as loading force, extension speed and tip geometry on the achievement of adhesion force and elasticity values, for both the Hertz and JKR models, on virgin and industrially fouled membranes have been performed These experiments were necessary to achieve both accurate and relevant data from RO membranes and to define the membrane characterization parameters in this proof of concept study.

A comparison study between the contact tip and the silica colloid probe was undertaken where the adhesion values demonstrate that the silica colloid probe is more sensitive to pH 3 than the contact tip, however the ranges of adhesion force, especially for pH 7 and

pH 9 are similar for both tip geometries. The range of values of Young's modulus for the fouled membrane achieved using the Hertz model are 419 +/- 191 to 567 +/- 180 kPa with a contact tip, while for the range of values of Young's modulus for the fouled membrane achieved using the Hertz model are 52.01 +/- 7.56 to 58.77 +/- 7.64 kPa with a silica colloid. The contact tip provided a much higher value of Young' modulus than those achieved using a colloid probe. Therefore it can be seen that tip geometry does have an effect on values achieved during force measurements, especially in the values of Young's modulus obtained. The silica colloid probe was chosen for the adhesion and indentation studies of the membranes due to its well defined tip geometry and silica being a possible contaminate within the Fujairah desalination plant.

The second AFM parameter to be investigated was the loading force applied to the membrane surface. This is a crucial parameter as the loading force influences the indentation depth into the sample surface and therefore where the measurements of elasticity will be taken from. Loading force was determined to have a negligible effect on the values of adhesion force for the virgin membrane, however for the fouled membrane, as the loading force increases so did the adhesion force experienced by the colloidal tip, which could be due to increased contact between the colloid and the foulant material on the membrane. Also for elasticity measurements on the virgin membrane, as the loading force increased there appeared to be a decrease in Young's modulus, with a decrease in standard deviation of the data however pH values did not seem to have a significant effect on Young's modulus obtained from the fouled membrane.

The third AFM parameter to be investigated is the extension speed applied to the colloid probe during a force measurement. The extension speed is the speed at which the tip approaches the surface. No trend for adhesion force could be established as the standard deviation of the data was relatively high for both the virgin and fouled membranes. In addition, the extension speed did not seem to have a significant effect on Young's modulus obtained for both the virgin and fouled membrane. A low loading force was chosen so that any plastic deformations which might occur are minor and the indentation into the thin film sample was small so that the underlying membrane would not have an effect on the values of elasticity.

The adhesion force measurements from the virgin membrane were the greatest in the environmental conditions of pH 3 and monovalent salt concentration. In the presence of monovalent ion at the ionic strength of 0.1M and 0.6M, the adhesion force decreases with increasing pH. Also there was a slight decrease in the adhesion force values obtained for 0.6M NaCl when compared to 0.1M NaCl, however the fouled membrane showed little variation in the adhesion force obtained for all salt conditions over the range of pH. The adhesion force from the virgin membrane and fouled membrane in the presence of the divalent ions at the ionic strength of 0.1M does not vary much over the range of pH when considering the standard deviations, apart from a slight rise in adhesion force at pH 9 for the divalent ions. This rise could be because of the absorption of $Ca^{2+}$ and $Mg^{2+}$ onto the membrane surface, decreasing the negativity of the membrane surface. Therefore within similar conditions to of 0.6M and pH 7, the virgin membrane adhesion force is not favourable for bacterial attachment. However as the pH of seawater can vary around 7.5 to 8.0, then the presence of $Ca^{2+}$ and $Mg^{2+}$ on the membrane surface could lead to a slightly greater value of adhesion force and therefore more favourable conditions for bacterial attachment to the RO membrane surface.

Elasticity values achieved using the Hertz model for the virgin membrane showed that the values of Young's modulus all for conditions of salt concentration did not significantly vary with pH, especially when considering the large values of standard deviation, however values achieved using the JKR model show a slight decrease from pH 3 to pH 7 for 0.1M and 0.6M NaCl and also for 0.1M ionic strength $MgCl_2$. Therefore the Hertz model suggest no dependence on salt concentration or pH values on the values of Young's modulus, however JKR suggests a slight dependence on pH values, especially at pH 3. However for the fouled membrane, there is evidence that there might be a weak dependence on pH and salt concentrations for the Young's modulus values. This could be due to the nature of the foulants within the fouling layer present on the membrane responding weakly to the environmental conditions and thereby slightly altering the value of Young's modulus achieved. Therefore the elasticity of the foulant surface present on the membrane surface could vary with industrially conditions. If the optimum conditions could be determine where the elasticity of the foulant layer is at its lowest, then cleaning regimes within Fujairah

desalination plant, such as cross-flow, could be more effect in removing and breaking up the foulant biofilm.

Adhesion force and elasticity values for both models performed at industrially relevant conditions were determined from force measurements achieved on purposefully fouled membranes with the chosen four isolated bacteria from the culture-dependent technique. There was no common trend for the adhesion force and elasticity measurements obtained from the bacteria and the standard deviation values obtained for all the adhesion force measurements were relatively high therefore it cannot be said conclusively that these individual bacterial species trends exist. However it is suggested that this variation of data could be due to the non-uniform bacterial film present on the membrane surface due to the high surface roughness of the RO membrane, so that the elasticity of the membrane had more of an effect on the elasticity value of the bacterial film when the bacterial film was present on the membrane peaks resulting in a thinner film depth, unlike at the valleys where the biofilm film has a greater depth and therefore the elasticity values are more indicative of the actual biofilm elasticity. The elasticity of the bacterial film was much lower than that obtained for the industrially fouled membrane, which could be due to a greater coverage of the RO membrane with foulant material and also due to the bacterial cells being freshly harvested and biologically functional. The results demonstrate that although the elasticity of the biofilm film is a lot lower than the industrially fouled membranes and therefore more susceptible to being broken up and detached from the membrane surface, the valleys located on the membrane surface could shield the biofilm from the mechanical cleaning forces which would therefore enable the biofilm to grow and develop and foul the surface.

AFM indentation experiments for determination of elasticity when applied to RO membranes as a method to elucidate the mechanisms of biofouling is extremely novel. There is limited literature about the indentation into commercially available membranes and biofilm, and no literature has been found for indentation experiments into process membranes using a silica and indentation of bacterial biofilms on membrane surfaces. This proof of concept study has been extended further by performing AFM indentation experiments at different salt concentrations and pH values. Therefore elasticity measurements are a novel technique as applied to RO membranes, and hold promise for further elucidation of the mechanisms involved in membrane bio-fouling. This proof of

concept study demonstrates that the methods utilised in this research could be standardised to allow for comparison between different fouled membranes and biofilms on different surfaces, such as food processing, heat exchangers and medical implants.

The use of the Hertz and the JKR model to determine Young's modulus has been applied throughout this present study into membrane and biofilm elasticity. The results showed that the JKR revealed slightly higher values of Young's modulus than those achieved for the Hertz model and in some cases revealed a slight trend in the data which was not seen when using the Hertz model. The JKR model was determined more suitable for use as the model takes into account adhesion force between the tip and the sample within the contact area, unlike the Hertz model which assumes completely elastic behaviour [92]. Most research groupings use the Hertz model due to its simplicity for analysis of biological samples, however it is flawed for biological analysis due to its inherent assumptions [86] and therefore should not be used for biological samples.

The method of plotting graphs of Young's modulus versus indentation for force indentation experiments on biofilm , as presented in this thesis, holds promise for a new way to examine multilayered biofilms, as Young's modulus at various layers within the biofilm can be measured. Also the biofilm layer depth from the surface can be determined from the indentation depth. No literature has been found where the elasticity of a biofilm has been investigated at various layers within the biofilm; however such information could aid in determining the ability to break up the developed biofilm on the surface of the membrane and reduce the foulant issue.

In conclusion, this thesis has shown the rigorous characterization of membrane fouling within a specific industrial context, through the use of both established and novel techniques when applied to RO membranes. Elasticity measurements are a novel technique as applied to RO membranes, and hold promise for further elucidation of the mechanisms involved in membrane bio-fouling. It is hoped that this encompassing research study within an industrial context will aid in developing a rational strategy for the prevention of biofilm formation with economic and effective cleaning within desalination processes which will maintain efficient membrane operation and prolong membrane life.

## 6.2 Recommendations for Future Research

The research detailed in this thesis has highlighted several areas of additional study which would add to the understanding of membrane fouling. These research areas are discussed below.

### 6.2.1 Studies of the uncultured bacterium isolate

One of the four bacterial isolates obtained from the fouled RO membrane could not be identified nor could the phylum to which it belongs, using 16S rDNA sequencing and comparing to sequence databases. The uncultured bacterium exhibited different surface cell charge behavior, shown in Chapter 3, to the other three studied bacteria isolates which all belong to the class *γ-Proteobacteria.* Studies should be conducted to determine the characteristics of this bacteria and to see if this bacteria can be identified within a certain phylum. The identification of this bacterium is important as the bacterial displays different surface charge behaviour of being positive in all salt and pH conditions (Chapter 3), however most bacterial species display a negative charge at standard growth conditions and neutral pH [10].

### 6.2.2 Extension of Force Measurement studies

There are a number of force curve experiments which could be extended for the production of more accurate data and also to obtain more process relevant data.

The contact point where the tip first comes into contact with the sample surface when force measurements are performed is required for the calculation of indentation depth into the sample. Contact point determination can be made when there is a sudden jump into contact as seen with other samples quoted in the literature, however not all samples display this type of interaction with the tip. Some research in the literature define the contact point as the height where the cantilever deflection begins to leave the horizontal axis on the deflection vs sample height curve [66], however this cannot be determined precisely. Therefore there is a need for a standardization method of the determination of the contact point. Experiments need to be performed over a wide range of surfaces

and tip geometry to determine a common and accurate method of contact point determination, especially when force measurements are performed on soft samples.

The force measurement study conducted on bacterial isolates filtered on RO membranes in varying salt solutions and pH for the determination of adhesion force and elasticity could be extended to perform force measurements on a mixed biofilm from all four bacteria isolates for a more representative process relevant membrane biofilm. Also as membrane fouling is a combination of inorganic fouling, colloidal fouling, biological fouling and organic fouling [7, 8], a RO membrane with a filter layer combined from different types of fouling, such as bacterial and colloidal fouling, would provide a more representative process relevant membrane biofilm.

The Young's modulus of the biofilm structure at various layers could be investigated, utilizing Young's modulus versus indentation plots to identify the values of elasticity throughout the biofilm. Firstly loading force and extension speed experiments need to be performed to determine the AFM parameters that would allow for multiple gradients within the approach curves, without the tip quickly compressing the biofilm which would mask multiple gradients within the approach curve.

Force curve analysis could be performed using a number of different models, such as Oliver-Pharr and Field-Swain, where they are described in Section 1.6.7 within the Introduction chapter. However these models still rely on the assumption of elastic behavior which is rarely exhibited in soft samples, therefore more research needs to be performed for the development of a force curve model which describes soft samples, such as biological samples, more accurately to enable an absolute values of Young's modulus to be obtained.

AFM force measurements for the purpose of measurements of elasticity of membrane and biofilm surfaces has been developed within this thesis, therefore there is scope for testing other membrane systems to determine the effect of surface elasticity on a range of industrial problems which utilise membrane technology.

Also, an interesting study would be to determine the influence of substrate surface on bacterial attachment and biofilm development, where a range of different elasticity process relevant surfaces could be investigated.

### 6.2.3 Hydrophobicity

Hydrophobocity is determined to be one of several factors which can influence the initial adhesion of bacteria to surfaces [176]. Investigations into the hydrophobicity of the bacteria types and the membrane could be conducted to further understand the mechanisms of adhesion of the bacteria to the membrane surface and to add to the wealth of information already gained from this study. The membrane hydrophobicity could be measured through the contact angle method and the hydrophobicity of the bacteria could be determined by partitioning bacteria between two aqueous phases, such as polyethylene glycol and dextran phase, as explained in literature by Loosdrecht *et al* [177].

### 6.2.4 Rheology

Rheology of biofilms formed from bacteria found on fouled membrane surfaces could be an interesting area of study which could be investigated for the elucidation of the mechanical properties of biofilms formed on membrane surfaces and provide information on the physical forces required for the failure and detachment of formed biofilms from the membrane surface. Biofilms mechanical properties will affect the shape and stability of the biofilm structure and therefore can determine the failure and detachment of a biofilm in reaction to a physical force such as fluid-induced shear and also the accumulation of such biofilms in industrial environments [154]. Through the understanding of these properties, a foundation of information for effective biofilm control within industrial environments can be established. However there only exist a handful of studies which have thoroughly investigated the mechanical properties of a limited number of biofilms, even though these properties are crucial in various biofilm processes and behaviors [154, 178, 179, 180]. This is due to the difficultly in testing biofilms mechanically and obtaining relevant data using conventional testing techniques. Some of the literature that does exist on biofilm rheology involves removing the biofilm from its natural environment and then testing the suspension

[178]. However this approach does not provide direct information regarding the *in situ* behavior of intact biofilms. Ideally the rheology of nearly undisturbed biofilms in their natural environments should be tested, as the testing of scraped biofilm will inevitably disrupt the sample. In the limited studies so far, observations, rheometry and measurements conducted on biofilm-agar mixtures have proposed that biofilms behave as viscoelastic polymeric fluids [181]. This exhibited behaviour in biofilms will explain the remarkable ability of biofilms to survive externally applied environmental mechanical stress. There are a few research teams who have developed techniques for obtaining relevant data from investigating the rheology of biofilms using rheometers. In Winston *et al* [154], the research team has used a TA Instruments AR 1000 Rheometer with parallel plate geometry to measure the rheological properties of both *Streptoccocus mutant* and mixed culture pond water biofilms. The biofilms were grown on the plates of the rheometer within a Rotating Disk Reactor (RDR) operating at batch culture for 24 hours then was switched to continuous culture for 48 hours, under a $CO_2$ headspace, to allow the biofilms to develop on the plates. The plates were then placed in the rheometer and subjected to constant shear creep tests. Both parameters of effective shear modulus $G$ and effective viscosity $\eta$ were measured and the Burger model was used for the analysis of the data. Both biofilms exhibit linearly viscoelastic behaviour within the range of stresses 3.5-5 Pa for *Streptoccocus* mutants and 0.1- 0.5 Pa for pond water biofilms and also the biofilms appeared to exhibit remarkable resemblance with the response of synthetic polymers. Using these types of methods, investigations into growing biofilms from the isolated bacteria on the metal rheometer plates should be conducted to determine the mechanical properties of these bacterial biofilms. This could lead to information about the mechanical behaviour of these biofilms under various process conditions, which could lead to the development of methods for the removal of these biofilms from the surface of the filtration membrane.

## References


1. **Flemming, H-C., Schaule, G., Griebe, T., Schmitt, J., Tamachkiarowa, A. (1997)**
'Biofouling – the Achilles Heel of Membrane Processes.'
Desalination., Vol. 113, pp. 215-225

2. **Flemming, H-C. (1997)**
'Reverse Osmosis Membrane Biofouling.'
Exp. Therm. Fluid Sci., Vol. 14, pp. 382-391

3. **Wyart, Y., Georges, G., Deumie, C., Amra, C., Moulin, P. (2008)**
'Membrane Characterization by Microscope Methods: Multiscale Structure.'
J. Memb. Sci., Vol. 315, pp. 82-92

4. **Pang, CM., Hong, P., Guo, H., Liu, W-T. (2005)**
'Biofilm Formation Characteristics of Bacterial Isolates Retrieved from Reverse Osmosis Membrane.'
Environ. Sci. Technol., Vol. 39, pp. 7541-7550

5. **Abd El Aleem, FA., Al-Sugair, KA., Alahmad, MI. (1998)**
'Biofouling Problems in Membrane Processes for Water Desalination and Reuse in Saudi Arabia.'
Int. Biodeterior. Biodegradation., Vol. 41, pp. 19-23

6. **Bowen, WR., Doneva, TA. (2000)**
'Atomic force microscopy studies of membranes: effect of surface roughness on double-layer interactions and particle adhesion.'
J. Colloid. Interface. Sci., Vol. 229, pp. 544-549

7. **Shirazi, S., Lin, C-J., Chen, D.**
"Inorganic fouling of pressure-driven membrane processes — A critical review."
Desalination., Article in Press

8. **Mitra, SS., Thomas, AR., Gang, GT. (2009)**
'Evaluation and characterization of seawater RO membrane fouling.'
Desalination., Vol. 249, pp. 94-107

9. **Garrett, TR., Bhakoo, M., Zhang, Z. (2008)**
'Review – Bacterial adhesion and biofilms on surfaces.'
Prog. Nat. Sci., Vol. 18, pp. 1049-1056

10. **Palmer, J., Flint, S., Brooks, J. (2007)**
"Bacterial cell attachment, the beginning of a biofilm."
J. Ind Microbial Biotcehnol., Vol. 34, pp. 577-588

11. **Chmielewski, RAN., Frank, JF. (2003)**
'Biofilm formation and control in food processing facilities.'
Comprehensive reviews in food science and food safety., Vol. 2, pp. 22-32

12. **Katsikogianni, M., Missirlis, Y.F. (2004)**
"Concise Review of Mechanisms of Bacterial Adhesion to Biomaterials and of Techniques used in Estimating Bacteria-Material Interactions."
J. Eur. Cell. Mater., Vol. 8, pp. 37

13. **ten Cate, JM. (2006)**
'Biofilms, a new approach to the microbiology of dental plaque.'
Odontology, Vol. 94, pp. 1-9

14. **Li, BY., Liang, YZ., Hu, Y., Du, YP., Song, YQ., Cui, H. (2003)**
'Evaluation of gas chromatography-mass spectrometry in conjunction with chemometric resolution for the identification of nitrogen compounds in crude oil.'
Talanta., Vol. 61, pp. 803-809

15. **Sekoulov, I., Brinke-Sciferth, S. (1999)**
'Application of biofiltration in the crude oil processing industry.'
Water Science and Technology., Vol. 39, pp. 71-76

16. **Wilson, WW., Wade, MM., Holman, SC., Champlin, FR. (2001)**
'Status of methods for assessing bacterial cell surface charge properties based on zeta potential measurements.'
J. Microbiol. Methods., Vol. 43, pp. 153-164

17. **Characklis, WG., Marshall, KC. (1990)**
'Biofilms.'
New York, John Wiley and Sons.

18. **Soni, KA., Balasubramanian, AK., Beskok, A., Pillai, SD. (2008)**
'Zeta potential of selected bacteria in drinking water when dead, starved or exposed to minimal and rich culture media.'
Curr. Microbiol., Vol. 56, No. 1, pp. 93-97

19. **Ahimou, F., Denis, FA., Touhami, A., Dufrene, YF. (2002)**
"Probing microbial cell surface charges by atomic force microscopy."
Langmuir., Vol. 18, pp. 9937-9941

20. **Poortinga, AT., Bos, R., Norde, W., Busscher, HJ. (2002)**
'Electric double layer interactions in bacterial adhesion to surfaces.'
Surf. Sci. Reports., Vol. 47, pp.1-32

21. **Hermansson, M. (1999)**
'The DLVO theory in microbial adhesion.'
Colloids. Surf. B. Biointerfaces., Vol. 14, pp. 105-119

22. **Lu, S., Pugh, RJ., Forssberg, E. (2005)**
'Interfacial separation of particles.'
Elsevier.

23. **Bowen, WR., Hilal, N. (2009)**
'Atomic force microscopy in process engineering – An introduction to AFM for improved processes and products.'
Butterworth-Heinemann, Oxford, UK

24. **Grasso, D., Subramaniam, K., Butkus, M., Strevett, K., Bergendahl, J. (2002)**
'A review of non-DLVO interactions in environmental colloidial systems.'
Reviews in Environmental Science and Bio/Technology., Vol.1, pp.17-38

25. **Erbil, HY. (2006)**
'Surface chemistry of solid and liquid interfaces.'
Blackwell Publishing

26. **Azeredo, J., Visser, J., Oliveira, R. (1999)**
'Exopolymers in bacterial adhesion: interpretation in terms of DLVO and XDLVO theories'
Colloids Surf B Biointerfaces., Vol. 14, pp.141-148

27. **Van Oss, CJ. (1989)**
'Energetics of Cell-Cell and Cell-Biopolymer interactions.'
Cell Biophysics., Vol.14, pp. 1-16.

28. **Ducker, WA., Senden, TJ., Pashley, RM. (1991)**
'Direct measurement of colloidal forces using an atomic force microscope.'
Nature, Vol. 353, pp. 239-241

29. **Marshall, KC., Stout, R., Mitchell, R. (1971)**
'Mechanism of initial events in the sorption of marine bacteria to surfaces.'
J. Gen. Microbiol., Vol. 68, pp. 337-348

30. **Schneider, RP., Ferreira, LM., Binder, P., Ramos, JR. (2005)**
'Analysis of foulant layer in all elements of an RO train.'
J. Memb. Sci., Vol. 261, pp. 152-162

31. **Weis, A., Bird, MR. (2001)**
'The influence of multiple fouling and cleaning cycles upon the membrane processing of lignosulphonates.'
Trans IChemE, Vol. 79, Part C.

32. **Bartlett, M., Bird, MR., Howell, JA. (1995)**
'An experimental study for the development of a qualitative membrane cleaning model.'
J. Memb. Sci., Vol. 105, pp. 147-157.

33. **Li, Q., Elimelech, M. (2004)**
'Organic Fouling and Chemical Cleaning of Nanofiltration Membranes: Measurement and Mechanisms.'
Environ. Sci. Technol., Vol. 38, pp. 4683-4693

34. **Amann, RI., Ludwig, W., Schleifer, K-H. (1995)**
'Phylogenetic identification and in situ detection of individual microbial cells without cultivation.'
Microbiol. Revs., Vol. 59, pp. 143-169

35. **Staley, JT. (2006).**
'The bacterial species dilemma and the genomic-phylogenetic species concept.'
Phil. Trans. R. Soc. B., Vol. 361, pp. 1899 – 1909

36. **Juck, D., Charles, T., Whyte, LG., Greer, CW. (2000).**
'Polyphasic microbial community analysis of petroleum hydrocarbon-contaminated soils from two northern Canadian communities.'
FEMS Microbiology Ecology., Vol. 33, pp. 241-249

37. **Cottrell, MT., Kirchman, DL. (2000)**
'Community composition of marine bacterioplankton determined by 16S rRNA gene clone libraries and fluorescence in situ hybridization.'
Appl. Environ. Microbiol, Vol. 66, pp. 5116-5122

38. **Butt, H-J., Cappella, B., Kappl, M. (2005)**
'Force measurements with atomic force microscope: Technique, interpretation and application.'
Surf. Sci. Rep., Vol. 59, pp. 1-152

39. **Weisburg, WG., Barns, SM., Pelletier, DA., Lane, DJ. (1991).**
'16S Ribosomal DNA amplification for phylogenetic study.'
J. Bacteriol., Vol. 173, pp.697-703

40. **Ha Thi Phuc. (2007)**
*'Enrichment, Performance and Microbial Diversity of Microbial Fuel Cell Fed with Formate.'*
Thesis for Master's Degree
Department of Environment Science and Engineering, Gwangju Institute of Science and Technology, South Korea

41. **Bereschenko, LA., Stams, AJM., Heilig, GHJ., Euverink, GJW., Nederlof, MM., Van Loosdrecht, MCM. (2007)**
'Investigation of microbial communities on reverse osmosis membranes used for process water production.'
Water. Sci. Technol., Vol. 55, No. 8-9, pp. 181-190

42. **Bereschenko, LA., Heilig, GHJ., Nederlof, MM., Van Loosdrecht, MCM., Stams, AJM., Euverink, GJW. (2008)**
'Molecular Characterisation of the Bacterial Communities in the Different Compartments of a Full-Scale Reverse-Osmosis Water Purification Plant.'
Appl. Environ. Microbiol., Vol. 74, No. 17, pp. 5297-5304

43. **Chen, C-L., Liu, W-T., Chong, M-L., Wong, M-T., Ong, SL., Seah, H., Ng, WJ. (2004)**
'Community Structure of microbial biofilms associated with membrane-based water purification processes as revealed using a polyphasic approach.'
Appl. Microbiol. Biotechnol., Vol. 63, pp. 466-473

44. **Binnig, G., Quate, CF., Gerber, Ch. (1986)**
'Atomic Force Microscope.'
Phys. Rev. Lett., Vol. 56, No. 9, pp. 930-933

45. **Dufrene, YF. (2002)**
'Atomic Force Microscopy, a Powerful Tool in Microbiology'
J. Bacteriol., Vol. 184, No. 19, pp. 5205-5213

46. **Wright, CJ., Armstrong, I. (2006)**
'The application of atomic force microscopy force measurements to the characterization of microbial surfaces.'
Surf. Interface. Anal., Vol. 38, pp. 1419-1428

47. **Bowen, WR., Lovitt, RW., Wright, CJ. (2000)**
'Application of atomic force microscopy to the study of micromechanical properties of biological materials'
Biotechnol. Lett., Vol. 22, pp. 983-903

48. **Bousso, K., Van der Bruggen, B., Volodin, A., Snauwaert, J., Van Hasendonck, C., Vandecasteele, C. (2005)**
'Roughness and Hydrophobicity studies of nanofilitration membranes using different modes of AFM.'
J. Colloid. Interface.Sci., Vol. 286, pp. 632-638

49. **Magonov, SN., Elings, V., Whangbo, M-H. (1997)**
'Phase Imaging and Stiffness in tapping mode – atomic force microscope.'
Surf. Sci. Lett., Vol. 375, pp. 385-391

50. **Babcock, KL., Prater, CB. (1995)**
'Phase Imaging: beyond topography.'
Application Note 11, Digital Instruments, Santa Barbara, CA.

51. **Yacoot, A., Koenders, L. (2008)**
'Aspects of scanning force microscope probes and their effects on dimensional measurement.'
J. Phys. D: Appl. Phys., Vol. 41, 103001 (46pp)

52. **Hutter, JL., Bechhoefer, J. (1993)**
'Calibration of atomic-force microscope tips.'
Rev. Sci. Instrum., Vol. 64, pp. 1868-1873

53. **Mendez-Vilas, A., Gonzalez-Martin, M.L., Labajos-Broncano, L., Nuevo, M.J. (2004)**
"Artifacts in AFM images revealed using friction maps."
Appl. Surf. Sci., Vol. 238, pp. 42

54. **Dufrene, Y.F. (2003)**
"Recent progress in the application of atomic force microscopy imaging and force spectroscopy to microbiology."
Curr. Opin. Microbiol., Vol. 6, pp. 317

55. **Dufrene, YF., Bonnaert, CJP., Van der Mei, HC., Busscher, HJ., Rouxhet, PG. (2000)**
'Probing molecular interactions and mechanical properties of microbial cell surfaces by atomic force microscopy.'
Ultramicroscopy., Vol. 86, pp. 113-120

56. **Ducker, WA., Senden, TJ., Pashley, RM. (1992)**
'Measurement of forces in liquids using a force microscope.'
Langmuir, Vol. 8, pp.1831-1836

57. **Butt, H-J. (1991)**
'Measuring electrostatic, van der Waals, and hydration forces in electrolyte solutions with an atomic force microscope.'
Biophys. J., Vol. 60, pp. 1438-1444

58. **Kappl, M., Butt, H-J. (2002)**
'The colloidal probe technique and its application to adhesion force measurements.'
Part. Part. Syst. Charact., Vol. 19, pp. 129-143

59. **Bowen, WR., Doneva, TA. (2000)**
'Atomic Force Microscopy studies of nanofiltration membranes: surface morphology, pore size distribution and adhesion.'
Desalination., Vol. 129, pp. 163-172

60. **Bowen, WR., Hilal, N., Lovitt, RW., Wright, CJ. (1999)**
'Characterisation of membrane surfaces: direct measurement of biological adhesion using an atomic force microscope.'
J. Memb. Sci., Vol. 154, pp. 205-212

61. **Bowen, WR., Doneva, TA., Yin, HB. (2002)**
'Atomic force microscopy studies of membrane-solute interactions (fouling).'
Desalination., Vol. 146, pp. 97-102

62. **Bowen, WR., Lovitt, RW., Wright, CJ. (2000)**
'Direct quantification of Aspergillus niger spore adhesion in liquid using an atomic force microscope.'
J. Colliod. Interface.Sci., Vol. 228, pp. 428-433

63. **Bastidas, JC., Pawlak, JJ., Venditti, RA., Heitmann, JA., Hubbe, MA., Kadla, JF. (2008)**
'A colloidal probe microscopy study of cellulose/gypsum interactions.'
Materials Characterization., Vol. 59, pp.144-150

64. **Iijima, M., Yoshimura, M., Tsuchiya, T., Tsukada, M, Ichikawa, H., Fukumori, Y., Kamiya, H. (2008)**
'Direct measurement of interactions between stimulation-responsive drug delivery vehicles and artificial mucin layers by colloid probe atomic force microscopy.'
Langmuir, Vol. 24, pp. 3987-3992

65. **Domke, J., Radmacher, M. (1998)**
'Measuring the elastic properties of thin polymer films with the atomic force microscope.'
Langmuir, Vol.14, pp.3320-3325

66. **Touhami, A., Nysten, B., Dufrene, YF. (2003)**
"Nanoscale mapping of the elasticity of microbial cella by atomic force microscopy."
Langmuir., Vol. 19, pp. 4539-4543

67. **Neumann, T.**
'Determining the elastic modulus of biological samples using atomic force microscopy.'
JPK Instruments Application Report, www.jpk.com

68. **Bowen, WR., Hilal, N., Lovitt, RW., Wright, CJ. (1998)**
'A new technique for membrane characterisation: direct measurement of force of adhesion of a single particle using an atomic force microscope.'
J. Memb. Sci., Vol. 139, pp. 269-274

69. **Vrijenhoek, EM., Hong, S., Elimelech, M. (2001).**
'Influence of membrane surface properties on initial rate of colloidal fouling of reverse osmosis and nanofiltration membranes.'
J. Memb. Sci., Vol, 188, pp. 115-128

70. **Norberg, D., Hong, S., Taylor, J., Zhao, Y. (2007).**
'Surface characterization and performance evaluation of commercial fouling resistant low-pressure RO membranes.'
Desalination., Vol. 202, pp.45-52

71. **Wong, PCY., Kwon, Y-N., Criddle, CS. (2009)**
'Use of Atomic Force Microscope and Fractal Geometry to characterize the roughness of nano-, micro-, and ultrafiltration membranes.'
J. Memb. Sci., Issues. 1-2, pp. 117-132

72. **Franceschini, EA., Corti, HR. (2009)**
'Elastic properties of nafion, polybenzimidazole and poly [2,5-benzimidazole] membranes determined by AFM tip nano-indentation.'
J. Power. Sources., Vol. 188, pp. 379-386

73. **Dufrene, YF. (2001)**
"Application of atomic force microscopy to microbial surfaces: from reconstituted cell surface layers to living cells."
Micron., Vol. 32, pp. 153-165

74. **Nunez, ME., Martin, MO., Chan, PH., Spain, EM. (2005)**
'Predation, death and survival in a biofilm: Bdellovibrio investigated by atomic force microscopy.'
Colloids Surf B Biointerfaces., Vol.42, pp.263-271

75. **Dufrene, YF. (2000)**
'Direct characterization of the physicochemical properties of fungal spores using functionalized AFM probes.'
Biophys. J., Vol. 78, pp. 3286-3291

76. **Thomson, NH., Kasas, S., Smith, B., Hamsma, HG., Hansma, PK. (1996)**
'Reversible binding of DNA to mica for AFM imaging.'
Langmuir, Vol.12, pp.5905-5908

77. **Kuznetsov, YG., Malkin, AJ., Lucas, RW., Plomp, M., McPherson, A. (2001)**
'Imaging of viruses by atomic force microscopy.'
J. Gen. Virology., Vol. 82, pp. 2025-2034

78. **Auerbach, ID., Sorensen, C., Hansma, HG., Holden, PA. (2000)**
'Physical Morphology and Surface Properties of Unsaturated *Pseudomonas putida* Biofilms.'
J. Bacteriol., Vol. 182, No. 13, pp. 3809-3815

79. **Oh, YJ., Jo, W., Yang, Y., Park, S. (2007)**
'Influence of culture conditions on Escherichia coli O157:H7 biofilm formation by atomic force microscopy.'
Ultramicroscopy., Vol. 107, pp. 869-874

80. **Rodriguez, A., Autio, W.R., McLandsborough, L.A. (2008)**
'Effects of Contact Time, Pressure, Percent Relative Humidity (%RH), and Material Type on Listeria Biofilm Adhesive Strength at a Cellular Level Using Atomic Force Microscopy (AFM)'.
Food. Biophys.. Vol. 3, pp. 305-311

81. **Oh, YJ., Lee, NR., Jo, W., Jung, WK., Lim, JS. (2009)**
'Effects of substrates on biofilm formation observed by atomic force microscopy.'
Ultramicroscopy., Vol. 109, pp. 874-880

82. **Fang, H.H.P., Chan, K.Y., Xu, L.C. (2000)**
'Quantification of bacterial adhesion forces using atomic force microscopy.' (AFM).
J. Microbiol. Methods, Vol. 40, pp. 89-97

83. **Heuberger, M., Dietler, G., Schlapbach, L. (1994)**
'Mapping the local Young's Modulus by analysis of the elastic deformations occurring in atomic force microscopy.'
Nanotechnology., Vol. 5, pp. 12-23

84. **Withers, JR., Aston, DE. (2006)**
'Nanomechanical measurements with AFM in the elastic limit.'
Adv. Colloid. Interface. Sci., Vol. 120, pp. 57-67

85. **Hertz, H. (1881)**
'Ueber den kontakt elastischer koerper.' 'On the contact of elastic solids.'
J. fure die Reine Angewandte Mathematik., Vol. 92, pp. 156

86. **Kuznetsova, TG., Starodubtseva, MN., Yegorenkov, NI., Chizhik, SA., Zhdanov, RI. (2007)**
'Atomic force microscopy probing of cell elasticity.'
Micron., Vol. 38, pp. 824-833

87. **Agee, P.**
'Instrumented Indentation Testing with the Agilent Nano Indenter G200.'
Agilent Application Note, www.agilent.com

88. **Sneddon, IN. (1965)**
'The relation between load and penetration in the axisymmetric boussinesq problem for a punch of arbitrary profile.'
Int. J. Eng. Sci., Vol. 3, No. 1, pp. 47-57

89. **McElfresh, M., Baesu, E., Balhorn, R., Belak, J., Allen, MJ., Rudd, RE. (2002)**
'Combining constitutive materials modeling with atomic force microscopy to understand the mechanical properties of living cells.'
PNAS, Vol. 99, pp. 6493-6497

90. **Kendall, K. (1969)**
Ph.D dissertation.
Cambridge University, England.

91. **Roberts, AD. (1968)**
Ph.D dissertation
Cambridge University, England.

92. **Johnson, K.L., Kendall, K., Roberts, D. (1971)**
'Surface energy and the contact of elastic solids.'
Proc. R. Soc. Lon. Ser. A., Vol. 324, pp. 301

93. **Butt, H-J., Jaschke, M., Ducker, W. (1995)**
'Measuring surface forces in aqueous electrolyte solution with the atomic force microscope.'
Bioelectrochem. Bioenerg., Vol. 38, pp. 191-201

94. **Chizhik, SA., Huang, Z., Gorbunov, VV., Myshkin, NK., Tsukruk, VV. (1998)**
'Micromechanical properties of elastic polymeric materials as probed by scanning force microscopy.'
Langmuir, Vol. 14, pp. 2606-2609

95. **Stillwell, NA., Tabor, D. (1961)**
'Elastic recovery of conical indentations.'
Proc. Phys. Soc. Lond., Vol: 78, pp. 169-178

96. **Tabor, D. (1947)**
'A simple theory of static and dynamic hardness.'
Proc. R. Soc. Lond. A., Vol: 192, pp. 247-274

97. **Pethica, JB., Hutchings, R., Oliver, WC. (1983)**
'Hardness measurement at penetration depths as small as 20nm.'
Philos. Mag. A., Vol: 48, pp. 593-606

98. **Oliver, WC., Hutchings, R., Pethica, JB. (1986)**
'Microindentation techniques in materials science and engineering.'
ASTM STP 889, Philadelphia, PA. pp. 90-108

99. **Doerner, MF., Nix, WD. (1986)**
'A method for interpreting the data from depth-sensing indentation instruments.'
J. Mater. Res., Vol:1, pp. 601-609

100. **Oliver, W.C., Pharr, G.W. (1992)**
'An improved technique for determining hardness and elastic modulus using load and displacement sensing indentation experiments.'
J. Mater. Res., Vol. 7, No. 6, pp. 1564 - 1583

101. **Oliver, WC., Pharr, GM. (2004)**
'Measurement of hardness and elastic modulus by instrumented indentation: Advances in understanding and refinements to methodology.'
J. Mater. Res., Vol. 19, No. 1, pp. 3-19

102. **Ebenstein, DM., Pruitt, LA. (2006)**
'Nanoindentation of biological materials.'
Nanotoday, Vol. 1, pp. 26-33

**103. Field, JS., Swain, MV. (1993)**
'A simple predictive model for spherical indentation'
J. Mater. Res., Vol. 8, pp. 297-306

**104. Fischer-Cripps, AC. (2000)**
'A review of analysis methods for sub-micron indentation testing.'
Vaccum, Vol. 58, pp. 569-585

**105. Zeta Instrumentation Explanation from Malvern Instruments**
www.malvern.com

**106. Al-Amoudi, A., Williams, P., Mandale, S., Lovitt, RW. (2007)**
'Cleaning results of new and fouled nanofiltration membrane characterized by zeta potential and permeability.'
Separation and Purification Technology, Vol. 54, pp. 234-240

**107. Fairbrother, F., Mastin, H. (1924)**
'CCCXII – Studies in electro-endosmosis. Part I.'
J.Chem. Soc., Trans., Vol. 125, pp. 2319-2330

**108. Abramson, HA. (1934)**
'Electrokinetic phenomena and their application to biology and medicine.'
ACS Monograph Series No.66. Chem Catalog. New York

**109. Electro Kinetic Analyser Instruction Manual Version 2.20 (2003)**
Anton Paar, Graz, Austria

**110. James, BJ., Jing, Y., Chen, XD. (2003)**
'Membrane fouling during filtration of milk – a microstructural structure.'
J. Food. Eng., Vol. 60, pp. 431-437

**111. Sanz, MA., Bonnelye, V., Cremer, G. (2007)**
'Fujairah reverse osmosis plant: 2 years of operation.'
Desalination., Vol. 203, pp. 91-99

**112. Prescott, LM., Harley, JP, Klein, DA (2005)**
'Microbiology, Sixth Edition'
Mcgraw Hill

**113. Gerischer, U. (2008)**
'Acinetobacter, Molecular Microbiology.'
Caister Academic Press, Norfolk, UK

**114. Vaneechoutte, M., Dijkshoorn, L., Tjernberg, I., Elaichouni, A., de Vos, P., Claeys, G., Verschraegen, G. (1995)**
'Identification of Acinetobacter genomic species by amplified ribosomal DNA restriction analysis.'
J. Clinical Microbiology., Vol: 33, pp. 11-15

115. **Yamamoto, S., Bouvet, PJM., Harayama, S. (1999)**
'Phylogenetic structures of the genus Acientobacter based on gyrB sequences: comparison with the grouping by DNA-DNA hybridization.'
Int. J. Syst. Bacteriol., Vol: 49, pp. 87-95

116. **Vaneechoutte, M., Nemec, A., Musilek, M., van der Reijden, TJ., van den Barselaar, M., Tjernberg, I., Calame, W., Fani, R., De Baere, T., Dijkshoorn, L. (2009).**
'Description of *Acientobacter venetianus* ex Di Cello et al. 1997 sp. Nov.'
Int J Syst Evol Microbiol., Vol. 59, pp.1376-1381

117. **Vaneechoutte, M., Tjernberg, I., Baldi, F., Pepi, M., Fani, R., Sullivan, ER, van der Toorn, J., Dijkshoorn, L. (1999)**
'Oil-degrading Acientobacter strain RAG-1and strains described as '*Acientobacter venetianus* sp. Nov.' belong to the same genomic species.'
Res Microbiol., Vol. 150, pp.69-73

118. **Thompson, FL., Austin, B., Swings, JG. (2006)**
'The biology of Vibrios.'
Wiley-Blackwell.

119. **Bergey, DH., Holt, JG. (2000)**
'Bergey's manual of determinative bacteriology.' Ninth Edition
Lippincott Williams and Wilkins

120. **Saeed, MO., Jamaluddin, IA., Tisan, IA., Lawrence, DA., Al-Amri, MM., Chida, K. (2000)**
'Biofouling in a seawater reverse osmosis plant on the red sea coast, Saudi Arabia.'
Desalination, Vol. 128, pp. 177-190

121. **Abdul Azis, PK., Al-Tisan, I., Sasikumar, N. (2001)**
'Biofouling potential and environmental factors of seawater at a desalination plant intake.'
Desalination, Vol. 135, pp. 69-82

122. **Lee, J., Jung, J-Y., Kim, S., Chang, IS., Mitra, SS., Kim, IS. (2008)**
'Selection of the most problematic biofoulant in fouled RO membrane and the seawater intake to develop biosensors for membrane biofouling.'
Desalination., Vol. 247, pp.125-136

123. **Bayer, ME., Sloyer, JL. (1990)**
'The electrophoretic mobility of gram-negative and gram-positive bacteria: an electrokinetic analysis.'
J. Gen. Microbiol., Vol.136, pp.867-874

124. **Blake II, RC., Shute, EA., Howard, GT. (1994)**
'Solubilization of minerals by bacteria: Electrophoretic mobility of Thiobacillus ferrooxidans in the presence of iron, pyrite and sulfur.'
Appl. Environ. Microbiol Vol. 60, pp. 3349-3357

125. **Van der Mei, HC., Leonard, AJ., Weerkamp, AH., Rouxhet, PG., Busscher, HJ. (1988).**
'Properties of oral streptococci relevant for adherence: Zeta potential, surface free energy and elemental composition.'
Colloid. Surf., Vol. 32, pp.291-305

126. **Burnett, P-G, Heinrich, H., Peak, D., Bremer, PJ., McQuillan, AJ., Daughney, CJ. (2006)**
'The effect of pH and ionic strength on proton adsorption by the thermophilic bacterium *Anoxybacillus flavithermus*.'
Geochimica et Cosmochimica Acta, Vol. 70, pp.1914-1927

127. **Phoenix, VR., Martinez, RE., Konhauser, KO., Ferris, FG. (2002)**
'Characterization and implications of the cell surface reactivity of Calothrix sp. Strain KC97.'
Appl. Environ. Microbiol, Vol. 68, pp.4827-4834

128. **Martienssen, M., Kohlweyer, RO. (2001)**
'Surface properties of bacteria from different wastewater treatment plants.'
Acta Biotechnologica., Vol.21, pp.207-225

129. **van Loosdrecht, MCM., Lyklema, J., Norde, W., Schraa, G., Zehnder, AJB. (1987)**
'Electrophoretic mobility and hydrophobicity as a measure to predict the initial steps of bacterial adhesion.'
Appl. Environ. Microbiol, Vol. 53, pp.1898-1901

130. **Chun, J., Lee. J-H., Jung, Y., Kim, M., Kim, S., Kim, BK., Lim, Y-W. (2007)**
'EzTaxon: a web-based tool for the identification of prokaryptes based on 16S ribosomal RNA gene sequences.'
International Journal of Systematic and Evolutionary Microbiology, Vol. 57, pp. 2259-2261

131. **Martinez, RE., Pokrovsky, OS., Schott, J., Oelkers, EH. (2008)**
'Surface charge and zeta-potential of metabolically active and dead cyanobacteria.'
J. Colloid. Interface. Sci, Vol. 323, pp.317-325

132. **Baldi, F., Ivosevic, N., Minacci, A., Pepi, M., Fani, R., Svetlicic, V., Zutic, V. (1999)**
'Adhesion of Acientobacter venetianus to diesel fuel droplets studied with in situ electrochemical and molecular probes.'
Appl. Environ. Microbiol., Vol. 65, pp. 2041-2048

133. **Dorobantu, LS., Bhattacharjee, S., Foght, M., Gray, MR. (2009)**
'Analysis of force interactions between AFM tips and hydrophobic bacteria using DLVO theory.'
Langmuir, Vol. 25, pp. 6968-6976

134. **Camprubf, S., Merino, S., Benedf, J., Williams, P., Tomas, JM. (1992)**
'Physicochemical surface properties of Klebsiella pneumoniae.'
Curr. Microbiol., Vol. 24, pp. 31-33

135. **Szabo, JG., Rice, EW., Bishop, PL. (2006)**
'Persistence of Klebsiella pneumoniae on stimlated biofilm in a model drinking water system.'
Environ. Sci. Technol., Vol. 40, pp. 4996-5002

136. **Morisaki, H., Nagai, S., Ohshima, H., Ikemoto, E., Kogure, K. (1999)**
'The effect of motility and cell-surface polymers on bacterial attachment.'
Microbiol., Vol. 145, pp. 2797-2802

137. **de Roever, EWF., Huisman, IF. (2007)**
'Microscopy as a tool for analysis of membrane failure and fouling.'
Desalination, Vol, 207, pp. 35-44

138. **Wijmans, JG., Baaij, JPB., Smolders, CA. (1983)**
'The mechanism of formation of microporous or skinned membranes produced by immersion precipitation.'
J. Memb. Sci, Vol. 14, pp. 263-266

139. **Kwak, S-Y., Jung, SG., Yoon, YS., Ihm, DW. (1999)**
'Details of surface features in aromatic polyamide reverse osmosis membranes characterised by scanning electron and atomic force microscopy.'
J. Polymer. Sci. Part B. Polymer Physics, Vol. 37, pp. 1429-1440

140. **Kwak, S-Y., Ihm, DW. (1999)**
'Use of atomic force microscopy and solid-state NMR spectroscopy to characterise structure-property-performance correlation in high flux reverse osmosis (RO) membranes.'
J. Memb. Sci, Vol. 158, pp. 143-153

141. **Bremer, PJ., Geese, GG., Drake, B. (1992)**
'Atomic force microscopy examination of the topography of a hydrated bacterial biofilm on a copper surface'
Curr. Microbiol., Vol. 24, No. 4, pp. 223-230

142. **Steele, A., Goddard, DT., Beech, IB. (1994)**
'An atomic force microscopy study of the biodeterioration of stainless steel in the presence of bacterial biofilms.'
Int. biodeterior. biodegradation., Vol. 34, No. 1, pp. 35-46

143. **Beech, IB., Cheung, CWS., Johnson, DB., Smith, JR. (1996)**
'Comparative studies of bacterial biofilms on steel surfaces using atomic force microscopy and environmental scanning electron microscopy.'
Biofouling., Vol. 10, pp. 65-77

144. **Arce, FT., Carlson, R., Monds, J., Veeh, R., Hu, FZ., Stewart, PS., Lal, R., Ehrlich, GD., Avci, R. (2009)**
"Nanoscale Structural and Mechanical Properties of Nontypeable *Haemophilus influenzae* Biofilms."
J. Bacteriol., Vol. 191, No. 8, pp. 2512-2520

145. **Chaw, KC., Manimaran, M., Tay, FEH. (2005)**
"Role of Silver Ions in Destabilization of Intermolecular Adhesion Forces Measured by Atomic Force Microscopy in *Staphylococcus epidermidis* Biofilms."
Antimicrob. Agents. Chemother., Vol.49, No.12, pp. 4853-485

146. **Karime, M., Bouguecha, S., Hamrouni, B. (2008)**
'RO membrane autopsy of Zarzis brackish water desalination plant.'
Desalination, Vol. 220, pp. 258-266

147. **Mohamedou, EO., Surarez, DBP., Vince, F., Jaouen, P., Pontie, M. (2010)**
'New lives for old reverse osmosis (RO) membranes.'
Desalination, Vol, 253, pp. 62-70

148. **Chan, R., Chen, V. (2004)**
'Characterisation of Protein Fouling on Membranes: Opportunities and Challenges.'
J. Memb. Sci., Vol. 242, pp. 169-188

149. **Nystrom, M., Lindstrom, M., Matthiasson, E. (1989)**
'Streaming potential as a tool in the characterization of ultrafiltration membranes.'
Colloid. Surf., Vol. 36, pp.297-312

150. **Elimelech, M., Chen, WH., Waypa, JJ. (1993)**
'Measuring the zeta (electrokinetic) potential of reverse osmosis membranes by a streaming potential analyser.'
Desalination, Vol. 95, pp. 269-286

151. **Deshmukh, SS., Childress, AE. (2001)**
'Zeta potential of commercial RO membranes: influence of source water type and chemistry.'
Desalination, Vol 140, pp. 87-95

152. **Burns, DB., Zydney, AL. (2000)**
'Buffer effects on the zeta potential of ultrafiltration membranes.'
J. Memb. Sci., Vol. 172, pp. 39-48

153. **Childress, AE., Elimelech, M. (1996)**
'Effect of solution chemistry on the surface charge of polymeric reverse osmosis and nanofiltration membranes.'
J. Memb. Sci., Vol. 119, pp.253-268

154. **Winston, W., Rupp, C.J., Vinogradov, A.M., Towler, B.W., Adams, H., Stoodley, P.**
"Rheology of Biofilms."
Internet Note from Department of Mechanical and Industrial Engineering, Montana State University Bozeman, MT 59717.
Email - vinograd@me.montana.edu

155. **Lee, S., Elimelech, M. (2006)**
'Relating organic fouling of reverse osmosis membranes to intermolecular adhesion forces.'
Envion. Sci. Technol., Vol. 40, pp. 980-987

156. **Pelham, RJ., Wang, Y-L. (1997)**
'Cell locomotion and focal adhesions are regulated by substrate flexibility.'
PNAS., Vol. 94, pp. 13661-13665

157. **Engler, AJ., Richert, L., Wong, JY., Picart, C., Discher, DE. (2004)**
'Surface probe measurements of the elasticity of sectioned tissue, thin gels and polyelectrolyte multilayer films: Correlations between substrate stiffness and cell adhesion.'
Surf. Sci., Vol. 570, pp.142-154

158. **Solon, J., Levental, I., Sengupta, K., Georges, PC., Janmey, PA. (2007)**
'Fibroblast adaptation and stiffness matching to soft elastic substrates.'
Biophys. J., Vol. 93, pp. 4453-4461

159. **Bakker, DP., Huijs, FM., de Vries, J., Klijnstra, JW., Busscher, HJ., van der Mei, HC. (2003)**
'Bacterial deposition to fluoridated and non-fluoridated polyurethane coatings with different elastic modulus and surface tension in a parallel plate and a stagnation point flow chamber.'
Colloids Surf B Biointerfaces, Vol, 32, pp. 179-190

160. **Lichter, JA., Thompson, MT., Delgadillo, M., Nishikawa, T., Rubner, MF., Van Vliet, KJ. (2008)**
'Substrata mechanical stiffness can regulate adhesion of viable bacteria.'
Biomacromolecules, Vol. 9, pp. 1571-1578

161. **Yeung, T., Georges, PC., Flanagan, LA., Marg, B., Ortiz, M., Funaki, M., Zahir, N., Ming, W., Weaver., V., Janmey, PA. (2005)**
'Effects of substrate stiffness on cell morphology, cytoskeletal structure, and adhesion.'
Cell. Motil. Cytoskeleton., Vol. 60, pp. 24-34

162. **Zhang, L., Ni, Q-Q., Natsuki, T. (2008)**
'Mechanical properties of polybenzimidazole reinforced by carbon nanofibers.'
Adv. Mater. Res., Vol. 47-50, pp. 302-305

163. **Xu, H., Chen, K., Guo, X., Fang, J., Yin, J. (2007)**
Synthesis of hyperbranched polybenzimidazoles and their membrane formation.'
J. Memb. Sci, Vol. 288, pp. 255-260

164. **Jee, A-Y., Lee, M. (2010)**
'Comparative analysis on the nanoindentation of polymers using atomic force microscopy.'
Poly. Test., Vol. 29, pp. 95-99

165. **Fang, T-H., Chang, W-J., Tsai, S-L. (2005)**
'Nanomechanical characterisation of polymer using atomic force microscopy and nanoindentation.'
Microelectronics. J., Vol. 36, pp. 55-59

166. **Xu, W., Mulhern, PJ., Blackford, BL., Jericho, MH., Firtel, M., Beveridge, TJ. (1996)**
'Modeling and measuring the elastic properties of an archaeal surface, the sheath of *Methanospirillum hungatei* and the implication for methane production.'
J. Bacteriol., Vol: 178, pp. 3106-3112

167. **Volle, CB., Ferguson, MA., Aidala, KE., Spain, EM., Nunez, ME. (2008)**
"Spring constants and adhesive properties of native bacterial biofilm cells measured by atomic force microscopy."
Colloids Surf B Biointerfaces., Vol. 67, pp. 32-40

168. **Nishino, T., Ikemoto, E., Kogure, K. (2004)**
"Application of Atomic Force Microscopy to Observation of Marine Bacteria."
Jounral of Oceanography., Vol. 60, pp. 219-225

169. **Zhao, C., Brinkhoff, T., Burchardt, M., Simon, M., Wittstock, G. (2009)**
'Surface selection, adhesion, and retention behavior of marine bacteria on synthetic organic surfaces using self-assembled monolayers and atomic force microscopy.'
Ocean Dynamics., Vol. 59, pp. 305-315

170. **Subramani, A., Hoek, EMV. (2008)**
'Direct observation of initial microbial deposition onto reverse osmosis and nanofilitration membranes.'
J. Memb. Sci, Vol. 319, pp.111-125

171. **Dimitriadis, EK., Horkay, F., Maresca, J., Kachar, B., Chadwich, RS. (2002)**
'Determination of elastic moduli of thin layers of soft material using the atomic force microscope.'
Biophys. J., Vol. 82, pp. 2798-2810

172. **Boubakri, A., Bouguecha, S. (2008)**
'Diagnostic and membrane autospy of Djerba Island desalination station.'
Desalination, Vol. 220, pp.403-411

**173. Xu, L-C., Vadillo-Rodriguez, V.,Logen, BE. (2005)**
'Residence time, loading force, pH and ionic strength affect adhesion forces between colloids and biopolymer-coated surfaces.'
Langmuir., Vol. 21, pp. 7491-7500

**174. Vrijenhoek, EM, Hong, S., Elimelech, M. (2001)**
'Influence of membrane surface properties on initial rate of colloidal fouling of reverse osmosis and nanofiltration membranes.'
J. Memb. Sci, Vol. 188, pp. 115-128

**175. Sheng, X., Ting, YP., Pehkonen, SO. (2008)**
'The influence of ionic strength, nutrients and pH on bacterial adhesion to metals.'
J. Colloid. Interface. Sci, Vol. 321, pp. 256-264

**176. Dahlback, B., Hermansson, M., Kjelleberg, S., Norkrans, B. (1981)**
'The hydrophobicity of bacteria – an important factor in their initial adhesion at the air-water interface.'
Arch. Microbial, Vol. 128, pp.267-270

**177. Loosdrecht, MCM., Lyklema, J., Norde, W., Schraa, G., Zehnder, AJB. (1987)**
'The role of bacterial cell wall hydrophobicity in adhesion.'
App. Environ. Microbiol., Vol. 53, pp. 1893-1897

**178. Hourai, A., Picard, J., Habarou, H., Galas, L., Vaudry, H., Heim, V., Di Martino, P. (2008)**
"Rheology of biofilms formed at the surface of NF membranes in a drinking water production unit."
Biofouling, Vol: 24, No: 4, pp. 235-240

**179. Vinogradov, A.M., Winston, M., Rupp,C.J., Stoodley, P. (2004)**
"Rheology of biofilms formed from the dental plaque pathogen *Streptococcus mutans*."
Biofilms, Vol: 1, pp. 49-56

**180. Towler, B.W., Rupp, C.J., Cunningham, A.L.B., Stoodley, P. (2003)**
"Viscoelastic Properties of a Mixed Culture Biofilm from Rheometer Creep Analysis."
Biofouling, Vol: 19 No: 5, pp.275-285

**181. Mayer, C., Moritz, R., Kirschner, C., Borchard, W., Maibaum, R., Wingender, J., Flemming, H-C. (1999)**
'The role of intermolecular interactions: studies on model systems for bacterial biofilms.'
International Journal of Biological Macromolecules, Vol: 26, pp. 3-16

# Appendix A – Young's modulus Explanation

The subject of Elasticity is concerned with the determination of the stresses and displacements in a body as a result of applied mechanical or thermal loads, for those cases in which the body reverts to its original state on the removal of the loads.

Young's modulus is a numerical constant that describes the elastic properties of a solid undergoing tension or compression in only one direction and was named after the 18th-century English physician and physicist Thomas Young. Young's modulus is defined as the ratio of the uniaxial stress over the uniaxial strain in the range of stress in which Hooke's Law holds. The following equations are related to the determination of Young's modulus:

$$E \equiv \frac{tensile\ stress}{tensile\ strain}$$

$$E = \frac{\sigma}{\varepsilon} = \frac{F/A_o}{\Delta L/L_o} = \frac{FL_o}{A_o \Delta L}$$

where E is the Young's modulus (modulus of elasticity) and has units in Pa or $N/m^2$, $\sigma$ is the tensile stress and has units in Pa or $N/m^2$, $\varepsilon$ is the tensile strain which is dimensionless, F is the force applied to the object and has units in N, $A_O$ is the original cross-sectional area through which the force is applied and has units in $m^2$, $\Delta L$ is the amount by which the length of the object changes has units in m and $L_O$ is the original length of the object has units in m.

During tensile tests conducted on a sample, Young's modulus can be experimentially determined from the slope of a stress-strain curve, where a material having a large Young's modulus is very stiff and difficult to deform. Certain equations relating to Young's modulus require the use of other material properties, such as Poisson's ratio.

# Appendix B – Membrane History

A presentation given by Dr. Sambhu Saran Mitra, Water System Manager in Furjairah RO process entilited 'Evaluation and Characterization of Seawater RO Membrane Fouling.' in a desalination conference within GIST in October 2008, gave information on the plants operational problems from the first pass on Line B from the RO plant. During the presentation, the following graphs were shown of the 1st pass, Line B RO membrane racks operational data, where it can be clearly seen at which point in the data the membrane units had to be replaced.

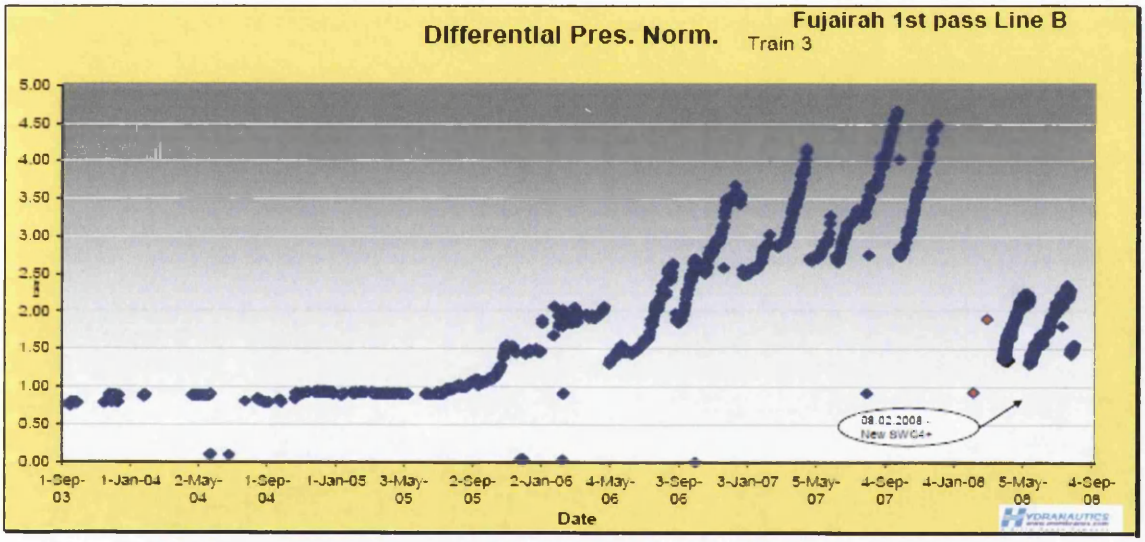


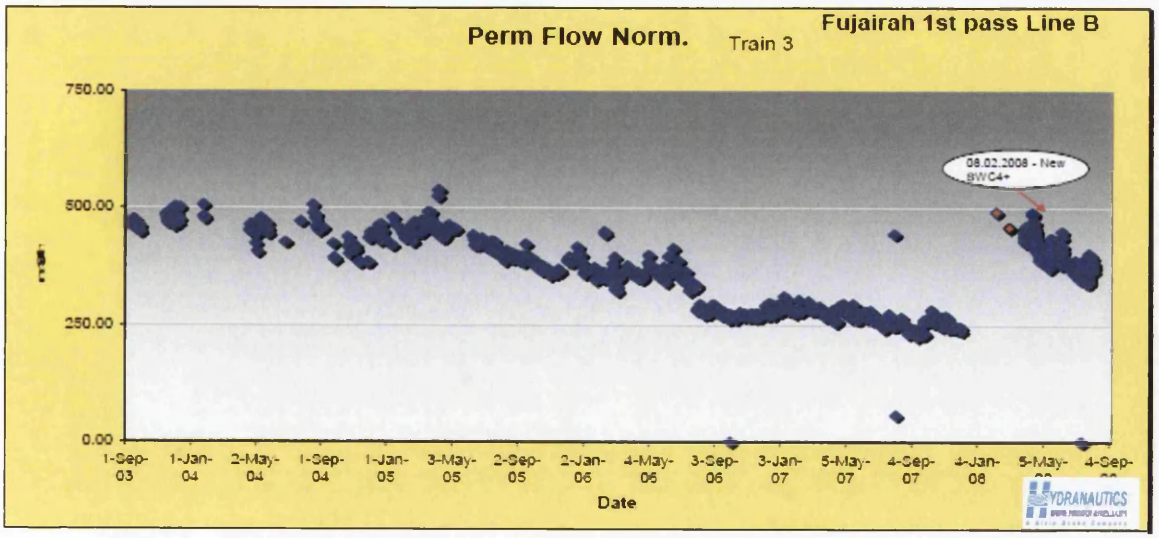

During the presentation Dr Mitra mentioned that the membrane units had to be replaced due to membrane fouling, which caused the increase in differential pressure and the decrease in normalized flow.

Even though it is not know what section of the plant the membrane analysed in this research work came from, the normalised flow and normalised differential pressure given above in the previous graphs date from September 2003 to September 2008 in the Fujairah RO plant and as the membranes were received in GIST in October 2008, the membranes used may have be subject to very similar conditions. The data gained from Dr Mitra presentation has given insight into the operation of the Fujairah RO plant and the operational values at which the membranes are determined to be too fouled and have to be replaced.

# Appendix C – Membrane Specification Sheet

NITTO DENKO HYDRANAUTICS www.membranes.com A Nitto Denko Company

## Membrane Element SWC3+

| | | |
|---|---|---|
| **Performance:** | Permeate Flow: | 7,000 gpd (26.5 $m^3/d$) |
| | Salt Rejection: | |
| | nominal: | 99.8 % |
| | minimum: | 99.7 % |
| **Type** | Configuration: | Spiral Wound |
| | Membrane Polymer: | Composite Polyamide |
| | Nominal Membrane Area: | 400 $ft^2$ |
| **Application Data*** | Maximum Applied Pressure: | 1200 psig (8.27 MPa) |
| | Maximum Chlorine Concentration: | < 0.1 PPM |
| | Maximum Operating Temperature: | 113 °F (45 °C) |
| | Feedwater pH Range: | 3.0 - 10.0 |
| | Maximum Feedwater Turbidity: | 1.0 NTU |
| | Maximum Feedwater SDI (15 mins): | 5.0 |
| | Maximum Feed Flow: | 75 GPM (17.0 $m^3/h$) |
| | Minimum Ratio of Concentrate to Permeate Flow for any Element: | 5:1 |
| | Maximum Pressure Drop for Each Element: | 10 psi |

* The limitations shown here are for general use. The values may be more conservative for specific projects to ensure the best performance and longest life of the membrane.

### Test Conditions

The stated performance is initial (data taken after 30 minutes of operation), based on the following conditions:

32,000 ppm NaCl
800 psi (5.5 MPa) Applied Pressure
77 °F (25 °C) Operating Temperature
10% Permeate Recovery
6.5 - 7.0 pH Range

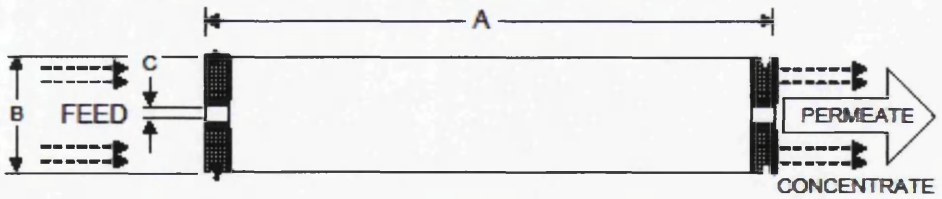


| A, inches (mm) | B, inches (mm) | C, inches (mm) | Weight, lbs. (kg) |
|---|---|---|---|
| 40.0 (1016) | 7.89 (200) | 1.125 (28.6) | 36 (16.4) |

Notice: Permeate flow for individual elements may vary + or - 15 percent. All membrane elements are supplied with a brine seal, interconnector, and o-rings. Elements are vacuum sealed in a polyethylene bag containing less than 1.0% sodium meta-bisulfite solution, and then packaged in a cardboard box.

Hydranautics believes the information and data contained herein to be accurate and useful. The information and data are offered in good faith, but without guarantee, as conditions and methods of use of our products are beyond our control. Hydranautics assumes no liability for results obtained or damages incurred through the application of the presented information and data. It is the user's responsibility to determine the appropriateness of Hydranautics' products for the user's specific end uses. 10/17/08

Hydranautics Corporate: 401 Jones Road, Oceanside, CA 92058
1-800-CPA-PURE Phone: 760-901-2500 Fax: 760-901-2578 info@hydranautics.com

# Appendix D - Results from DNA Analysis of RO Membrane using Culture Dependent method

| Phylogenetic lineages | Closest Relative in Gen Bank | No of Isolates | Similarity % |
|---|---|---|---|
| Alphaproteobacteria | Alpha proteobacterium C06 | 2 | 99 |
| | Martelella mediterranea | 2 | 99 |
| | Alpha proteobacterium IMCC1702 | 3 | 99 |
| | Novosphingobium capsulatum (Sphingomonas capsulata) | 1 | 99 |
| Betaproteobacteria | Alcaligenes sp. S-SL-5 | 1 | 99 |
| Gammaproteobacteria | Acinetobacter venetianus | 16 | 100 |
| | Acinetobacter venetianus Strain ACI555 | 4 | 100 |
| | Acinetobacter sp. TS IW 07 | 2 | 100 |
| | Balneatrix alpaca | 1 | 96 |
| | Enterobacter cloacae | 1 | 100 |
| | Enterobacter sp. AAJ3 | 1 | 99 |
| | Gamma proteobacterium 12IX/A01/168 | 1 | 98 |
| | Gamma proteobacterium B32 | 1 | 100 |
| | Klebsiella pneumoniae subsp. Pneumonia | 1 | 100 |
| | Marinobacter hydrocarbonoclasticus | 5 | 99 - 100 |
| | Marinobacter hydrocarbonoclasticus strain S6-02 | 1 | 100 |
| | Marinobacterium litorale | 1 | 97 |
| | Microbacterium sp. S15-C | 1 | 100 |
| | Oceanimonas denitrificans | 1 | 99 |

| | | | |
|---|---|---|---|
| | Oceanimonas denitrificans strain F13-1 | 2 | 99 |
| | Pseudomonas sp. D6-6 | 1 | 100 |
| | Pseudomonas pseudoalcaligenes | 2 | 99 |
| | Pseudomonas sp. BWDY-42 | 2 | 99 |
| | Pseudomonas sp. FSB | 1 | 99 |
| | Rheinheimera aquimaris | 2 | 100 |
| | Rheinheimera aquimaris strain SW-369 | 2 | 99 |
| | Vibrio sp. PM6A | 4 | 99 |
| Firmicutes | Bacillus sp. CNJ733 PL04 | 2 | 99 - 100 |
| | Uncultured Virgibacillus sp. | 1 | 100 |
| | Clostridium sp. enrichment culture clone MB3_7 | 1 | 99 |
| | Halobacillus sp. B298Ydz-ds | 2 | 99 - 100 |
| | Halobacillus sp. NT N163 | 1 | 99 |
| | Exiguobacterium sp. TL | 2 | 99 |
| | Caldanaerocella colombiensis | 3 | 95 |
| Sphingobacteria | Cytophaga sp. SA1 | 1 | 99 |
| Unknown Group | bacterium K2-53A | 2 | 100 |
| | Endophytic bacterium S02 | 1 | 99 |
| Environmental sample | uncultured bacterium | 6 | 99 - 100 |

# Appendix E - Surface Roughness Measurements

## *Virgin Membrane*

| Membrane scan area | RMS (nm) | Peak to Valley (nm) |
|---|---|---|
| 1 | 71 | 399 |
| 1 | 82.7 | 572 |
| 1 | 55.4 | 362 |
| ***average*** | 69.70 | 444.33 |
| ***st dev*** | 13.70 | 112.10 |

| Membrane scan area | RMS (nm) | Peak to Valley (nm) |
|---|---|---|
| 10 | 98.7 | 667 |
| 10 | 118 | 900 |
| 10 | 107 | 791 |
| ***average*** | 107.90 | 786.00 |
| ***st dev*** | 9.68 | 116.58 |

| Membrane scan area | RMS (nm) | Peak to Valley (nm) |
|---|---|---|
| 100 | 154 | 1494 |
| 100 | 164 | 1583 |
| 100 | 203 | 2847 |
| ***average*** | 173.67 | 1974.67 |
| ***st dev*** | 25.89 | 756.77 |

## *Process Fouled Membrane*

| Membrane scan area | RMS (nm) | Peak to Valley (nm) |
|---|---|---|
| 1 | 77.89 | 614 |
| 1 | 99.80 | 408 |
| 1 | 84.62 | 449 |
| **average** | 87.45 | 490.24 |
| ***st dev*** | 11.21 | 109.57 |

| Membrane scan area | RMS (nm) | Peak to Valley (nm) |
|---|---|---|
| 10 | 90.2 | 704 |
| 10 | 116 | 927 |
| 10 | 92.6 | 842 |
| **average** | 99.60 | 824.33 |
| ***st dev*** | 14.25 | 112.54 |

| Membrane scan area | RMS (nm) | Peak to Valley (nm) |
|---|---|---|
| 100 | 265 | 2676 |
| 100 | 348 | 4543 |
| 100 | 280 | 4292 |
| **average** | 297.67 | 3837.00 |
| ***st dev*** | 44.23 | 1013.26 |

## *1μm x 1μm area surface roughness measurements*

| | Process fouled membrane | | Virgin Membrane | |
|---|---|---|---|---|
| | **RMS (nm)** | **P - V (nm)** | **RMS (nm)** | **P - V (nm)** |
| | 55.7 | 305 | 95.2 | 451 |
| | 50.8 | 277 | 65.9 | 446 |
| | 53.1 | 271 | 78.1 | 436 |
| | 43.8 | 224 | 94.9 | 535 |
| | 38.6 | 194 | 90.7 | 463 |
| | 31.5 | 180 | 68.4 | 360 |
| | 34.6 | 214 | 83.3 | 407 |
| | 42.6 | 234 | 102 | 443 |
| | 38.0 | 241 | 68.5 | 376 |
| | 34.1 | 224 | 70.7 | 353 |
| | 44.8 | 209 | 99.7 | 546 |
| | 45.7 | 209 | 99.7 | 654 |
| | 38.8 | 196 | 82.5 | 480 |
| | 37.1 | 196 | 94.1 | 383 |
| | 30.9 | 183 | 76.9 | 421 |
| | 67.9 | 325 | 93.2 | 482 |
| | 67.8 | 313 | 86.5 | 470 |
| | 41.4 | 200 | 107 | 575 |
| | 40.8 | 169 | 72 | 430 |
| | 41.9 | 253 | 97.4 | 525 |
| | 17.2 | 98.3 | 89.5 | 503 |
| | 35.3 | 192 | 101 | 656 |
| | 36.4 | 191 | 70 | 455 |
| | 43.4 | 198 | 93.3 | 410 |
| | 32.2 | 210 | 76.4 | 388 |
| | 18.8 | 112 | 116 | 548 |
| | 32.6 | 156 | 110 | 476 |
| | 72.6 | 448 | 116 | 540 |
| Average | 41.48 | 221.01 | 93.01 | 484.23 |
| St. Dev | 12.53 | 66.40 | 25.32 | 100.85 |